

Dissertation

zur Erlangung des Doktorgrades
der Fakultät für Chemie und Pharmazie
der Ludwig-Maximilians-Universität München

Gelatin Nanoparticles as Delivery System for Nucleotide-Based Drugs

vorgelegt von

Klaus Zwioerek

aus München

2006

Erklärung

Diese Dissertation wurde im Sinne von § 13 Abs. 3 bzw. 4 der Promotionsordnung vom 29. Januar 1998 von Herrn Prof. Dr. Gerhard Winter betreut.

Ehrenwörtliche Versicherung

Diese Dissertation wurde selbstständig, ohne unerlaubte Hilfe erarbeitet.

München, am 03. August 2006

Klaus Zwiorek

Dissertation eingereicht am 03.08.2006

1. Gutachter: Prof. Dr. Gerhard Winter

2. Gutachter: Prof. Dr. Wolfgang Frieß

Mündliche Prüfung am 24.10.2006

Meinen Eltern
in Liebe und Dankbarkeit
gewidmet

Table of contents

Preface

General introduction, aims and organization of this thesis

1.	General introduction.....	1
2.	Aims of this thesis.....	2
3.	Organization of this thesis.....	2
4.	References.....	4

Chapter I

Optimized preparation of gelatin nanoparticles

1.	Introduction.....	5
2.	Materials and Methods.....	12
2.1	Reagents.....	12
2.2	Preparation of gelatin nanoparticles by two-step desolvation.....	12
2.3	Particle size determination.....	13
2.3.1	Dynamic light scattering (DLS).....	13
2.3.2	Asymmetrical flow field-flow fractionation (AF4) in combination with multi-angle light scattering (MALS).....	15
2.3.3	Scanning electron microscopy (SEM).....	16
2.4	Molecular weight analysis of gelatin.....	16
2.4.1	Size exclusion HPLC (SE-HPLC) analysis of various gelatin samples.....	16
2.4.2	AF4 analysis of gelatin.....	17
2.5	Zetapotential (ζ potential) determination of gelatin.....	17

3. Results and Discussion	18
3.1 Comparison of different analytical tools for gelatin nanoparticle size determination.....	18
3.2 Molecular weight characterization of gelatin.....	22
3.3 Optimization of the two-step desolvation technique.....	27
3.3.1 Temperature at the first and second desolvation step.....	27
3.3.2 Amount of sediment after the first desolvation step.....	28
3.3.3 pH value before the second desolvation step.....	30
3.3.4 Acetone addition-rate during the second desolvation step.....	32
3.3.5 Amount of the applied crosslinking reagent.....	33
3.3.6 Evaluation of the conditions for tailor-made nanoparticles.....	34
3.4 Gelatin nanoparticles by one-step desolvation.....	35
4. Conclusion	40
5. References	41

Chapter II

Cationic gelatin nanoparticles as non-viral gene delivery system

1. Introduction	45
2. Materials and Methods	49
2.1 Reagents.....	49
2.2 Preparation of cationized gelatin nanoparticles.....	49
2.3 Cell culture.....	51
2.4 Plasmid DNA (pDNA) and oligonucleotide (ODN) loading of gelatin nanoparticles.....	52
2.4.1 Experiments to determine the maximum pDNA or ODN payload on surface-modified nanoparticles.....	52
2.4.2 pDNA loading of cholamine-modified nanoparticles for subsequent in vitro application.....	52

2.5	Preparation and pDNA loading of cationic liposomes.....	52
2.6	Preparation of PEI polyplexes.....	53
2.7	Transfection.....	53
2.8	Luciferase assay.....	53
2.9	Cell viability.....	54
2.10	Hemolysis assay.....	54
3.	Results and Discussion	55
3.1	Characterization of the surface-modified nanoparticles.....	55
3.2	Nucleotide loading efficiency of surface-modified nanoparticles.....	58
3.3	Optimized pDNA transfection conditions with cholamine-modified gelatin nanoparticles.....	61
3.4	Cytotoxicity of cationized gelatin nanoparticles.....	65
4.	Conclusion	68
5.	References	69

Chapter III

In vitro delivery of immunogenic CpG oligonucleotides

1.	Introduction	73
1.1	The immune system and the role of toll-like receptors.....	73
1.2	History and mechanism of action of CpG ODNs.....	75
1.3	Synthetic CpG ODN classes for humans and their effects on the immune system.....	77
1.4	Fields of applications for synthetic CpG ODNs.....	79
1.5	Clinical trials with CpG ODNs.....	82
1.6	CpG ODN transport by delivery systems and aim of the study.....	82

2. Materials and Methods	84
2.1 Materials	84
2.1.1 Reagents	84
2.1.2 Fluorescent dyes and monoclonal antibodies	85
2.1.3 Applied ODNs	85
2.1.4 Cell culture reagents	86
2.2 Preparation of cationized gelatin nanoparticles	86
2.3 Preparation of fluorescent gelatin nanoparticles	86
2.3.1 Covalent linkage of aminoreactive fluorescent dyes	86
2.3.2 Incorporation of dextran-linked fluorescent dyes	87
2.4 Preparation of fluorescent HSA nanoparticles	87
2.5 Preparation of fluorescent PLGA nanoparticles	87
2.6 Characterization of the nanoparticles	87
2.7 ODN loading of cationized gelatin nanoparticles	88
2.8 Experiments with murine myeloid dendritic cells (MDCs)	88
2.8.1 Culture of MDCs	88
2.8.2 FACS analysis of nanoparticle uptake by MDCs	88
2.8.3 Visualization of nanoparticle uptake by MDCs via CLSM	89
2.8.4 Quantification of cytokine secretion	89
2.8.5 Special conditions for kinetic experiments	89
2.9 Experiments with primary human blood cells	90
2.9.1 Isolation of PBMCs	90
2.9.2 Isolation of PDCs	90
2.9.3 Isolation of B cells	91
2.9.4 Cell cultures	91
2.9.5 Cytokine quantification by ELISA	91
2.9.6 CLSM experiments	91
3. Results and Discussion	93
3.1 Comparative uptake study of various biodegradable colloidal carrier systems into murine myeloid dendritic cells (MDCs)	93
3.1.1 Nanoparticle characterization via DLS	93
3.1.2 FACS analysis of the cellular uptake	93

3.1.3	Visualization of the cellular uptake by CLSM.....	95
3.1.4	Discussion and Summary.....	95
3.2	Delivery of CpG ODN-loaded nanoparticles (CpG-GNPs) into murine MDCs.....	96
3.2.1	Characterization of the nanoparticles.....	96
3.2.2	FACS analysis of CpG-GNP uptake by MDCs.....	98
3.2.3	Visualization of CpG-GNP uptake by CLSM.....	99
3.2.4	Phenotypic maturation of MDCs following treatment with CpG-GNPs.....	100
3.2.5	Cytokine secretion following treatment of MDCs with CpG-GNPs.....	101
3.2.6	Assessment of CpG-GNP uptake and immune-stimulation kinetics.....	105
3.2.7	Discussion and summary.....	109
3.3	Transfer from murine setup to primary human cells.....	113
3.3.1	Activation of CpG ODN sensitive human cell-lines after CpG-GNP treatment.....	113
3.3.1	Morphological investigations of CpG-A ODN 2216.....	116
3.3.2	Effects of CpG ODN-loading on particle mean size and homogeneity.....	117
3.3.3	Is enhanced cellular uptake the key for the enhanced activation of the immune system?.....	119
3.3.4	Discussion and summary.....	121
4.	Conclusion	124
5.	References	126

Chapter IV

In vivo characterization of CpG ODN-loaded gelatin nanoparticles – Application as efficient and safe vaccine adjuvant

1.	Introduction	135
1.1	Novel vaccine adjuvants.....	135
1.2	Aim of the study and potential safety hazards.....	139
2.	Materials and Methods	141
2.1	Reagents.....	141

Table of contents

2.2	Preparation of gelatin nanoparticles.....	141
2.2.1	Cationized gelatin nanoparticles.....	141
2.2.2	Gelatin nanoparticles with encapsulated OVA.....	141
2.3	CpG ODN or OVA loading of cationized gelatin nanoparticles.....	142
2.4	Mice.....	142
2.5	Immunostimulation in vivo and immunization.....	142
2.6	Quantification of cytokines in serum.....	143
2.7	OVA-specific immune response.....	143
2.8	Biodistribution studies via CLSM.....	144
2.9	FACS analysis of lymph node tissue.....	144
2.10	Gelatin-specific immune response.....	144
3.	Results and Discussion	145
3.1	Systemic immunogenic activity of CpG-GNPs in vivo.....	145
3.1.1	Intravenous injection.....	145
3.1.2	Subcutaneous injection.....	147
3.1.3	In vivo localization of fluorescence labeled CpG-GNPs.....	148
3.1.4	Summary.....	151
3.2	CpG-GNPs as immunization adjuvant for chicken egg ovalbumin (OVA) as model protein vaccine.....	152
3.2.1	Orientation study to evaluate the applicability of CpG-GNPs as adjuvant for OVA....	152
3.2.2	Rational design of an applicable OVA delivery by gelatin nanoparticles.....	153
3.2.3	Comparison of the adjuvant potential of CpG-GNPs vs. soluble CpG ODN.....	156
3.2.4	Summary.....	157
3.3	Do gelatin nanoparticles induce anti-gelatin IgGs in mice?.....	158
4.	Conclusion	160
5.	References	161

Chapter V**PEGylation and biodistribution of gelatin nanoparticles –
Initial experiments**

1. Introduction	165
1.1 Biodistribution of nanoparticles.....	165
1.2 Real-time biodistribution analysis of gelatin nanoparticles via positron emission tomography (PET).....	167
1.3 Aim of the study.....	169
2. Materials and Methods	170
2.1 Reagents.....	171
2.2 Preparation of plain and PEGylated gelatin nanoparticles.....	171
2.3 Quantitative monitoring of nanoparticle PEGylation by AF4.....	172
2.4 Atomic force microscopy analysis of plain and PEGylated cationized gelatin nanoparticles.....	172
2.5 Synthesis of 4-Nitrophenyl 2-[¹⁸ F]fluoropropionate ([¹⁸ F]NPPF).....	174
2.6 Adopted synthesis of N-succinimidyl-[¹⁸ F]fluorobenzoate ([¹⁸ F]SFB).....	174
2.7 ¹⁸ F-radiolabeling of gelatin nanoparticles with [¹⁸ F]SFB/ [¹⁸ F]NPPF.....	175
2.8 ¹²⁵ I/ ¹²³ I labeling of gelatin nanoparticles.....	175
2.9 Biodistribution experiments.....	176
2.10 PET imaging.....	176
2.11 γ -camera imaging.....	177
3. Results and Discussion	178
3.1 PEGylation of gelatin nanoparticles.....	178
3.1.1 Quantitative analysis of the PEGylation properties of gelatin nanoparticles via AF4.....	178
3.1.2 Visual comparison of the surface morphology of plain and PEGylated gelatin nanoparticles by AFM.....	181
3.1.3 Summary.....	183
3.2 Biodistribution experiments with radiolabeled gelatin nanoparticles.....	184

Table of contents

3.2.1	Evaluation of the applicability of prosthetic groups for radioactive ^{18}F labeling of gelatin nanoparticles.....	184
3.2.2	Biodistribution experiments with ^{18}F -labeled gelatin nanoparticles.....	186
3.2.3	Biodistribution experiments with $^{123}\text{I}/^{125}\text{I}$ -labeled gelatin nanoparticles.....	189
3.2.4	Summary.....	194
4.	Conclusion	196
5.	References	197
 Final summary and conclusions of this thesis		201
 List of abbreviations		207
 Publications and presentations associated with this work		211
 Acknowledgments		213
 Curriculum Vitae		215

Preface

General Introduction, aims and organization of this thesis

1. GENERAL INTRODUCTION

In expert opinions, nanobiotechnology is expected to revolutionize or at least significantly improve the pharma and life science market within the next 15 years (Rehm & Schueler 2005). However, imaginations concerning what exactly will be possible in future are rather divergent. Visions, such as the ones of the controversially discussed American physicist K. E. Drexler, that one day it will be possible to build nanorobots, which will be able to assemble atom-by-atom anything mankind needs (Drexler *et al.* 1993), appear rather like utopian illusions from a science fiction novel. Nevertheless, nanotechnology is the rage of today's research world that forces the American government to spend 1.3 billion \$ for funding in 2006 alone (www.nano.gov/html/about/funding.html).

Concerning nanodevices suitable for drug delivery, there has already been tremendous progress within the last 30 years, from the first liposomal approach (Gregoriadis *et al.* 1974) to various present colloidal systems that enable temporal and spatial site-specific delivery. Typical properties of these novel nanocarriers are (Couvreur & Vauthier 2006):

- a) Protection of the drugs from degradation
- b) Enhancement of the drug absorption by facilitating the diffusion through the epithelium
- c) Modification of the pharmacokinetics and the drug tissue distribution profile
- d) Improvement of the intracellular penetration and distribution

One very popular subtype of these colloidal delivery systems are nanoparticles. They are by definition solid, submicron-sized particles that possess a matrix structure typically based on polymers or macromolecular substances (Kreuter 1978). Drugs or tracers to be delivered with these particles can either be adsorbed onto the surface, entrapped in the particle matrix or dissolved in the particle core (Allemann *et al.* 1993). When searching for potential matrix-molecules, good particle preparation properties are just one aspect. Aside from this, potential

candidates should ideally be highly biocompatible and biodegradable, feature various accessible sites to e.g. attach targeting ligands, and finally, be easy to obtain and cheap in production. Due to this, approaches based on natural macromolecules and proteins that originally go back to the early days of colloidal carrier system development (Speiser & Pharmaceutical Society of Victoria 1974; Marty *et al.* 1978), have performed a certain renaissance within the last years. Back in time, these approaches failed due to limited reproducibility as well as instabilities and inhomogeneities of the produced nanoparticles. Nowadays, technological and scientific progress offer new and highly precise tools that facilitate the development of new preparation procedures for high quality nanoparticles based on the originally old approaches.

2. AIMS OF THIS THESIS

The present thesis deals with the development of nanoparticles based on the proteinaceous macromolecule gelatin as delivery system for various nucleotide-based drugs. Since a method to produce homogenous nanoparticles was already described in principle (Coester *et al.* 2000), it was the first approach to characterize, optimize, and standardize this manufacturing process.

The next goal was to advance these plain gelatin nanoparticles via modification of the surface towards a delivery system for nucleotide-based drugs. Subsequent to this, the newly established carrier system should be evaluated in preclinical trials.

In addition to these main projects, it was also an aim of this study to investigate and influence the biodistribution of gelatin nanoparticles.

3. ORGANIZATION OF THIS THESIS

Due to the multitude of independent projects, the present work is divided into five self-contained chapters.

In **Chapter I**, fundamental research data concerning the preparation of gelatin nanoparticles is described. Thereby, the work was focused on process optimization of the existing preparation procedure. Moreover, new analytical tools to characterize gelatin and the gelatin nanoparticles are introduced.

Chapter II features the data that were produced in cooperation with the Department of Pharmaceutical Biotechnology at Ludwig-Maximilians-University Munich. In this cooperation, plasmid DNA was bound onto the surface of previously modified gelatin nanoparticles by electrostatic interactions. Subsequent preparation optimization, this simple non-viral gene delivery system was investigated *in vitro* on murine melanoma cells.

The major project of this work, the development and evaluation of gelatin nanoparticles as carrier system for immunogenic so called CpG oligonucleotides is presented in **Chapter III** and **Chapter IV**. The data has been generated in cooperation with the Department of Internal Medicine at the Ludwig-Maximilians-University Munich and initially during a 3-month research stay at the Faculty of Pharmacy at the University of Alberta in Edmonton, Canada.

Chapter III features extensive *in vitro* investigations on the respective primary murine and human target cells such as dendritic cells and B cells, whereas in **Chapter IV**, the results of *in vivo* experiments are presented. Here, the immunogenic effects of CpG oligonucleotide-loaded nanoparticles alone and their adjuvant activity in combination with the model protein antigen ovalbumin (OVA) were explored.

In the final chapter, **Chapter V**, first PEGylation experiments of gelatin nanoparticles are described, with special emphasis on the establishment of new analytical tools for the quality control of the PEGylation process. In the second part of this chapter, radiolabeling strategies were developed in cooperation with the Department of Nuclear Medicine (TU Munich) to enable real-time *in vivo* tracking of the gelatin nanoparticles via positron emission tomography (PET).

4. REFERENCES

Allemann, E., Gurny, R., and Doelker, E.; (1993) Drug-loaded nanoparticles. Preparation methods and drug targeting issues. *EUROPEAN JOURNAL OF PHARMACEUTICS AND BIOPHARMACEUTICS*, 39, 173-191.

Coester, C. J., Langer, K., Von Briesen, H., and Kreuter, J.; (2000) Gelatin nanoparticles by two step desolvation-a new preparation method, surface modifications and cell uptake. *JOURNAL OF MICROENCAPSULATION*, 17, 187-193.

Couvreur, P., and Vauthier, C.; (2006) Nanotechnology: Intelligent Design to Treat Complex Disease. *PHARMACEUTICAL RESEARCH*, 23[7], 1417-1450.

Drexler, K. E., Peterson, C., and Pergamit, G.; (1993) Unbounding the Future: The Nanotechnology Revolution. Quill, New York.

Gregoriadis, G., Wills, E. J., Swain, C. P., and Tavill, A. S.; (1974) Drug-carrier potential of liposomes in cancer chemotherapy. *LANCET* 1[7870], 1313-1316.

Kreuter, J.; (1978) Nanoparticles and nanocapsules. New dosage forms in the nanometer size range. *PHARMACEUTICA ACTA HELVETIAE*, 53, 33-39.

Marty, J. J., Oppenheim, R. C., and Speiser, P.; (1978) Nanoparticles - a new colloidal drug delivery system. *PHARMACEUTICA ACTA HELVETIAE*, 53, 17-23.

Rehm, B. and Schueler, D.; (2005) Small, smaller, smallest. in: *Biotechnology 2020: From the Transparent Cell to the Custom-Designed Process*; European Commission, Directorate-General for Research, Report.

Speiser, P. and Pharmaceutical Society of Victoria.; Injectable compositions. (1974) Australian Patent, 38036/75[1516348].

Chapter I

Optimized preparation of gelatin nanoparticles

1. INTRODUCTION

In the development process of a nanoparticulate drug delivery system for *in vivo* application, biodegradability without toxic by-products is one of the major claims, a potential matrix molecule has to fulfill. Within the past decades, a multitude of protocols described in literature used synthetic or natural base products for the preparation of biodegradable nanoparticles. Instead of a complete listing of all approaches, only a selection of the most significant biodegradable nanoparticle types will be reviewed here.

With regards to nanoparticles based on synthetic polymers, polylactide (PLA), polyglycolide (PLG), and poly(D,L-lactide-co-glycolide) (PLGA) nanoparticles represent the most extensively investigated ones (Panyam & Labhasetwar 2003). Further polymers discussed as promising approaches are poly(cyanoacrylate) (PCA), poly(alkylcyanoacrylate) (PACA) (Vauthier *et al.* 2003), poly(ϵ -caprolactone) (PCL) (Potineni *et al.* 2003), and poly(ester-anhydride) (PEA) (Pfeifer *et al.* 2004).

In addition to these polymers, natural biopolymers and macromolecules such as chitosan (Janes *et al.* 2001), sodium alginate (Rajaonarivony *et al.* 1993), albumin (Kreuter 1978), collagen (Lee *et al.* 2001) and gelatin represent a second fundamental class of base materials for nanoparticles. Among these, nanoparticles of proteinaceous origin, e.g. albumin, collagen and gelatin have raised specific interest. Due to their intrinsic protein structure with the high number of different accessible functional groups, they bear multiple modification opportunities for coupling of e.g. targeting-ligands, crosslinkers, and shielding substances.

In the present work, gelatin nanoparticles have been chosen as promising drug delivery system candidate. Typically, this natural biopolymer is present in other fields of our daily life. It gives gummi bears consistency and without gelatin containing icing, ingredients such as fruits would not stick to a cake. Consequently, the foodstuff industry is the major purchaser of the tonnages of gelatin that are produced every year. However, the amount of gelatin being applied in pharmaceutical industry is not negligible, as far as capsules and ointments are concerned (Djagny *et al.* 2001). But also for current research in fields of delivery

vehicles for the controlled release of biomolecules such as proteins and nucleotides, gelatin has generated increased interest (Young *et al.* 2005). While gelatin and the delivery systems based on this polymer are biocompatible and biodegradable without toxic degradation products (Ward *et al.* 1977; Tabata & Ikada 1998; Kawai *et al.* 2000; Yamamoto *et al.* 2001), they are furthermore known for high physiological tolerance and low immunogenicity since decades (Schwick & Heide 1969). However, rare ethnologically caused cases of hypersensitivity reactions in the Japanese population have been described in literature (Kelso 1999; Saito *et al.* 2005). But the basically beneficial properties of gelatin contributed to its proven record of safety which is also documented by the classification as “Generally Recognized as Safe” (GRAS) excipient by the US Food and Drug Administration (FDA). So, gelatin derivatives are even constituent of intravenously administered applications as plasma expanders (e.g. Gelafundin™, Gelafusal™) and used as sealant for vascular prostheses (Kuijpers *et al.* 2000).

The natural source of gelatin are animals. It is obtained by mainly acidic or alkaline, but also thermal or enzymatic degradation of the structural protein collagen. Collagen represents 30% of all vertebrate body protein. More than 90% of the extracellular protein in the tendon and bone and more than 50% protein in the skin consist of collagen (Friess 1998). The characteristic molecular feature of collagen being responsible for its high stability is the unique triple-helix structure consisting of three polypeptide α -chains. Among the 27 collagen types that have been isolated so far (Brinckmann *et al.* 2005), only collagen type I (skin, tendon, bone), type II (hyaline vessels) and type III are utilized for the production of gelatin (Babel 1996).

According to origin and pretreatment of the utilized collagen, two major types of gelatin are commercially produced (Fig. 1). Gelatin type A (**a**cid) is obtained from porcine skin with acidic pre-treatment prior to the extraction process. The second prevalent gelatin species, type B (**b**asic), is extracted from ossein and cut hide split from bovine origin. Thereby, an alkaline process, also known as “liming” is applied. During this extraction also the amide groups of asparagine and glutamine are targeted and hydrolyzed into carboxyl groups, thus converting many of the residues to aspartate and glutamate (Tabata & Ikada 1998; Young *et al.* 2005). Consequently, the electrostatic nature is affected, in contrast to collagen and gelatin type A having an isoelectric point (IEP) of pH 9.0, the higher number of carboxyl groups per molecule reduces the IEP to pH 5.0.

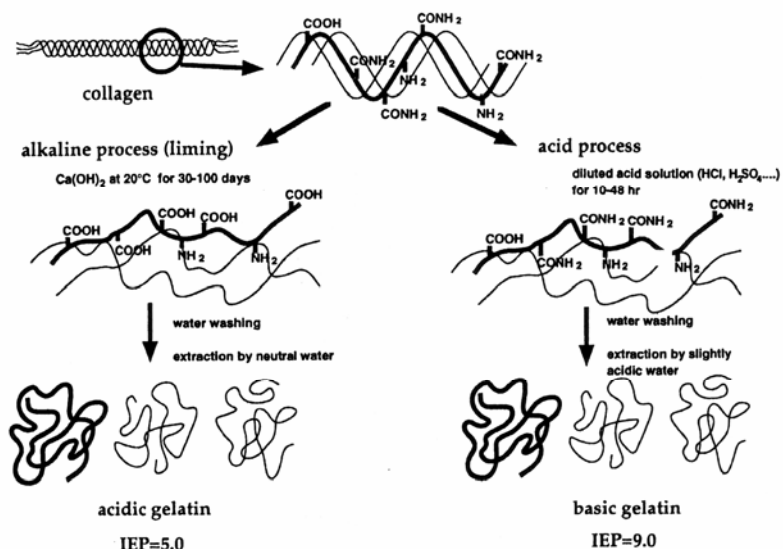


Fig. 1: Preparative process for acidic and basic gelatins from collagen (Tabata & Ikada 1998)

Aside from the two major gelatin types, mixtures of both, resulting in specific intermediate IEPs and cold water fish gelatin do exist. Latterly, FibroGen (South San Francisco, CA, USA) offers synthetic gelatin produced by recombinant DNA technology via a yeast system (*pichia pastoris*). Thus, the potential theoretical hazards of animal-derived materials do no longer exist. However, the current price of 750\$ per g (www.fibrogen.com) is immense in comparison to the low price of commercially available highly purified, sterile, and pyrogen-free natural gelatin.

The amino acid composition of collagen and hence of gelatin is dominated by about 33% glycine and a further 22% proline and 4-hydroxyproline; the remaining 45% comprise 17 amino acids. This specific distribution profile can be attributed to the characteristic triple-helical structure of collagen. Thus, Gly-X-Y represents the continuously repeating amino acid sequence. Since glycine does not possess a side chain, it is oriented into the core of the triple-helix, which represents the closest packed formation. Proline can typically be found in X-position and 4-hydroxyproline in Y-position (Friess 1998). But they can be substituted by any other amino acid as well. In addition to these repetitive sequences, there are regions of 9-26 amino acids at each end flanking the helical structure. These non-helical regions are named telopeptides and show a high variation in amino acids. The overall amino acid composition (rounded per 1000) of type I collagen and gelatin is given in Table 1.

Table 1: Amino acid composition of collagen type I and gelatin. (rounded per 1000) (Babel 1996)

Amino acid	Type I collagen	Type A gelatin	Type B gelatin
Alanine	113	111	117
Arginine	51	49	48
Asparagine	16	16	-
Aspartic acid	29	29	46
Glutamine	25	25	-
Glutamic acid	48	48	72
Glycine	331	329	335
Histidine	4	4	4
Hydroxylysine	104	91	93
Hydroxyproline	5	6	4
Isoleucine	11	10	11
Leucine	24	24	24
Lysine	28	27	28
Methionine	6	4	4
Phenylalanine	13	14	14
Proline	114	131	125
Serine	35	35	34
Threonine	17	18	18
Tyrosine	4	3	1
Valine	22	26	22
Total	1000	1000	1000

During the extraction process of collagen, covalent intra- and intermolecular bonds responsible for the stability and insolubility of collagen undergo cleavage (Courts 1959). The resulting tropocollagen is further denatured by the breakage of hydrogen- and hydrophobic bonds that stabilize the triple-helix structure (Flory & Weaver 1960). Instead of a homogeneous decomposition product, a heterogeneous proteinaceous material with a broad range of molecules with various molecular weights is generated since some peptide bonds remain stable and others, especially those with glycine are rather labile. Furthermore, partial renaturation can occur dependent on external factors such as pH or temperature (Farrugia & Groves 1999).

The molecular heterogeneity of gelatin can be characterized via various molecular weight fractions (Farrugia 1998; Farrugia & Groves 1999):

- a) Low molecular weight fraction (< 50 kDa) and sub- α fraction (50-80 kDa); consisting of hydrolysis fragments (Steckert *et al.* 1992)
- b) α fraction (80-125 kDa); corresponding to the α -chains derived from tropocollagen (Piez *et al.* 1960)
- c) β fraction (125-230 kDa); corresponding to α -chain dimers, also known as β -chain (Piez *et al.* 1960; Piez *et al.* 1961)
- d) γ fraction (230-340 kDa); corresponding to α -chain trimers, also known as γ -chain (Veis *et al.* 1962)
- e) ϵ fraction (340-700 kDa); corresponding to γ -chain dimers
- f) ζ fraction (700-1000kDa); corresponding to γ -chain trimers
- g) δ fraction (1000-1800 kDa); corresponding to γ -chain tetramers with a high degree of crosslinking (Veis *et al.* 1962)
- h) Microgel (> 1800 kDa); corresponding to γ -chains multimers

Due to this molecular heterogeneity of gelatin, the preparation of homogeneous micro- and especially nanoparticulate formulations is challenging. Nevertheless, there is a number of preparation techniques described since the 1970s, most of them adopted from other proteins such as albumin. Basically two major approaches can be described:

- a) Preparation via a biphasic system: emulsifying an aqueous solution of gelatin within an oily phase.
- b) Desolvation of the protein: adding a non-solvent, salting out, or adjusting the pH to the IEP of gelatin.

Most of the emulsification techniques that are described in literature use simple W/O-emulsions. Thereby, e.g. sesame oil, chloroform, toluene or isopropylpalmitate are chosen as organic phase (Yoshioka *et al.* 1981; Tabata & Ikada 1989; Kreuter 1992; Cascone *et al.* 2002). The preparation itself is typically performed with emulsifiers, but in some cases also without surfactant (Esposito *et al.* 1995; Li *et al.* 1998).

Even though a lot of emulsion techniques are described in literature, all of them contain certain drawbacks, such as low yield (30%) or broad size distributions. Furthermore, complex and tedious purification procedures are necessary to get rid of the sometimes toxic organic phase and remaining emulsifier. Finally, high energetic methods, such as ultrasound, high-speed-, or high-pressure-homogenization have to be applied to achieve adequate particle sizes.

The first method using a desolvation technique was already described in the 1970s (Speiser & Pharmaceutical Society of Victoria 1974; Marty *et al.* 1978). Thereby, gelatin nanoparticles are prepared by the addition of sodium- or ammonium sulfate as salting-out agents or ethanol as non-solvent.

This method is appropriate for the preparation of nanoparticles based on proteins with defined molecular weight such as albumin. For the use with bulk gelatin having a wide molecular weight spectrum, it lacks robustness in reproducibility and homogeneity of the produced particles. So it is described that different batches of nominally the same gelatin require different experimental conditions and even a slight excess of the dehydrating agent ethanol leads to mass aggregation and precipitation of the nanoparticles. Moreover, polydispersity indices obtained by dynamic light scattering analysis (DLS) are mostly unacceptably large, indicating the presence of a broad size distribution (Farrugia & Groves 1999).

It is mandatory that problems like these get eliminated before gelatin nanoparticles gain attractiveness as alternative colloidal carrier system. An important step towards a solution was the development of the two-step desolvation technique (Coester *et al.* 2000); a higher molecular weight fraction is separated from a lower molecular weight fraction during a first desolvation step, before the particles are prepared in a second desolvation step. This new protocol enabled the production of homogeneous colloidal gelatin spheres.

But thinking of the applicability of nanoparticles as future drug delivery systems, aside from uniformity, reproducibility in size is another prerequisite for commercial production. Hitherto, first investigations had been made, leading to a better understanding of the complexity of the process and resulting nanoparticles (Coester 2000; Weber *et al.* 2000).

It was the aim of the present study to further optimize the two-step desolvation technique and to characterize the utilized gelatin fractions, preparation conditions, and resulting nanoparticles. So, the gelatin fractions and the resulting nanoparticles

are scrutinized with well established analytical tools in comparison to novel approaches. Finally, the impact of several preparation parameters was investigated, to determine a size range where homogeneous gelatin nanoparticles can be reproducibly prepared within.

2. MATERIALS AND METHODS

2.1 Reagents

Reagent	Description	Supplier
Acetone	p.a.	VWR International GmbH (Ismaning, Germany)
Gelatin type A	175 Bloom	Sigma-Aldrich GmbH (Taufkirchen, Germany)
Glutaraldehyde	25% sol. in water	Sigma-Aldrich GmbH (Taufkirchen, Germany)
HCl	1 N	VWR International GmbH (Ismaning, Germany)
NaCl	p. a.	VWR International GmbH (Ismaning, Germany)
Na ₂ HPO ₄ *2H ₂ O	p.a.	Sigma-Aldrich GmbH (Taufkirchen, Germany)
NaH ₂ PO ₄ *H ₂ O	p.a.	Sigma-Aldrich GmbH (Taufkirchen, Germany)
NaOH	1 N	VWR International GmbH (Ismaning, Germany)

2.2 Preparation of gelatin nanoparticles by two-step desolvation

The original preparation procedure is described as following (Coester *et al.* 2000):

1.25g of gelatin type A (Bloom175) are dissolved in 25 mL water (5% w/w) under gentle heating. A first desolvation step is initiated by the addition of 25 mL acetone. After sedimentation of precipitated gelatin fractions for a certain time, the supernatant consisting of some desolvated gelatin as well as gelatin in solution has to be discarded. Now, the sediment is getting dissolved again by the addition of 25 mL water under heating and the pH has to be adjusted to 2.5. In situ gelatin nanoparticles are formed during a second desolvation step by dropwise addition of 50 mL acetone under stirring (500 rpm). After 10 min, 200 µl of glutaraldehyde (25%) are added to the reaction vessel to crosslink the nanoparticles. Finally, after stirring for 12 hours, the particles have to be purified by three-fold centrifugation (16000 g for 20 min) and redispersion in acetone/water (30/70). The purified

nanoparticles are stored as dispersion in highly purified water (conductivity < 0.04 $\mu\text{s}/\text{cm}$) at 4-8 °C.

Except stated otherwise, the following standard parameters were chosen for nanoparticle preparation:

- a) Temperature before the first and second desolvation step: 50°C
- b) stirring speed: 500-700 rpm
- c) precipitation time after the first desolvation step: 60 sec
- d) speed of acetone addition (second desolvation step): 3-5 mL/min

2.3 Particle size determination

Particle size determination was performed with three different methods. In addition to the two state-of-the-art techniques dynamic light scattering and scanning electron microscopy, a new sizing method was evaluated. The applied new analytical tool was an asymmetric flow field-flow fractionation unit with a multi-angle light scattering detector. The asymmetrical flow field-flow fractionation data was generated in cooperation with my former colleague Dr. Wolfgang Fraunhofer. Dr. Norbert Stock (Physical Chemistry, LMU Munich) assisted at the scanning electron microscopy experiments.

2.3.1 Dynamic light scattering (DLS)

DLS is also often referred as photon correlation spectroscopy (PCS) or quasi-elastic light scattering (QELS). In DLS experiments, the Brownian motion of the analytes within the dispersion medium is detected. More precisely, this is done by measuring the angular distribution of time-dependent scattered light intensity due to density and/or concentration fluctuations (Chu & Liu 2000). From these fluctuations an autocorrelation function is derived, which is inverted to determine the diffusion coefficient of the analyzed sample. The diffusion coefficient in turn represents the velocity of the analyte's Brownian motion. The size of the analyte is now calculated based on the measured velocity with respect to two further factors having significant impact on this calculation; medium viscosity and temperature (Hodgson 2000).

Thus, the hydrodynamic diameter ($d(H)$) can be calculated by the Stokes-Einstein equation:

$$d(H) = \frac{kT}{3\pi\eta D}$$

$d(H)$ = hydrodynamic diameter

k = Boltzmann's constant

η = viscosity

T = absolute temperature (K)

D = diffusion coefficient

Thereby, the measured diameter $d(H)$ describes how the particles move within a liquid, but cannot be set equivalent with the actual particle diameter.

The calculated DLS results are displayed as average mean sizes. However, these mean sizes represent only intensity-based average values and do not further clarify the prevailing size distributions. For this purpose a second benchmark, the polydispersity index (PI) is stated to give information about the actual distortion of the monomodal light scattering signal. The PI can have values from 0-1 and is equivalent to the variance σ^2 of the distribution (Rawle 1993).

DLS experiments were performed with a Zetamaster (Malvern Instruments, Worcestershire, England) detecting the scattered light at a fixed angle of 90°. Additionally, recent samples were analyzed with a Nanosizer ZS (Malvern Instruments, Worcestershire, England) using NIBS™-technology (**N**on **I**nvasive **B**ack **S**cattering) at a static detection angle of 173°. Except stated otherwise, the nanoparticles were diluted in sterile filtered, highly purified water and measured in concentrations between 30 and 100 µg/mL. Due to these low concentrations, the nanoparticles did not influence the viscosity of the dispersion, so that the viscosity was set as pure water (i.e. 0.8872 cP at 25°C). The experiments were performed at room temperature or set to 25°C in Nanosizer ZS experiments.

2.3.2 Asymmetrical flow field-flow fractionation (AF4) in combination with multi-angle light scattering (MALS)

As novel analytical approach for size determinations we chose a combination of an asymmetrical flow field-flow fractionation (AF4) unit for analyte fractionation and a static light scattering (SLS) detector to determine the analyte's size or molecular weight. SLS, also known as classic light scattering measures in contrary to DLS the angular distribution of time-averaged scattered light intensities (Chu & Liu 2000). Whereas DLS is the light scattering technique of choice, if no further fractionation of the analyte can be applied, it is inappropriate for on-line detection subsequent to a chromatographic separation, as autocorrelation and size calculation take too much time. On the other hand it is mandatory for accurate SLS detection to separate varying analytes before detection. However, SLS with a single photodiode to collect the scattered light intensity of analytes at a defined angle is not adequate for correct signal detection of gelatin nanoparticles. This experimental setup is only appropriate for analytes with diameters $< \lambda/20$. Solely these samples induce isotropic light scattering with the same intensity to every direction according to the Rayleigh theory. Analytes $> \lambda/20$ instead induce anisotropic light scattering, as the light is in correlation with increasing analyte size more and more forward scattered (Fig. 2).

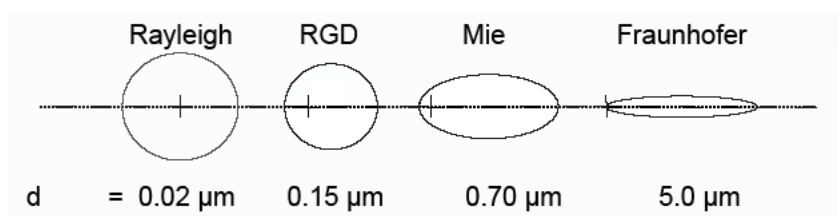


Fig. 2: Illustration of the particular light scattering profiles of various sized analytes

Hence, these analytes that are best described by the theories of Rayleigh-Gans-Debye (RGD), Mie, or Fraunhofer cannot be determined exactly by measuring only a single light intensity at a static angle. In consequence, a multi-angle measurement is necessary for correct analysis of samples within this size range. This is possible by the use of a 18-angle multi-angle light scattering (MALS) unit (DAWN EOS, Wyatt Technology, Santa Barbara, USA). For the present size calculation of gelatin nanoparticles, a Debye-based method was chosen.

The fractionation of the various sized nanoparticles was performed by an HRFFF-10.000 AF4 system, comprising separation channel, pumps controlling the injection flow, forward flow, and cross-flow, in-line solvent filter (0.1 μm , PTFE), degasser (PN7505) and autoinjection system (PN5200) (all from Postnova Analytics, Landsberg, Germany). The channel height was 350 μm and the flow rate at the channel outlet was 1.0 mL/min. The applied regenerated cellulose ultrafiltration membrane (Nadir Filtration, Wiesbaden, Germany) had a cut-off of 5 kDa.

The concentration signal, which is necessary to calculate the particle size, was obtained from on-line UV-spectrophotometrical detection at 280 nm wavelength (SpectraSystem UV 1000, Thermoquest, Darmstadt, Germany) and dn/dc values were determined with a deflection type differential RI detector (Δn -1000, $\lambda = 620$ nm; WGE Dr. Bures, Dallgow, Germany).

The experiments were performed at 24 °C, using a buffer with pH 7.4 (5 mM $\text{Na}_2\text{HPO}_4 \cdot 2\text{H}_2\text{O}$ and 14 mM NaCl).

2.3.3 Scanning electron microscopy (SEM)

Gelatin nanoparticles were analyzed by SEM to characterize the surface morphology of dry, non-dispersed nanoparticles. The pictures were taken with a field emission scanning electron microscope (JSM-6500 F, Jeol, Ebersberg, Germany) at 5.0 kV and a working distance of 9.7 mm. For sample preparation gelatin nanoparticles were dispersed in acetone at a concentration of 20 $\mu\text{g}/\text{mL}$ and applied on a specifically polished sample grid. The samples were vacuum-dried over 12 hours and finally metallized with a 2 nm gold layer before microscopical analysis.

2.4 Molecular weight analysis of gelatin

Size exclusion HPLC and AF4 analytics of gelatin were performed under the technical guidance of my colleague Jan Zillies and my former colleague Dr. Wolfgang Fraunhofer.

2.4.1 Size exclusion HPLC (SE-HPLC) analysis of various gelatin samples

The molecular weight distribution of dissolved gelatin type A (Bloom 175) was analyzed using a TSKgel G 3000 SW column (7.5 mm x 30 cm; Tosoh Biosep,

Stuttgart, Germany). The further HPLC instrumentation consisted of a LKB 2248 pump (Pharmacia Corp., Germany), a Spectra Series AS 100 (Thermoquest, Darmstadt, Germany) autosampler, and a vacuum in-line degasser (Thermoquest). Quantitative detection was performed with a UV detector (Thermoquest) at 280nm wavelength. The light scattering signal was measured by a MiniDawn™ (Wyatt Technology, Santa Barbara, USA) static light scattering detector.

The separation experiments were performed at 24 °C, using a phosphate buffer pH 6.0 (2 mM Na₂HPO₄*2H₂O and 14 mM NaCl) as mobile phase. The refractive index increment dn/dc for molecular weight calculation of gelatin was set to 0.174 mL/g and the second virial coefficient was set to 0.

2.4.2 AF4 analysis of gelatin

The molecular weight analysis of gelatin type A (Bloom 175) was performed with the identical AF4/MALS instrumentation as described for the nanoparticle characterization (see 2.3.2), except the RI detector. Analogous to the SE-HPLC analysis, we used 0.174 mL/g as dn/dc and set the second virial coefficient at 0. As mobile phase, the same phosphate buffer pH 6.0 as in the SE-HPLC experiments (see 2.4.1) was chosen.

2.5 Zetapotential (ζ potential) determination of gelatin

As the ζ potential can not be measured directly, it is calculated from the electrophoretic mobility of an analyte, according to the Debye-Hückel-theory and the Helmholtz-Smoluchowski-equation.

For the present study, we used a NanoSizer ZS (Malvern Instruments, Worcestershire, UK) equipped with ZetaPals™ technology. Measurements were performed in specific disposable cuvettes at concentrations of 20 µg/mL. To provide sufficient ionic background, measurements were performed in 1 mM NaCl (conductivity: 0.7-1.0 mS/cm).

3. RESULTS AND DISCUSSION

3.1 Comparison of different analytical tools for gelatin nanoparticle size determination

As already mentioned in the introduction, the two-step desolvation method enables the preparation of homogeneous nanoparticles. Quality control of the resulting nanoparticles is done by DLS measurements, the state-of-the-art sizing technique for colloidal analytes. Typical narrow size distributions of gelatin nanoparticles are characterized by PIs below 0.1, so DLS analysis will suggest them to be monomodal. In Fig. 3 a size distribution as plotted by DLS is displayed (Zetamaster; fixed 90° detection angle). This nanoparticle batch (ZW030121-1) was prepared under the previously stated standard conditions (see 2.2), except for the pH value before the second desolvation step, which was adjusted to 3.0. The Zetamaster software calculated 255.7 ± 1.8 nm as averaging mean size of these particles with a PI of 0.028 ± 0.012 (mean of 3 measurements with 10 individual subruns each).

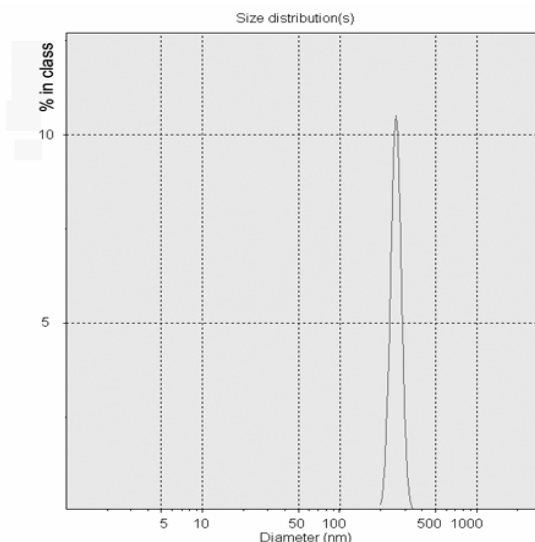


Fig. 3: DLS results of batch ZW030121-1 (size distribution by intensity)

We additionally analyzed this nanoparticle batch by SEM to visualize the particles and investigate their morphology. SEM revealed the sample as smooth spheres (Fig. 4), but a significant discrepancy could be seen between the visible size distribution of the nanoparticles in the SE micrograph (150-260 nm) and the DLS results. Obviously, the accuracy of DLS data needed to be reconsidered. Certainly,

according to the measurement principle of both analytical methods, the nanoparticles could not be measured under equal conditions. For DLS analysis, the particles need to be dispersed in sterile filtered water, whereas SEM detection has to be performed with dried analytes under vacuum conditions.

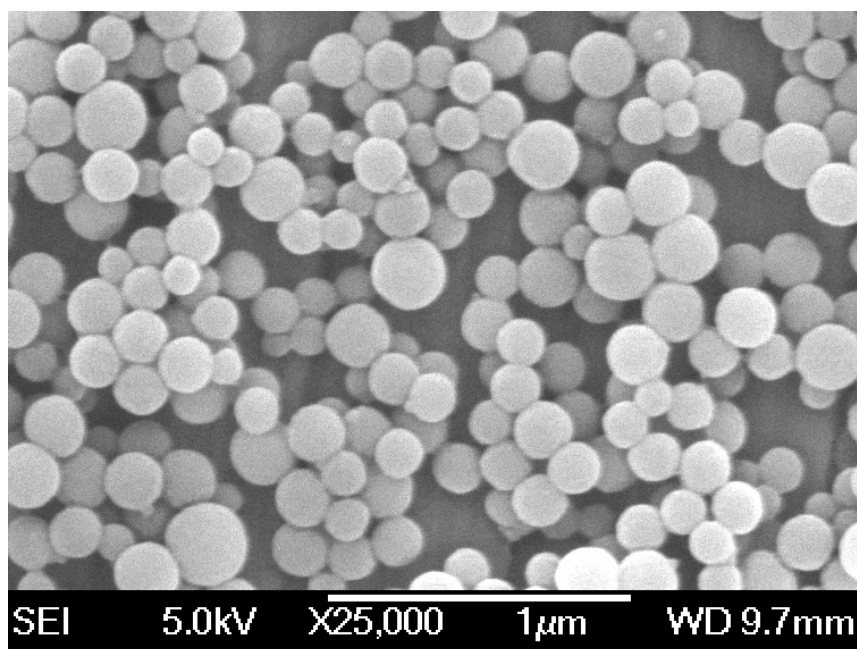


Fig. 4: SE micrograph of gelatin nanoparticle batch ZW030121-1

Consequently, a certain shrinking or even tendencies towards collapsing seem possible when preparing nanoparticles for SEM analysis. DLS in contrary measures the hydrodynamic diameter ($d(H)$) of analytes which is higher than their real diameter. Same observations were already described in literature for other polymer-based nanoparticles (Finsy *et al.* 1992; Bootz *et al.* 2004).

Exact knowledge of the nanoparticle size and a narrow size distribution are essential. However, the variety of appropriate analytical tools is rather limited. Solely analytical ultracentrifugation has been recently described as promising alternative tool to SEM and PCS (Bootz *et al.* 2004).

Our attempt was to use MALS to determine the exact nanoparticle size. The multi-angle geometry spacing 18 photodetectors around a flow cell ensures exact detection of colloidal anisotropic scattering analytes within shortest time. The second big advantage of this detector is its ability to determine molar masses without reference standards, as MALS is an absolute method and all necessary constants can be measured.

A requirement for the exact size determination via MALS is a sufficient previous fractionation of different nanoparticle populations. SE-HPLC as state-of-the-art separation unit being utilized in conjunction with MALS is inappropriate since no adequate columns are commercially available for the separation of nanoparticles. Typically, the upper threshold for samples that can be analyzed via SE-HPLC is 10^9 kDa (~ 50 nm). Above this threshold, no separation occurs and finally columns are destroyed by clogging. For particles within this range other fractionation techniques as for example capillary hydrodynamic chromatography (CHDF) and field-flow fractionation (FFF) are presently the methods of choice (Dos Ramos & Silebi 1993; Wyatt 1998).

So we chose the FFF sub-type AF4 as fractionation unit for the nanoparticles. AF4 can easily be applied for insoluble analytes up to some micrometers because the fractionation is driven by specific flows in a channel instead of a package-material filled separation column.

Dealing with nanoparticles with an expectable narrow size distribution, it has to be the goal to achieve a possibly high resolution. The key is to increase the separation force, i.e. the cross-flow (Wahlund *et al.* 1986). However, an increased cross-flow increases also the potential risk of sample-sample and sample-membrane interactions due to sample concentration at the ultrafiltration membrane (Andersson *et al.* 2001). Hence, we decided to apply a procedure of stepwise approximation to find optimal fractionation conditions. Thereby, we started with an initial cross-flow rate of 5% which was applied for 10 min and increased run by run in 5% intervals. At 5% cross-flow rate, the resolution was too low to enable accurate calculation of the nanoparticle size distribution. Very small analytes were not separated enough from each other to enable distinct detection in the MALS detector (Fig. 5). Moreover, their MALS signal is overpowered by stronger light scattering signal of simultaneously eluted bigger analytes at the beginning of the elution process. An increase to 10% cross-flow already led to adequate resolution with a separated elution profile according to the particle size. This could be proven as we exerted 15% cross-flow, indeed nanoparticle elution profile was further delayed, but no different size distribution data were calculated by MALS software.

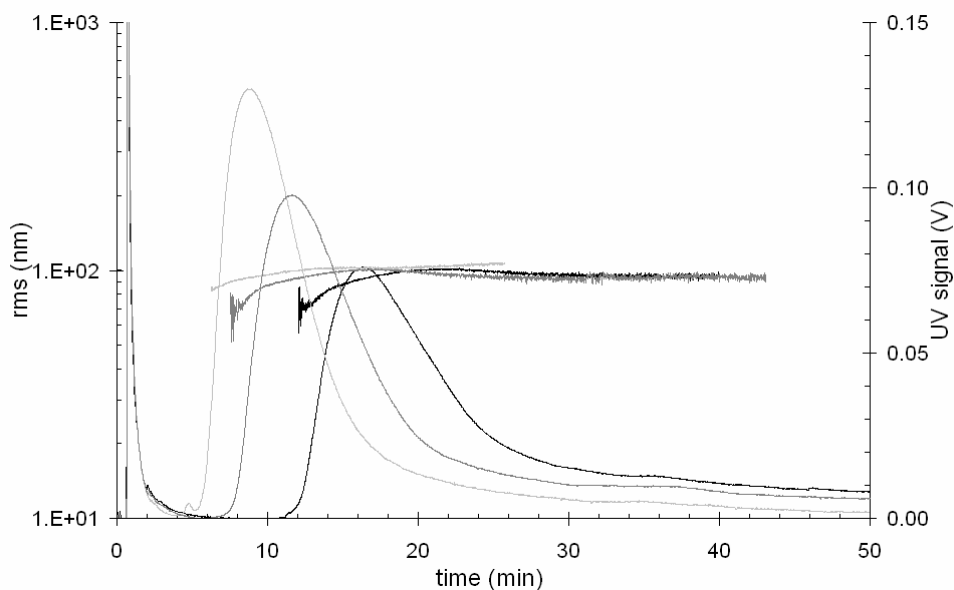


Fig. 5: Characterization of gelatin nanoparticles via AF4/MALS using 5% cross-flow (light grey line), 10% cross-flow (grey line), and 15% cross-flow (black line)

To further verify our data we finally increased the injected nanoparticle concentration (from 0.5 to 0.9 mg/mL). Thereby the assessed increase of UV's AUC values was in sound agreement with the sample concentrations (from $A=1.56-2.80$). Size distribution data was not further affected, thus our new sizing method was further substantiated.

MALS software calculates the original dimension data as root mean square (rms) radii (Fig. 5), also known as radii of gyration (R_G). Anyways, these values can easily be converted into the hydrodynamic diameters ($d(H)$) by the following equation:

$$d(H) = \sqrt{\frac{20}{3}} (R_G)^2$$

$d(H)$ = hydrodynamic diameter

R_G = radius of gyration or root mean square radius

Calculating the size distribution based on the obtained MALS data with a cross-flow rate of 10% (R_G distribution 60-98 nm), resulted with a hydrodynamic diameter range between 155 and 253 nm.

Comparing these data with the results of the other analytical methods it can be summarized, that DLS analysis using the Zetamaster system (Malvern, Worcestershire, United Kingdom) is obviously unable to produce data with the

same high accuracy as SEM or AF4/MALS. An explanation for this can be found in the sample measuring setup, since the plain probe is measured without further separation. According to the Rayleigh approximation, differences in particle size have an amplification factor of 10^6 on the scattered light intensity (Rawle 1993). Thus, it is quite difficult to detect small nanoparticles along with larger ones. During sample preparation special attention has to be paid to the avoidance of contaminations. Otherwise, DLS analysis is a method that requires no specific preparation and is performed in a short time.

The big advantage of SEM is the detailed information about shape and morphology of the samples. A clear disadvantage is the complex sample preparation. Moreover, preparation steps like vacuum drying and contrasting feature a potential risk of changes in particle properties. The determination of size distributions demands further software. Although, only random samples can be captured, so that due to the low number of samples only poor statistical data are generated.

Regarding to the calculated size distribution, AF4/MALS resulted with presumably more accurate data than DLS. In contrast to SEM, no tedious sample preparation with its potential risks is necessary and far more individual particles can be detected. A slight disadvantage of the method is, that it is not ready to use for any analyte at anytime, in contrast to DLS. So, sensitive tuning of the fractionation conditions is necessary to enable accurate sample analysis. Concerning time and effort, the new technique consumes more than the less precise DLS analysis, which produces sizing data within seconds, but is also far less complex than SEM analysis. Thus, DLS as quick state-of-the-art technique is acceptable as quality control for homogeneous samples as analyzed here. Nevertheless, it can be expected that the new hybrid will have great potential especially for heterogeneous samples.

3.2 Molecular weight characterization of gelatin

The present fundamental data concerning the molecular weight distribution of different gelatin fractions was generated under the major guidance of Dr. Wolfgang Fraunhofer. Parts of the presented data, such as the ones depicted in Fig. 6 – Fig. 8, are already published (Fraunhofer *et al.* 2004).

SE-HPLC is the method of choice routinely used for process control and product development, to monitor the molecular mass distribution of gelatin (Meyer &

Morgenstern 2003). The use of a UV detector requires previous calibration of the retention times via globular molecular weight standards resulting in more or less straight calibration lines. The accuracy of these calibrations in connection with gelatin is rather questionable, since gelatin has no globular structure. Thus, previous molecular weight findings based on UV detection alone (Coester 2000; Weber *et al.* 2000) have to be considered as approximations only. In the present study we additionally measured the light scattering signals of the separated gelatin fractions employing a static light scattering (SLS) detector. As soluble gelatin is below the diameter boundary of $\lambda/20$ (see 2.3.2), a 3-angle light scattering detector is sufficient for correct analysis.

Investigating gelatin with our experimental settings, the resulting chromatogram (Fig. 6) of a bulk gelatin solution demonstrated the large molecular heterogeneity of this biopolymer. MALS determined a molecular weight range from about 4 – 1000 kDa. Moreover, two distinct fractions could be identified at 280 nm wavelength. The first fraction comprised high molecular weight (hmw) components >100 kDa and the second one low molecular weight (lmw) components < 100 kDa.

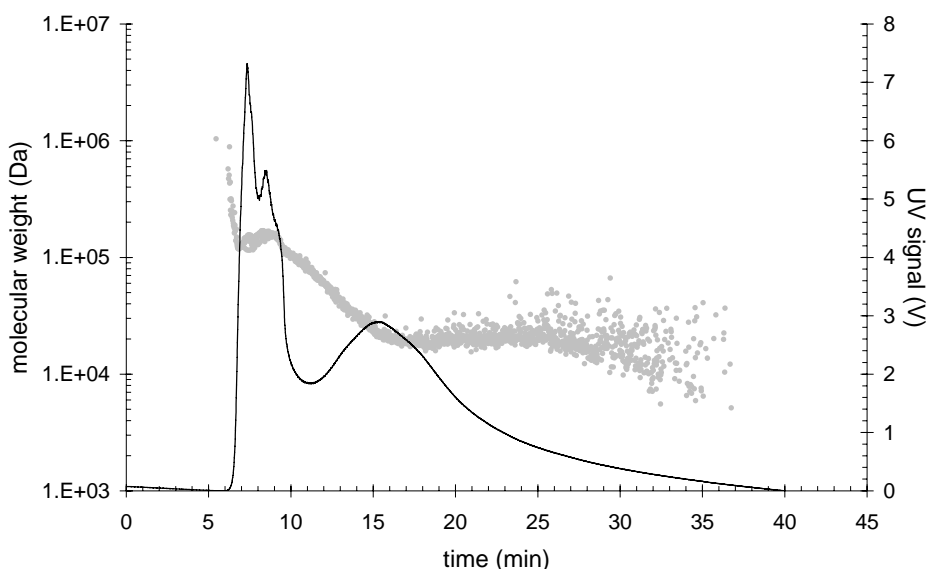


Fig. 6: SE-HPLC analysis via UV_{280} and MALS; flow rate: 0.7 mL/min

Adopting the previously described classification scheme for the different gelatin molecular weight fractions (Farrugia 1998; Farrugia & Groves 1999), the borderline between both fractions corresponds to the α -fraction of gelatin (80-125 kDa),

which consists of soluble tropocollagen α -chains. Consequently, the first peak summarizes the higher molecular weight fractions (β -, γ -, ϵ -, ζ -, δ -, and microgel-fraction) i.e. the multimers of the tropocollagen α -chain, whereas the hydrolysis products classified as sub- α and low molecular weight fraction are responsible for the second peak. The initial steepness of the first peak has to be attributed to an artifact of the separation column, because the molecular weight of the eluted protein was above the maximum separable molecular weight. Thus, these very large components were already eluted with the void volume.

Based on these chromatographic data for bulk gelatin, we further analyzed solutions of the two phases after the first desolvation step: the precipitated sediment which would be further processed for nanoparticle preparation and the supernatant that has to be discarded (Fig. 7). Comparing the chromatograms, both gelatin samples revealed high and low molecular components as well. But as supposed, a higher amount of the hmw components could be found in the sediment. The percentage of hmw components was 58% in the sediment sample compared to 38% in bulk gelatin. A percentage of only 29% of hmw components remained in the supernatant.

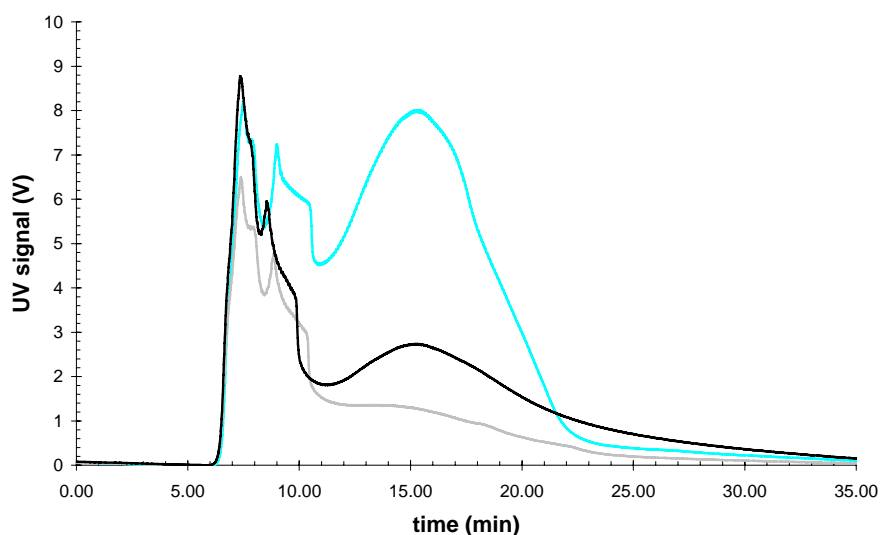


Fig. 7: SE-HPLC chromatograms of bulk gelatin (black), sediment (grey) and supernatant (blue) before the first desolvation step

Even though SE-HPLC is the method of choice to characterize the molecular weight of gelatin (Barth *et al.* 1994; Farrugia 1998), our experiments demonstrated that variations of the analytical settings have significant impact on the determined

ratios between the hmw and lmw components of the samples. Lowering the flow rate led to an intense reduction of the hmw component percentage throughout the analyzed samples; e.g. a reduction of the flow rate to 0.3 mL/min reduced the hmw component content to 24% (sediment), 15% (bulk), and 13% (supernatant). Apparently, the change of the flow rate prohibits to state absolute quantitative values for the molecular weight distribution of gelatin.

Since our major interest was to get a more detailed idea about the actual molecular weight distributions of the gelatin samples, we evaluated AF4/MALS as alternative analytical tool. Applying mild cross-flow conditions (5%), a separation of the bulk gelatin into two fractions was not observed (Fig. 8). However, the molecular weight results, calculated from these experiments, differed remarkable from the results obtained with SE-HPLC. With a molecular weight distribution of 20 – 10,000 kDa, the calculated maximal molar mass was about one order of magnitude higher.

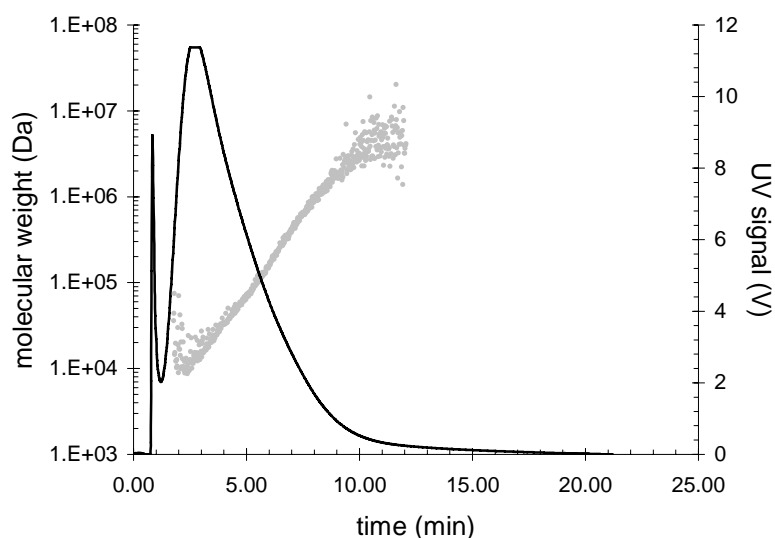


Fig. 8: AF4 fractogram of bulk gelatin (5% cross-flow)

However, these results seem to describe more precisely the actual molar mass distribution of gelatin solutions. It is supposable that these very hmw components could either not pass the separation column in SE-HPLC or got degraded by abrasive shear forces caused by the column package material (Barth *et al.* 1994). In AF4 experiments, this problem does not occur because the separation channel itself is free of package material. Additionally, the field of force that is exerted on

the sample can be minimized by reducing the cross-flow. So, even very delicate analytes can be kept from degradation during the analytical run.

If higher cross-flows are applied, the fractograms of gelatin reveal two populations analogous to the SE-HPLC chromatogram. These two separated fractions can already be generated with 40% initial cross-flow. The molecular weight borderline between these two fractions was not 100 kDa but approximately 450 kDa, thus the the hmw peak represented a lower amount of total gelatin than in SE-HPLC experiments. Nevertheless, most hmw components could be detected in the sediment (27%), followed by 17 % in bulk gelatin and 10% in the supernatant sample (Fig. 9)

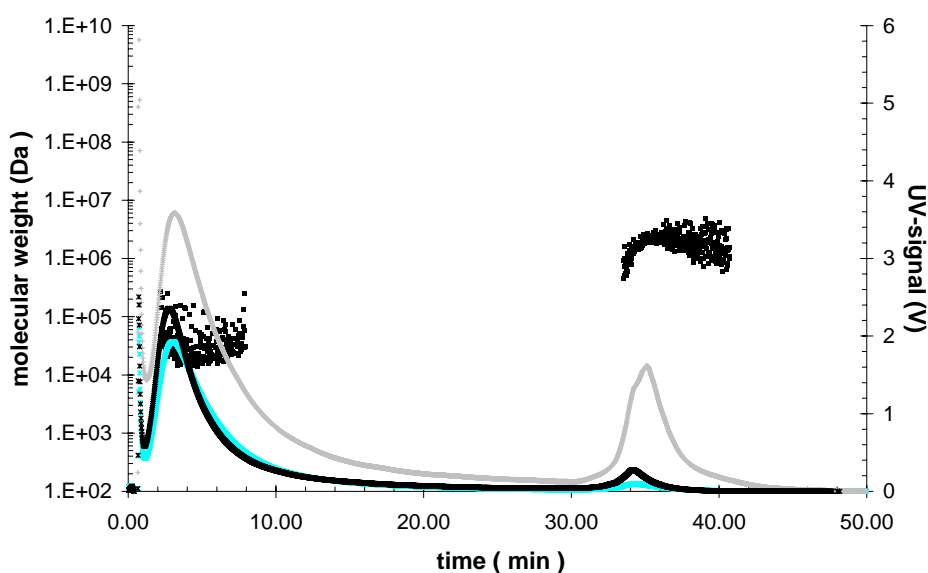


Fig. 9: AF4 fractograms of bulk gelatin (black), sediment (grey), and supernatant (blue) after the first desolvation step (40% cross-flow)

Even though augmentations of the cross-flow intensity influenced the absolute values of the hmw ratios, the relative proportions of the individual samples to each other concerning the hmw content remained constant (data not shown). Thus, no sample degradation occurred.

So, it can be summarized that AF-4 analysis exceeded SE-HPLC in the present study, as it delivered more accurate molecular weight distributions of the applied gelatin solutions. This can be attributed to the milder and more flexible separation conditions the samples were committed to.

3.3 Optimization of the two-step desolvation technique

To achieve pre-defined settings for the reproducible preparation of specifically sized nanoparticles, we had to characterize the influence of diverse variables in the manufacturing process. We expected the following factors to be most important and decided to investigate their impact on the resulting nanoparticles:

- a) temperature at the first and second desolvation step
- b) amount of sediment after the first desolvation step
- c) pH value before the second desolvation step
- d) speed of acetone addition during the second desolvation
- e) amount of crosslinking reagent applied

Batch size, geometry and size of the reaction vessel, and the applied homogenization speed were not further varied or investigated.

3.3.1 Temperature at the first and second desolvation step

The first parameters we investigated were the prevailing temperatures before the induction of the first respectively the second desolvation step. It is well known from literature, that temperature has significant impact on the apparent molecular weight distribution of gelatin, due the occurrence of denaturation or renaturation processes (Farrugia 1998; Farrugia & Groves 1999). Gelatin solutions incubated at 56°C and above exhibit partially reversible denaturation of the higher molecular weight fractions. Enhanced renaturation occurs at lower temperatures, which results in sol-gel transition of gelatin solutions. The sol-gel transition temperature of gelatin solutions is typically at 35-40°C (Peyrelasse *et al.* 1996). In addition to the temperature, the pH of the solution does also have an impact on these denaturation/renaturation phenomena. Thus, denaturation is suppressed and renaturation favored by the lack of net charge on the individual polypeptide units (Farrugia 1998).

As we performed our experiments according to the standard preparation protocol, we chose 35-60°C as temperature range to be tested. The upper limit of the tested temperature spectrum was constituted with respect to the boiling temperature of the later applied desolvation reagent acetone. The lower limit was constituted with

respect to the expected sol-gel transition temperature. Each condition was tested in triplicate.

Contrary to our expectance, variations of the gelatin solutions' temperatures did not induce significant differences in the resulting particles. At least, concerning the temperature before the first desolvation step a slight trend could be seen. The highest (60°C) and the lowest (35°C) temperature conditions led to the biggest and most inhomogeneous particles (Fig. 10A). In terms of the temperature at the second desolvation step, only a minimal trend could be observed favoring 50-55°C as optimal temperature for the production of small nanoparticles (Fig. 10B). So it can be concluded that the chosen standard conditions (50°C for both) also seem to represent the ideal setup as well.

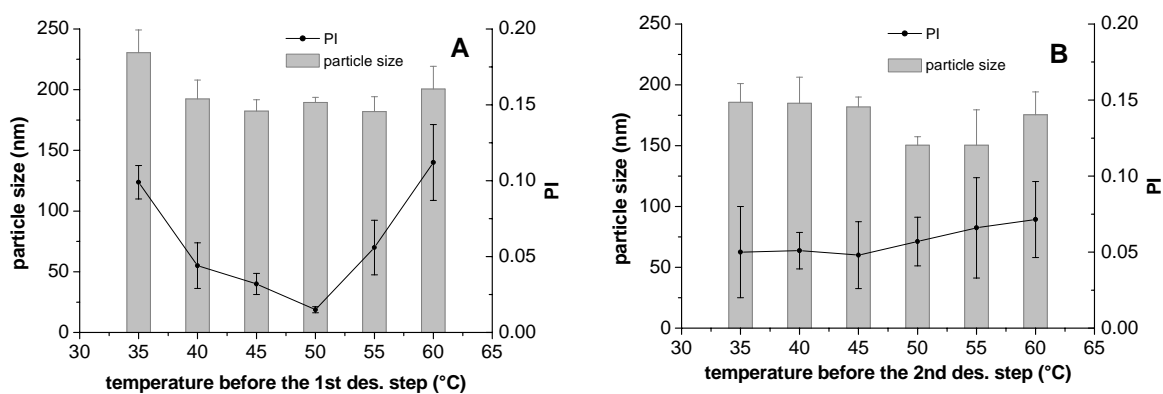


Fig. 10: Correlation between the temperature of the gelatin solutions before each desolvation step and the resulting nanoparticles; A: temperature before the first desolvation step; B: temperature before the second desolvation step ($n=3$)

3.3.2 Amount of sediment after the first desolvation step

As described in the original protocol, the quick addition of acetone causes a rapid precipitation of gelatin. Within seconds a highly viscous, hydrogel-like gelatin sediment appears, which can easily be separated from its supernatant by decantation. Waiting for 10 minutes leads to complete precipitation of insoluble gelatin fractions. But as displayed in Table 2, the majority of insoluble gelatin is already precipitated after 90 seconds. In addition to this sedimentation kinetics information, Table 2 also illustrates that the averaging percentage of gelatin within the hydrogel-like sediment remains constant with $23.6 \pm 1.2\%$ (w/w). Thus, while

we start with originally 1.25 g gelatin before the first desolvation step, the final particles are prepared with a fraction of 26 – 51% (w/w) of the original gelatin amount.

Table 2: Relationship between sedimentation time, amount of resulting hydrous sediment and the actual protein content within this sediment.

Prec. time (s)	hydrogel-like sediment (g)	Dried protein (g)	Protein content (%)
30	1.334	0.330	24.7
40	1.851	0.415	22.5
50	2.050	0.462	22.4
60	2.168	0.540	24.9
90	2.669	0.642	24.1
120	3.132	0.699	22.3
1200	3.430	0.834	24.3

Starting with different amounts of the hydrogel-like sediment, we redissolved the respective sediment in 25 mL highly purified water at a temperature of 50°C. Before the slow addition of acetone (3-5 mL/min), the pH was adjusted to 3.0.

DLS resulted with average sizes of 125 – 300 nm for the various nanoparticle batches (Fig. 11).

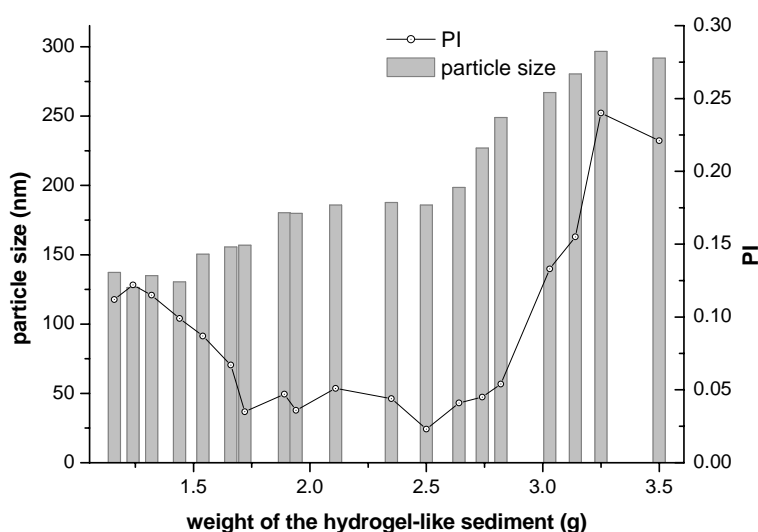


Fig. 11: Correlation between the weight of the hydrogel-like sediment after the first desolvation step and the resulting nanoparticle quality.

The results demonstrate that the final protein concentration of the solution prior to the second desolvation step has crucial influence on the particle size. A higher protein density within the solution obviously facilitates inter-molecular interactions and finally the co-aggregation of gelatin during the second desolvation step. Thus, bigger nanoparticles are the result. It has to be mentioned that 125-140 nm represents a certain lower size limit for nanoparticles prepared under the applied conditions. Furthermore, for sediment weights below 1.25 g (~0.31 g dry protein) the standard addition of 50 mL acetone was unable to induce complete desolvation of the protein. Accessory amounts of acetone had to be added which continuously worsened the PIs of the nanoparticles. This is due to the fact that higher concentrations of the desolvation agent apparently enforce aggregation tendencies of the nanoparticles. Sediments above 3.0 g (~0.70 g dry protein) likewise led to worse PIs above 0.1. So, slower precipitating gelatin components with probably lower molecular weight seem to facilitate aggregation as well.

3.3.3 pH value before the second desolvation step

The net charge of low charge density polyelectrolytes such as gelatin in solution is strongly affected by the prevalent pH conditions. Hence, changing the pH led to strong alterations in final particle size (Fig. 12). The pH region we observed was between pH 2.0 and 4.5. Since gelatin type A has an IEP of pH 9.0, it had a positive net charge at all tested conditions. Under standardized conditions as previously described (see 2.2), it was possible to produce gelatin nanoparticles within a range of pH 2.3 – 4.0. Above pH 4.0 the produced gelatin nanoparticles tended strongly towards aggregation and precipitation. Obviously, this pH value is too close to the IEP of gelatin type A. Thus the remaining net charge of gelatin is too weak to prevent the freshly in-situ formed nanoparticles from instabilities. Within the favorable pH region, increasing acidic conditions correlated with the reduction of the particle's mean sizes. The produced nanoparticles had sizes between 115.0 and 425.8 nm (Fig. 12). Highly homogenous nanoparticles with PIs below 0.1 could be produced between pH 2.3 and 3.8.

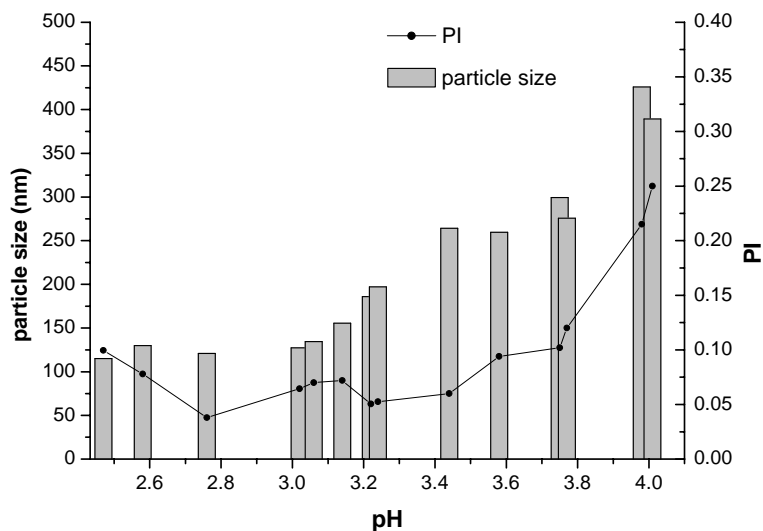


Fig. 12: Correlation between the adjusted pH value before the second desolvation step and the resulting nanoparticle quality.

Performing the dropwise addition of 50 mL acetone to generate the nanoparticles it was noticed that a first turbidity, indicating phase separation, and the generation of nanoparticles appeared at a later point of acetone addition by shifting the pH towards lower values. Thus, at pH 2.3 additional 25 mL acetone were necessary to induce the phase separation. Below this pH even additional 50 mL of acetone could not induce any phase separation. The net charge of the gelatin molecules was apparently too intense, so that the intermolecular repulsion forces stabilizing the characteristic three-dimensional protein shape prevented it from collapse and aggregation induced by the desolvation agent.

In the pH regions where nanoparticles can be produced, the same reasons seem to be responsible for the smaller particle sizes. Intermolecular electrostatic repulsion forces obviously hinder the inter-molecular co-aggregation.

In Fig. 13, the ζ potentials of gelatin before the second desolvation step at various pH values are illustrated. Referring to these data, the averaging ζ potential of the polypeptide molecules has to be approximately between 9 and 16 mV (in 1 mM NaCl) to enable the production of nanoparticles.

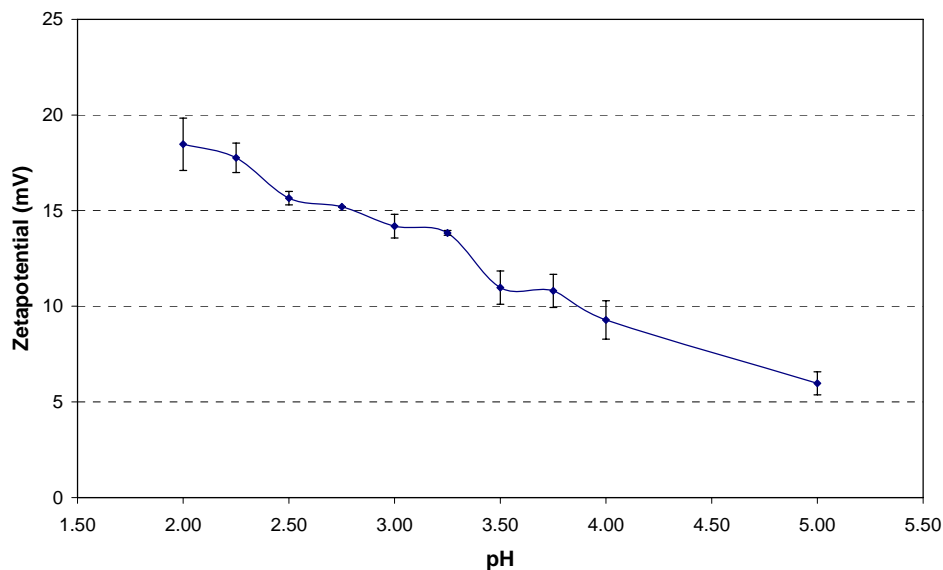


Fig. 13: ζ potential values of redissolved gelatin sediments in correspondence to the pH ($n=3$)

3.3.4 Acetone addition-rate during the second desolvation step

In this study we wanted to determine the maximum applicable rate for the addition of acetone. As depicted in Fig. 14, the resulting nanoparticles were not negatively influenced up to a rate of 5 mL/min.

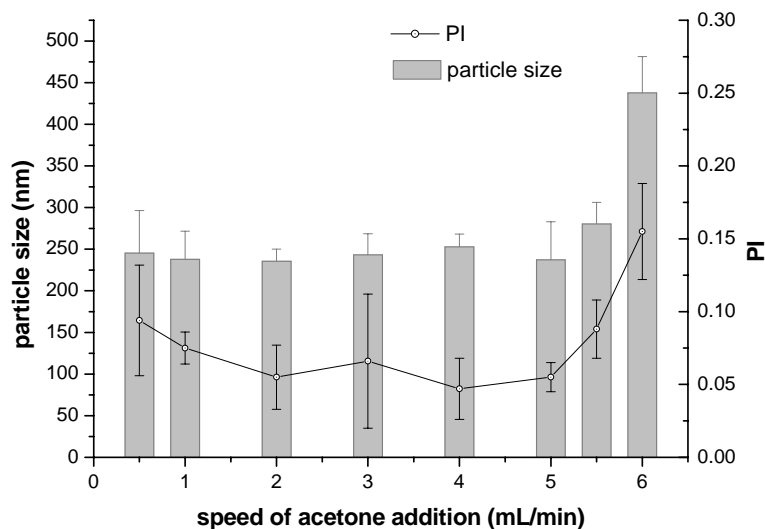


Fig. 14: Correlation between the speed of acetone addition during the second desolvation step and the resulting particle quality ($n=3$)

Beyond this limit, mean particle sizes along with their corresponding PIs increased exponentially, thus indicating either particle aggregation or appearance of inhomogeneous nanoparticles. Consequently, no higher rate seems advisable if no further changes of the standard conditions (e.g. enhanced stirring) are applied. Below 5 mL/min the process is very robust against variations in acetone addition rates.

3.3.5 Amount of the applied crosslinking reagent

Crosslinking has to be done to prevent the in situ formed nanoparticles from disintegration when the desolvation agent acetone is evaporated. It can be performed with non-zero length and zero length agents. Zero-length crosslinking agents (e.g. EDC) activate carboxylic acid residues to react directly with amine groups on adjacent protein chains. For gelatin nanoparticles glutaraldehyde (GTA) is the agent of choice, since it is a highly reactive and efficient crosslinking agent. GTA is a non-zero length crosslinker as it operates by intra-particulate bridging of residual amino groups. But, GTA is due to its high reactivity also the most hazardous reagent being utilized for gelatin nanoparticle preparation. The potential toxicological hazards of GTA in conjunction with proteinaceous materials have been discussed in literature (Lin *et al.* 1998; Ulubayram *et al.* 2002; Zeiger *et al.* 2005). In the present study we prepared gelatin nanoparticles according to the standard conditions (see 2.2; sediment weight after the first desolvation: ~2.5 g; adjusted pH: 3.0) and varied the amount of applied GTA from 6.25-75 mg per sample. Each condition was prepared in triplicates.

As depicted in Fig. 15, the particle size decreases steadily along with higher amounts of GTA applied. Even though, the further size reduction is decelerated from an amount of ~30 mg GTA on. But in total we can state in consensus with other authors (Cascone *et al.* 2002) that increasing amounts of crosslinks lead to denser and smaller nanoparticles.

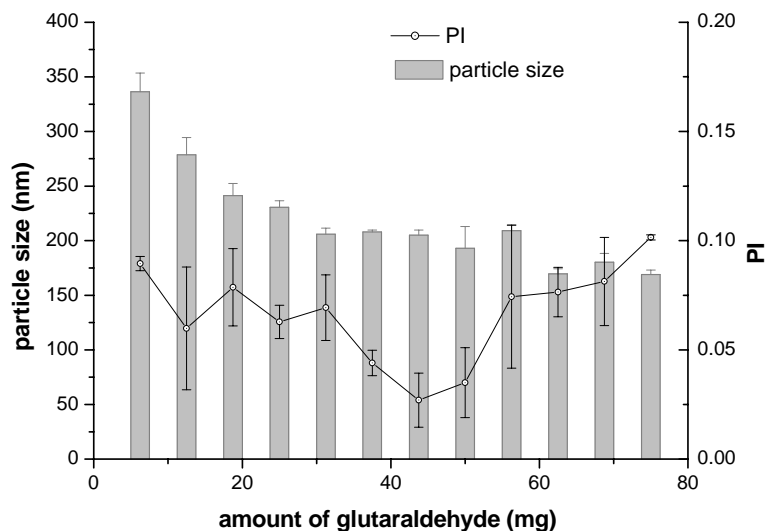


Fig. 15: Correlation between the amount of GTA applied for crosslinking and the resulting particle quality ($n=3$)

With regards to the measured PI values, 43.75 mg represent an optimum with the most homogeneous nanoparticles resulting. The slight increase of the PI values beyond this point might be addressed to stronger interparticulate aggregation tendencies which are facilitated by higher amounts of GTA.

From a toxicological point of view, it would be advisable to keep the amount of GTA as low as possible. But there are further aspects that have to be taken in consideration. The number of crosslinks of gelatin nanoparticles is also responsible for a later degradation and the release kinetics of potentially incorporated drugs. Finally, the number of functionally available amino groups for covalent bonding of amino-reactive ligands is also affected by the number of crosslinks.

The goal of the present experiments was to optimize the particle preparation and not to achieve specific release kinetics of incubated drugs. So, 43.75 mg GTA were chosen as advisable standard amount. At these conditions, the most homogeneous nanoparticles could be produced.

3.3.6 Evaluation of the conditions for tailor-made nanoparticles

Summarizing the results of all parameters evaluated, we finally defined conditions for the preparation of the three different nanoparticle sizes: 100 nm, 150nm, and 300 nm (Table 3). To verify the reproducibility of the nanoparticles produced under these conditions, we repeated every experiment 6 times.

Table 3: Evaluation of optimized conditions for the reproducible preparation of distinctive nanoparticles

conditions/ results \ particle size	300 nm	150 nm	100 nm
Temp. before 1 st desolvation (°C)	50	50	50
Precipitation time (sec.) / weight of hydrous sediment (g)	100 / 2.8	40 / 1.8	30 / 1.3
Temp. before 2 nd desolvation (°C)	50	50	50
pH before 2 nd desolvation	3.75	2.75	2.25
speed of acetone addition (2 nd desolvation) (mL/min)	<5	<5	<5
Amount of acetone (2 nd desolvation)	50	50	75
Amount of GTA for crosslinking (mg)	43.75	43.75	43.75
Mean particle size (nm) (n=6)	293.4 ± 9.9	150.8 ± 2.1	108.77 ± 14.4
PI (n=6)	0.066± 0.021	0.026± 0.015	0.106± 0.022

It can be assumed, that all tested conditions yielded very close to their target sizes with a high reproducibility. The results for the 150 nm particles were definitely outstanding, as they exactly hit their mark and were very homogeneous. But also the results of the other two batches were satisfying. Although it can be concluded that 100nm and 300 nm approximately represent the respective limits for the production of predictable high quality gelatin nanoparticles by two-step desolvation.

3.4 Gelatin nanoparticles by one-step desolvation

Even though the preparation of gelatin nanoparticles by two-step desolvation is already a very elegant and robust technique, it would be a further advantage to prepare nanoparticles from specific gelatin after one desolvation step. By default, gelatin type A (Bloom 175) purchased from Sigma-Aldrich (Taufkirchen, Germany) is used for nanoparticle preparation. With regards to the analytical data solutions of bulk gelatin, the sediment, and the supernatant after the first desolvation step (see

3.2), it was assumed that an increase of hmw components and/or a reduction of lmw components are beneficial for the production of stable and homogenous nanoparticles. This was also suggested by literature (Farrugia 1998). We contacted Gelita AG (Eberbach, Germany), one of the world's largest gelatin producers and asked them to produce specific gelatin batches with modified molecular weight profiles. The respective batches were screened for their suitability to produce stable and homogeneous nanoparticles at various pH conditions and concentrations in one desolvation step.

As an analytical support to this work, Jan Zillies contributed the AF4/MALS analyses to characterize the molecular weight profile of the particularly applied gelatin batches. Parts of these analytical data (Fig. 16 - Fig. 18) are cited in the present chapter but will be part of his thesis (Zillies 2007).

Via a specific preparation procedure, Gelita was able to produce gelatin lots with reduced amounts of peptides <65 kDa. The analysis of Sigma bulk gelatin via AF4/light scattering revealed a content of >50% of these low molecular peptides (Fig. 16) compared to the total protein content.

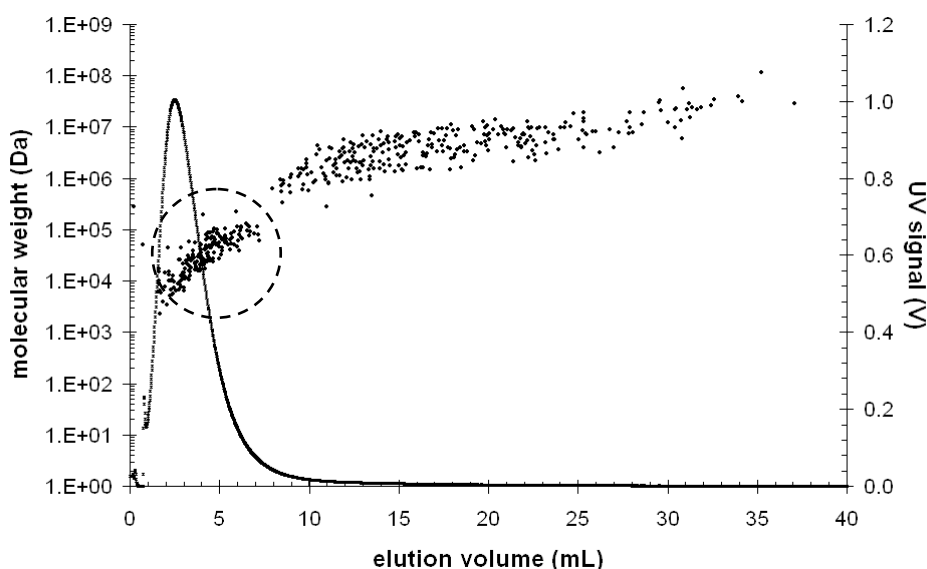


Fig. 16: AF4/SLS fractogram of Gelatin type A (Bloom175) from Sigma-Aldrich (Taufkirchen, Germany, Productnr.: G-2326/LOT: 155469654). (Zillies 2007)

The first specific gelatin batch from Gelita we investigated (PN307779), featured a <65kDa peptide content reduced to <40% of total peptide. Yet, we were unable to produce stable gelatin nanoparticles using this batch.

The second batch (VP 433), again featured a <65 kDa peptide content of <40% of the total gelatin. But additionally, Gelita had introduced an extra high amount of high molecular weight components $>10^7$ kDa to this gelatin batch via specific crosslinking. But also this approach failed to produce nanoparticles. Finally, we could successfully produce gelatin nanoparticles during a single desolvation step with two qualities of gelatin that contained amounts of <20% of <65kDa peptides (VP306/VP413-2) without extra hmw fraction (Fig. 17).

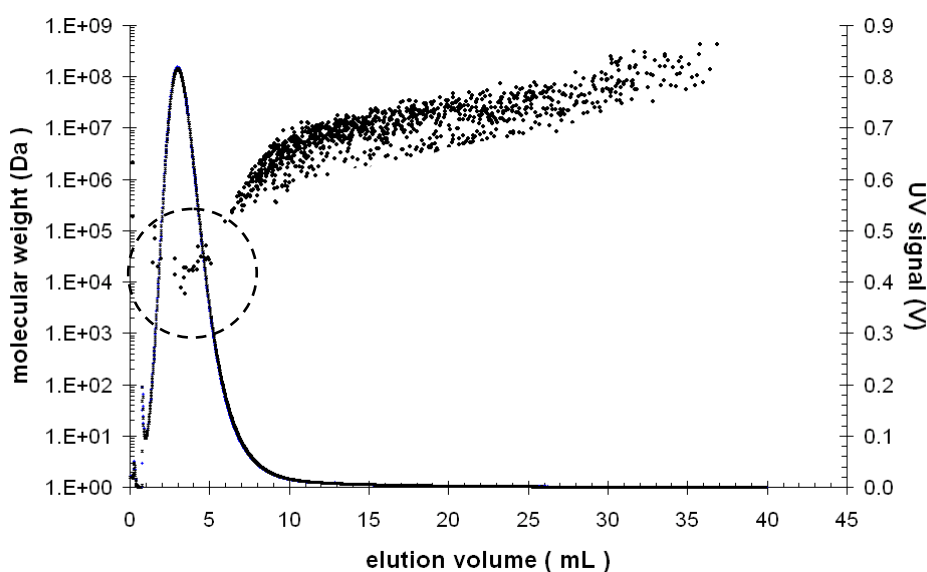


Fig. 17: AF4/light scattering fractogram of gelatin (VP 306) produced by Gelita which enables the production of stable and homogeneous gelatin nanoparticles by a single desolvation step. (Zillies 2007)

In this new simplified preparation approach, it was no longer necessary to perform an initial desolvation step to discard the disturbing gelatin fraction. Thus, gelatin was dissolved at a certain concentration under constant heating and stirring (50°C; 500rpm). Similar to the gelatin solution before the usually second desolvation step, the pH was now adjusted to acidic values before nanoparticles were generated by dropwise addition of acetone. Finally nanoparticle crosslinking with GTA and purification were performed identically to the original two-step desolvation method.

In the present screening, protein concentration (2-6% [w/w]) and pH-range (pH 2.25-3.0) were varied to determine a first range of conditions where stable nanoparticles can be prepared by this new method. It can be derived from Table 4 that monomodal size distributed nanoparticles could be produced within a range

from 180-250 nm. Even though it has to be mentioned, that the applicable pH range is narrower than in two-step desolvation experiments.

Table 4: Overview of the successful preparation conditions screening with gelatin batch VP 306 (n=3)

conc. / pH (% [w/w])	2.25	2.5	2.75	3.0
2.0	no desolvation*	no desolvation*	no desolvation*	no desolvation*
3.0	no desolvation*	180.7±2.7 nm PI: 0.007±0.001	221.5±13.5 nm PI: 0.057±0.014	instable particles**
4.0	no desolvation*	199.7±5.7 nm PI: 0.025±0.011	248.7±27.4 nm PI: 0.105±0.021	instable particles**
6.0	precipitation***	instable particles**	instable particles**	precipitation***

Even excessive addition of acetone did not induce any desolvation of gelatin.

** Desolvation with acetone led to nanoparticles which aggregated and precipitated within a few hours.

*** Addition of acetone led to the formation of an amorphous sediment.

To further characterize these gelatin batches, we analyzed the mean molecular weight of this gelatin via light scattering software (ASTRA 4.73, Wyatt Technology) and compared them with sediment and supernatant of Sigma gelatin after the first desolvation step (Fig. 18).

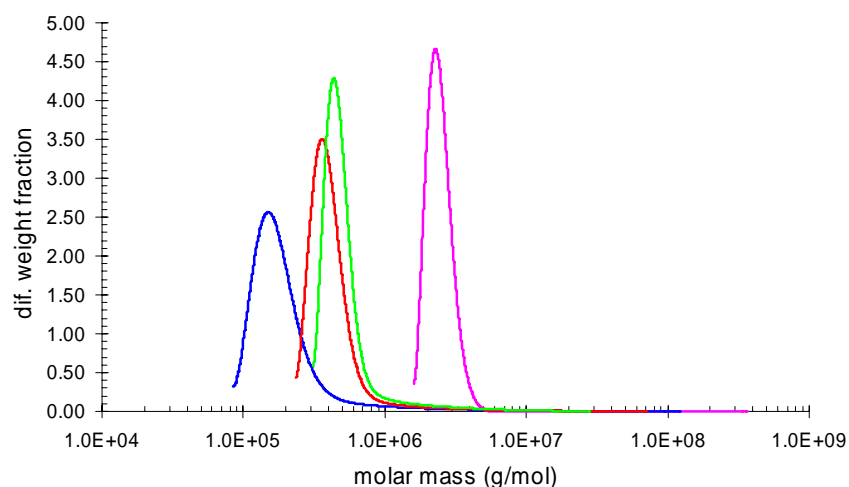


Fig. 18: Mean molecular weight analysis via light scattering analysis of supernatant (blue), gelatin batch VP306 (red), gelatin batch VP413-2 (green), and sediment (pink). (Zillies 2007)

Supernatant and sediment fractions revealed mean molecular weights of ~ 150 kDa respectively ~ 2300 kDa. Both specific gelatin batches resulted between supernatant and sediment (VP306: ~ 380 kDa; VP413-2: ~ 440 kDa). So it can be derived from the present data, that gelatin does not necessarily have to contain an increased amount of hmw components for the production of stable and homogeneous colloidal spheres as stated by other authors (Farrugia & Groves 1999). In fact, the absence or strong reduction of very low molecular weight components (<65 kDa) seems to be essential for the stability and homogeneity of the nanoparticles.

4. CONCLUSION

The repetitive standardized preparation of homogeneous batches is a clear must to bring gelatin nanoparticles closer to the clinical use as a drug delivery system.

Along with better manufacturing processes, high precision analytics are also needed to characterize the base material and the resulting nanoparticles. The new established combination of AF4 and MALS has proven to be a promising tool to close the gaps left by current analytical methods. With this new tool we could moreover clarify the molecular weight distribution of the heterogeneous biopolymer gelatin. The generated data helped to further specify hmw fractions of gelatin as being beneficial. However, the absence or strong reduction of lmw peptides < 65 kDa and not a predominant presence of extra-hmw fractions could be determined as the essential factor for the preparation of stable and homogeneous nanoparticles. In our process optimization studies, we were able to define specific conditions for the preparation of homogeneous (PI <0.15) nanoparticles with a predictability of better than ± 15 nm of the resulting diameter within the range of 100-300 nm. The two crucial factors to control the result are the protein amount and the pH value before the second desolvation step. But also the amount of crosslinking is of high importance, especially if later release of entrapped drugs and degradation kinetics are concerned.

In summary, the preparation of specific homogeneous and stable gelatin nanoparticles is now very well predictable. Consequently, gelatin nanoparticles can be considered as a ready to upscale, promising colloidal drug delivery system.

5. REFERENCES

- Andersson, M., Wittgren, B., and Wahlund, K. G.; (2001) Ultrahigh molar mass component detected in ethyl hydroxyethyl cellulose by asymmetrical flow field-flow fractionation coupled to multi-angle light scattering. *ANALYTICAL CHEMISTRY*, 73, 4852-4861.
- Babel, W.; (1996) Gelatine - Ein vielseitiges Biopolymer. *CHEMIE IN UNSERER ZEIT*, 30, 1-11.
- Barth, H. G., Boyes, B. E., and Jackson, C.; (1994) Size exclusion chromatography. *ANALYTICAL CHEMISTRY*, 66[12], 595R-620R.
- Bootz, A., Vogel, V., Schubert, D., and Kreuter, J.; (2004) Comparison of scanning electron microscopy, dynamic light scattering and analytical ultracentrifugation for the sizing of poly(butyl cyanoacrylate) nanoparticles. *EUROPEAN JOURNAL OF PHARMACEUTICS AND BIOPHARMACEUTICS*, 57[2], 369-375.
- Brinckmann, J., Notbohm, H., Mueller, P. K., and Editors.; (2005) Collagen: Primer in Structure, Processing and Assembly, Springer, Berlin/New York
- Cascone, M. G., Lazzeri, L., Carmignani, C., and Zhu, Z.; (2002) Gelatin nanoparticles produced by a simple W/O emulsion as delivery system for methotrexate. *JOURNAL OF MATERIALS SCIENCE: MATERIALS IN MEDICINE*, 13, 523-526.
- Chu, B. and Liu, T.; (2000) Characterization of nanoparticles by scattering techniques. *JOURNAL OF NANOPARTICLE RESEARCH*, 2[1], 29-41.
- Coester, C.; (2000) Entwicklung peptidischer oberflächenmodifizierter nanopartikulärer Trägersysteme für Antisense-Wirkstoffe und präklinische Testung gegen HIV, Dissertation, Frankfurt.
- Coester, C. J., Langer, K., Von Briesen, H. & Kreuter, J.; (2000) Gelatin nanoparticles by two step desolvation - a new preparation method, surface modifications and cell uptake. *JOURNAL OF MICROENCAPSULATION*, 17, 187-193.
- Courts, A.; (1959) N-Terminal amino acid residues of gelatin. IV. Chain weight and rigidity of relation in fractionated gelatins. *BIOCHEMICAL JOURNAL*, 73, 596-600.
- Djagny, K. B., Wang, Z., and Xu, S.; (2001) Gelatin: A valuable protein for food and pharmaceutical industries: Review. *CRITICAL REVIEWS IN FOOD SCIENCE AND NUTRITION*, 41[6], 481-492.
- Dos Ramos, J. G. and Silebi, C. A.; (1993) Submicron particle size and polymerization excess surfactant analysis by capillary hydrodynamic fractionation (CHDF). *POLYMER INTERNATIONAL*, 30, 445-450.
- Esposito, E., Pastesini, C., Cortesi, R., Gambari, R., Menegatti, E., and Nastruzzi, C.; (1995) Controlled release of 1-b-D-arabinofuranosylcytosine (ara-C) from hydrophilic gelatin microspheres: in vitro studies. *INTERNATIONAL JOURNAL OF PHARMACEUTICS*, 117, 151-158.

Farrugia, C. A. and Groves, M. J.; (1999) Gelatin behaviour in dilute aqueous solution: designing a nanoparticulate formulation. *JOURNAL OF PHARMACY AND PHARMACOLOGY*, 51[6], 643-649.

Farrugia, C. A.; (1998) The formulation of gelatin nanoparticles and their effect on melanoma growth in vivo, Dissertation, Chicago

Finsy, R., De Jaeger, N., Sneyers, R., and Gelade, E.; (1992) Particle sizing by photon correlation spectroscopy. Part III. Mono and bimodal distributions and data analysis. *PARTICLE & PARTICLE SYSTEMS CHARACTERIZATION*, 9[2], 125-137.

Flory, P. J. and Weaver, E. S.; (1960) Helix \leftrightarrow coil transitions in dilute aqueous collagen solutions. *JOURNAL OF THE AMERICAN CHEMICAL SOCIETY*, 82, 4518-4525.

Fraunhofer, W., Winter, G., and Coester, C.; (2004) Asymmetrical Flow Field-Flow Fractionation and Multiangle Light Scattering for Analysis of Gelatin Nanoparticle Drug Carrier Systems. *ANALYTICAL CHEMISTRY*, 76, 1909-1920.

Friess, W.; (1998) Collagen. Biomaterial for drug delivery. *EUROPEAN JOURNAL OF PHARMACEUTICS AND BIOPHARMACEUTICS*, 45[2], 113-136.

Hodgson, R. J. W.; (2000) Genetic Algorithm Approach to Particle Identification by Light Scattering. *JOURNAL OF COLLOID AND INTERFACE SCIENCE*, 229[2], 399-406.

Janes, K. A., Calvo, P., and Alonso, M. J. (2001) Polysaccharide colloidal particles as delivery systems for macromolecules. *ADVANCED DRUG DELIVERY REVIEWS*, 47[1], 83-97.

Kawai, K., Suzuki, S., Tabata, Y., Ikada, Y., and Nishimura, Y.; (2000) Accelerated tissue regeneration through incorporation of basic fibroblast growth factor-impregnated gelatin microspheres into artificial dermis. *BIOMATERIALS*, 21[5], 489-499.

Kelso, J. M.; (1999) The gelatin story. *THE JOURNAL OF ALLERGY AND CLINICAL IMMUNOLOGY*, 103[2 Pt 1], 200-202.

Kreuter, J.; (1978) Nanoparticles and nanocapsules. New dosage forms in the nanometer size range. *PHARMACEUTICA ACTA HELVETIAE*, 53, 33-39.

Kreuter, J.; (1992) Nanoparticles and Nanocapsules.; in Donbrow M.; Nanoparticles-preparation and applications. Microcapsules and nanoparticles in medicine and pharmacy. CRC-press, Boca Raton, 125-148.

Kuijpers, A. J., Engbers, G. H., Krijgsveld, J., Zaat, S. A., Dankert, J., and Feijen, J.; (2000) Cross-linking and characterisation of gelatin matrices for biomedical applications. *JOURNAL OF BIOMATERIALS SCIENCE. POLYMER EDITION*, 11[3], 225-243.

Lee, C. H., Singla, A., and Lee, Y.; (2001) Biomedical applications of collagen. *INTERNATIONAL JOURNAL OF PHARMACEUTICS*, 221[1-2], 1-22.

Li, J. K., Wang, N., and Wu, X. S.; (1998) Gelatin nanoencapsulation of protein/peptide drugs using an emulsifier-free emulsion method. *JOURNAL OF MICROENCAPSULATION*, 15, 163-172.

- Lin, F. H., Yao, C. H., Sun, J. S., Liu, H. C., and Huang, C. W.; (1998) Biological effects and cytotoxicity of the composite composed by tricalcium phosphate and glutaraldehyde crosslinked gelatin. *BIOMATERIALS*, 19, 905-917.
- Marty, J. J., Oppenheim, R. C., and Speiser, P.; (1978) Nanoparticles - a new colloidal drug delivery system. *PHARMACEUTICA ACTA HELVETIAE*, 53, 17-23.
- Meyer, M. and Morgenstern, B.; (2003) Characterization of Gelatin and Acid Soluble Collagen by Size Exclusion Chromatography Coupled with Multi Angle Light Scattering (SEC-MALS). *BIOMACROMOLECULES*, 4[6], 1727-1732.
- Panyam, J. and Labhasetwar, V.; (2003) Biodegradable nanoparticles for drug and gene delivery to cells and tissue. *ADVANCED DRUG DELIVERY REVIEWS*, 55, 329-347.
- Peyrelasse, J., Lamarque, M., Habas, J. P., and El Bounia, N.; (1996) Rheology of gelatin solutions at the sol-gel transition. *PHYSICAL REVIEW E: STATISTICAL PHYSICS, PLASMAS, FLUIDS, AND RELATED INTERDISCIPLINARY TOPICS*, 53[6-B], 6126-6133.
- Pfeifer, B. A., Burdick, J. A., and Langer, R.; (2004) Formulation and surface modification of poly(ester-anhydride) micro- and nanospheres. *BIOMATERIALS*, 26[2], 117-124.
- Piez, K. A., Lewis, M. S., Martin, G. R., and GROSS, J.; (1961) Subunits of the collagen molecule. *BIOCHIMICA ET BIOPHYSICA ACTA*, 53, 596-598.
- Piez, K. A., Weiss, E., and Lewis, M. S.; (1960) The separation and characterization of the alpha- and beta-components of calf skin collagen. *JOURNAL OF BIOLOGICAL CHEMISTRY*, 235, 1987-1991.
- Potineni, A., Lynn, D. M., Langer, R. & Amiji, M. M.; (2003) Poly(ethylene oxide)-modified poly(b-amino ester) nanoparticles as a pH-sensitive biodegradable system for paclitaxel delivery. *JOURNAL OF CONTROLLED RELEASE*, 86, 223-234.
- Rajaonarivony, M., Vauthier, C., Couarraze, G., Puisieux, F., and Couvreur, P.; (1993) Development of a new drug carrier made from alginate. *JOURNAL OF PHARMACEUTICAL SCIENCES*, 82[9], 912-917.
- Rawle, A.; (1993) PCS in 30 minutes. Application note, Malvern Instruments Ltd., Worcestershire, UK.
- Saito, A., Kumagai, T., Kojima, H., Terai, I., Yamanaka, T., Wataya, Y., Umetsu, M., Umetsu, A., and Yano, S.; (2005) A sero-epidemiological survey of gelatin sensitization in young Japanese children during the 1979-1996 period. *SCANDINAVIAN JOURNAL OF IMMUNOLOGY*, 61[4], 376-379.
- Schwick, H. G. and Heide, K.; (1969) Immunochemistry and immunology of collagen and gelatin. *BIBLIOTHECA HAEMATOLOGICA (BASEL)*, 33, 111-125.
- Speiser, P. and Pharmaceutical Society of Victoria. Injectable compositions. (1974) Australian Patent, 38036/75[1516348].
- Steckert, J. J., Kramer, D. L., and Brand, J. S.; (1992) Preparative chromatography and analysis of molecular weight fractions of gelatin. *JOURNAL OF PHOTOGRAPHIC SCIENCE*, 40, 134-137.

Tabata, Y. and Ikada, Y.; (1989) Synthesis of gelatin microspheres containing interferon. *PHARMACEUTICAL RESEARCH*, 6, 422-427.

Tabata, Y. and Ikada, Y.; (1998) Protein release from gelatin matrixes. *ADVANCED DRUG DELIVERY REVIEWS*, 31[3], 287-301.

Ulubayram, K., Aksu, E., Gurhan, S. I. D., Serbetci, K., and Hasirci, N.; (2002) Cytotoxicity evaluation of gelatin sponges prepared with different cross-linking agents. *JOURNAL OF BIOMATERIALS SCIENCE, POLYMER EDITION*, 13, 1203-1219.

Vauthier, C., Dubernet, C., Fattal, E., Pinto-Alphandary, H., and Couvreur, P.; (2003) Poly(alkylcyanoacrylates) as biodegradable materials for biomedical applications. *ADVANCED DRUG DELIVERY REVIEWS*, 55[4], 519-548.

Veis, A., Anesey, J., and Cohen, J.; (1962) The characterization of the γ -component of gelatin. *ARCHIVES OF BIOCHEMISTRY AND BIOPHYSICS*, 98, 104-110.

Wahlund, K. G., Winegarner, H. S., Caldwell, K. D., and Giddings, J. C.; (1986) Improved flow field-flow fractionation system applied to water-soluble polymers: programming, outlet stream splitting, and flow optimization. *ANALYTICAL CHEMISTRY*, 58[3], 573-578.

Ward, A. C., Courts, A., and Editors.; (1977) Food Science and Technology. The Science and Technology of Gelatin. Academic Press, London/New York, 564.

Weber, C., Coester, C., Kreuter, J. & Langer, K.; (2000) Desolvation process and surface characterization of protein nanoparticles. *INTERNATIONAL JOURNAL OF PHARMACEUTICS*, 194, 91-102.

Wyatt, P. J.; (1998) Submicrometer particle sizing by multiangle light scattering following fractionation. *JOURNAL OF COLLOID AND INTERFACE SCIENCE*, 197, 9-20.

Yamamoto, M., Ikada, Y., and Tabata, Y.; (2001) Controlled release of growth factors based on biodegradation of gelatin hydrogel. *JOURNAL OF BIOMATERIALS SCIENCE. POLYMER EDITION*, 12[1], 77-88.

Yoshioka, T., Hashida, M., Muranishi, S., and Sezaki, H.; (1981) Specific delivery of Mitomycin C to the liver, spleen and lung: nano- an microspherical carriers of gelatin. *INTERNATIONAL JOURNAL OF PHARMACEUTICS*, 81, 131-141.

Young, S., Wong, M., Tabata, Y., and Mikos, A. G.; (2005) Gelatin as a delivery vehicle for the controlled release of bioactive molecules. *JOURNAL OF CONTROLLED RELEASE*, 109[1-3], 256-274.

Zeiger, E., Gollapudi, B., and Spencer, P.; (2005) Genetic toxicity and carcinogenicity studies of glutaraldehyde-a review. *MUTATION RESEARCH*, 589[2], 136-151.

Zillies, J.; Dissertation, Munich, to be published 2007.

Chapter II

Cationic gelatin nanoparticles as non-viral gene delivery system

1. INTRODUCTION

It is the aim of gene therapy to heal genetic and acquired diseases on a biomolecular level following the concept that hereditary diseases can be cured by substitution with plasmids encoding for the correct genes. Gene therapeutic strategies for acquired diseases, such as cancer or AIDS, are either to activate the body's own immune defense, or to introduce suppression genes.

One way to introduce genes to their target tissues is to transfect cells with genes *ex vivo* and to (re-)implant them into the patients afterwards. The second is to administer the plasmids *in vivo* to the patients. Thereby, the easiest way is the direct injection of naked DNA into the target tissue or organ. But this approach is limited to only a few applications as for example injection into solid tumors (Vile & Hart 1993) or muscle tissue (Wolff *et al.* 1990). For most applications direct injection is not efficient enough due to enzymatic degradation and electrostatic repulsion between both negatively charged cell membrane and DNA, consequently inhibiting efficient cellular uptake.

Thus, a carrier system, either viral or non-viral, is necessary. Statistics covering all clinical trials worldwide that are currently dealing with gene delivery reveal that viral vectors are still the clear number one, being used in more than 70% of all protocols (www.wiley.co.uk/genmed/clinical/). This can be attributed to the fact that viral vectors deliver genes with the highest efficiency, as it is the intrinsic feature of viruses to shuttle their genome into cells. The most commonly used viral vectors are adenoviruses, retroviruses, adeno-associated viruses, and herpes viruses (Boulaiz *et al.* 2005; Ciftci & Gupte 2006). Lastly, lentiviruses are presently discussed as promising new vectors (Romano 2005). Nevertheless, having the advantage of the highest efficiency in delivery, viral vectors comprise also major drawbacks with respect to safety hazards.

A first tragic incident concerning viral gene delivery was on September 17, 1999 as 18-year-old Jesse Gelsinger, who participated as a volunteer in a gene therapeutic trial, died from an immune reaction against the adenoviral vector (Ferber 2001).

Recently, it has been reported from clinical trials of γ c-mediated gene therapy for X-linked severe combined immunodeficiency (X-SCID) that 3 out of 17 patients have developed T cell leukaemia as a consequence of the retroviral treatment (Anson 2004; Couzin & Kaiser 2005). Aside from these safety issues, difficulties in the scale-up process and high production costs of viral vectors are further restrictive factors.

These substantial reasons made the development of non-viral alternatives highly desirable. Alternative delivery methods are either physical methods to transfer genetic material directly into the target cell or even the nucleus, or chemical methods using non-viral vectors. Electroporation, gene gun, particle bombardment, ultrasound, jet injection and micro injection represent the most common physical gene delivery methods. (Boulaiz *et al.* 2005). Chemical nonviral vectors are either complexes of nucleic acids with cationic polymers, i.e. polyplexes (De Smedt *et al.* ; Felgner *et al.* 1997), or based on cationic lipids, i.e. lipoplexes (Felgner *et al.* 1997; Felgner 1997). Furthermore, plasmid DNA (pDNA) can be loaded on the surface of previously formed cationic nanoparticles due to electrostatic interactions. But although a variety of efforts have been made in the past, the ideal system has not been found yet.

However, efficient gene delivery represents also a very complex issue. Before the final gene expression, a non-viral vector has to shuttle the pDNA across various barriers until it reaches its final destination. Consequently, an ideal delivery system has to fulfil various requirements:

- a) Complexation of pDNA into colloidal dimensions
- b) Protection against extracellular inactivation
- c) Selective and effective internalization into the target cell
- d) Quick release from the endo/lysosomal compartment
- e) pDNA transfer to the nucleus and activation of the transcription
- f) Degradation of the vector without toxic by-products

The escape from the endosome is a crucial bottleneck for most existing non-viral gene delivery systems. Thus, e.g. poly(L-lysine) (PLL) polyplexes, need the additional administration of endosomolytic agents, such as chloroquine, to generate efficient transfection results (Wagner *et al.* 1992) The polycationic polymer polyethylenimine (PEI) which was originally introduced as polyplex agent by the

research group of Jean-Paul Behr (Boussif *et al.* 1995) represents the most significant polycation for polyplex compositions at the moment. Due to the presence of unprotonated nitrogens at neutral pH, PEI features a so called ‘proton sponge’ character (Kichler *et al.* 1999). It is assumed that the low pH within the endosome forces PEI to cause an osmotic imbalance facilitating the endosomal release. Regarding to this, especially linear PEI with an average molecular weight of 22 kDa represents currently the ‘gold standard’ amongst the present non-viral gene delivery systems. However, a severe handicap of PEI is its high *in vitro* and *in vivo* toxicity (Chollet *et al.* 2002; Boeckle *et al.* 2004) and non-biodegradability. Nevertheless, a very promising new approach that utilizes degradable and less toxic polymers consisting of reversibly crosslinked low molecular oligoethylenimines with e.g. 1,6-hexanediol-diacrylate was just recently described (Kloeckner 2006).

The idea of the present study was to introduce a cationic net charge onto the surface of gelatin nanoparticles. This should enable the loading of nucleotides onto the particle’s surface due to electrostatic interactions. Comparable approaches for nanoparticles based on other matrix materials, such as solid-lipid nanoparticles (Olbrich *et al.* 2001), silica nanoparticles (Kneuer *et al.* 2000a), polylactide (PLA) nanoparticles (Munier *et al.* 2005), poly(D,L-lactide-co-glycolide) (PLGA) nanoparticles (Kumar *et al.* 2004), HSA nanoparticles (Wartlick 2004), chitosan nanoparticles, and chitosan-modified poly(ϵ -caprolactone) (PCL) nanoparticles (Haas *et al.* 2005) can be found in literature.

Our research group focuses on gelatin as potential matrix material for colloidal carrier systems. Positive results of other groups that have already shown the potential of gelatin (Truong-Le *et al.* ; Leong *et al.* 1998; Truong-Le *et al.* 1999) and cationized gelatin (Hosseinkhani *et al.* 2002; Fukunaka *et al.* 2002; Kushibiki *et al.* 2003) as complexing agent or hydrogel matrix for gene delivery encouraged our plans. The first aim of this study was to evaluate a variety of surface-modified gelatin nanoparticles as nucleic acid carriers in for their zeta potential (ζ potential) increase and loading efficiency. After finding ideal conditions, the next step was to test the most appropriate formulations *in vitro*.

Besides the optimization of experimental conditions, a second focus of the study was to monitor the cell toxic effects of the system, to prove the thesis that gelatin nanoparticles are physiologically very well tolerated. To enable an assessment of the achieved transfection results we compared the cationized gelatin nanoparticles with

the 'gold standard' PEI polyplexes. Cell toxicological experiments were performed in comparison to pDNA-loaded cationic liposomes and PEI polyplexes.

2. MATERIALS AND METHODS

2.1 Reagents

Reagent	Description	Supplier
Acetone	p.a.	VWR International GmbH (Ismaning, Germany)
cholaminechloride hydrochloride	(2-aminoethyl)-trimethyl-ammoniumchloride hydrochloride	Sigma-Aldrich GmbH (Taufkirchen, Germany)
DOPC	1,2-dioleoyl-sn-glycero-3-phosphocholine	Avanti Polar –Lipids Inc. (Alabaster, AL, USA)
DOTAP	1,2-dioleoyl-3-trimethylammonium-propane chloride	Avanti Polar –Lipids Inc. (Alabaster, AL, USA)
EDC	1-ethyl-3-(3-dimethyl-aminopropyl) carbodiimide hydrochloride	Sigma-Aldrich GmbH (Taufkirchen, Germany)
Gelatin type A	175 Bloom	Sigma-Aldrich GmbH (Taufkirchen, Germany)
Glutaraldehyde	25%	Sigma-Aldrich GmbH (Taufkirchen, Germany)
Spermine	98.5%, crystalline	Sigma-Aldrich GmbH (Taufkirchen, Germany)
TEPA	Tetraethylenpentamine, 98.5%	Merck-Schuchardt OHG (Hohenbrunn, Germany).
TETA	Triethylentetramine; 97-99%	Merck-Schuchardt OHG (Hohenbrunn, Germany).
Exgen 500	Linear poly(ethylenimine) with average 22 kDa (PEI 22)	Euromedex (Souffelweyerheim, France)

The pDNA used in our studies was pCMVLuc (Photinus pyralis luciferase under the control of the CMV enhancer/promoter) as previously described (Plank *et al.* 1992). The single-stranded DNA oligonucleotide (ODN) applied for loading studies had a random sequence (TCG-CTC-GAT-AGC-TCG-ATC) and was kindly donated by MWG Biotech (Ebersberg, Germany).

2.2 Preparation of cationized gelatin nanoparticles

Plain gelatin nanoparticles were produced in reference to previously established optimized conditions (see Chapter I). In order to bind DNA by electrostatic interactions onto the particle's surface, various amines such as the quaternary amine

cholamine (Mw 175.10 Da), or the polyamines spermine (Mw 202.35 Da), TEPA (Mw 189.30 Da), and TETA (Mw 146.24 Da) were covalently coupled onto the surface and later evaluated for their nucleotide binding properties. The chemical structures of the particular molecules are depicted in Fig. 1.

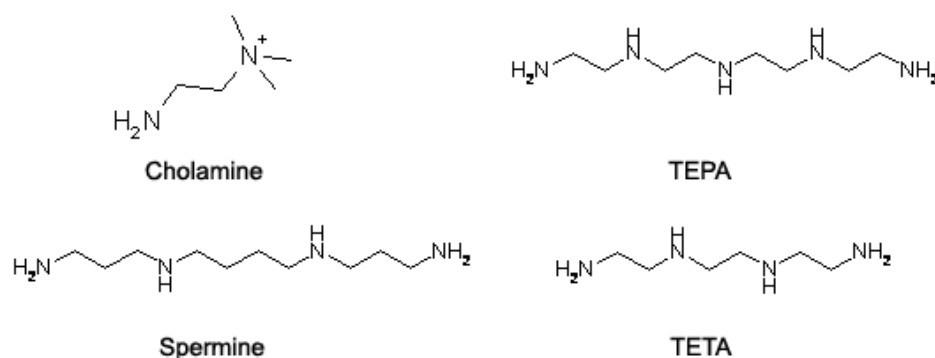


Fig. 1: Chemical structures of the applied cationization agents

The used cationization procedure was a further modified and optimized version of a procedure previously described for cholamine (Coester 2003). In this new, optimized version, an aqueous dispersion of native nanoparticles has to be adjusted to pH 4.5 and a molar excess of the cationization agent (e.g. 50 mg per 500 mg nanoparticles) was added under constant stirring. After 5 minutes of incubation, a molar excess of EDC (50 mg) was added to activate free carboxyl groups on the particles to react with cholamine. During the cationization reaction the primary amino groups of the particular agents can react with two possible functional groups on the nanoparticle's surface, as exemplified for cholamine in Fig. 2. The first interaction sites are residual aldehyde groups derived from only mono-functionally bound crosslinking reagent glutaraldehyde. Furthermore, the primary amino groups can react with activated carboxyl groups on the nanoparticles surface. The reaction is stopped after 1 h and the nanoparticles were purified by 3-fold centrifugation and redispersion, analogous to the purification of plain nanoparticles (see Chapter I. – 2.2)

The final particles were characterized by size determination via dynamic light scattering and measurement of the ζ potential. The determinations of both parameters were conducted with a Zetamaster (Malvern Instruments, Worcestershire, UK). Each assigned size and corresponding polydispersity index

was the mean of 10 subruns. The ζ potential was determined by the same instrument and calculated as the mean of 10 individual measurements.

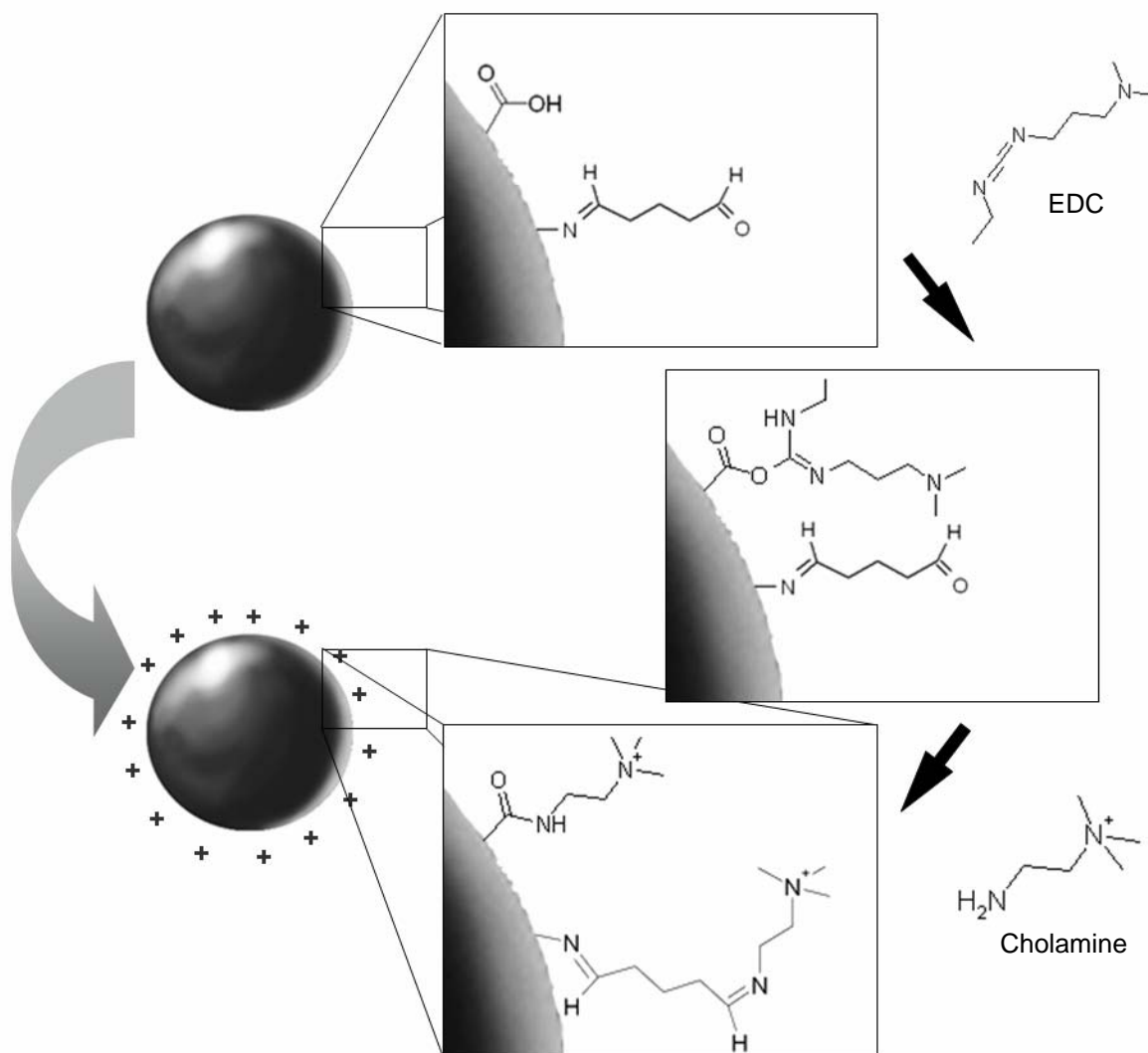


Fig. 2: Schematic illustration of the surface cationization of gelatin nanoparticles with cholamine; step 1: activation of the carboxyl groups with EDC; step 2: covalent bonding of cholamine with residual aldehyde groups and activated carboxyl groups

2.3 Cell culture

Cell culture media, fetal calf serum (FCS) and antibiotics were purchased from Invitrogen GmbH (Karlsruhe, Germany).

B16F10 cells were grown in Dulbecco's Modified Eagle's Medium (DMEM) (1.0 g glucose/L) supplemented with 10% FCS at 37°C in 5% CO₂ humidified atmosphere.

2.4 Plasmid DNA (pDNA) and oligonucleotide (ODN) loading of gelatin nanoparticles

Various batches of cationized nanoparticles were loaded with different amounts of pDNA or ODN (0.33 – 10% [w/w]) in varying conjugation media to find optimized conditions. The used conjugation media were highly purified water, phosphate buffered saline (PBS) 7.4, PBS 7.0/water (1:1 ratio), HEPES-buffered glucose (HBG, 5 % [w/w] glucose, 20 mM HEPES, pH 7.1), or HEPES-buffered saline (HBS, 20mM HEPES, 150mM NaCl, pH 7.1).

2.4.1 Experiments to determine the maximum pDNA or ODN payload on surface-modified nanoparticles

Various amounts of ODN or pDNA were co-incubated over 2-20 min. with nanoparticles at ambient temperature in one of the selected conjugation media. After this incubation period, the amount of unbound oligonucleotide was determined UV spectrophotometrically (260nm, UV1, Thermo Spectronic, Dreieich, Germany) in the supernatant of the reaction media after the separation of the nanoparticles by centrifugation at 14000g (neo lab 16/18, Hermle Labortechnik, Wehingen, Germany).

2.4.2 pDNA loading of cholamine-modified nanoparticles for subsequent *in vitro* application

In order to bind the pDNA onto the nanoparticles, a dispersion of nanoparticles was pipetted to a solution of pDNA (c=4 µg/mL) in buffer and mixed vigorously. After an incubation period of 2 min, 50 µL nanoparticle dispersion containing 200 ng pDNA (luciferase pDNA) loaded in various pDNA to nanoparticle ratios was directly added to each well.

2.5 Preparation and pDNA loading of cationic liposomes

The applied cationic liposome batch (FG56) was kindly prepared by Dr. Friedrich Gruber. For detailed preparation conditions see his PhD thesis (Gruber 2004). Shortly summarized, they were prepared by a film method followed by extrusion through a 200 nm sterile filter at ambient temperature. The total lipid concentration was 5mM in 5% glucose solution. Thereby, DOTAP and DOPC were utilized in a

molar ratio of 1:1. The overall batch volume was 10 mL. Right after the extrusion, the samples were aliquoted in glass vials at 500 μ L/vial and lyophilized. The reconstituted liposomes had a mean diameter of 188.7 nm and a PI of 0.122. The ζ potential of the liposomes reconstituted in water was +45.6 mV.

pDNA was identically loaded onto the liposomes as described for cationic gelatin nanoparticles (see 2.4).

2.6 Preparation of PEI polyplexes

For complex preparation, PEI was used at a 1 mg/mL working solution, neutralized to pH 7.0 with HCl.

DNA complexes were prepared by first diluting PEI 22 in HBS pH 7.1. This PEI-conjugate buffer solution was pipetted to pDNA diluted in HBS and mixed vigorously. Complexes were formed at a molar ratio of PEI nitrogen atoms to DNA phosphate (N/P) of 6. Complexes were allowed to stand for at least 20 min at room temperature before use. The final concentration of DNA (luciferase pDNA) in complexes was 20 μ g/mL. Complexes containing 200 ng pCMVLuc were added directly to each well.

2.7 Transfection

5.0×10^3 cells per well were seeded out into 96-well plates (TPP, Trasadingen, Switzerland). After 16 h of incubation with the different formulations, the transfection medium was removed and replaced by fresh medium containing 10% FCS. After 24 h medium was again replaced. During transfection and for the following 24h 100 U/mL penicillin and 100 μ g/mL streptomycin were present in the media.

2.8 Luciferase assay

For luciferase detection, cells were washed once with PBS, lysed in 50 μ L of Promega cell lysis solution (Promega, Mannheim, Germany), and assayed as previously described (Carlisle *et al.* 2001). Luciferase activity was determined from 20 μ L samples of the lysate using the Luciferase Assay system (Promega);

measurements were performed in a luminometer (Lumat LB9507, Berthold, Bad Wildbad, Germany).

Values are given as light units and represent the total luciferase activity per 5.0×10^3 cells as mean \pm s.d. of at least triplicates. 2 ng of recombinant luciferase (Promega) corresponded to 10^7 light units.

2.9 Cell viability

In comparison to PEI polyplexes, cell viability studies with loaded and unloaded nanoparticles were performed using a CellTiter-Glo™ Luminescent Cell Viability Assay (Promega, Mannheim, Germany) according to the manufacturer's instructions. This assay is based on quantification of the ATP content of viable cells.

2.10 Hemolysis assay

Human erythrocytes were isolated from fresh citrate-treated blood and washed in PBS by 3 centrifugation cycles, each at 1000 g for 20 min at 4°C. The final cell suspension was adjusted to a concentration of 5% erythrocytes as stock suspension. Erythrocyte stocks were used within 24 h and the particular concentrations were determined using a specific Fuchs-Rosenthal counting chamber. Erythrocyte stocks were stored before usage at 4°C. 50 μ l of the erythrocyte stock suspension were added to 950 μ l of pDNA-loaded nanoparticle dispersions or unloaded nanoparticles. The particle dispersions had a concentration of 500 μ g/mL nanoparticles loaded with 5 μ g of pCMV-LUC. DOTAP/DOPC liposomes (1:1 ratio) were loaded in the same ratio and tested in comparison.

Each sample was co-incubated with the erythrocytes at 700 rpm on a Thermomixer comfort (Eppendorf AG, Hamburg, Germany) for 30 min (37°C). Afterwards, the samples were centrifuged at 1000 g to separate the erythrocytes. The supernatant was then centrifuged at 16000 g for another 20 min to separate the nanoparticles or liposomes. This final supernatant was then quantified UV-metrically at $\lambda=576$ nm to determine the haemoglobin release.

For the calibration of the assay, PBS solution containing 1% Triton X-100 was added to achieve complete hemolysis. To obtain a calibration curve, dilutions of this 100% value were measured.

3. RESULTS AND DISCUSSION

3.1 Characterization of the surface-modified nanoparticles

Starting with one homogeneous plain gelatin nanoparticle batch, particular modifications were performed and the final modified nanoparticles were then monitored for changes regarding their mean particle size and homogeneity (Table 1).

Table 1: Nanoparticle sizes measured with DLS

	mean particle size (nm)	PI
Gelatin	205.4	0.043
Cholamine	212.7	0.075
TETA	245.7	0.144
TEPA	237.5	0.131
Spermine	270.8	0.215

Overall, gelatin nanoparticles remain more or less homogeneous and stable after modification. Increases in the particle mean size and PI can be attributed to the fact that after the activation of the carboxyl groups with EDC, the reactive intermediate can also interact with primary amino groups on the surface of other particles. Thus, inter-particulate covalent linking occurs. Whereas, PI values are rather abstract numbers, the worsening particle quality of higher PI values could be very well visualized by overlay-plots of the respective size distributions by volume (Fig. 3). Spermine-modified gelatin nanoparticles which resulted with the highest PI value had also the most inhomogeneous size distribution graph with initial signs of a dimeric or multimeric peak.

The statistical chance for particle-particle interactions is rather low, since the cationization agent is added in molar excess and is more flexible to interact with activated carboxyl groups on the nanoparticles surface than sterically hindered nanoparticles. However, the polyamines (TETA, TEPA, and spermine) apparently tend more towards inter-particulate crosslinking as they contain reactive primary

amino groups at both ends of the molecule. Consequently, this might cause the increased mean sizes and PIs. Cholamine-modified particles remained almost unchanged in mean size and homogeneous according to the low PI.

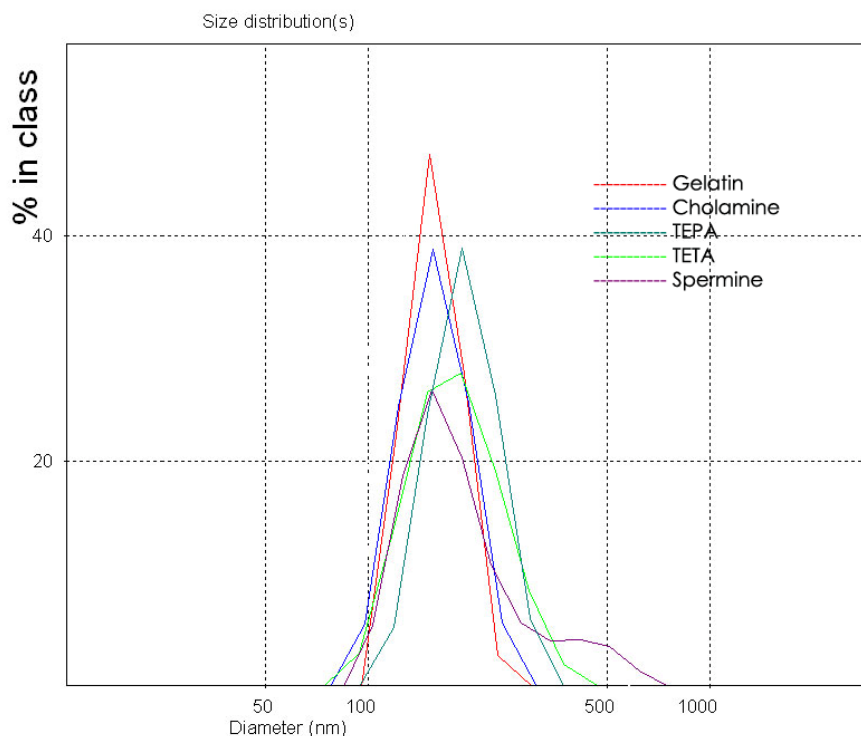


Fig. 3: DLS size-distribution by volume of plain gelatin nanoparticles and the 4 differently surface-modified batches

An elegant method to track a successful cationization of nanoparticles is to compare their particular ζ potentials. The two main factors having significant impact on the detectable potential are the prevailing pH and conductivity of the nanoparticle dispersion (Rawle 2004). The presence of ions attenuates the detectable net charge signal, so increasing ionic strength reduces the extent of the detectable potential values. In a first experiment, we measured the various prepared nanoparticles directly as dispersion in highly purified water (conductivity: 0.02-0.04 mS/cm) without further pH adjustment (Table 2). The detected pH of the aqueous particle dispersions was always between 4.0 and 5.0.

Table 2: ζ potentials (mV) of plain gelatin nanoparticles and the various surface-modified gelatin nanoparticles in highly purified water (aq. disp.) and 10 mM NaCl adjusted to pH 7.0 (10 mM NaCl pH 7.0); the particular conductivities are put in parentheses

	aq. disp.	10 mM NaCl pH 7.0
Gelatin	26.23 \pm 0.48 mV (0.03 mS/cm)	-3.78 \pm 0.08 mV (1.46 mS/cm)
Cholamine	46.93 \pm 0.93 mV (0.03 mS/cm)	11.70 \pm 0.58 mV (1.52 mS/cm)
TETA	49.77 \pm 0.83 mV (0.02 mS/cm)	-3,51 \pm 0.04 mV (1.50 mS/cm)
TEPA	39.31 \pm 0.38 mV (0.03 mS/cm)	-3.47 \pm 0.07 mV (1.61 mS/cm)
Spermine	35.92 \pm 1.12 mV (0.04 mS/cm)	-3,14 \pm 0.05 mV (1.59 mS/cm)

ζ potential calculation performed at these conditions resulted for all nanoparticle types, even unmodified gelatin nanoparticles in positive values. Furthermore, it could be noticed that all surface modifications led to an increase of the particles' net charge in comparison to plain gelatin nanoparticles. However, these acidic conditions might be applied for nucleotide loading but do not represent the later physiological conditions the delivery system will encounter *in vivo*. Thus, we chose neutral pH 7.0 as second measurement point. In order to enable the adjustment of the pH with HCl/NaOH without causing too many alterations concerning the ionic background, we chose 10 mM NaCl as standard background (conductivity: 1.46-1.61 mS/cm). As depicted in Table 2, only the cholamine-modified particles had a positive ζ potential of + 11.70 mV at pH 7.0. The amino groups of the polyamines are obviously not protonated at neutral conditions, whereas the quaternary amino group of cholamine induces a pH-independent positive net charge.

To prove this thesis, we determined the ζ potentials of cholamine-modified gelatin nanoparticles compared to unmodified gelatin nanoparticles with an ionic background of 1mM NaCl (Fig. 4).

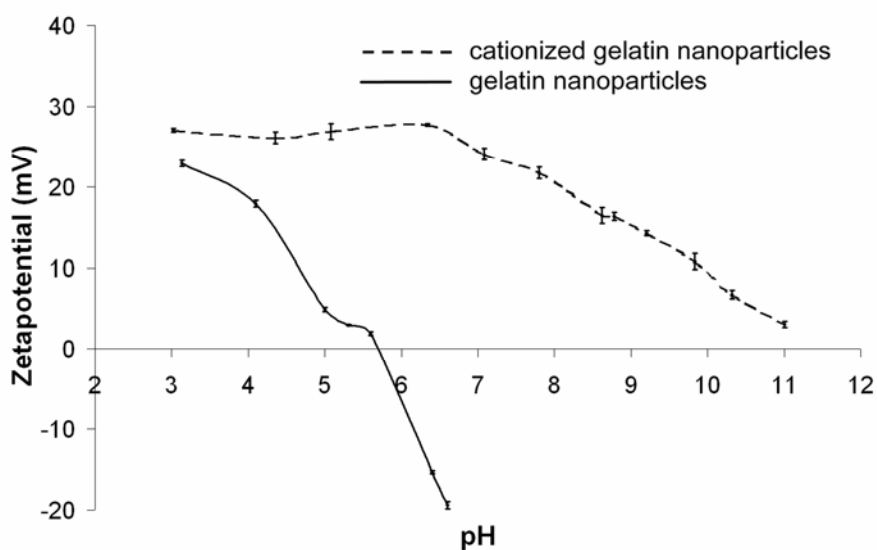


Fig. 4: ζ potential measured in correlation to the pH value (ionic background: 1 mM NaCl; conductivity: 0.16-0.19 mS/cm)

Whereas plain gelatin nanoparticles resulted in an IEP of ~ 5.7 , the nanoparticles modified with cholamine remained positively charged within the whole measured pH range. Consequently, the pH of the physiological environment should not have an effect on the DNA loading.

3.2 Nucleotide loading efficiency of surface-modified nanoparticles

The introduction of further nitrogen groups to the nanoparticle surface does not automatically mean, that this enables efficient loading of nucleotides at any conditions. The results of our nucleotide loading experiment using comparatively big double-stranded pDNA consisting of a few thousand base-pairs and small single-stranded 18-mer ODN were quite different.

The small ODN could be completely loaded onto all surface-modified nanoparticle batches up to a concentration of 100 μg ODN per mg nanoparticles (10% [w/w]) (Fig. 5). The experiments were performed in PBS pH 7.4 and did not show any tendency towards aggregation during 2 hours. Without any surface modification, gelatin nanoparticles were only able to adsorb 38% of the offered ODN onto their surface.

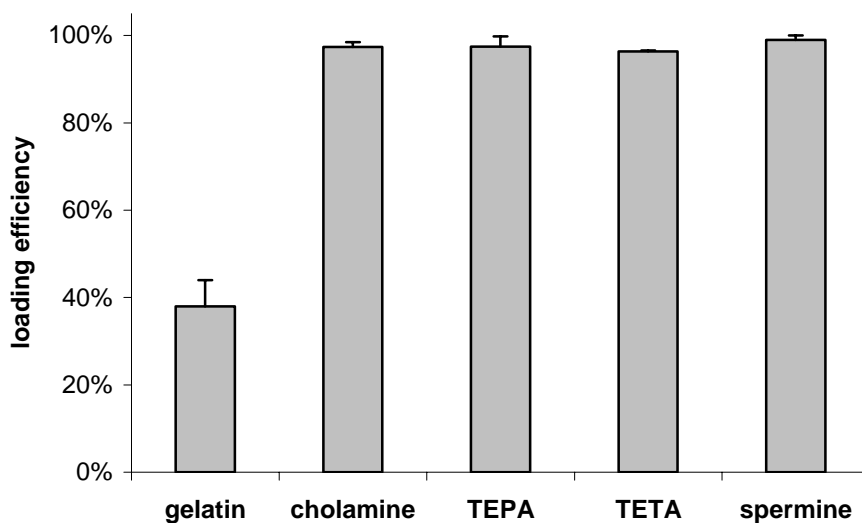


Fig. 5: Random 18-mer ODN loading efficiency in PBS 7.4; applied ODN amount: 10% (w/w); $n=3$

As we performed similar experiments with larger, double-stranded pDNA, several nanoparticle batches modified with polyamines and the non-modified nanoparticle batch failed to adsorb significant amounts of pDNA in PBS 7.4 (Fig. 6). Solely the cholamine particles, which represent the only modification with positive ζ potential at neutral conditions (see 3.2) were able to bind the pDNA quantitatively. The maximum amount of complete pDNA loading that could be achieved with cholamine-modified gelatin nanoparticles was $50 \mu\text{g}/\text{mg}$ (5% [w/w]). But these formulations were very instable and agglomerated, respectively precipitated very quickly. This rapid process could only be stopped by reducing the amount of loaded pDNA to $20 \mu\text{g}/\text{mg}$ (2% [w/w]).

If the pDNA was co-incubated with the various nanoparticle formulations under the acidic and 'ion-free' conditions in highly purified water, now all surface-modified nanoparticle types were able to bind up to $50 \mu\text{g}/\text{mg}$ (5% [w/w]) pDNA completely. Non-modified gelatin nanoparticles were only able to adsorb 26% of the total pDNA amount. Again the same aggregation tendencies were visible as in PBS 7.4. Thus, the presence of disturbing ions is not the reason for the aggregation of the nanoparticles loaded with amounts higher than $20 \mu\text{g}/\text{mg}$ pDNA. In fact, the larger structure of pDNA in comparison to the small ODN seems to be responsible for these instabilities and facilitates the aggregation of the nanoparticle formulations. The present aggregation results correlate very nicely with findings concerning cationic silica nanoparticles (Kneuer *et al.* 2000b) where the authors

demonstrated at comparable loading ratios, that nanoparticles and pDNA tend to form complex structures, that can be described with a spaghetti-meatball model. They visualized via atomic force microscopy, that the DNA is wound around and sandwiched by multiple nanoparticles. Obviously, this aggregation tendency is hindered, when the relative amount of pDNA is reduced. Size determinations of cholamine-modified nanoparticles loaded with 2% (w/w) pDNA by DLS and AF4/MALS demonstrated, that the nanoparticles did not show any aggregation tendency at this loading ratio (Fraunhofer 2003; Fraunhofer *et al.* 2004).

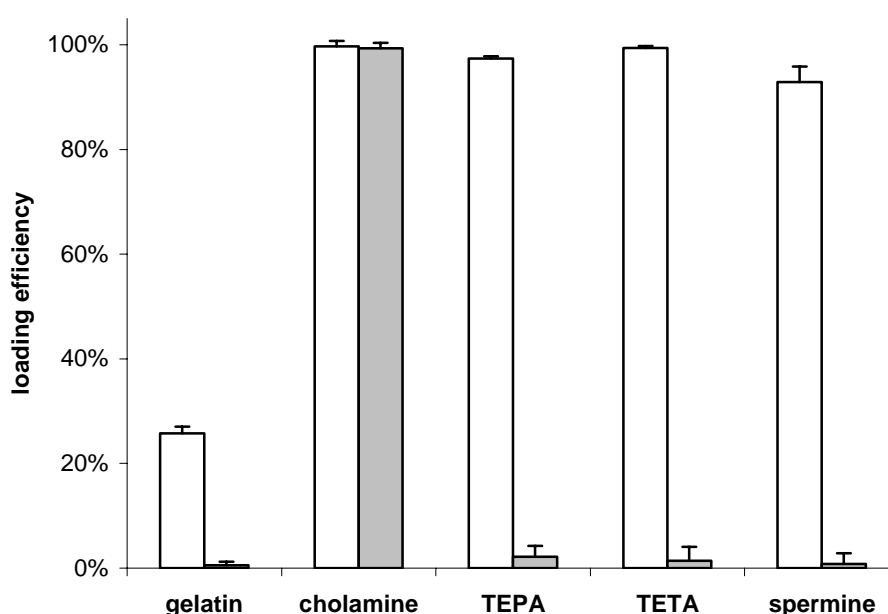


Fig. 6: pDNA loading efficiency in PBS 7.4 (grey) and highly purified water (white); applied pDNA amount: 2% (w/w); n=3

Summarizing the results of the various surface modifications, it can be concluded, that the ζ potential of the nanoparticles has significant impact on the pDNA binding abilities of the gelatin nanoparticles, in contrast to the nucleotide adsorption of short single-stranded ODNs.

Experiments with other types of nucleotide-based drugs gave further indications that loading properties of various nucleotides onto cationic gelatin nanoparticles cannot be generalized. Preliminary experiments with single-stranded mRNA consisting of a few hundred nucleotides and cholamine-modified gelatin nanoparticles exhibited also certain aggregation tendencies comparable to pDNA, but in an alleviated manner. Jan Zillies demonstrated that short 22-mer double-

stranded NF- κ B decoys with phosphorothioated backbone can be loaded onto cholamine-modified gelatin nanoparticles comparable to short single-stranded ODNs. 21-mer double-stranded siRNA with phosphodiester backbone however, revealed only weak binding properties with cholamine-modified particles (Zillies & Coester 2004).

As a consequence, we decided to choose cholamine surface-modified nanoparticles as favored type of cationized gelatin nanoparticles for the following *in vitro* transfection experiments. Furthermore the cationization procedure with cholamine preserved the original homogeneous particle quality and did not induce instabilities. Nevertheless the polyamines are worth to be kept in mind, as they might be beneficial for applications with pH-controlled release, or could be used in combination with cholamine to induce a quicker release of the delivery system from the endosome, according to the ‘proton sponge’ theory.

3.3 Optimized pDNA transfection conditions with cholamine-modified gelatin nanoparticles

In the previous drug loading studies (see 3.2), we found that the maximum amount of pDNA that should be loaded onto cationized nanoparticles without causing rapid instabilities is 20 $\mu\text{g}/\text{mg}$ (2% [w/w]). As we performed the previous experiments only in PBS and highly purified water, we wanted to test also other conjugation media, to investigate if the loading amount can be increased. Therefore we tested HEPES-buffered glucose (HBG, 5 % [w/w] glucose, 20 mM HEPES, pH 7.1), and HEPES-buffered saline (HBS, 20mM HEPES, 150mM NaCl, pH 7.1) as alternatives, as they have shown good potential as conjugation media for polyplexes (Kloeckner 2006). But as for PBS, incubating our formulations within these media led to same results in case of HBS and an even stronger tendency towards aggregation in case of HBG. So, PBS 7.4 and PBS 7.0 diluted with highly purified water (1:1 ratio) were chosen as standard conjugation media.

Conducting first transfection experiments with formulations that were loaded with 20 $\mu\text{g}/\text{mg}$ (2% [w/w]), failed to induce any gene expression. Instead we found that only formulations loaded between 3.3 $\mu\text{g}/\text{mg}$ and 10 $\mu\text{g}/\text{mg}$ (0.33-1% [w/w]) showed significant transfection results. Searching for reasons, we investigated the ζ potentials of formulations containing different DNA to nanoparticle ratios (Fig. 7).

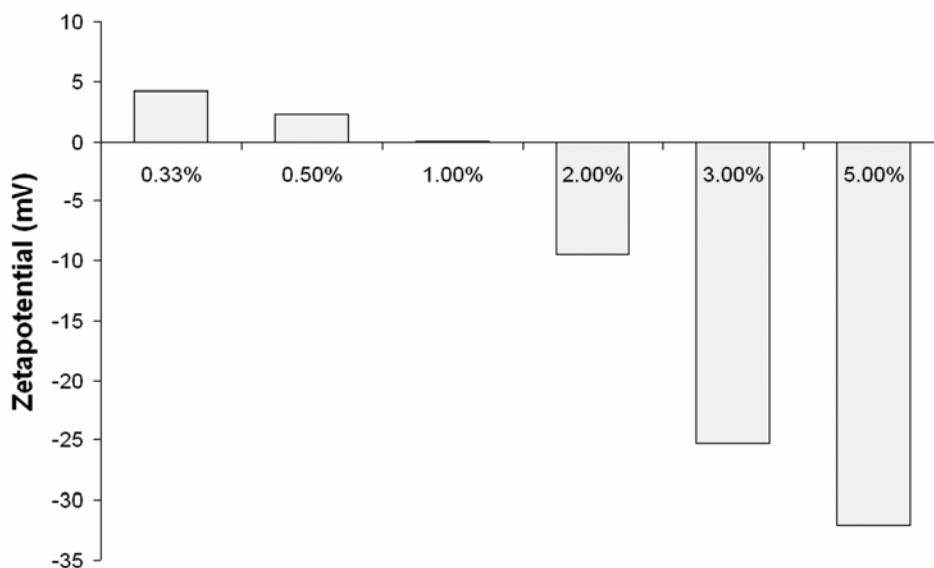


Fig. 7: ζ potential determination of formulations with various ratios of DNA to nanoparticles (w/w).

The measurements were performed in physiological PBS 7.4. Formulations containing 3-5% (w/w) payload tended towards quick agglomeration and resulted in strong negative ζ potentials. Reducing the DNA content to 2% (w/w) prevented aggregations and correlated with a characteristic reduction of the formulations' ζ potential to -9.5 mV. Finally, the formulations that were able to transfect the B16 cells (0.33-1% [w/w]) had all either a neutral or slightly positive ζ potential, which appears to be crucial for successful gene delivery as it facilitates the passage through the negatively charged cell membrane.

The two nanoparticle batches used in this study had a mean size of 288.3 nm (ZWgen288+) and 182.7 nm (ZWgen182+). Dynamic light scattering suggested a uni-modal size distribution for both batches, having low PIs of 0.067 (ZWgen288+) and 0.101 (ZWgen182+).

For nanoparticulate pDNA formulations loaded in PBS 7.4, none of the three different loading concentrations showed any significant gene expression after 24 h. However the PEI polyplexes showed their strongest gene expression (1.46×10^7 RLU [relative light units]) at this point (Fig. 8).

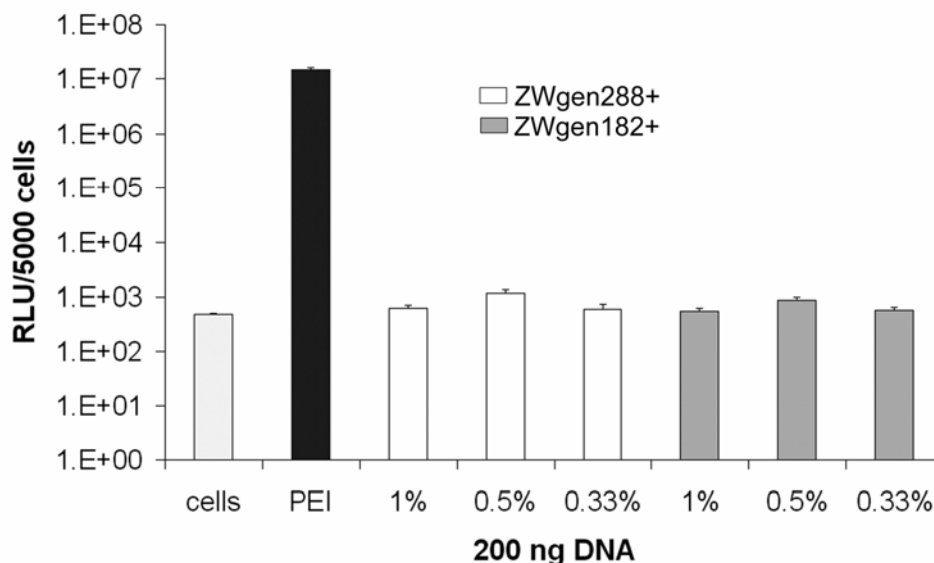


Fig. 8: Transfection efficiency of cationized gelatin nanoparticles after 24 h; conjugation buffer: PBS 7.4; cells: untreated cells; PEI: standard polyplex; 1%, 0.5%, 0.33%: relative amount of pDNA loaded onto gelatin nanoparticles (w/w)

Performing the DNA loading of the particles in PBS 7.0/water (1:1 ratio) instead of PBS 7.4 led to first detectable gene expressions for the formulations loaded with 0.5% pDNA (w/w) after 24 h (Fig. 9).

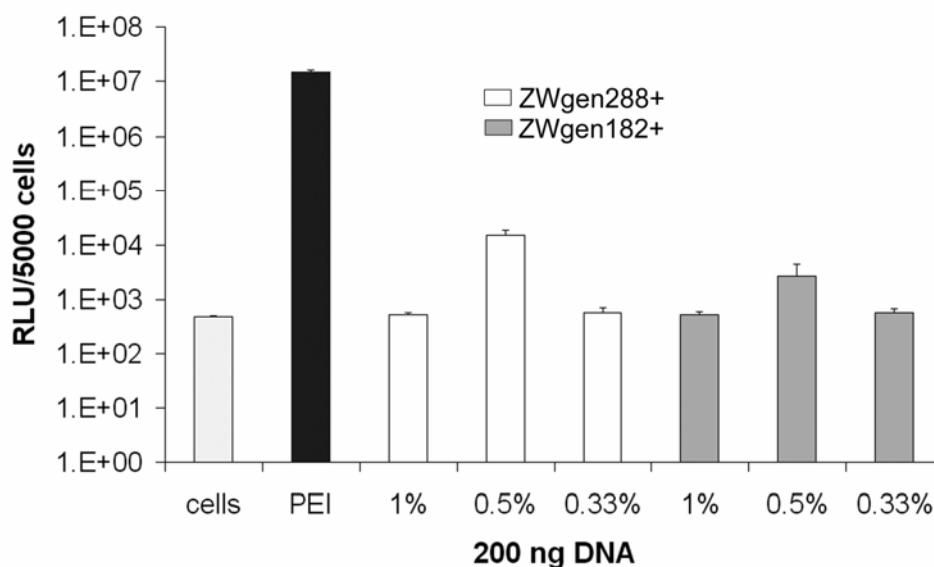


Fig. 9: Transfection efficiency of cationized gelatin nanoparticles after 24 h; conjugation buffer: PBS 7.0/water (1:1 ratio); cells: untreated cells; PEI: standard polyplex; 1%, 0.5%, 0.33%: relative amount of pDNA loaded onto gelatin nanoparticles (w/w)

After 72 h, both the nanoparticles incubated in PBS 7.4 (Fig. 10) and in PBS 7.0/water (1:1 ratio) (Fig. 11) resulted in distinct increases of gene expression.

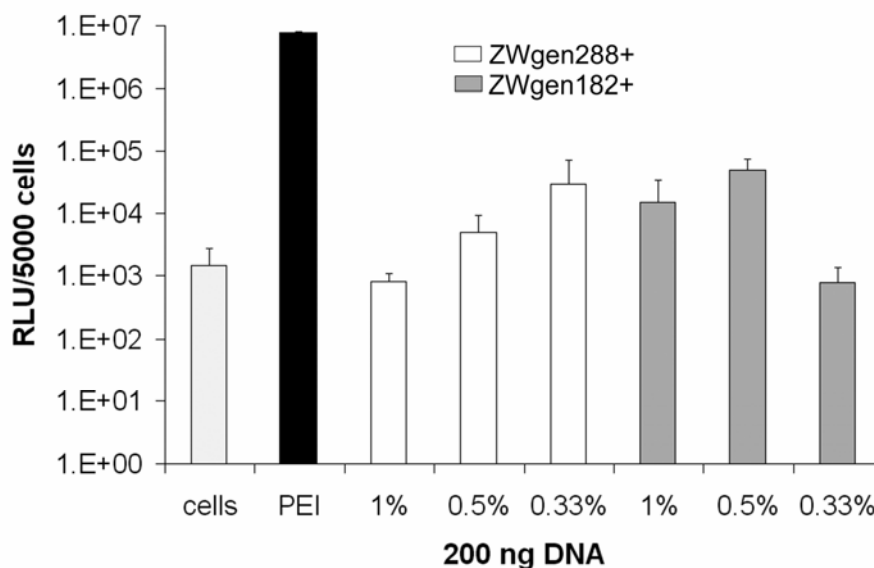


Fig. 10: Transfection efficiency of surface-modified gelatin nanoparticles after 72 h; conjugation buffer: PBS 7.4; cells: untreated cells; PEI: standard polyplex; 1%, 0.5%, 0.33%: relative amount of pDNA loaded onto gelatin nanoparticles (w/w) and in PBS 7.0/water (1:1 ratio) (Figure 6) resulted in distinct increases of gene expression.

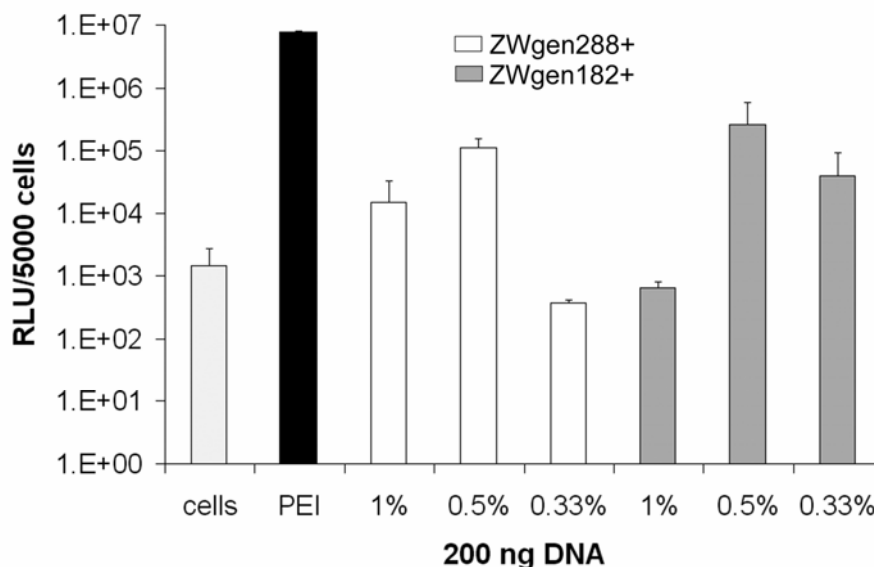


Fig. 11: Transfection efficiency of surface-modified gelatin nanoparticles after 72 h; conjugation buffer: PBS 7.0/water (1:1 ratio); cells: untreated cells; PEI: standard polyplex; 1%, 0.5%, 0.33%: relative amount of pDNA loaded onto gelatin nanoparticles (w/w)

Formulations prepared in PBS 7.4 showed already noticeable outcomes with 2.98×10^4 RLU for the larger nanoparticles (ZWgen288+) containing 0.33% pDNA loading (w/w) and 4.94×10^4 RLU for ZWgen182+ (0.5% [w/w] pDNA). The best gene expressions could be achieved in PBS 7.0/water (1:1 ratio) with 1.12×10^5 RLU for ZWgen288+ and 2.63×10^5 RLU for ZWgen182 (both 0.5% [w/w] pDNA).

Overall, there is a tendency favoring the use of 182.7 nm large particles as carrier (ZWgen182+) with a relative amount of 0.5% pDNA (w/w) loaded onto the particles. As for the conjugation buffer, further studies have to be performed to find ideal media. Compared to PEI, the peak gene expression occurs with a certain delay and a one order of magnitude lower efficiency. One reason could be a prolonged intracellular processing due to slow endosomal escape or a different cellular uptake mechanism.

3.4 Cytotoxicity of cationized gelatin nanoparticles

Since cytotoxicity of our formulations was the second focus of our experiments, we monitored the viability of the transfected B16 F10 cells simultaneously (Fig. 12).

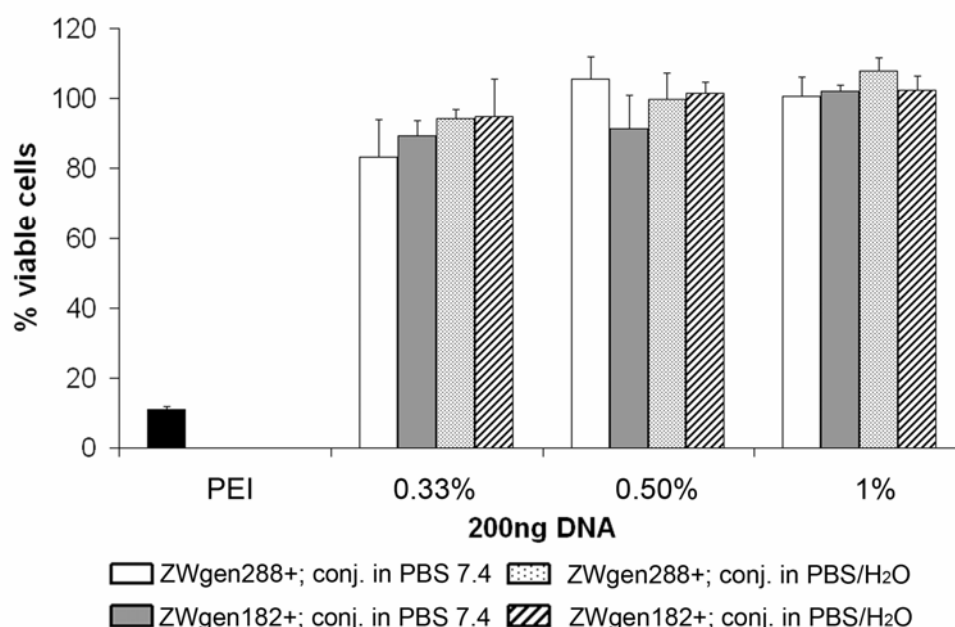


Fig. 12: Cell viability of B16 F10 cells after 72 h of incubation; PEI: standard polyplex; 1%, 0.5%, 0.33%: relative amount of pDNA loaded onto gelatin nanoparticles (w/w)

After a total time of 72 h, only averaging 10.9% of the B16 F10 cells transfected with PEI polyplexes remained viable, whereas the viability of all cells that have been transfected with gelatin nanoparticle formulations was between 83.3 and 100%. For transfection, PEI formulations are typically incubated with cells for 4 h instead of 16 h as in this study. This might explain the low cell viability of cells transfected with PEI polyplexes but also demonstrates the good physiological tolerance of gelatin nanoparticle formulations. A trend was observed, that formulations loaded with less relative pDNA amount are more toxic. The reason for this might be that the higher remaining positive net charge of the formulations induces lower cell viability. Furthermore, a marginal tendency towards formulations conjugated in PBS 7.4 showing less cell viability can be seen but in general, the cell toxicological effects of our formulations are minimal compared to PEI polyplexes.

In addition to this cytotoxicity data we characterized also the hemolytical activity of our formulations on human erythrocytes. Since erythrocytes are one of the first cell species, nanoparticles will face when administered intravenously, this experiment provides valuable information concerning *in vivo* practicability. To rate the achieved results we compared cationized gelatin nanoparticles with plain gelatin nanoparticles and DOTAP/DOPC liposomes (1:1 ratio). These liposomes represent another well recognized effective non-viral gene delivery system (Fig. 13).

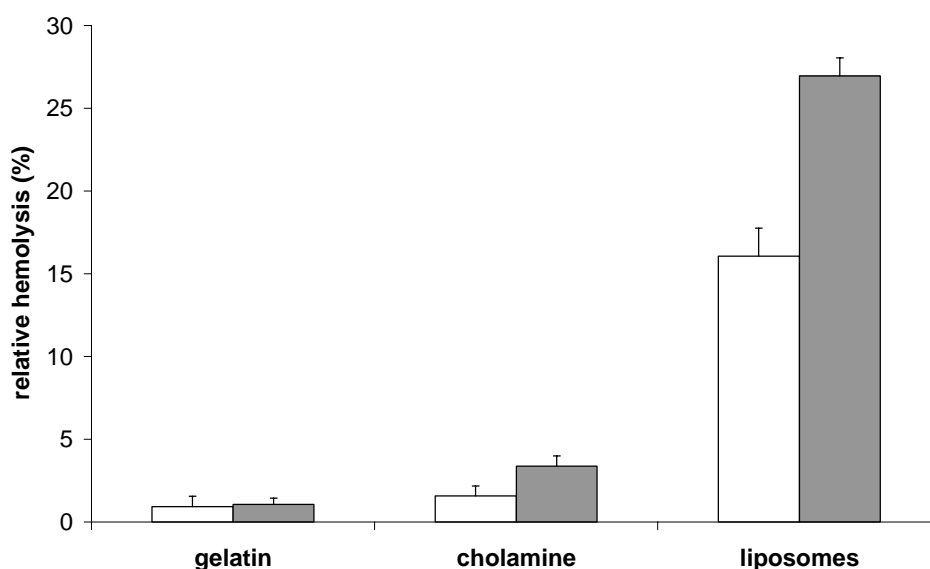


Fig. 13: Relative hemolysis of unloaded (grey) and 20 µg/mg pDNA-loaded (white) cholamine-modified nanoparticles vs. DOTAP/DOPC liposomes

Plain gelatin nanoparticles hardly induced any erythrocyte lysis ($0,94\% \pm 0,62$). The activity of loaded and unloaded plain gelatin nanoparticles was as expected similar, because no pDNA loading was expected, so the pDNA remained in solution. pDNA-loaded cationized nanoparticles also did not induce any significant release of hemoglobin ($1.58\% \pm 0.59$). Even unloaded cationized gelatin nanoparticles were only slightly haemolytic ($2.98\% \pm 0.30$). If these results are compared with DOTAP/DOPC liposomes, unloaded cationized gelatin nanoparticles are still far below the hemolytic activity of the loaded liposomes ($17.60\% \pm 1.02$). Some might argue that this occurred possibly due to a higher remaining ζ potential of the loaded liposomes, since unloaded liposomes had a higher potential in highly purified water ($+45.6$ mV). But this was not the case as pDNA-loaded liposomes had an ζ potential of $+6.9$ mV in PBS 7.4, whereas less toxic unloaded cationized gelatin nanoparticles had a ζ potential of $+11.4$ mV and can be referred as almost ideal physiologically tolerated according to these present *in vitro* results.

4. CONCLUSION

According to the results of this study, it is possible to bind ODNs and pDNA to surface-modified gelatin nanoparticles. In case of ODNs this is pH-independently possible with all modification-types tested in this study.

The pH-independent binding of pDNAs is limited to the cholamine-modification. Amino groups of the polyamine-modifications need to be protonated to adsorb pDNAs. This fact offers the chance for pH-dependent controlled release.

Aside from the tested approaches it is as well possible to combine the binding of cholamine or other quaternary amino groups with the binding of polyamines. The quaternary amino group ensures pH-independent drug loading whereas the polyamines with their amino groups as protonable tools could potentially accelerate the endosomal escape after cellular uptake.

In the second part of this study we were able to demonstrate *in vitro* that cholamine-modified gelatin nanoparticles are a promising new non-viral carrier system for gene therapy. A major benefit is not only the very low cytotoxicity, but also their simple and reproducible production, which would facilitate future upscaling. Low costs of the base material gelatin make this approach commercially attractive. Gene transfer efficiency of our formulations are only approximately one order of magnitude lower than the efficiency of the ‘gold standard’ cationic PEI polyplexes; these *in vitro* transfection rates are significant and quite remarkable considering that we are still at an early stage of formulation optimization. Of course other approaches are already further on their way towards the ideal non-viral delivery system, the so-called ‘artificial virus’ (Wagner 2004), as they are highly sophisticated intelligent systems. Nevertheless, the already achieved results with this simple system are very promising.

One advantage offered by the amino acid side-chains of the gelatin matrix molecule is the option of multiple further modifications. This could be used for coupling of ligands to improve targeting diseased tissues, to enhance specific cellular uptake or affect intracellular distribution.

5. REFERENCES

- Anson, D. S.; (2004) The use of retroviral vectors for gene therapy-what are the risks? A review of retroviral pathogenesis and its relevance to retroviral vector-mediated gene delivery. *GENETIC VACCINES AND THERAPY*, 2[9], 1-13.
- Boeckle, S., von Gersdorff, K., van der Piepen, S., Culmsee, C., Wagner, E., and Ogris, M.; (2004) Purification of polyethylenimine polyplexes highlights the role of free polycations in gene transfer. *JOURNAL OF GENE MEDICINE*, 6[10], 1102-1111.
- Boulaiz, H., Marchal, J. A., Prados, J., Melguizo, C., and Aranega, A.; (2005) Non-viral and viral vectors for gene therapy. *CELLULAR AND MOLECULAR BIOLOGY*, 51[1], 3-22.
- Boussif, O., Lezoualc'h, F., Zanta, M. A., Mergny, M. D., Scherman, D., Demeneix, B., and Behr, J. P.; (1995) A versatile vector for gene and oligonucleotide transfer into cells in culture and in vivo: polyethylenimine. *PROCEEDINGS OF THE NATIONAL ACADEMY OF SCIENCES OF THE UNITED STATES OF AMERICA*, 92[16], 7297-7301.
- Carlisle, R. C., Bettinger, T., Ogris, M., Hale, S., Mautner, V., and Seymour, L. W.; (2001) Adenovirus hexon protein enhances nuclear delivery and increases transgene expression of polyethylenimine/plasmid DNA vectors. *MOLECULAR THERAPY*, 4[5], 473-483. 2001.
- Chollet, P., Favrot, M. C., Hurbin, A., and Coll, J.; (2002) Side-effects of a systemic injection of linear polyethylenimine-DNA complexes. *THE JOURNAL OF GENE MEDICINE*, 4[1], 84-91.
- Ciftci, K. and Gupte, A.; (2006) Gene therapy: an overview of the current viral and nonviral vectors. *PHARMACEUTICAL BIOTECHNOLOGY*, 2, 333-378.
- Coester, C.; (2003) Development of a new carrier system for oligonucleotides and plasmids based on gelatin nanoparticles. *NEW DRUGS*, 1, 14-17.
- Couzin, J. and Kaiser, J.; (2005) Gene therapy: As Gelsinger case ends, gene therapy suffers another blow. *SCIENCE*, 307[5712], 1028.
- De Smedt, S. C., Demeester, J., and Hennink, W. E.; (2000) Cationic polymer based gene delivery systems. *PHARMACEUTICAL RESEARCH*, 17, 113-126.
- Felgner, P. L.; (1997) Nonviral strategies for gene therapy. *SCIENTIFIC AMERICAN* 276[6], 102-106.
- Felgner, P. L., Barenholz, Y., Behr, J. P., Cheng, S. H., Cullis, P., Huang, L., Jessee, J. A., Seymour, L., Szoka, F., Thierry, A. R., Wagner, E., and Wu, G.; (1997) Nomenclature for synthetic gene delivery systems. *HUMAN GENE THERAPY*, 8[5], 511-512.
- Ferber, D.; (2001) Gene therapy: Safer and virus-free? *SCIENCE*, 294, 1638-1642.
- Fraunhofer, W.; (2003) Asymmetrical Flow-Field-Flow-Fractionation in Pharmaceutical Analytics – Investigations in Aggregation Tendencies of Pharmaceutical Antibodies. Dissertation, Munich.
- Fraunhofer, W., Winter, G., and Coester, C.; (2004) Asymmetrical Flow Field-Flow Fractionation and Multiangle Light Scattering for Analysis of Gelatin Nanoparticle Drug Carrier Systems. *ANALYTICAL CHEMISTRY*, 76, 1909-1920.

Fukunaka, Y., Iwanaga, K., Morimoto, K., Kakemi, M., and Tabata, Y.; (2002) Controlled release of plasmid DNA from cationized gelatin hydrogels based on hydrogel degradation. *JOURNAL OF CONTROLLED RELEASE*, 80[1-3], 333-343.

Gruber, F.; (2004) Untersuchungen zur Encapsulierung von Paclitaxel in kationische Liposomen. Dissertation, Munich.

Haas, J., Ravi Kumar, M. N. V., Borchard, G., Bakowsky, U., and Lehr, C.; (2005) Preparation and characterization of chitosan and trimethyl-chitosan-modified poly-(epsilon-caprolactone) nanoparticles as DNA carriers. *AAPS PHARMSCITECH*, 6[1], E22-E30.

Hosseinkhani, H., Aoyama, T., Ogawa, O., and Tabata, Y.; (2002) Ultrasound enhancement of in vitro transfection of plasmid DNA by a cationized gelatin. *JOURNAL OF DRUG TARGETING*, 10[3], 193-204.

Kichler, A., Behr, J. P., and Erbacher, P.; (1999) Polyethylenimines: a family of potent polymers for nucleic acid delivery. in *Non-viral vectors for gene therapy*; Hung, M. C., Huang, L., and Wagner, E., Academic Press, San Diego, 191-206.

Kloeckner, J.; (2006) Novel Biodegradable Gene Carriers Based on Oligomerized Polyamines. Dissertation, Munich.

Kneuer, C., Sameti, M., Haltner, E. G., Schiestel, T., Schirra, H., Schmidt, H., and Lehr, C. M. (2000a) Silica nanoparticles modified with aminosilanes as carriers for plasmid DNA. *INTERNATIONAL JOURNAL OF PHARMACEUTICS*, 196[2], 257-261.

Kneuer, C., Sameti, M., Bakowsky, U., Schiestel, T., Schirra, H., Schmidt, H., and Lehr, C. M.; (2000b) A Nonviral DNA Delivery System Based on Surface Modified Silica-Nanoparticles Can Efficiently Transfect Cells in Vitro. *BIOCONJUGATE CHEMISTRY*, 11, 926-932.

Kumar, M. N. V. R., Mohapatra, S. S., Kong, X., Jena, P. K., Bakowsky, U., and Lehr, C. M., (2004) Cationic poly(lactide-co-glycolide) nanoparticles as efficient in vivo gene transfection agents. *JOURNAL OF NANOSCIENCE AND NANOTECHNOLOGY*, 4[8], 990-994.

Kushibiki, T., Tomoshige, R., Fukunaka, Y., Kakemi, M., and Tabata, Y.; (2003) In vivo release and gene expression of plasmid DNA by hydrogels of gelatin with different cat-ionization extents. *JOURNAL OF CONTROLLED RELEASE*, 90[2], 207-216.

Leong, K. W., Mao, H. Q., Truong-Le, V. L., Roy, K., Walsh, S. M., and August, J. T.; (1998) DNA-polycation nanospheres as non-viral gene delivery vehicles. *JOURNAL OF CONTROLLED RELEASE*, 53[1-3], 183-193.

Munier, S., Messai, I., Delair, T., Verrier, B., and Taman-Oenal, Y.; (2005) Cationic PLA nanoparticles for DNA delivery: Comparison of three surface polycations for DNA binding, protection and transfection properties. *COLLOIDS AND SURFACES, B: BIOINTERFACES*, 43[3-4], 163-173.

Olbrich, C., Bakowsky, U., Lehr, C. M., Muller, R. H., and Kneuer, C.; (2001) Cationic solid-lipid nanoparticles can efficiently bind and transfect plasmid DNA. *JOURNAL OF CONTROLLED RELEASE*, 77[3], 345-355.

Plank, C., Zatloukal, K., Cotten, M., Mechtler, K., and Wagner, E.; Gene transfer into hepatocytes using asialoglycoprotein receptor mediated endocytosis of DNA complexed with an artificial tetra-antennary galactose ligand. *BIOCONJUGATE CHEMISTRY*, 3[6], 533-539.

- Rawle, A.; (2004) Zetapotential in 30 minutes. Application note, Malvern Instruments Ltd., Worcestershire, UK.
- Romano, G.; (2005) Current development of lentiviral-mediated gene transfer. *DRUG NEWS AND PERSPECTIVES*, 18[2], 128-134.
- Truong-Le, V. L., August, J. T., and Leong, K. W.; (1998) Controlled gene delivery by DNA-gelatin nanospheres. *HUMAN GENE THERAPY*, 9, 1709-1717.
- Truong-Le, V. L., Walsh, S. M., Schweibert, E., Mao, H. Q., Guggino, W. B., August, J. T., and Leong, K. W.; (1999) Gene transfer by DNA-gelatin nanospheres. *ARCHIVES OF BIOCHEMISTRY AND BIOPHYSICS*, 361, 47-56.
- Vile, R. G. and Hart, I. R.; (1993) Use of tissue-specific expression of the herpes simplex virus thymidine kinase gene to inhibit growth of established murine melanomas following direct intratumoral injection of DNA. *CANCER RESEARCH*, 53[17], 3860-3864.
- Wagner, E.; (2004) Strategies to Improve DNA Polyplexes for in Vivo Gene Transfer: Will "artificial viruses" be the answer? *PHARMACEUTICAL RESEARCH*, 21, 8-14.
- Wagner, E., Plank, C., Zatloukal, K., Cotten, M., and Birnstiel, M. L.; (1992) Influenza virus hemagglutinin HA-2 N-terminal fusogenic peptides augment gene transfer by transferrin-polylysine-DNA complexes: Toward a synthetic virus-like gene-transfer vehicle. *PROCEEDINGS OF THE NATIONAL ACADEMY OF SCIENCES OF THE UNITED STATES OF AMERICA*, 89[17], 7934-7938.
- Wartlick, H.; (2004) Albumin-Nanopartikel als Trägersysteme für Antisense-Oligonukleotide zur Anwendung in der Brustkrebstherapie. Dissertation, Frankfurt.
- Wolff, J. A., Malone, R. W., Williams, P., Chong, W., Acsadi, G., Jani, A., and Felgner, P. L.; (1990) Direct gene transfer into mouse muscle in vivo. *SCIENCE*, 247, 1465-1468.
- Zillies, J. and Coester, C.; (2004) Evaluating gelatin based nanoparticles as a carrier system for double stranded oligonucleotides. *JOURNAL OF PHARMACY AND PHARMACEUTICAL SCIENCES*, 7[4], 17-21.

Chapter III

In vitro delivery of immunogenic CpG oligonucleotides

1. INTRODUCTION

1.1 The immune system and the role of toll-like receptors

The human immune system represents a collective of cells, tissues, and organs that defends the human body against foreign pathogenic invaders such as viruses, bacteria, parasites, and fungi. It can be divided into innate and adaptive or acquired components. The innate immune system is the first quick line of defense. But neither are pathogens specifically recognized, nor mechanisms of safety against repetitive future infections initiated. Important elements of the innate immune system are the humoral component i.e. the complement system and the cellular components i.e. phagocytotic cells such as macrophages, granulocytes, and natural killer (NK) cells. Even though the innate immune system is very quick, it mostly fails to abolish the pathogen completely due to its lack of specificity. But, it triggers the acquired immune system which consists of antibodies as humoral components and lymphocytes as cellular components. Characteristic for the acquired immune system are its high specificity against pathogens and its memory function. Via clonal selection lymphocytes specific for one pathogenic antigen are produced. Some of these lymphocytes are differentiated to memory cells. The lymphocytes can be subdivided in B cells and T cells. B cells produce antibodies, whereas T cells act either as T helper cells (T_H cells), supporting other immune cells or cytotoxic T lymphocytes (CTL) that are able to induce the death of infected cells. T_H cells are positive for the antigen CD4 (cluster of differentiation antigen 4), whereas CTLs are positive for CD8. Naïve $CD4^+$ T-cells (T_{H0} cells) are activated via antigens that are presented by antigen presenting cells (APCs) such as macrophages and dendritic cells (DCs). According to the co-administered cytokines, the naïve T_{H0} cells are further differentiated to either T_{H1} or T_{H2} cells. T_{H1} cells support cellular immune responses, while T_{H2} cells support the activation of B cells to produce antibodies, thus inducing a humoral immune response. Within the immune system, APCs and especially DCs play a major role because they connect innate and acquired immune response.

Activation of the innate immune system occurs by the exposure to pathogen-associated molecular patterns (PAMPs) that are expressed by diverse infectious microorganisms (Medzhitov & Janeway 1997b). These PAMPs are recognized by specific pattern recognition receptors (PRRs) that are mainly present in APCs. Although PAMPs represent a very heterogeneous group, all PAMPs have in common their specificity for microbial pathogens that cannot be found in the host organism. Furthermore, PAMPs are part of the respective pathogenicity and are indispensable for the pathogen's survival (Medzhitov & Janeway 1997a). The PRRs that exist in vertebrates are lectin receptors (Stahl *et al.* 1998), scavenger receptors (Peiser *et al.* 2002), and toll-like receptors (TLRs).

Presently, there are 10 human TLRs described in literature, although some of their natural ligands have not been identified so far. Most of these ligands are of microbial origin. But, there are also supposed to be endogenous ligands that are released during inflammation reactions due to cellular stress or damage (Matzinger 2002). An overview of the known TLRs and their corresponding ligands is given in Table 1 (Kaisho & Akira 2002).

Table 1: TLRs and ligands

TLR	PAMP	Origin of ligand	Reference
TLR1	cooperates with TLR2		
TLR2	Lipoproteins	Gram-positive bacteria	(Yoshimura <i>et al.</i> 1999; Underhill <i>et al.</i> 1999)
	Zymosan	Yeast	(Underhill <i>et al.</i> 1999)
	Lipoarabinomannan	Mycoplasma	(Means <i>et al.</i> 1999a; Means <i>et al.</i> 1999b)
	MALP-2	Mycobacteria	(Takeuchi <i>et al.</i> 2000; Takeuchi <i>et al.</i> 2001)
TLR3	Double-stranded RNA	Virus	(Alexopoulou <i>et al.</i> 2001)
TLR4	LPS	Gram-negative bacteria	(Qureshi <i>et al.</i> 1999; Hoshino <i>et al.</i> 1999)
	F protein	Respiratory syncytial virus	(Kurt-Jones <i>et al.</i> 2000)
	HSP60	Host	(Ohashi <i>et al.</i> 2000; Vabulas <i>et al.</i> 2001)
	Fibronectin EDA domain	Host	(Okamura <i>et al.</i> 2001)
TLR5	Flagellin	Bacteria with flagella	(Hayashi <i>et al.</i> 2001)

TLR6	Cooperates with TLR2		(Takeuchi <i>et al.</i> 1999)
TLR7	Guanosine analogs, single-stranded RNA		(Hornung <i>et al.</i> 2004)
TLR8	Guanosine analogs		(Jurk <i>et al.</i> 2002)
TLR9	CpG motifs	Bacteria, viruses	(Hemmi <i>et al.</i> 2000)
TLR10	unknown		

TLR1, 2, 4, 5, and 6 are specialized on the recognition of ligands that are unique in bacteria and cannot be produced by the infected host itself. TLR3, 7, 8, and 9 are responsible for the detection of viral pathogens and the recognition of nucleic acids that do not only exist in microbial organisms. In these cases, the differentiation between own and foreign DNA does not only rely on the type of ligand but also on the accessibility of the particular TLRs. Thus, these TLRs are located in subcellular compartments.

1.2 History and mechanism of action of CpG ODNs

As described in Table 1, bacterial or viral DNA is recognized by TLR9 via non-methylated cytosine-phosphate-guanosine dinucleotides in particular sequence contexts (CpG motifs) that are sensed as the key danger signals (Krieg *et al.* 1995). Concerning the immunogenicity of viral or bacterial DNA, first findings were already made more than 100 years ago. Back in 1890, William Coley introduced the deliberate use of bacterial extracts for the treatment of cancer (Wiemann & Starnes 1994). Even though temporary tumor-restitution and a surprising complete remission rate of 10% (Coley 1991) were achieved, this approach was not further established since it lacked reproducibility and was ruled out by other methods such as radiotherapy. It took until the 1970ies before a second approach was conducted using attenuated mycobacteria *Bacillus Calmette Guerin* (BCG) for tumor therapy which was finally established as standard therapy for human bladder cancer (Morales 1978). Other research groups explored later that the anti-tumoral effect of the vaccination with BCG was related to a stimulation of the immune system (Tokunaga *et al.* 1984). More precisely, the bacterial DNA was responsible for the induction of natural killer cell (NK cell) activity and the production of type 1 and type 2 interferons (Yamamoto *et al.* 1992). After further investigations, the researchers concluded that self-complementary palindromes in the nucleotide sequence containing at least one cytosine-phosphate-guanosine (CpG) dinucleotide

(Kuramoto *et al.* 1992) were responsible for this stimulation of the immune system. Another research group independently reported that purified bacterial DNA as well as poly-(dG,dC) nucleotides in contrast to vertebrate DNA, induced the proliferation of murine B cells and immunoglobulin secretion (Messina *et al.* 1991). Furthermore this group explored that the mitogenicity of poly-(dC,dG)-nucleotides was abolished by methylation of cytosine (Pisetsky & Reich, III 1998). So they suggested that methylation interferes the formation of unique higher order structures, which are responsible for the immunogenic effect.

During experiments with antisense ODNs in 1995, Arthur M. Krieg coincidentally observed immune stimulatory effects such as strong B cell proliferation and immunoglobulin secretion of certain ODNs. After further analysis of the ODNs, Krieg found out that CpG dinucleotides in particular sequence contexts (XCGY whereas X can be random but C and Y can be random but G) are decisive to induce a stimulation of the immune system. Inversion of the base sequence (GpC) as well as methylation of cytosine abolished the immune stimulation. Concomitantly, it could be disproved that the formation of higher order structures related to a palindrome sequence is necessary for action (Krieg *et al.* 1995).

Summarizing all these insights, it can be explained how TLR9 succeeds to differentiate between own and foreign DNA (Bird *et al.* 1987):

- a) CpG dinucleotides are statistically underrepresented in vertebrate DNA (1:60), whereas nucleotide utilization in bacterial DNA is random (1:16).
- b) The majority of cytosines (70%) in CpG dinucleotides are methylated in vertebrate, but not in microbial DNA.

With this knowledge various synthetic ODNs were developed which were highly effective concerning their immune stimulation in murine *in vitro* and *in vivo* experiments. But it was noticed that optimized sequences and settings of the murine experiments could not be transferred to nonhuman primates and humans, as there are significant evolutionary based differences in the recognition of CpG motifs. Whereas GACGTT was determined as the optimized CpG motif to activate the immune system of mice (Rankin *et al.* 2001) it is GTCGTT for nonhuman primates and humans (Hartmann & Krieg 2000) (Table 2). Moreover, the cell-types that contain TLR9 differ remarkably. In mice, TLR9 is also present in cells of the myeloid lineage such as myeloid dendritic cells (MDCs; CD11c⁺ DCs). In humans the receptor is exclusively present in plasmacytoid dendritic cells (PDCs; CD11c⁻

DCs) and B cells (Rothenfusser *et al.* 2002). Murine MDCs are often utilized in *in vitro* models, since these cells are conveniently derivable from bone marrow precursors being treated with GM-CSF. But TLR9 is not present in human MDCs, so the significance of the data produced with this *in vitro* model is limited. Caution seems advisable when extrapolating murine CpG ODN data to primates and humans.

1.3 Synthetic CpG ODN classes for humans and their effects on the immune system

With respect to the induced immunological effects, there are two major classes of CpG ODNs described for humans which are called CpG-A (also known as ODN type D (Klinman 2004)) and CpG-B (also known as ODN type K (Klinman 2004)).

Table 2: Nucleotide sequences of CpG ODN 1826 (prototype murine CpG ODN), CpG ODN 2216 (prototype CpG-A class), and CpG ODN 2006 (prototype CpG-B class).

CpG ODN type	Description	Sequence (5'-3')
1826	murine CpG ODN	TCCATGAC CG TTTCCTGAC CG TT*
2216	CpG-A ODN	GGgggac cg atc gcg GGGGg*
2006	CpG-B ODN	TCGTCG TTTTGT CG TTTTGT CG TT*

* capital letters: nucleotides with phosphorothioated backbones;
others: phosphodiester backbones

CpG-A with its prototype ODN 2216 (Krug *et al.* 2001) (Table 2) is known to stimulate the production of high amounts of IFN- α/β (type I interferons). The ODNs of this class possess characteristic structural features (Krug *et al.* 2001):

- chimeric backbone with phosphorothioate-modified 5' and 3' ends and a phosphodiester center portion
- poly-G sequences at both ends
- central palindrome sequence
- CpG dinucleotide within the palindrome

However, the B cell activation of CpG-A ODNs is only weak. On the other hand, CpG-B ODNs selectively activate PDCs and induce their maturation, but are unable to initiate the secretion of IFN- α/β . Moreover, CpG-B ODNs are able to activate B cells. The sequence prototype ODN 2006 (Hartmann & Krieg 2000) (Table 2) is currently tested in various clinical trials as ODN 7909 (ProMune™, Coley Pharmaceutical Group, Wellesley, MA, USA). A more detailed overview of the effects of CpG ODNs on the two cell types that are directly activated in the human immune system is given in Fig. 1 (Rothenfusser *et al.* 2002):

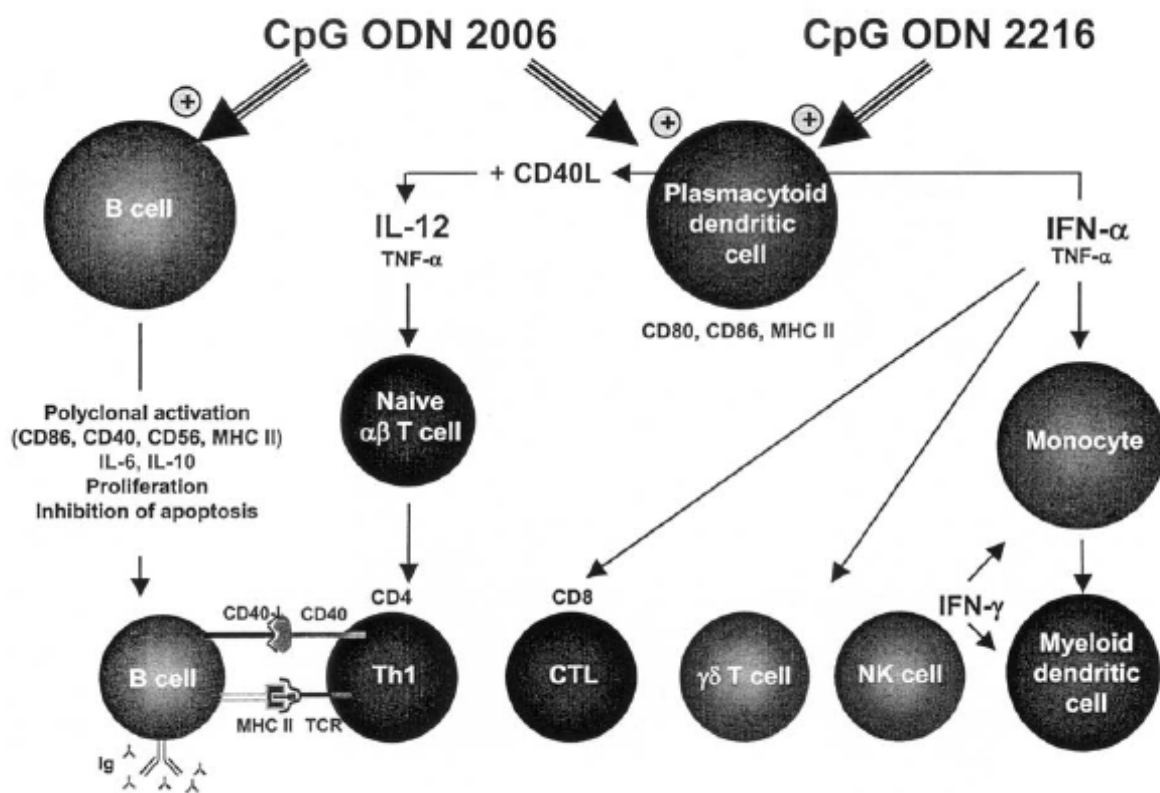


Fig. 1: Effects of CpG ODN on the human immune system (Rothenfusser *et al.* 2002)

Whereas PDCs and B cells are directly activated by CpG ODNs, other immune cell subsets such as monocytes, MDCs, T cells and NK cells are only indirectly activated.

Effects mediated via CpG-A class ODNs are:

- a) partial activation of CD8 cytotoxic T lymphocytes (CTL) (Hornung *et al.* 2002)
- b) strong activation of NK cells (→ production of IFN- γ and lytic activity) (Rothenfusser *et al.* 2001)
- c) promotion of proliferation, IFN- γ production, and lytic activity of $\gamma\delta$ T cells (Rothenfusser *et al.* 2001)

Effects mediated via CpG-B class ODNs are:

- a) direct activation of B cells (Hartmann & Krieg 2000)
- b) synergistic stimulation of IL-12 with CD40 L in PDCs leading to priming of naïve CD4 T cells and the development of T_H1 cells (Rothenfusser *et al.* 2002)

Both CpG ODN classes upregulate co-stimulatory molecules in monocytes and MDCs.

Recently, with the CpG-C class, a new class of CpG ODNs was introduced. These CpG ODNs activate both, the secretion of IFN- α in PDCs and the proliferation of B cells (Hartmann *et al.* 2003; Poeck *et al.* 2004; Vollmer *et al.* 2004).

1.4 Fields of applications for synthetic CpG ODNs

Potential fields of application for synthetic CpG ODNs are illustrated in Fig. 2 (Klinman 2004). They can be applied as immunoprotective stand-alone agent, inhibitor of T_H2-cell-mediated allergic reactions, adjuvant for vaccine applications, and for the immunotherapy of cancer.

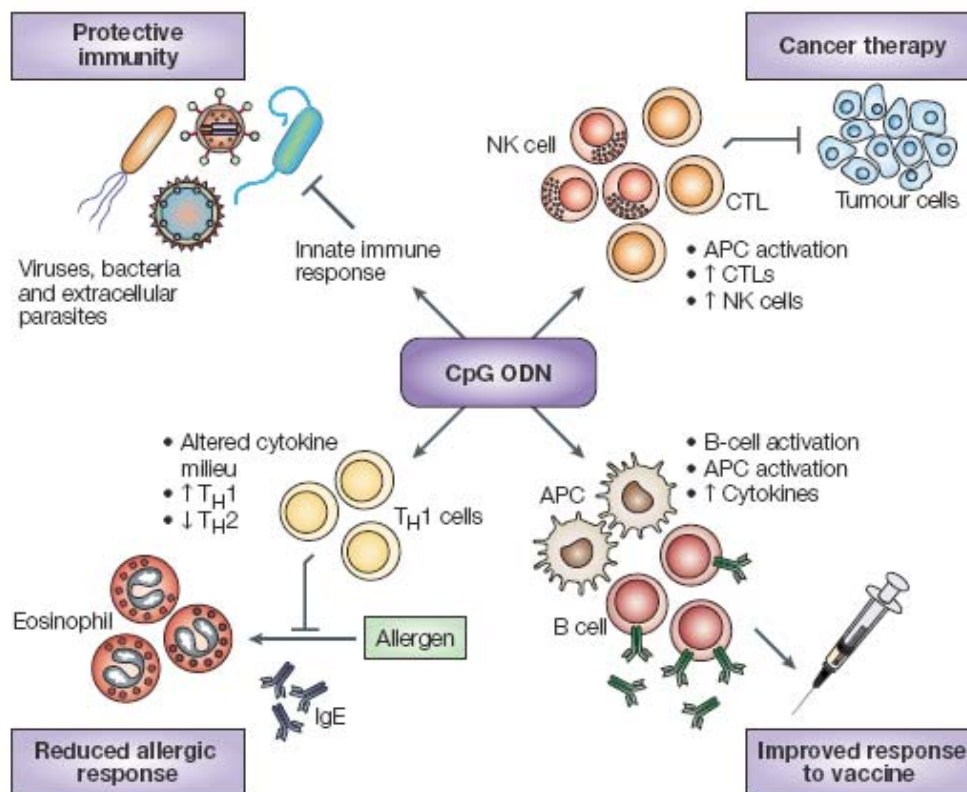


Fig. 2: Potential therapeutic uses of CpG ODNs (Klinman 2004)

Immunoprotective activity of CpG ODNs

Various research groups have proven *in vivo* that the prophylactic administration of CpG ODNs and bacterial DNA induces protection against various viruses, bacteria and extracellular parasites. So, pretreated mice were e.g. resistant versus bacteria inducing listeria and tularaemia (Krieg *et al.* 1998; Klinman *et al.* 1999; Elkins *et al.* 1999). Similar results could be achieved for the protection from viral pathogens such as the herpes simplex virus and the cytomegalovirus (Pyles *et al.* 2002; Ashkar *et al.* 2003) as well as from parasites inducing leishmaniasis and malaria (Zimmermann *et al.* 1998; Gramzinski *et al.* 2001). Thereby, the immunoprotective activity reached its maximum after several days and lasted for several weeks. In first experiments with primates (macaques), the malignance of infections was strongly reduced when the monkeys were pretreated with CpG-A ODN (Verthelyi *et al.* 2003). Finally, it was also demonstrated in this study that the CpG-induced immunoprotection is mainly PDC-related, since PDC-deficient mice treated with CpG ODNs did not show any protection against infections.

Prevention and treatment of allergies

Allergic asthma, an inflammatory disease of the respiratory tract, is associated with T_H2 -biased activation mainly via the cytokines IL-4 and IL-5 (Robinson *et al.* 1992). Furthermore it is known that cytokines that induce a T_H1 -type immune response, such as INF- γ and IL-12, strongly reduce the symptoms by inhibiting the T_H2 -pathway (Sur *et al.* 1996). Research groups demonstrated in mouse models that allergic asthma could be attenuated or even cured when CpG ODNs were co-administered with allergens (Kline *et al.* 1998; Sur *et al.* 1999). Intratracheally administered CpG ODN shifted the balance between INF- γ - and IL-4-secreting cells towards INF- γ , reduced the number of allergen specific IgE-producing cells and diminished the allergen-induced eosinophil recruitment (Sur *et al.* 1999).

Immunotherapy of cancer

CpG ODNs have shown great potential in murine tumor models. Effective anti-tumor immunity can be achieved with CpG ODNs in both, monotherapy and in combination with chemo- or radiotherapy (Ballas *et al.* 2001; Heckelsmiller *et al.* 2002; Weigel *et al.* 2003; Milas *et al.* 2004; Meng *et al.* 2005; Bourquin *et al.* 2006). These anti-tumoral effects appear, because the immune cascade that is elicited by CpG ODNs results in the activation of NK cells and cytotoxic T lymphocytes (CTLs). Even complete tumor remission in mice could be achieved and due to the presence of memory immune cells, no recidivisms occurred (Heckelsmiller *et al.* 2002). However, the published results indicate that the type of tumor, as well as the type of administered CpG ODN is crucial for the success of a prophylactic or therapeutic application.

Adjuvant for vaccine applications

CpG ODNs induce the production of cytokines and chemokines that create an supportive environment for antigen-specific immune response. In addition, CpG ODNs activate professional APCs and induce their maturation. Consequently, CpG ODNs are discussed as potent vaccine adjuvants, as they strongly enhance the immunogenicity of co-administered antigens. In agreement with the production of T_H1 -type cytokines, CpG ODNs activate the production of INF- γ that promotes the production of IgG2a antibodies and facilitates the development of antigen

specific CTLs (Moldoveanu *et al.* 1998; Eastcott *et al.* 2001). These issues are further investigated in Chapter IV of this thesis.

1.5 Clinical trials with CpG ODNs

Due to the promising *in vivo* data derived from animal studies, CpG ODNs have made their way straight forward towards clinical trials. Until 2004, CpG ODNs have been administered in more than 12 clinical trials (Klinman 2004). Most of these studies are in Phase I or Phase II. Applications tested are either CpG ODNs alone, or in combination with allergens, vaccines, or antibodies. So, CpG ODNs are evaluated for the treatment of various allergies, asthma, cancer, and as vaccine adjuvant.

So far, the results of two clinical trials have been described in literature. In these experiments, CpG ODN 7909 (= CpG-B ODN 2006 sequence) has been used as vaccine adjuvant. In a first randomized double-blind study, CpG ODN 7909 was co-administered by intramuscular injection with Engerix-B[®] (GlaxoSmithKline) a commercial hepatitis B vaccine. This co-administration led to 13 - 45-fold higher antibody titers than with Engerix-B[®] alone (Halperin *et al.* 2003; Cooper *et al.* 2004a). In a second double-blind study where CpG ODNs were co-administered with the influenza virus vaccine Fluarix[®] (GlaxoSmithKline), humoral responses were not significantly enhanced by the addition of CpG 7909, except in individuals with pre-existing immunity (Cooper *et al.* 2004b). However, co-administered CpG ODN induced significantly higher INF- γ secretion from peripheral blood mononuclear cells (PBMCs). Thus, CpG ODN 7909 may allow the use of reduced Fluarix[®] doses without reducing the immunogenicity.

1.6 CpG ODN transport by delivery systems and aim of the study

Professional antigen presenting cells naturally phagocytose bacteria, viruses, and other microorganisms and process their proteins for antigen presentation to T cells for the induction of antigen specific immune responses. Colloidal particulate formulations fall within the same size range as microorganisms and thus are preferentially phagocytosed by MDCs. Hence, particulate vaccine delivery systems have proven to be advantageous for subunit vaccines based on proteins, peptides and DNA (Raychaudhuri & Rock 1998; Singh & O'Hagan 2002).

Following this concept, enhanced T_H1 -biased immune responses have been observed in mice subsequent the delivery of CpG ODNs via liposomes (Joseph *et al.* 2002; Suzuki *et al.* 2004) and micro- or nanoparticulate delivery systems (Singh *et al.* 2001; Diwan *et al.* 2002; Fearon *et al.* 2003; Diwan *et al.* 2004). Our cooperation partners at the University of Alberta already demonstrated the advantage of CpG ODNs after incorporation in biodegradable poly(D,L-lactic-co-glycolide acid) (PLGA) nanoparticles (Diwan *et al.* 2002; Diwan *et al.* 2004). Another research group (Singh *et al.* 2001) achieved very promising results using CpG ODNs adsorbed onto cationized Polylactide-co-glycolide (PLG) microparticles due to electrostatic interactions. The advantage of this system is the direct presentation of CpG ODNs on the carrier's surface. This might result in a quicker activation compared to carrier-incorporated CpG ODNs since no diffusion or particle degradation is necessary before ODNs can interact with the receptor.

It was the aim of the present study to evaluate CpG ODN-loaded cationized gelatin nanoparticles (CpG-GNPs). Thereby the same cholamine-modified cationized gelatin nanoparticles were applied as already introduced as non-viral gene delivery system (Chapter II).

At first *in vitro* uptake of plain gelatin nanoparticles into murine myeloid dendritic cells (MDCs) was studied in competition with other established nanoparticulate carrier system. At the same time we started to evaluate the loading behavior of CpG ODNs onto cationized gelatin nanoparticles. Optimized CpG-GNPs were then investigated in this previously established murine *in vitro* model. However, due to differences in the distribution of TLR9 and the ideal CpG ODN sequences comparing murine and human organisms, these data allow only to draw limited conclusions. Hence, primary human blood cells were utilized in the third part of this study, where immunological effects of all three CpG ODN classes that exist for humans and non-human primates were evaluated.

2. MATERIALS AND METHODS

2.1 Materials

2.1.1 Reagents

Reagent	Description	Supplier
Acetone	p.a.	VWR International GmbH (Ismaning, Germany)
Chloroform	HPLC grade	Fisher (Nepean, ON, Canada)
Cholaminechloride hydrochloride	(2-aminoethyl)-trimethyl-ammoniumchloride hydrochloride	Sigma-Aldrich GmbH (Taufkirchen, Germany)
DABCO	1,4-Diaza[2.2.2]bicyclooctane; 98%	Sigma-Aldrich GmbH (Taufkirchen, Germany)
DMSO	Dimethyl Sulfoxide; ≥99.9%	Sigma-Aldrich GmbH (Taufkirchen, Germany)
EDC	1-ethyl-3-(3-dimethyl-aminopropyl) carbodiimide hydrochloride	Sigma-Aldrich GmbH (Taufkirchen, Germany)
Gelatin type A	175 Bloom	Sigma-Aldrich GmbH (Taufkirchen, Germany)
Glutaraldehyde	25%	Sigma-Aldrich GmbH (Taufkirchen, Germany)
Glycerol	For molecular biology	Sigma-Aldrich GmbH (Taufkirchen, Germany)
HCl	1 N	VWR International GmbH (Ismaning, Germany)
HSA	Human serum albumin (lyophilized; ≥99.9%)	Sigma-Aldrich GmbH (Taufkirchen, Germany)
Mowiol™ 4-88		Calbiochem (La Jolla, CA, USA)
NaCl	p. a.	VWR International GmbH (Ismaning, Germany)
NaOH	1 N	VWR International GmbH (Ismaning, Germany)
PLGA	poly(D,L-lactic-co-glycolic acid) polymer (ratio 50:50)	BPI (Birmingham, AL, USA)
Polyvinyl alcohol	87-89% hydrolyzed; Mw. 31,000-50,000	Aldrich (Milwaukee, WI, USA)
Paraformaldehyde	Solution (4%)	Sigma-Aldrich GmbH (Taufkirchen, Germany)
Water for injection		Wyeth Pharma (Muenster, Germany)

2.1.2 Fluorescent dyes and monoclonal antibodies

Reagent	Description	Supplier
Alexa™ Fluor 488 Concanavalin A		Molecular Probes (Leiden, Netherlands)
Alexa™ Fluor 596 Concanavalin A		Molecular Probes (Eugene, OR, USA)
Alexa™ Fluor 488 succinimidyl ester	Mixed isomers	Invitrogen (Karlsruhe, Germany)
CD11c antibody	+ FITC-conjugated secondary antibody	BD Pharmingen (Mississauga, Canada)/(Heidelberg, Germany)
CD86 antibody	+ FITC-conjugated secondary antibody	BD Pharmingen (Mississauga, Canada)
MHC II antibody	+ FITC-conjugated secondary antibody	BD Pharmingen (Mississauga, Canada)
Texas Red-X™ succinimidyl ester	Mixed isomers	Molecular Probes (Leiden, Netherlands)

2.1.3 Applied ODNs

Name	Description	Supplier
ODN 1826	Mouse specific CpG ODN 5' TCCATGAC CG TTTCCTGAC CG TT 3' [*]	Operon Technologies Inc. (Alameda, USA).
ODN 1911	Control ODN 5' TCCAGGACTTTCCTCAGGT 3' [*]	Operon Technologies Inc. (Alameda, USA).
ODN 2006	Prototype CpG-B ODN 5' TCGT CG TTTTGT CG TTTTGT CG TT 3' [*]	Coley Pharmaceutical Group (Wellesley, MA, USA)
ODN 2216	Prototype CpG-A ODN 5' Gggggac cgatcgtc GGGGGg 3' [*]	Coley Pharmaceutical Group (Wellesley, MA, USA)
ODN M362	Prototype CpG-C ODN 5' TCGT CG TCGT TCGAACGACG TTGAT 3' [*]	Coley Pharmaceutical Group (Wellesley, MA, USA)
ODN M383	GC pendant to ODN M362 5' TGCTGCTGCTTGCAAGCAGCTTGAT 3' [*]	Coley Pharmaceutical Group (Wellesley, MA, USA)

* capital letters: nucleotides with phosphorothioated backbones;
others: phosphodiester backbones

2.1.4 Cell culture reagents

Reagent	Description	Supplier
FCS	Fetal calf serum	GibcoBRL (Paisley, UK)
Human AB-serum		BioWhittaker Inc. (Wakersville, MD, USA)
HSA	Human serum albumin; $\geq 97\%$	Pharmacia & Upjohn (Erlangen, Germany)
L-glutamine		PAA (Linz, Austria)
Penicilline		PAA (Linz, Austria)
RPMI-1640	medium	Biochrom AG (Berlin, Germany)
Streptomycine		PAA (Linz, Austria)

2.2 Preparation of cationized gelatin nanoparticles

Cationized gelatin nanoparticles were prepared according to the procedure described in Chapter II. – 2.2. Cholamine was chosen as cationization agent for the nanoparticle surface. In order to prevent contaminations, which might influence the immune response, all preparation steps were performed under aseptic conditions.

2.3 Preparation of fluorescent gelatin nanoparticles

To enable the detection of the gelatin nanoparticles in CLSM and FACS experiments, they were labeled with fluorescent dyes. The labeling was conducted during the particle preparation process.

2.3.1 Covalent linkage of aminoreactive fluorescent dyes

For fluorescence labeling, 2 mg of the aminoreactive dye, e.g. Texas Red-X™ succinimidylester, were added to the redissolved gelatin solution after the first desolvation step. This mixture was constantly stirred over 2 hours. After this, we proceeded with the standard preparation method.

2.3.2 Incorporation of dextran-linked fluorescent dyes

2 mg TMR dextran (Mw. 40,000) was added to the redissolved gelatin solution after the first desolvation step and encapsulated into the nanoparticle matrix during the second desolvation step.

2.4 Preparation of fluorescent HSA nanoparticles

HSA nanoparticles were prepared using a previously described desolvation technique (Marty *et al.* 1978; Weber *et al.* 2000). 200 mg HSA was dissolved in 2.0 mL highly purified water. To incorporate a fluorescent dye, 1 mg TMR dextran was added to this solution. Desolvation of this protein solution was initiated by dropwise addition of 6.0 mL ethanol. 80 μ L of 25% aqueous glutaraldehyde solution were added to stabilize the in-situ formed particles by crosslinking. After stirring over 24 h, the resulting nanoparticles were purified by 3-fold centrifugation and redispersion with injectable water.

2.5 Preparation of fluorescent PLGA nanoparticles

TMR dextran containing PLGA nanoparticles were kindly prepared by our cooperation partner Praveen Elamanchili (University of Alberta) with a double emulsion solvent evaporation technique as described earlier (Elamanchili *et al.* 2004).

2.6 Characterization of the nanoparticles

The size of the prepared nanoparticles and CpG-A ODN 2216 was measured by dynamic light scattering using a Zetasizer 3000 HSA or a Nanosizer ZS (Malvern, Worcestershire, UK). The resulting mean size was calculated on the basis of 10 individual subruns. Zeta potential (ζ potential) measurements were conducted in 1 mM NaCl at pH 7.0 (Zetasizer 3000 HSA, Malvern, Worcestershire, UK) if not stated otherwise.

2.7 ODN loading of cationized gelatin nanoparticles

600 µg nanoparticles were incubated with 30 µg of ODN in 400 µL of physiological PBS 7.4 for 30 min under gentle shaking at room temperature. In analogy to pDNA experiments (see Chapter II), the nanoparticle dispersion was centrifuged and the supernatant was analyzed UV-spectrophotometrically at 260 nm wavelength for unbound ODN.

2.8 Experiments with murine myeloid dendritic cells (MDCs)

2.8.1 Culture of MDCs

MDCs were generated from murine bone marrow precursors following the method previously described (Lutz *et al.* 1999). Briefly, 2×10^6 bone marrow cells obtained from the femurs of C57BL/6 mice were plated in bacteriological grade petri dishes in 10 mL of RPMI-1640 medium containing 20 ng/mL of GM-CSF (complete media) and incubated at 37°C and 5% CO₂. On day 3, the cells were supplemented with 10 mL of complete media and on day 6, half of the media was removed and replaced with fresh complete media. The purity of the semi-adherent and non-adherent DC populations on day 7 was found to be greater than 80% (based on the expression of CD11c).

2.8.2 FACS analysis of nanoparticle uptake by MDCs

Seven days old DCs were incubated for 12 hours with CpG ODN-loaded formulations (ZWCaTMR) or unloaded nanoparticles. After 12 hours, the cells were harvested and washed thoroughly in cold staining buffer (PBS containing 10% FBS and 0.05% sodium azide) and transferred into FACS tubes. For phenotypic analysis of cells that have taken up the nanoparticles, surface staining was performed after 12 h of incubation with fluorescence-labeled nanoparticles using monoclonal antibodies specific for CD11c, CD86, and MHC-II molecules (along with their respective isotype controls) and appropriate FITC-conjugated secondary antibodies. The samples were then transferred into FACS tubes and analyzed using a FACSort. All events were collected by gating on the total live cell populations without further specific gating of particular subpopulations. A minimum of 10,000 events was collected.

2.8.3 Visualization of nanoparticle uptake by MDCs via CLSM

Day 7 DC primary cultures were transferred into Lab-Tek II eight well chamber slides (Nalge Nunc International, Rochester, USA) at 4×10^5 cells in 300 μL of medium. The cells were incubated with 8 μg of CpG ODN-loaded Texas Red-X-labeled nanoparticles (ZWCaTEX; containing 400 ng of CpG ODN) in a final volume of 500 μL . Control wells were treated with the phagocytosis inhibitor Cytochalasin B (5 $\mu\text{g}/\text{mL}$) 30 min prior addition of nanoparticles and throughout the whole incubation. After incubation for 8 hours, the supernatant in the chamber slide cultures was carefully removed. The cells were washed thrice with PBS and stained with a CD11c specific primary antibody followed by a FITC-labeled secondary antibody. After the final washing step, cells were fixed with 4% paraformaldehyde. Chamber slides were finally prepared with a solution of 2.5% DABCO and PBS/glycerol (1:1) and visualized under a Zeiss 510 LSM NLO confocal laser scanning microscope (Carl Zeiss Microscope Systems, Jena, Germany).

2.8.4 Quantification of cytokine secretion

1×10^6 cells of 7 days old MDCs were transferred into 50 mm petri dishes in 5 mL of complete RPMI-1640. The MDCs were incubated with 200 μg of two differently sized cationized gelatin nanoparticle batches (ZWCa01 and ZWCa02) containing a payload of 10 μg (5% [w/w]) CpG ODN each. In addition, some MDC groups were incubated with 10 μg of soluble CpG ODN or nanoparticles that contained 10 μg of non-stimulatory control ODN or 200 μg of unloaded cationized gelatin nanoparticles. After 24 hours, the supernatant of each group was collected and frozen for later cytokine analysis. Quantitative cytokine analysis for IL-6, IL-12p70, and TNF- α was performed using specific ELISA Ready-SET-Go kits (eBioscience Inc., San Diego, USA) according to the manufacturer's instructions.

2.8.5 Special conditions for kinetic experiments

Different from the experiments we performed on our own, our cooperation partners Dr. Dr. Carole Bourquin and Philip von der Borch at LMU's Division of Clinical Pharmacology purified CD11c⁺ MDCs from other cells by magnetic-activated cell sorting (MACS) (Miltenyi Biotech, Bergisch Gladbach, Germany). All experiments were performed in 96-well plates (BD Biosciences, Heidelberg,

Germany) containing 5×10^4 MDCs in 200 μ L RPMI-1640 medium. Standard CpG-GNP concentration per well was 60 μ g/mL. Thus, 600 ng CpG ODN loaded onto 12 μ g cationized gelatin nanoparticles were administered per 5×10^4 cells. CpG-GNP uptake into MDCs was examined by flow cytometry (FACSCalibur, BD Biosciences). Data were analyzed using CellQuest software (BD Biosciences). Cytokine concentrations were determined by ELISA for IL-6 (BioSource, Solingen, Germany) and IL-12p70 (BD Biosciences) according to the manufacturer's protocol.

2.9 Experiments with primary human blood cells

The present *in vitro* experiments testing CpG-GNPs on primary human PBMCs, PDCs, and B-cells, were performed in cooperation with Julia Battiany and PD Dr. Gunther Hartmann from the Division of Clinical Pharmacology at the Department of Internal Medicine at LMU Munich, Germany.

2.9.1 Isolation of PBMCs

Human PBMCs (monocytes and lymphocytes) were isolated from buffy coats (leucocytes obtained by centrifugation from the whole blood) provided by the blood bank of the University of Greifswald, Germany. Blood donors were between 18 to 65 years old healthy women and men, which were tested to be negative for HIV, HBV, and HCV. Further exclusion criteria were manifest infections during the last 4 weeks, fever, symptomatic allergies, abnormal blood cell counts, increased liver enzymes or medication of any kind except vitamins and oral contraceptives. PBMCs were prepared from buffy coats by Ficoll-Hypaque density gradient centrifugation (Biochrom, Berlin, Germany). Thereby, PBMCs are separated from other formed elements in the blood. The sample is layered onto a Ficoll-sodium metrizoate gradient of specific density; following centrifugation, lymphocytes are collected from the plasma-Ficoll interface.

2.9.2 Isolation of PDCs

PDCs were positively isolated using an anti-BDCA-4 antibody according to the manufacturer's protocol (BDCA-4 Cell-Isolation-Kit, Miltenyi Biotec, Bergisch-Gladbach, Germany). The purity of the isolated PDC cultures was 96-98% as assessed by flow cytometric analysis.

2.9.3 Isolation of B cells

Purified B cells were obtained by using the CD19 B cell isolation kit from Miltenyi Biotec. Briefly, B cells were labeled with anti-CD19 antibody coupled to colloidal paramagnetic microbeads and passed through a magnetic separation column (LS, Miltenyi Biotec). The purity of isolated B cells was >95% as assessed by flow cytometric analysis with no PDCs detectable (<0.005%).

2.9.4 Cell cultures

The various isolated cells were resuspended in RPMI 1640 medium supplemented with 8% human AB-serum, 1.5 mM L-glutamine, 100 U/mL penicillin, and 100 µg/mL streptomycin. Cells were cultured in 96-well round-bottom plates (200 µL medium/well; final concentration PBMCs: 2×10^6 /mL, PDCs: 2.5×10^5 /mL, B cells: 2×10^5 /mL). All compounds were purchased endotoxin-tested. Viability of isolated cells was determined by trypan-blue exclusion.

2.9.5 Cytokine quantification by ELISA

IFN- α was quantified with the IFN- α module set from Bender MedSystems (Vienna, Austria; detection range 8-500 pg/mL). This ELISA detects most of the IFN- α isoforms, except IFN- α B and IFN- α F. IL-6 was measured by using the human IL-6 OptEIA ELISA (Bender Med Systems; detection range 4.7-300 pg/mL).

2.9.6 CLSM experiments

Uptake experiments into PDCs were performed with CpG ODNs that were previously labeled (3'terminal) with fluoresceine (Coley Pharmaceutical Group). 5×10^4 isolated PDCs in 200 µL of medium were transferred into Lab-Tek II eight well chamber slides (Nalge Nunc International). The medium additionally contained 2 ng IL-3. The cells were incubated with 12 µg of fluorescence-labeled (3'terminal) CpG-A ODN 2006-loaded cationized gelatin nanoparticles (containing 600 ng of CpG ODN). After incubation for 8 hours, the supernatant in the chamber slide cultures was carefully removed. The cells were washed thrice with PBS and stained with 100 µL of a 0.0005% Alexa Fluor™ 594 Concanavalin A solution in PBS for 1 min (unspecific cell membrane stainer). After the final

washing step, cells were fixed with 4% paraformaldehyde. Chamber slides were finally prepared with a solution of 2.5% DABCO and PBS/glycerol (1:1) and visualized under a Zeiss 510 LSM NLO confocal laser scanning microscope (Carl Zeiss Microscope systems, Jena, Germany).

3. RESULTS AND DISCUSSION

3.1 Comparative uptake study of various biodegradable colloidal carrier systems into murine myeloid dendritic cells (MDCs)

Our cooperation partners have already shown in the past that nanoparticles based on poly(D,L-lactic-co-glycolic acid) (PLGA) are potent vehicles for various drugs, such as peptides and plasmid DNA to generate immune response *in vivo* (Diwan *et al.* 2002). Besides PLGA particles, further biodegradable and physiologically very well tolerated colloidal carriers exist, such as nanoparticles based on gelatin and human serum albumin (HSA). Both of them are discussed as interesting alternative delivery systems due to their protein structure, which offers a multitude of selective linking opportunities. Hence, we compared in this initial study the potential of these 3 different nanoparticle types as drug vehicles into MDCs.

3.1.1 Nanoparticle characterization via DLS

All prepared particles had sizes within the colloidal range. Concerning particle homogeneity, DLS suggested unimodal size distributions for all batches as displayed by low polydispersity indices (Table 3).

Table 3: DLS data of the applied nanoparticle batches

particle type	mean size (nm)	polydisp. index
HSA	277.9	0.0756
PLGA	387.6	0.1083
Gelatin	216.2	0.0782

3.1.2 FACS analysis of the cellular uptake

The purity of the MDCs being cultured according to the previously described method was assessed via FACS analysis of CD11c positive cells to be 75%. One million of 7 days old MDCs were incubated with 200 μ g of different fluorescence-labeled nanoparticulate formulations each. After the incubation period of 24 hours, all nanoparticulate formulations were basically taken up by MDCs. However, distinct differences could be detected. Whereas 68% of the cells incubated with gelatin nanoparticles and 52% of those incubated with HSA nanoparticles were

positive for nanoparticles, only 41% were positive for PLGA nanoparticles (Fig. 3). Due to the higher averaging fluorescence detected within the cells that were incubated with gelatin or HSA nanoparticles, a higher number of those nanoparticles was obviously taken up. Moreover, analyzing the FACS dot-plots (data not shown), the highest shift towards MDCs with increased size and granularity compared to untreated MDCs could be seen with gelatin nanoparticles. Indeed, the prepared PLGA nanoparticles were larger in size, but this issue should not have such a crucial impact on the cellular uptake, since we haven't seen those differences in preliminary studies where we used differently sized gelatin nanoparticles (data not shown).

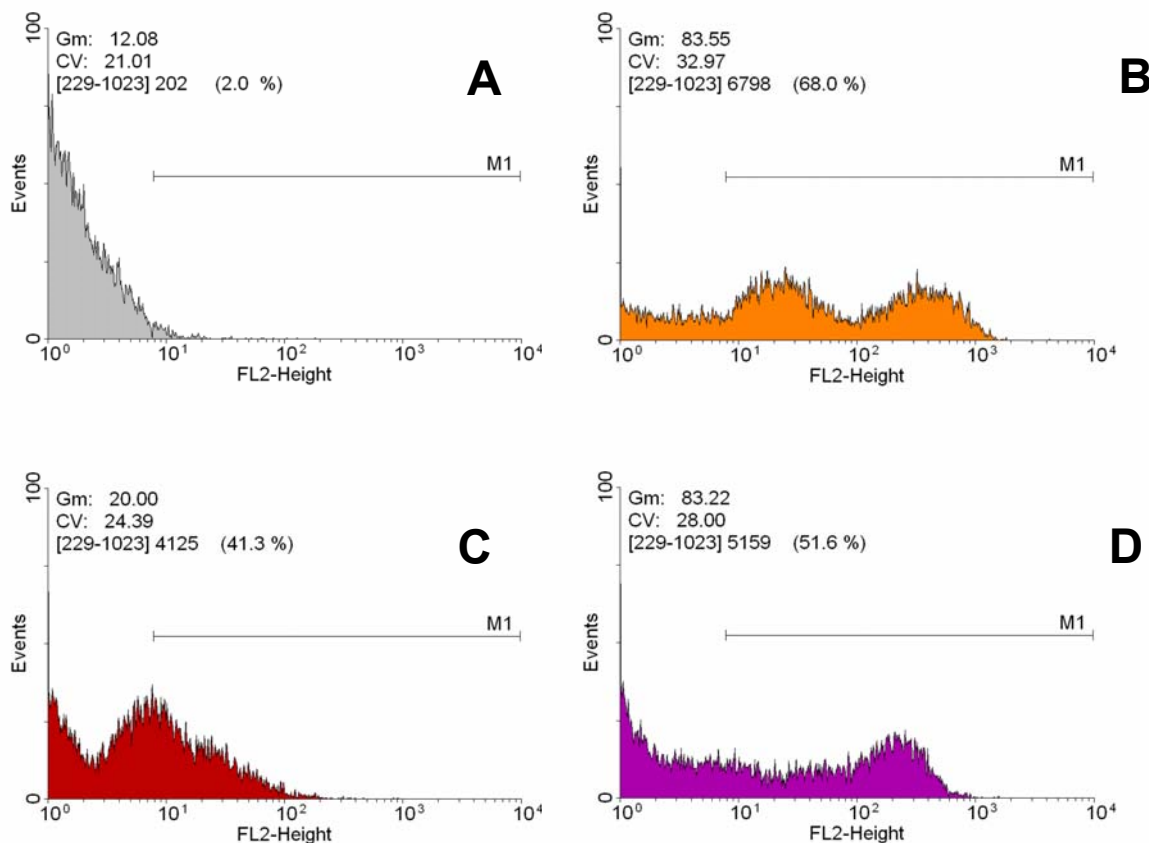


Fig. 3: Uptake of various nanoparticulate formulations into MDCs. FACS histogram plots (FL2-height) of untreated MDCs (A), MDCs incubated with gelatin nanoparticles (B), MDCs incubated with PLGA nanoparticles (C), MDCs incubated with HSA nanoparticles (D).

3.1.3 Visualization of the cellular uptake by CLSM

FACS data indicated that all of the tested nanoparticles are taken up by MDCs. But FACS is unable to differentiate between surface adsorbed and internalized nanoparticles. So, CLSM studies were employed to pin point the localization of these nanoparticles. Surprisingly, only gelatin and PLGA nanoparticles could be localized within the cells. The majority of HSA nanoparticles in contrast, was adsorbed onto the cell membrane (Fig. 4).

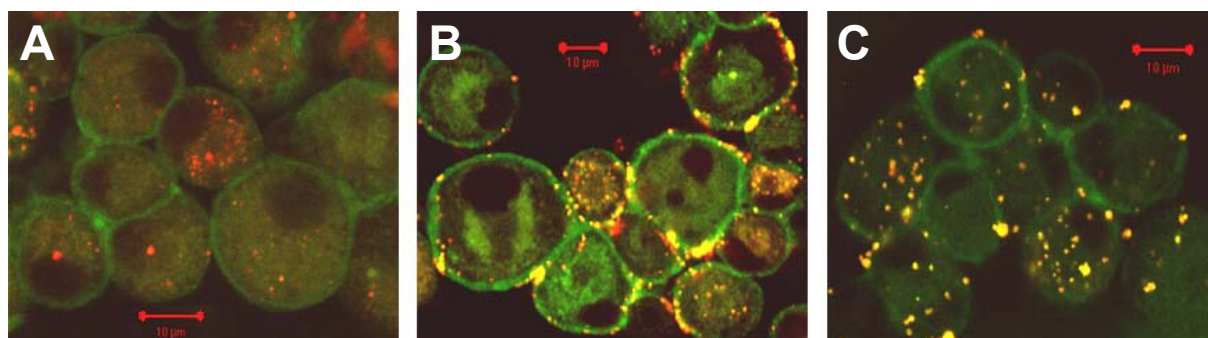


Fig. 4: CLSM pictures of MDCs incubated with various formulations: gelatin nanoparticles (A); HSA nanoparticles (B); PLGA nanoparticles (C).

3.1.4 Discussion and Summary

Summarizing the data generated in this study, we found significant differences between three types of biodegradable nanoparticles in terms of delivery into MDCs. In fact, only PLGA and gelatin nanoparticles were effectively internalized into MDCs, whereas HSA nanoparticles remained mainly sticking to the cell membrane. Since e.g. antigen delivery with the objective of subsequent presentation requires the uptake into the MDCs, HSA nanoparticles appear relatively unsuitable for this purpose. Moreover most of the other potential applications with DCs as target, such as the delivery of various PAMPs to their target TLRs require intracellular uptake. Thus, only a few potential applications remain where it might be advantageous to achieve only cell-membrane delivery. One example might be the adjuvant monophosphoryl lipid A (MPLA) that has its target receptor, TLR4, located on the cell membrane of APCs.

Quantitative FACS analysis revealed that gelatin nanoparticles were most efficiently taken up by the MDCs. Hence, gelatin nanoparticles seem well armed for competing PLGA nanoparticles as potential delivery system into DCs.

3.2 Delivery of CpG ODN-loaded cationized gelatin nanoparticles (CpG-GNPs) into murine MDCs

Based on the promising data with cholamine-modified cationized gelatin nanoparticles during gene therapeutic experiments (see Chapter II) we decided to evaluate the applicability of this nucleotide delivery system with immunogenic short single-stranded CpG oligonucleotides. In 3.1, uptake data of gelatin nanoparticles into MDCs had been shown.

3.2.1 Characterization of the nanoparticles

Most of the nanoparticles used in our experiments ranged from 230 to 260 nm (Table 4). We chose smaller, 133.8 nm sized nanoparticles (batch ZWCa01) as an additional sample to investigate a possible impact of the particle size. Dynamic light scattering (DLS) characterized all nanoparticle batches as very homogeneous. The respective size distributions were very narrow as displayed by polydispersity indices below 0.1.

Table 4: Sizing data obtained by DLS of unloaded vs. CpG ODN-loaded gelatin nanoparticles batches (5% [w/w] payload).

	unloaded		loaded	
	Mean particle size (nm)	PI*	Mean particle size (nm)	PI*
ZWCa01	133.8	0.0763	135.3	0.0891
ZWCa02	244.3	0.0625	245.0	0.0759
ZWCaTEX	232.7	0.0342	233.2	0.0411
ZWCaTMR	255.4	0.0881	259.2	0.0911

*PI = polydispersity index

Cationization of the nanoparticles was monitored by measuring the ζ potential of the formulations. The linking of cholamine introduces a pH independent cationic net charge onto the nanoparticles due to the quaternary amino group. Consequently, the ζ potentials of all batches were positive independent of the persisting pH conditions. In contrast, plain gelatin nanoparticles are negatively charged at neutral pH due to their isoelectric point at pH 5.7 (see Chapter II - 3.1).

After CpG ODN loading of the nanoparticles in PBS 7.4, no significant changes, neither in mean size nor in size distribution, were detectable (Table 4).

To find the optimal CpG ODN payload of the nanoparticles we tried to load increasing amounts of ODN onto the nanoparticles. After an incubation of 30 min the formulations were analyzed via UV spectroscopy for complete ODN loading (see 2.7). Furthermore, we visually monitored aggregation tendencies and measured the respective ζ potentials of the formulations. Results indicated that up to 100 μg CpG ODN 1826 could be completely loaded onto 600 μg (16.7% [w/w]) nanoparticles in 400 μL PBS 7.4. However, these nanoparticles were not stable in physiological PBS and tended to aggregate, most probably due to their neutral net charge (Table 5) that facilitates aggregation since inter-particulate electrostatic repulsion forces are absent (Müller 1996). This aggregation tendency could be circumvented by reducing the amount of payload to 60 μg per 600 μg nanoparticles (10% [w/w]). In our gene therapeutic experiments (see Chapter II) we have demonstrated that the highest transfection efficiency can be achieved with nanoparticle formulations bearing a final ζ potential of $\sim +3$ mV in PBS 7.4. Based on this knowledge we chose 30 μg CpG ODN per 600 μg nanoparticles (5% [w/w]) as payload of choice for all later *in vitro* experiments with murine MDCs, since the respective averaging ζ potentials of the formulations was around the favored value, e.g. $+3.90 \pm 0.87$ mV for ZWCa02 (Table 5).

Table 5: ζ potential values and visible aggregation tendencies of cationized gelatin nanoparticles (batch ZWCa02) loaded with various amounts of CpG ODN 1826 after 30 min of incubation; measurements were performed in PBS 7.4; respective conductivity values are put in parentheses

Payload (w/w)	ζ potential (Conductivity)	Aggregation
unloaded	$+7.39 \pm 0.35$ mV (17,03 mS/cm)	no
5.0%	$+3.90 \pm 0.87$ mV (16.34 mS/cm)	no
10.0%	$+1.33 \pm 0.25$ mV (16.08 mS/cm)	no
16.7%	-0.63 ± 0.17 mV (17.33 mS/cm)	yes

Comparing the amounts of loaded CpG ODN 1826 with the maximum payloads of pDNA, the achieved maximum of stable payload of CpG ODNs is one order of magnitude higher (see Chapter II). Apparently 10-30mer single-stranded ODNs

can be better adsorbed onto the nanoparticle surface than comparatively huge pDNA consisting of some thousand base-pairs. The huge double-stranded ring structure of pDNA complicates the complexation on only one single nanoparticle and facilitates possible interactions with other nanoparticles resulting in aggregates. Performing experiments with various other single- and double-stranded RNA and DNA oligonucleotides has shown that it is difficult to declare universally valid principles for the loading of nucleotides onto cationized gelatin nanoparticles (Zillies & Coester 2004; unpublished data). Summarizing all our nucleotide loading experiments, we can state as rules of thumb that short single-stranded DNA is easier to be adsorbed on cationized gelatin nanoparticles without causing aggregates than large double-stranded DNA. In addition DNA seems to be more convenient than RNA.

3.2.2 FACS analysis of CpG-GNP uptake by MDCs

As we had shown in 3.1, plain gelatin nanoparticles are efficiently taken up by MDCs. So, our first focus was to compare the uptake of CpG ODN-loaded cationized gelatin nanoparticles (ZWCaTMR) by MDCs with that of plain gelatin nanoparticles. MDCs incubated with nanoparticulate formulations displayed an increased forward and side scatter, indicating an increase in size and granularity of the cells as a result of the particle uptake (Fig. 5).

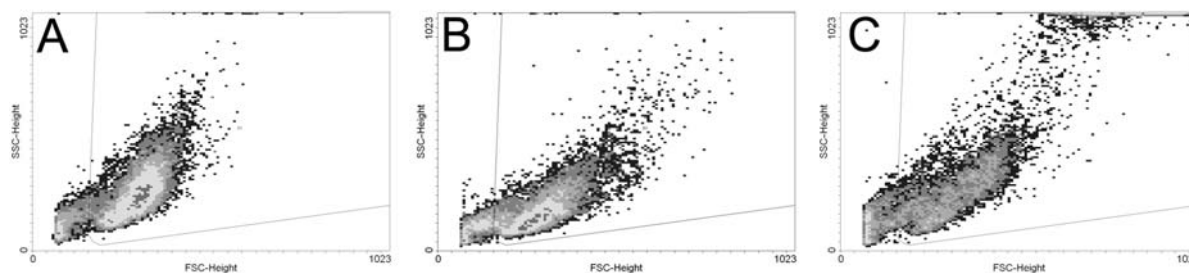


Fig. 5: FACS dotplots of untreated MDCs (A), MDCs incubated with plain non-cationized gelatin nanoparticles (B) and MDCs incubated with CpG-GNPs (C).

Furthermore, these results showed that MDCs had an immature phenotype at the time of nanoparticle pulsing and thus efficiently internalized the nanoparticle formulations. To determine the number of cells that had taken up the nanoparticles, the rhodamine fluorescence signal (FL-2) emitted from the MDCs was analyzed. As depicted in Fig. 6, 33% of the cells were TMR-dextran positive

when incubated with plain non-cationized gelatin nanoparticles whereas 68% were positive when the cells were incubated with CpG-GNPs.

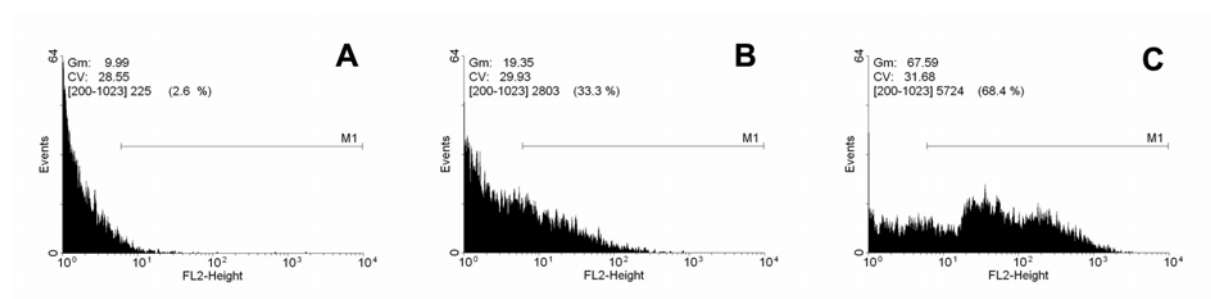


Fig. 6: FACS histogram plots (FL-2 Height) of untreated MDCs (A), MDCs incubated with plain non-cationized gelatin nanoparticles (B) and MDCs incubated with CpG-GNPs (C).

3.2.3 Visualization of CpG-GNP uptake by CLSM

Although the current FACS data indicated that CpG-GNPs are efficiently taken up by MDCs, we performed CLSM experiments to exactly localize these formulations. This time, MDCs in the chamber slides were identified by CD11c antibody-staining. Scanning various planar sections, CpG ODN-loaded and Texas Red-X-labeled nanoparticles (ZWCaTEX) could be observed as distinct dots within the cells (Fig. 7A). Furthermore, inhibition of nanoparticle uptake by MDCs following treatment with phagocytosis inhibitor Cytochalasin B revealed that phagocytosis was the main mechanism involved in the nanoparticle uptake process (Fig. 7B).

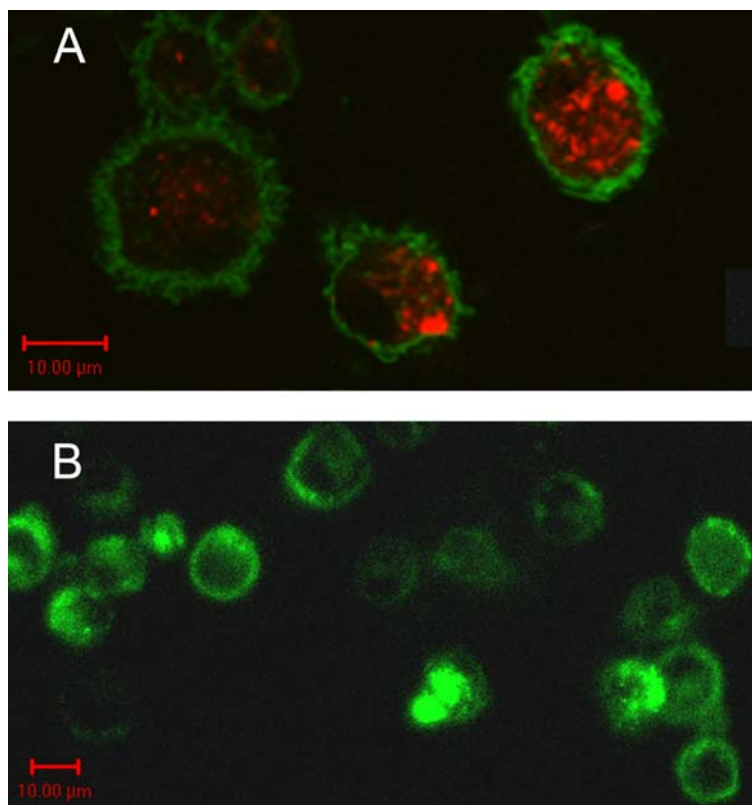


Fig. 7: CLSM images of MDCs incubated with fluorescent CpG-GNPs (A) and MDCs treated with Cytochalasin B before and during incubation with CpG-GNPs (B)

3.2.4 Phenotypic maturation of MDCs following treatment with CpG-GNPs

Subsequent to the recognition of a danger signal, immature MDCs upregulate their surface expression of MHC and co-stimulatory molecules and transform into mature MDCs. In the current study, the efficiency of CpG-GNPs to activate MDCs was investigated based on the augmentation in expression of MHC class II and CD86 molecules. As shown in Fig. 8, MDCs treated with CpG-GNPs upregulated their expression of MHC-II and CD86 molecules. These results thus indicated that delivery of CpG ODN loaded onto cationized gelatin nanoparticles could efficiently activate MDCs and cause their maturation.

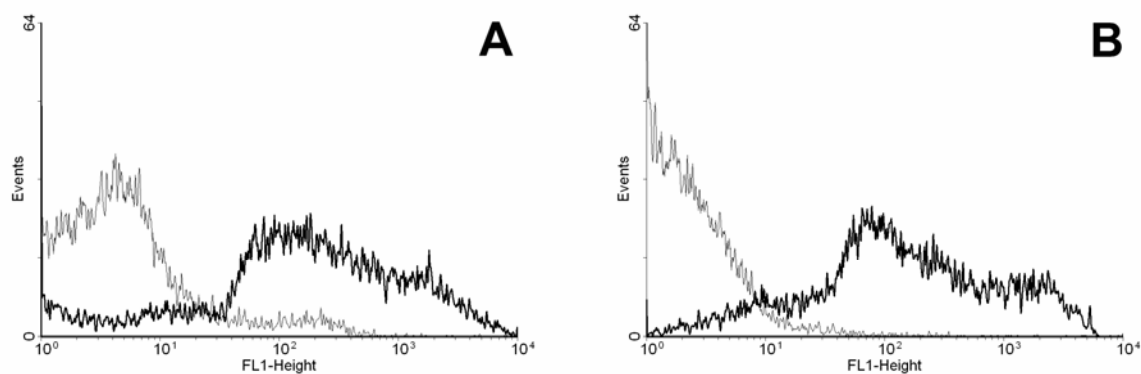


Fig. 8: FACS histogram plots (FL-1 Height); A: MHC II antibody staining; untreated MDCs (grey) vs. CpG-GNP treated MDCs (black); B: CD 86 antibody staining; untreated MDCs (grey) vs. CpG-GNP treated MDCs (black)

3.2.5 Cytokine secretion following treatment of MDCs with CpG-GNPs

The transformation of phenotypically immature MDCs to mature following treatment with CpG-GNPs prompted the assessment of the functionality of these MDCs with regard to their cytokine secretion profile. To qualitatively determine the type of cytokines and chemokines being secreted, the supernatants of the MDC cultures treated with the different CpG ODN formulations were initially screened with cytokine microarray membranes (TranSignalTM Mouse Cytokine Antibody Arrays, Panomics, Redwood City, USA) (Fig. 9).

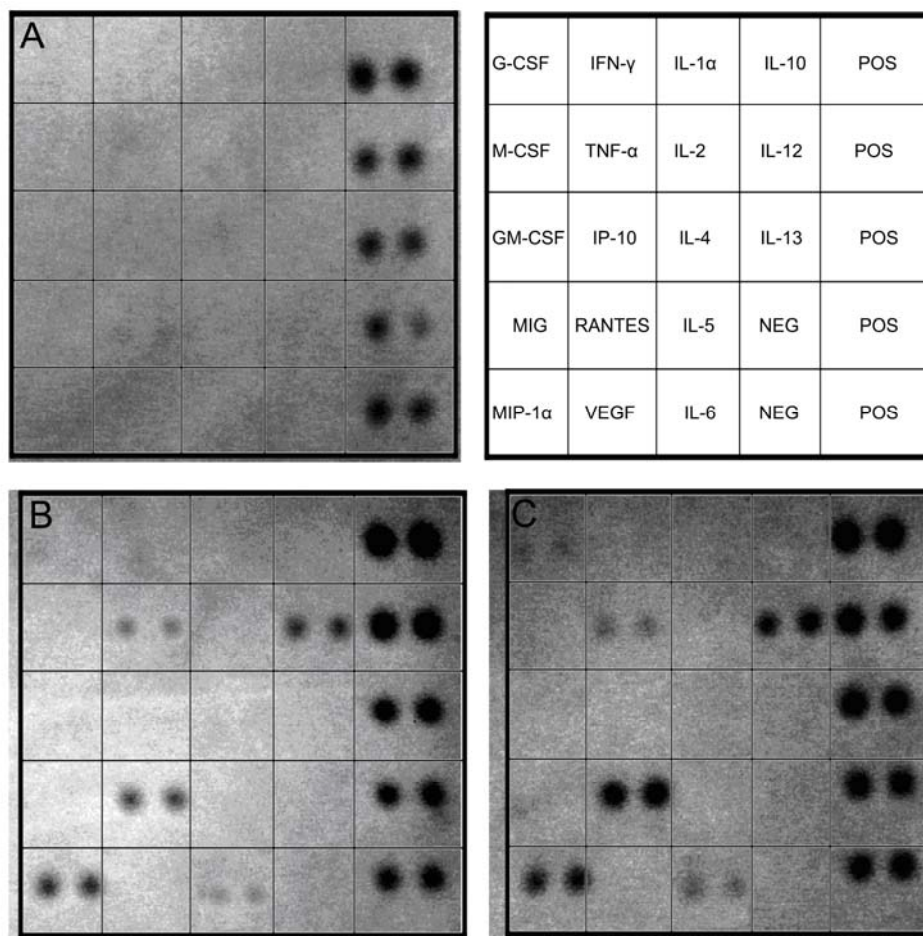


Fig. 9: Qualitative microarray membrane analysis of the secreted cytokines and chemokines when treated with plain cationized GNP (A), soluble CpG ODN (B), and CpG-GNPs (C).

No detectable cytokine secretion could be observed following treatment with plain nanoparticles (Fig. 9A) whereas soluble CpG ODN treatment induced the secretion of IL-6, IL-12p40/70, TNF- α , and chemokines like RANTES (regulated upon activation, normal T cell expressed and secreted) and macrophage inflammatory protein 1 α (MIP-1 α) (Fig. 9B). MDCs treated with CpG-GNPs qualitatively had the same cytokine and chemokine secretion profile as soluble CpG ODN. Overall, the cytokine and chemokine secretion patterns correlated with previously described induction patterns polarizing the stimulation towards T_H1-type immune response (Jakob *et al.* 1999; Krieg 2002) (Fig. 9C). T_H2-polarizing cytokines such as IL-4, IL-5, or IL-10 could not be detected in any of the cell supernatants.

Based on these data we decided to perform quantitative ELISAs of IL-12, IL-6 and TNF- α to receive detailed information on the particular cytokine amounts secreted

after 24 hours. In all of these experiments, no measurable amounts of the cytokines could be detected in the supernatants of the untreated control cells and cells treated with plain gelatin nanoparticles or gelatin nanoparticles loaded with non-stimulating ODN (Fig. 10A-C).

IL-12 is the key cytokine directing immune response towards T_H1 . Two subtypes of IL-12 do exist, IL-12p40 and its bioreactive heterodimer IL-12p70. To get more precise information about the actual T_H1 polarization potential, it was decided to quantify only the rare bioreactive IL-12p70 (Fig. 10A).

Collecting cell supernatants of the samples after 24 hours, 266 ± 53 pg/mL IL-12p70 was secreted by MDCs following stimulation with $10 \mu\text{g}$ ($2 \mu\text{g/mL}$) soluble CpG ODN whereas the two batches of CpG-GNPs were able to induce the secretion of averaging 595 ± 107 pg/mL (ZWCa01) and 690 ± 56 pg/mL (ZWCa02). So we achieved 2-3 fold cytokine induction by loading CpG ODN onto 244.8 nm sized gelatin nanoparticles (ZWCa02). TNF- α which is a key inflammatory cytokine that induces MDC maturation (Arrighi *et al.* 2001; Iijima *et al.* 2003) was minimally secreted following soluble CpG ODN treatment whereas CpG ODN loading onto nanoparticles increased its secretion 7-9 times (Fig. 10B). Again, the larger sized nanoparticles (ZWCa02) resulted with a slightly higher signal. Lastly, no significant difference in the secretion of IL-6 by MDCs was observed following delivery of CpG ODN in nanoparticulate or soluble form (Fig. 10C).

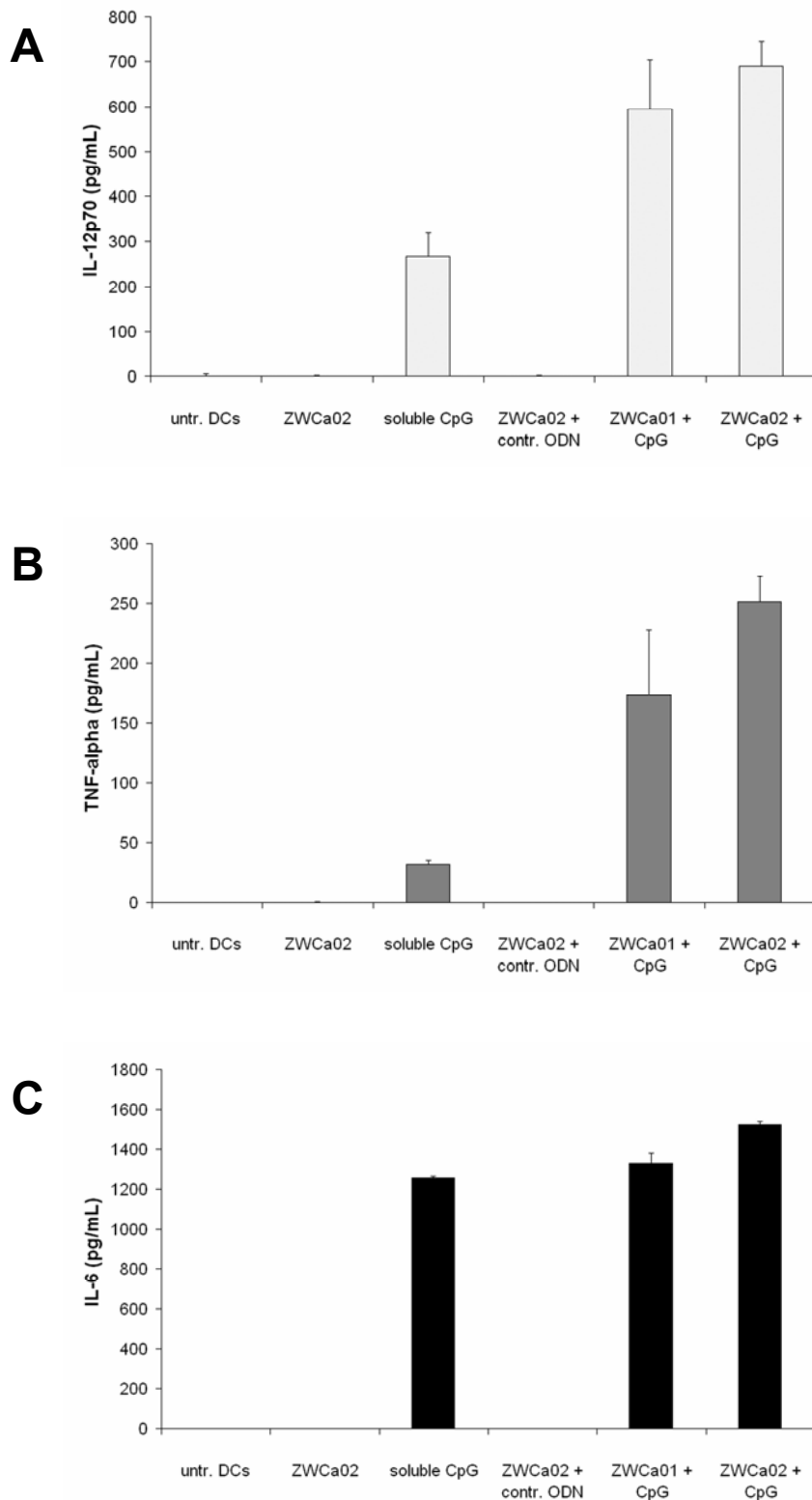


Fig. 10: Levels of IL-12p70 (A), TNF- α (B), and IL-6 (C) per mL cell supernatant after 24 hours incubation: untreated MDCs (untr. DCs); unloaded gelatin nanoparticles ZWCa02 (ZWCa02); soluble CpG ODN (soluble CpG ODN); non-stimulating control ODN-loaded gelatin nanoparticles ZWCa02 (ZWCa02 + CpG); CpG ODN-loaded gelatin nanoparticles ZWCa01 (ZWCa01 + CpG); CpG ODN-loaded gelatin nanoparticles ZWCa02 (ZWCa02 + CpG)

3.2.6 Assessment of CpG-GNP uptake and immune-stimulation kinetics

In cooperation with our partners Dr. Dr. Carole Bourquin and Philip von der Borch (Department of Internal Medicine, Division of Clinical Pharmacology, LMU Munich) we wanted to take a closer look on the respective kinetics of CpG-GNP uptake into MDCs and the related activation of the immune system.

Conducting a critical retrospective of the data we generated so far (see 3.2.1-3.2.5), a certain weakness was the purity of the MDC cell population. Following the described procedure (Lutz *et al.* 1999) generating MDCs from murine bone marrow precursors, implicates a maximum purity of CD11c⁺ MDCs of ~ 80%. Thus, data derived from the whole cell population always contains a certain imprecision. Together with our cooperation partners we were able to isolate highly purified MDC populations via magnetic -activated cell sorting (MACS). The so derived averaging purity of MDCs was between 96-98%.

The first issue we investigated with Alexa FluorTM488-labeled CpG-GNPs were the cellular uptake kinetics of the formulations. The chosen fluorescence dye is excited at comparable wavelengths as fluorescein-isothiocyanate (FITC) but with higher stability against bleaching.

In previous experiments, we had already shown, that plain gelatin nanoparticles (see 3.1) and CpG-GNPs (see 3.2.2) are preferentially taken up by MDCs after 24 h. Now, we wanted to determine the velocity and saturation tendencies of the internalization process.

Incubation of 5×10^4 MDCs with 12 μg CpG-GNPs (containing 600 ng CpG ODN) in 200 μL medium/well (\rightarrow administered CpG ODN concentration: 3 $\mu\text{g}/\text{mL}$) led to an immediate uptake as depicted in Fig. 11.

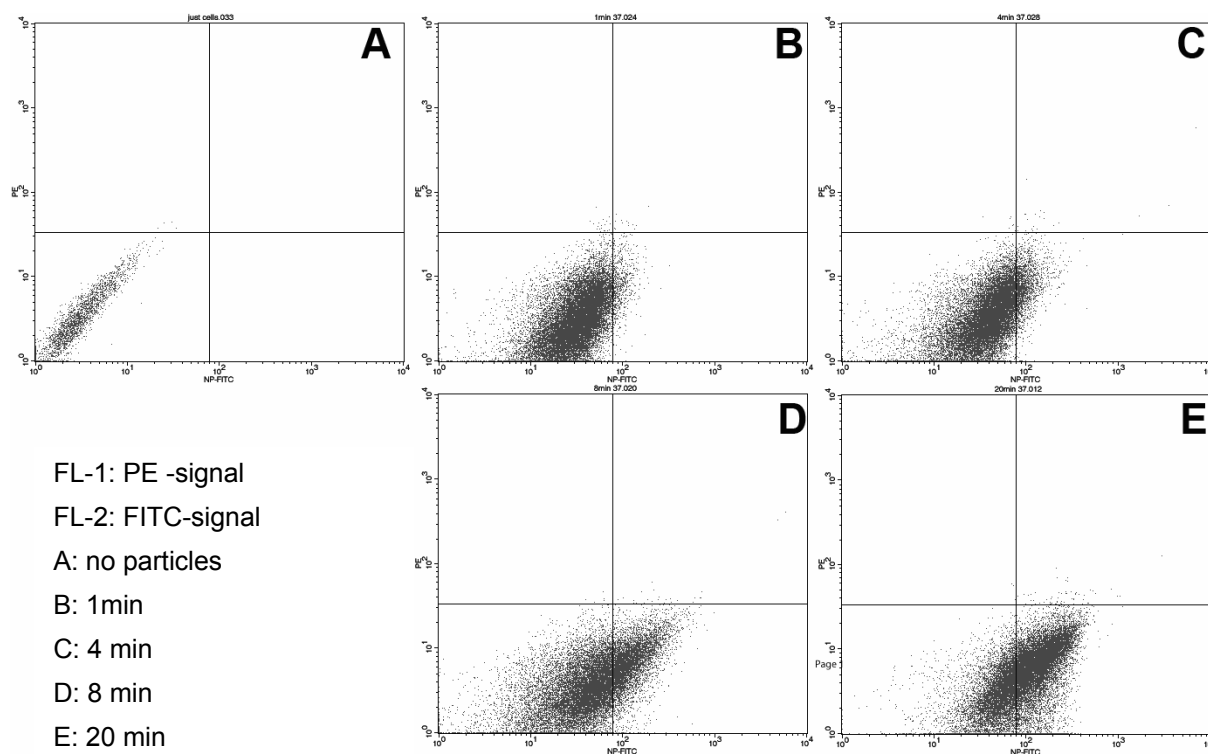


Fig 11: FACS analysis of Alexa Fluor™ 488-labeled CpG-GNP internalization into MDCs (5×10^4 cells) at various points of time; administered amount of CpG-GNPs per well: $12 \mu\text{g}$ (containing 600 ng CpG ODN). FL-1: green FITC-fluorescence (x-axis); FL-2: red PE-fluorescence (y-axis); Lower left quadrant: cells gated as MDCs without nanoparticles; lower right quadrant: cells gated as nanoparticle containing MDCs; upper quadrants: cells that were not considered for calculation.

To give more detailed information on the impact of MDC autofluorescence, it was decided to present the data in a two-dimensional quadrant plot, with additional acquired red PE (Phycoerythrin) FL-2 signal instead of an FL-1 histogram plot view only. Already after 1 min, significant uptake or at least adherence of Alexa Fluor™ 488-labeled CpG-GNPs could be detected by FACS (Fig. 11A). A state of certain saturation was achieved after 20 min (Fig. 11D). From this point, no further cells could be detected positive for CpG-GNPs (data not shown). The respective fluorescence intensities, indicating the uptake of more nanoparticles in cells that have already internalized CpG-GNPs, were also not further increased. The maximum amount of MDCs that were CpG-GNP positive after the administration of $12 \mu\text{g}$ CpG-GNPs per 5×10^4 MDCs, remained constant at $\sim 63\%$ from 20 minutes until the last reading point of the study at 4 h.

In the next experiments the impact of various administered CpG-GNP concentrations on the cellular uptake was screened. It was our aim to determine the maximum *in vitro* administrable amount of CpG-GNPs without causing distinct

cytotoxicity. Starting with a very low concentration of 3 μg CpG-GNPs per 5×10^4 cells in 200 μL medium (Fig. 12B), the administered amount was elevated up to 100 μg CpG-GNPs (Fig. 12E).

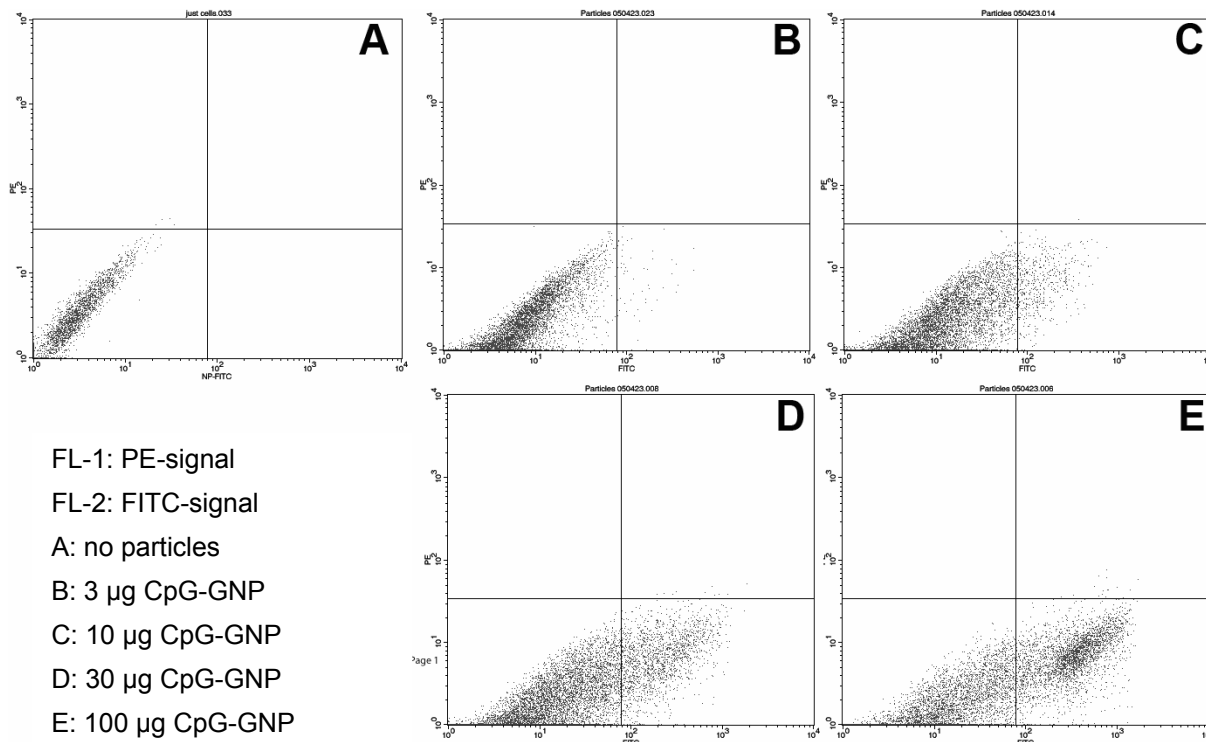


Fig. 12: FACS analysis of Alexa Fluor™ 488-labeled CpG-GNP internalization into MDCs (5×10^4 cells) at various CpG-GNP amounts administered per well; incubation time: 4 h; FL-1: green FITC-fluorescence (x-axis); FL-2: red PE-fluorescence (y-axis); lower left quadrant: cells gated as MDCs without nanoparticles; lower right quadrant: cells gated as nanoparticle containing MDCs; upper quadrants: cells that were not considered for calculation.

Even at this high amount of CpG-GNPs, no significant cytotoxicity was visually detected under the microscope by trypan-blue exclusion. However in contrast to lower administered CpG-GNP amounts, cells treated with 100 μg CpG-GNPs very strongly aggregated and formed cell clusters (Fig. 13), which are undesirable *in vivo* since embolisms might be induced.

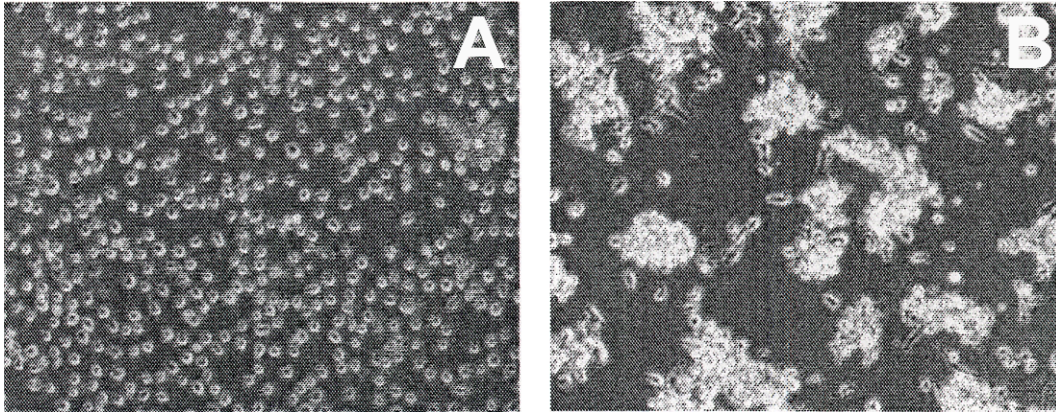
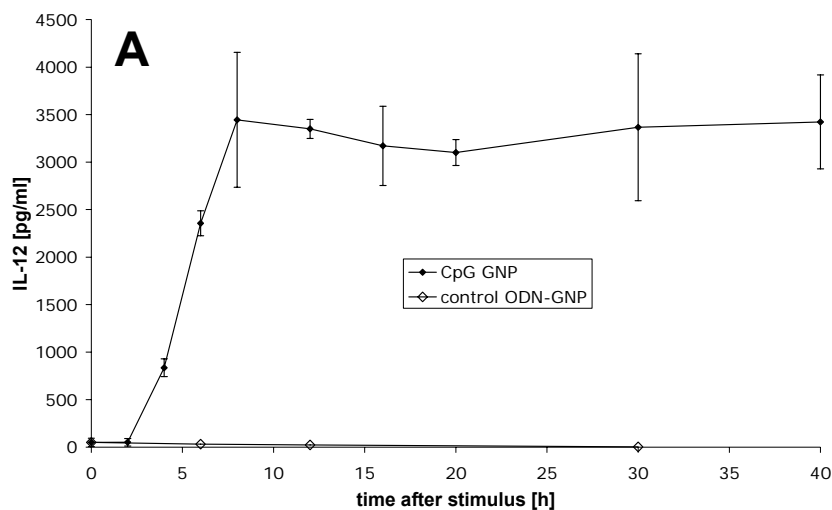


Fig. 13: Micrographs of MDCs (5×10^4 cells) being incubated with various amounts of CpG-GNP after 4 hours of incubation; A: 12 μg CpG-GNPs (containing 600 ng CpG ODN) in 200 μL medium/well; B: 100 μg CpG-GNPs (containing 5 μg CpG ODN) in 200 μL medium/well

Finally, the kinetics of the immune system's activation were investigated. Therefore we analyzed the respective secreted amounts of IL-12p70 (Fig. 14A) and IL-6 (Fig. 14B) at distinct time-points after the addition of CpG-GNPs. After a certain lag time, the secreted amounts of both cytokines increased after 2.5 hours past administration. IL-12 reached a maximum plateau phase after 8 h and was not further elevated until 40 h after administration. For IL-6 this plateau was reached after 12 h.



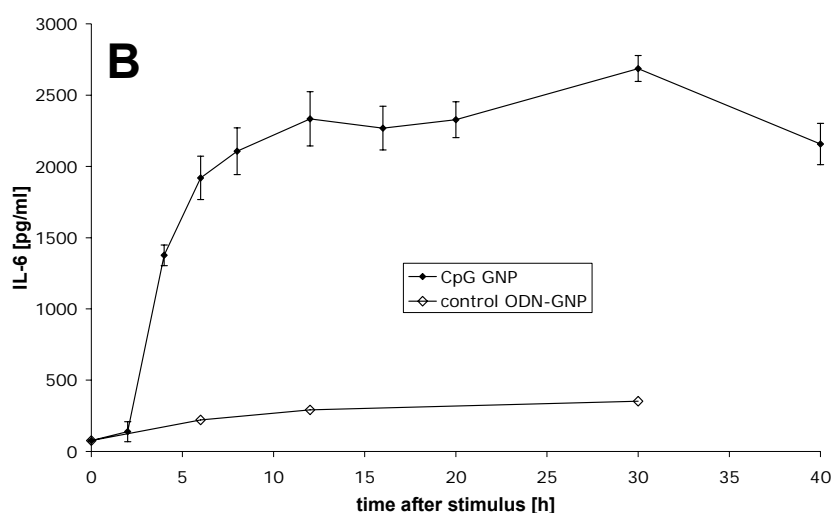


Fig. 14: Cytokine secretion kinetics of CpG-GNPs over 40 h after administration on 5×10^4 MDCs; administered amount: $12 \mu\text{g}$ CpG-GNPs (containing 600 ng CpG ODN) in $200 \mu\text{L}$ medium /well ($n=3$); A: Induction of IL-12p70; B: Induction of IL-6

Comparing the cytokine kinetics data of CpG-GNPs with those from soluble CpG ODN (unpublished data Philip von der Borch), no delay was visible, neither concerning the initial point of cytokine secretion nor the achievement of a plateau-phase. Thus only a higher amount of cytokines was secreted within the same period of time.

Since no delayed signal recognition occurred in case of CpG-GNPs in comparison to soluble CpG ODN, neither release of CpG from the particle surface nor particle degradation seem necessary to allow interaction between CpG ODN and its endosomal receptor TLR9. Apparently, CpG ODNs fixed onto the surface of nanoparticles are able to directly activate TLR9, but in an amplified manner. One explanation for this might be an enhanced phagocytotic uptake of CpG ODN when loaded onto the nanoparticle surface. Another could be that a highly concentrated presentation of CpG motifs on nanoparticles enforces these increased immune reactions.

3.2.7 Discussion and summary

The use of delivery systems for CpG ODNs to enhance the ODNs activity is currently one of the immunological topics that are discussed e.g. to be utilized as adjuvant formulation or as all-in-one vaccine formulation with a co-delivered antigen. In this context, our partners at University of Alberta and others have shown that the immunogenicity can be increased by its delivery in biodegradable

micro- or nanoparticles (Singh *et al.* 2001; Diwan *et al.* 2002; Diwan *et al.* 2004). In this study we used for the first time cationized gelatin nanoparticles as carrier for CpG ODNs. Gelatin offers several advantages as a biomaterial for preparation of colloidal drug carriers. In the current study, we set out to demonstrate that CpG ODN could be efficiently loaded onto cationized gelatin nanoparticles and that these formulations could effectively be internalized by MDCs. A loading ratio between 10:1 and 20:1 (w/w) of nanoparticles to CpG ODN was found to be favorable since the formulations remained stable within physiological media and had a slightly positive net charge. These positively charged nanoparticles have been reported to be better phagocytosed by MDCs and macrophages than neutral or negatively charged particulate formulations (Roser & Kissel 1993; Thiele *et al.* 2001; Foged *et al.* 2005). In agreement with this, MDCs internalized the positively charged CpG ODN nanoparticles more efficiently than the non-cationized gelatin nanoparticles, which have a partially negative ζ potential (see Chapter II - 3.1). CLSM studies showed that the uptake of nanoparticles was inhibited by treatment of MDC cultures with Cytochalasin B, an inhibitor of intracellular actin-myosin polymerization, an essential step in phagocytosis (Davis *et al.* 1971). Thus, the observed uptake of the cationized gelatin particles by MDCs could be assumed to be driven by active phagocytosis, and neither due to mere adherence of the particles to cell surfaces, nor due to pinocytosis. Upregulation of MHC and co-stimulatory molecules on the MDC surface improves the ability of MDCs to activate and prime T cells. The results of our study indicated that CpG ODN loaded onto the gelatin nanoparticles superiorly upregulates MHC-II and CD86 molecules. These data also indicated that MDCs were in their immature state at the time of phagocytosis and CpG that ODN loaded onto the cationized nanoparticles efficiently induced MDC maturation. Similar to soluble CpG ODN which promotes the secretion of T_H1 polarizing cytokines and cytotoxic immune response by MDCs (Chu *et al.* 1997; Krieg *et al.* 2000), CpG-GNPs induced the secretion of IL-12p70, IL-6, and TNF- α . However, the extent of secretion of IL-12p70 and TNF- α was amplified in comparison to soluble CpG ODN treatment. No significant difference in the extent of cytokine secretion was observed for the secretion of IL-6. Since IL-6 is discussed to have adverse effects on the T_H1 differentiation (Diehl & Rincon 2002), this circumstance would favor a bias towards T_H1 immune response even more. Regarding particle size, overall CpG ODN loaded on the batch with larger particle size, ZWCa02 (245.0 nm), induced

slightly higher immune stimulation than loaded on ZWCa01, having a mean size of 135.3 nm. This finding is in agreement with Foged et al. (Foged *et al.* 2005), who tested the phagocytosis activity of various polystyrene particles in a diameter range between 0.04-15 μm and found that particle diameters around 0.5 μm and slightly below were optimal for uptake into MDCs. Consequently, our system might be advantageous compared to already established microparticulate carrier systems.

The absence of cytokine secretion following the treatment of MDC cultures with plain nanoparticles, or control nonstimulatory ODN, indicated a basic biocompatibility of the nanoparticles and the preparation process, as any endotoxin contamination would have triggered cytokine secretion by MDCs.

Investigating the reaction kinetics of CpG-GNP uptake into MDCs, it was noticed that the formulations were quickly internalized within 20 min. The amount of the internalized CpG-GNPs can be influenced by the administered concentration. Congruent to the cell toxicological data we generated for cationized gelatin nanoparticles in gene therapeutic experiments, even huge amounts of CpG-GNPs (100 μg per 2×10^4 MDCs) did not cause significant cell death. However, cell clustering occurred at this high amount of administered CpG-GNPs. So it seems to be advisable to reduce the amount of CpG-GNPs below this value.

Cytokine secretion can be detected within 3-12 h after CpG-GNP administration. In comparison to soluble CpG ODN, no retarded or sustained cell activation could be observed. Thus, CpG ODNs seem to be still attached onto the nanoparticles when interacting with TLR9. This apparently induces enhanced but not prolonged activation of the immune system.

Interestingly, polymers known for their good properties in non-viral gene delivery due to quick endosomal release (e.g. PEI) lead to less activation when administered as polyplex with CpG ODNs than soluble CpG ODN alone (Ilardia *et al.* 2006; unpublished data Dr. Dr. Bourquin). But since TLR9 is located within the endosome, quick endosomal release is undesirable in this case. In pDNA transfection experiments with cationized gelatin nanoparticles, the gene expression occurred with certain delay (see Chapter II). Due to the present CpG ODN data it appears obvious that this delay was caused by sustained endosomal release in comparison to PEI polyplexes. Summarizing, it seems that these properties of choline-modified cationized gelatin nanoparticles that are rather unfavorable for gene transfection, are ideal for CpG ODN delivery.

CpG ODNs are reported to be less toxic than other investigated adjuvants (Weeratna *et al.* 2000). However, other studies have reported dose-dependent systemic adverse effects for CpG ODN (Klinman *et al.* 1996; Lipford *et al.* 2000; Heikenwalder *et al.* 2004). Significant dose reduction would be expected to minimize the risk of side effects of this new class of immune adjuvants. Nanoparticulate CpG ODN delivery decreases the effective dose needed to generate or increase an immune response in the present *in vitro* data.

The present data is a promising first step towards the application of cationized gelatin nanoparticles in the field of immuno therapeutics. Even though, correlation of the murine *in vitro* data with humans or non human primates seems, due to the previously mentioned different cellular distribution of TLR9, doubtful. So, further experiments with primary human B cells and plasmacytoid dendritic cells (PDCs) were indispensable in addition to the present data.

3.3 Transfer from murine setup to primary human cells

DCs are the sentinels of the immune system (Banchereau & Steinman 1998). Within the human body two different phenotypic subtypes of DCs are known in the peripheral blood: myeloid CD11c⁺ DCs (MDCs) and plasmacytoid CD11c⁻ DCs (PDCs). Both of them are containing TLRs. Performing immunological experiments, it is cheap in early stages to gain primary cell cultures for first *in vitro* experiments from murine origin. When transferring *in vitro* experiments to *in vivo*, the species that are chosen for first experiments are mice. Surveying CpG, there is unfortunately a significant discrepancy between humans and rodents concerning the TLR9 expression pattern. TLR9 in humans is in contrast to mice only expressed in PDCs instead of MDCs being utilized in previous experiments (see 3.2). To get an exact correlation of the data it was necessary to substantiate this murine model data with *in vitro* data from human PDCs.

As already mentioned in the introduction, three classes of CpG ODNs have been assessed by scientists. CpG-A ODNs activate the secretion of large amounts of IFN- α in PDCs. CpG-B ODNs are known for the activation of B cells, but are rather poor in inducing the secretion of IFN- α . Finally, CpG-C ODNs can activate both with intermediate strength. Thus, we decided to scrutinize how the activation pattern of the immune response is influenced when the prototypes of each class CpG ODN 2216 (CpG-A), CpG ODN 2006 (CpG-B), and CpG ODN M362 (CpG C) are loaded onto cationized gelatin nanoparticles.

3.3.1 Activation of CpG ODN sensitive human cell-lines after CpG-GNP treatment

Analogous to the *in vitro* experiments with murine MDCs, we compared again two differently sized nanoparticle batches: GNP-H1 (mean size: 160 nm; PI: 0.099) and GNP-H2 (mean size: 293 nm; PI: 0.039). The nanoparticles were loaded with CpG ODN at a ratio of 50 μ g ODN per mg nanoparticles, i.e. 5% (w/w).

In a first experiment, we refrained from further cell purification and measured the secretion of IFN- α of the whole population of primary human peripheral blood mononuclear cells (PBMCs). In analogy to our experiments with murine MDCs, the total amount of CpG ODN administered per well either in soluble form or

bound onto nanoparticles was 600 ng CpG-ODN in 200 μ L media (3 μ g/mL). Each well contained 4×10^5 PBMCs (Fig. 15).

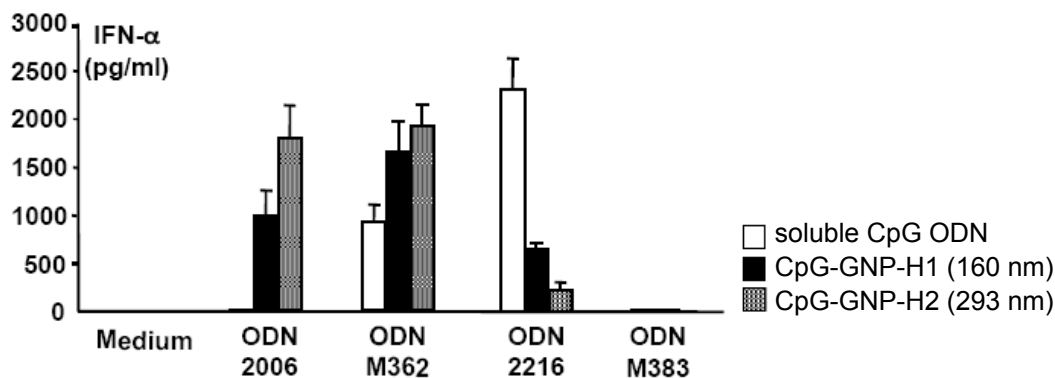


Fig. 15: Induction of IFN- α in human PBMCs (4×10^5 PBMCs/well) after 48h; CpG ODNs were administered in soluble form (white columns) or loaded onto cationized gelatin nanoparticles: CpG-GNP-H1 (black columns, 160 nm) and CpG-GNP-H2 (grey columns; 293 nm). The CpG ODNs tested were CpG-B (ODN 2006), CpG-C (ODN M362), CpG-A (ODN 2216) and the corresponding GpC control ODN (ODN 383) to CpG-C. Results are based on the mean values \pm s.d. of 8 individual experiments each.

Within PBMCs, adsorption of the CpG ODNs 2006 (CpG-B) and M362 (CpG-C) onto nanoparticles led to enhanced stimulation of IFN- α . Soluble CpG-B and CpG-C only led to weak or almost no secretion. More precisely, the IFN- α inducing effect of CpG-C was doubled by particulate administration and in soluble form non-inducing CpG-B was able to induce IFN- α secretion when attached onto nanoparticles. The detected IFN- α amounts were remarkable and reached depending on the applied nanoparticle batch almost the values of soluble CpG-A ODN (ODN 2216), the ‘gold-standard’ CpG ODN for the induction of IFN- α . However, the ability of CpG-A to induce IFN- α was strongly reduced by binding it onto the surface of cationic gelatin nanoparticles.

It could be proven that the presence of CpG motifs is still mandatory for the stimulation of the immune system, since nanoparticles loaded with the corresponding GpC-control ODN (M383) did not induce any stimulation. So, gelatin nanoparticles alone are no stimulus for the IFN- α production in PDCs. Noticeable were the significant differences between the detected amounts of IFN- α when using the two different sized nanoparticle batches CpG ODN loaded

GNP-H2 (293 nm) was far more effective than GNP-H1 (160 nm). These data correlate very well with murine MDC experiments (see 3.2).

To confirm the hypothesis that nanoparticulate bound CpG ODNs behave similar to soluble CpG ODNs and directly stimulate the secretion of IFN- α , the experiments were repeated in purified PDCs. In these experiments, the same amount of CpG ODN was administered (600 ng/200 μ L media) on 5×10^4 purified PDCs per well.

The IFN- α signal augmentation by nanoparticulate formulations of CpG-B ODN and CpG-C ODN could be proven (Fig. 16A). In addition, also the IFN- α pattern of CpG-A ODN and control ODN M383 as determined in PBMC experiments could be reproduced. Depending on the utilized nanoparticle batch, we were able to exceed the IFN- α levels of the ‘gold-standard’, soluble CpG-A ODN 2216.

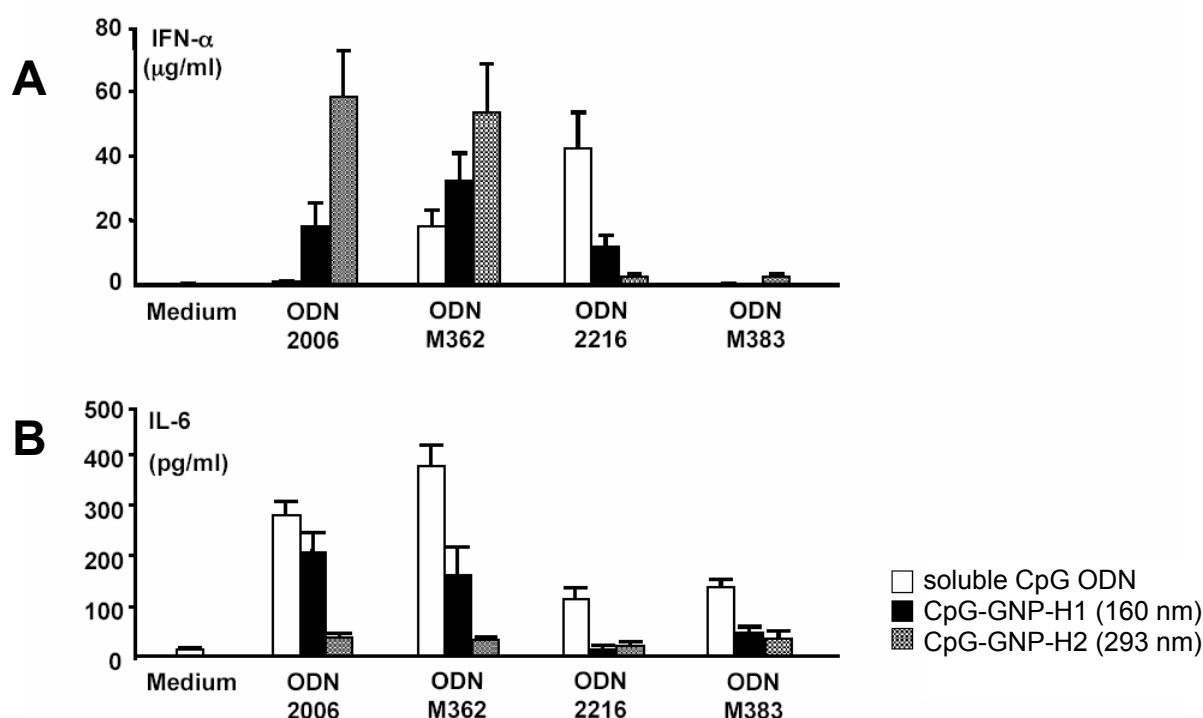


Fig. 16: CpG-GNP induced immunostimulatory activity on PDCs and B cells. Both cell populations were incubated for 48 hours with CpG-GNP formulations. The size of the applied nanoparticle batches was 160 nm and 300 nm; IFN- α was quantified in the supernatants of PDC cultures (A), whereas B cells were analyzed for IL-6 (B). The depicted data represent average values \pm s.d. of 5 individual experiments respectively.

In another experiment we used purified B cells to measure their activation by the formulations, since they are the second cell type that contains TLR9 in humans. In these experiments also 600 ng CpG ODN were administered in 200 μ L medium on 2×10^5 purified B cells per well (Fig. 16B).

CpG-B ODNs and CpG-C ODNs are known to directly activate B cells. Subsequently, B cells start to proliferate and secrete IL-6 as first cytokine after activation with CpG ODNs. The results of the experiments were quite surprising, since no enhanced B cell stimulation was induced with any of the CpG-GNP formulations in comparison to soluble CpG ODN. Moreover the effects of CpG ODNs were attenuated for CpG-GNP-H1 (160 nm) and CpG-GNP-H2 (293 nm) did almost diminish any activation.

Evidently, particulate presentation of CpG-B and CpG-C promotes the activation of TLR9 in PDCs, but simultaneously it also interferes the activation of B cells. An explanation might be that particulate bound CpG ODNs are not taken up into B cells. But, preliminary FACS data indicated that both particulate bound CpG-B ODN and CpG-C ODN in contrast to CpG-A were internalized into B cells in similar quantities as their respective soluble form (data not shown).

3.3.2 Morphological investigations of CpG-A ODN 2216

According to our data, particulate presentation of CpG ODNs is beneficial for the induction of IFN- α in PDCs. Similar findings were just recently published for polystyrene nanoparticles (Kerkmann *et al.* 2005). Concerning the ODN sequences, CpG-A ODN 2216 is the prototype being applied to achieve IFN- α induction in PDCs. This ODN possesses both, a central palindrome sequence and terminal poly(G) motifs at the 5' and 3' end, which are known to enforce the formation of inter- and intra-molecular bonds (Krug *et al.* 2001). Thus, CpG-A spontaneously forms stable nanoparticulate structures under physiological conditions consisting of up to 30 ODN strands (Marshall *et al.* 2003) with an average mean size of 20-100 nm (Costa *et al.* 2004). To verify these statements we performed own DLS and SEM experiments with soluble CpG-A ODN 2216. Measuring the ODN 2216 in sterile filtered PBS resulted in an average mean size of 99.4 nm (PI:0.352). This indicated the presence of quite heterogeneous particulate ODN aggregates. However, the absoluteness of the suggested mean size should not be overestimated because DLS accuracy is limited for such heterogeneous samples.

Surveying vacuum-dried samples of ODN 2216 also revealed particulate ODN aggregates which are apparently the key for the activation of IFN- α secretion in PDCs (Fig. 17).

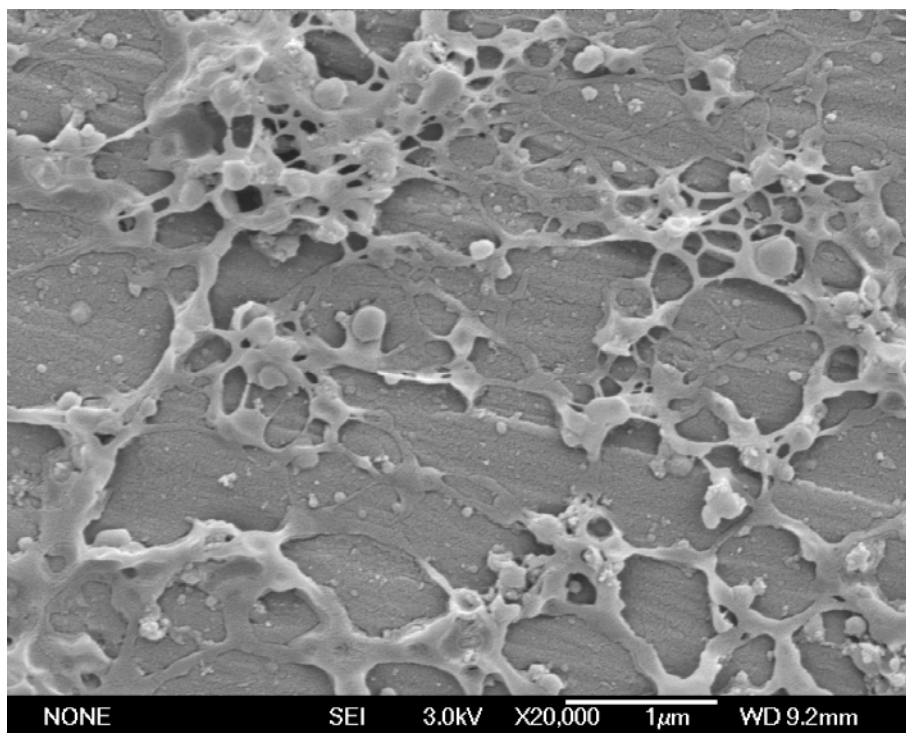


Fig. 17: SEM image of ODN 2216 revealing its particle-like aggregated structure

Overall, the generated DLS and SEM data of CpG-A ODN 2216, were in sound agreement with just recently published data (Costa *et al.* 2004; Kerkmann *et al.* 2005). Moreover, the resolutions achieved in SEM images exceeded those of published AFM images; thus gave new detailed insights on the aggregated morphology of CpG-A ODN 2216.

3.3.3 Effects of CpG ODN-loading on particle mean size and homogeneity

According to our experiments with mouse specific CpG ODN 1826, we simply adopted the established settings for the loading of the human specific CpG ODNs. But since CpG-A ODN 2216 is known for its aggregation tendencies, it was mandatory to monitor if any changes in nanoparticle size occur, when any of the three CpG ODN classes is loaded onto cationized gelatin nanoparticles. As depicted in Table 6, the averaging mean sizes of the nanoparticles did not change, when loading increasing amounts of CpG-B ODN 2006 and CpG-C ODN M362

onto the nanoparticles. The results were analogous to the ones derived from mouse specific CpG ODN 1826. Hence, no aggregation tendencies could be detected up to a payload of 10% (w/w). In contrast to that, enforced aggregation could be monitored with increasing CpG-A ODN amounts already after 30 min of incubation. The occurrence of these huge aggregates is evidently responsible for the hindrance of the immunogenic activation with nanoparticulate bound CpG-A ODN 2216.

Table 6: DLS size determination of cationized gelatin nanoparticles that were loaded with each CpG ODN class in various payloads; incubation time: 30 min in PBS (n=1)

ODN- Payload (w/w)	ODN- type	CpG-A (ODN 2216)	CpG-B (ODN 2006)	CpG-C (ODN M362)
unloaded		209.2 nm	209.2 nm	209.2 nm
2.5%		422.7 nm	208.1 nm	204.2 nm
5%		1203.4 nm	202.1 nm	212.1 nm
7.5%		4100.6 nm	201.2 nm	205.3 nm
10%		6475.8 nm	201.1 nm	199.9 nm

Another aspect we wanted to investigate further was the previously assessed optimum payload of 5% (w/w). For murine MDC experiments, this number was only determined by comparing the measured ζ potential data with the experiences from the *in vitro* gene transfection experiments (Chapter II). Now, the optimum was determined via measuring the ability of various loading ratios to induce IFN- α on PDCs. Performing these experiments with CpG-B ODN and CpG-C ODN, our theoretically predicted optimum payloads were substantiated, since the highest IFN- α amounts were achieved between 5-10% (w/w) (Fig. 18).

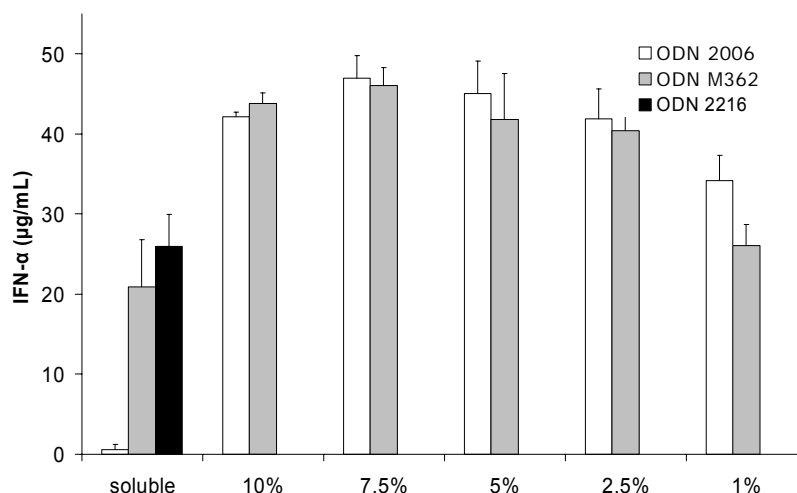


Fig. 18: CpG-GNP induced immunostimulatory activity on PDCs of various applied payloads (1-10%); PDCs were incubated for 48 hours with CpG-GNP formulations or soluble CpG ODNs ($n=3$).

3.3.4 Is enhanced cellular uptake the key for the enhanced activation of the immune system?

Searching for an answer, we performed CLSM and FACS experiments with fluorescence-labeled CpG ODNs. FACS experiments (data not shown) did not show any remarkable differences comparing uptake of ODN 2216, ODN 2006 and nanoparticulate bound ODN 2006. The data even suggested that the uptake of particulate ODN 2006 was slightly lower than that of soluble CpG 2006, which does not induce the release of significant amounts of IFN- α .

CLSM images of soluble CpG-A ODN 2216, particulate bound CpG-B ODN 2006, and soluble CpG-B ODN 2006, proved that all three were internalized into PDCs. Furthermore, no significant differences could be seen concerning the respective amount of ODN that was taken up. Solely, soluble ODN 2006 appears rather diffuse on the images, whereas particulate CpG-B 2006 and soluble ODN 2216 could be identified as distinct dots within PDCs (Fig. 19).

However, some research groups suggest that the enhanced immunogenic activity of CpG ODNs bound onto a particulate or liposomal delivery system is based on an enhanced cellular uptake (Gursel *et al.* 2001; Fearon *et al.* 2003). Whereas other research groups have assessed contrary statements (Marshall *et al.* 2004; Kerkmann *et al.* 2005) in agreement with the data we have generated.

For ODNs containing poly-G-motifs, such as CpG-A ODNs it has been postulated that they are preferentially internalized into APCs thus being more

efficient (Dalpke *et al.* 2002; Gursel *et al.* 2002). It has been described that this enhanced uptake occurs due to the recognition of the polyguanosine-motifs by scavenger receptors (Dalpke *et al.* 2002). But this statement was only proven for macrophages, monocytes, and murine CD11⁺ MDCs (Lee *et al.* 2000; Gursel *et al.* 2002). Recent results revealed that scavenger receptors are not expressed in PDCs (Dr. Simon Rothenfusser, unpublished data).

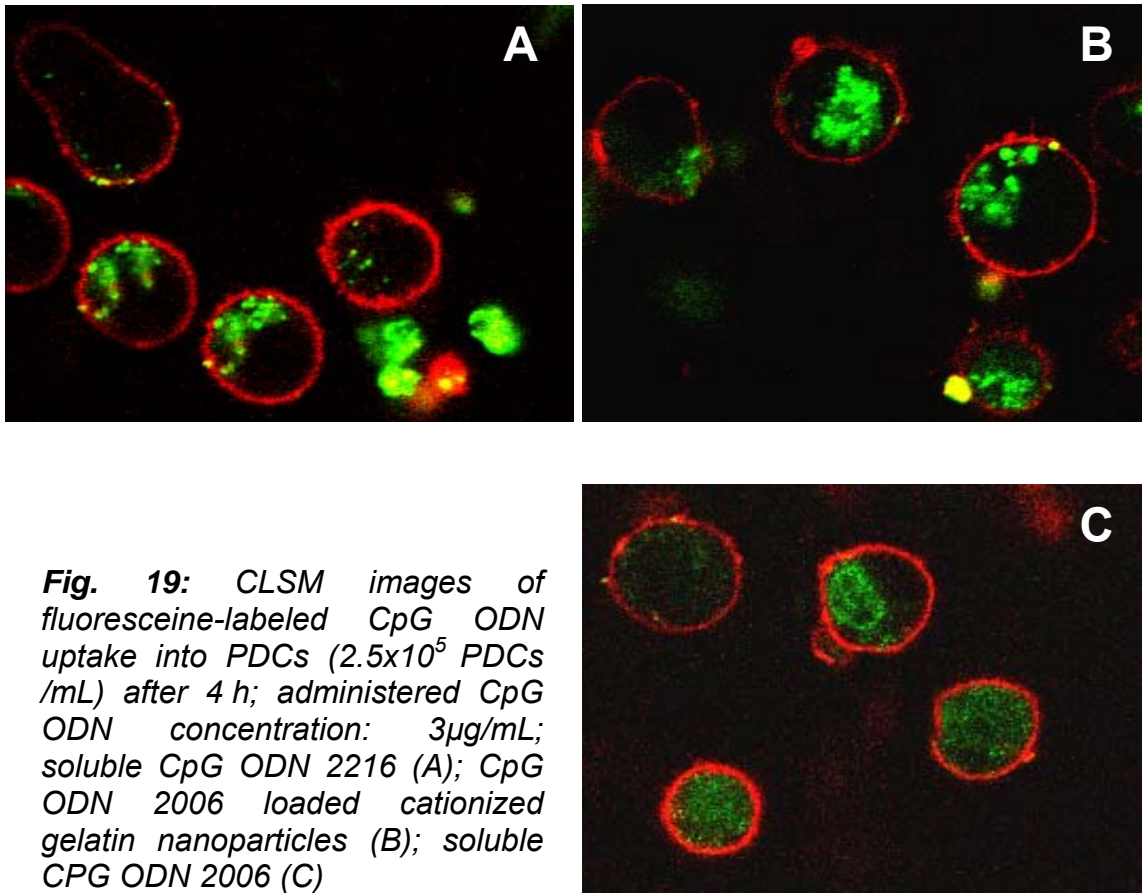


Fig. 19: CLSM images of fluoresceine-labeled CpG ODN uptake into PDCs (2.5×10^5 PDCs/mL) after 4 h; administered CpG ODN concentration: $3 \mu\text{g/mL}$; soluble CpG ODN 2216 (A); CpG ODN 2006 loaded cationized gelatin nanoparticles (B); soluble CPG ODN 2006 (C)

Surveying B cells, preliminary FACS data with soluble CpG ODN and CpG GNP demonstrated that both were internalized into B cells (data not shown). But contrary to PDCs the particulate delivery of CpG ODNs did not induce enhanced secretion of IL-6 the key cytokine of B cell activation (see 3.3 – Fig. 18). Instead, a reduction of the immunogenic effect occurred that was even stronger for larger nanoparticles (~ 300 nm). Thus, the immune stimulation of B cells is induced by conditions converse to those of PDCs.

3.3.5 Discussion and summary

In the present study we demonstrated that CpG-GNPs are internalized into human PDCs and B cells, the respective cells being sensitive for CpG motifs in humans. Based on the results with the various established classes of CpG ODNs for humans, we were able to show that the structural prerequisites for the successful presentation of CpG ODNs to B cells and PDCs differ remarkably. Comparable INF- α levels with CpG-B and CpG-C being adsorbed onto the surface of our cationized nanoparticles indicated that the activation of PDCs is driven by the nanoparticulate structure instead of a specific sequence. These findings are in sound agreement with the results of other research groups using cationic PLGA microparticles (Fearon *et al.* 2003) or microparticles based on the polycationic antibiotic polymyxin B (Marshall *et al.* 2004). Adsorption of CPG-A ODN 2216 on nanoparticles, which possesses already a particulate structure, led to huge aggregates, which are obviously unable to be internalized into PDCs and/or to act as signal transducer. Aside from this structural component, a stimulating sequence with CpG motifs is still necessary to activate PDCs, as proven with the control-ODN M383, which represents the corresponding GpC pendant to ODN M362 (CpG-C) but does not induce any activation of the immune system when being adsorbed onto gelatin nanoparticles.

IFN- α could already be measured after 3 hours when ODN release is not yet expected. Furthermore, CpG ODN could be identified as distinct particles in the CLSM pictures. Thus it can be stated that the interaction with TLR9 apparently occurs while CpG ODN is still attached onto the nanoparticles. This hypothesis was furthermore substantiated by the kinetics data we had previously generated in our murine model (see 3.2.6). Scanning literature, there are further hints that dense and close assembly of CpG motifs on the particles' surface induces clustering of TLR9. Interaction of only one receptor with one ligand represents just a simplified reflection of the actual incidents. Investigations of the interaction between DC and T-cell have demonstrated that the whole scenery is far more complex than what is described in textbooks (Monks *et al.* 1998). A multitude of receptors accumulates in most cases at defined areas of the cell membrane which are called lipid rafts (Pralle *et al.* 2000). This receptor clustering enables enhanced and efficient signal transduction. Other groups have described that multimeric presentation induces crosslinking of TLR9 in PDCs, thus leading to the enhanced secretion of IFN- α .

Consequently, soluble monomeric CpG-B ODN fails to induce significant IFN- α secretion (Fearon *et al.* 2003; Marshall *et al.* 2004; Wu *et al.* 2004). Presumably, the presentation of CpG ODN in particulate matter allows various receptor-ligand interactions and amplifies the transcription of IFN- α .

Thus, an optimized primary sequence for immune stimulation of PDCs such as the one of ODN2216 (palindrome, chimeric backbone, poly-G ends) is not mandatory. CpG-B ODN 2006 attached onto gelatin nanoparticles revealed identical immunogenic activation patterns. The specific ODN sequence is just necessary to form a particulate structure of the CpG ODN by self-assembly. The recognition by TLR9 occurs by the CpG motif alone. Intermediate activation of IFN- α secretion by soluble CpG-C ODNs can be explained with findings that these ODNs tend to form dimers in physiological media due to a central palindrome structure in their ODN sequence (Battiany 2006).

In contrast, the activation of B cells seems mainly to be driven by the sequence of the CpG ODN, whereas particulate delivery seems rather disadvantageous. However, particulate bound CpG-B ODN 2006 and particulate bound CpG-C ODN M362 are still able to activate B cells as well. Apparently, the respective degree of B cell activation depends on the size of the utilized nanoparticles. Nevertheless, the present data demonstrate that optimized activation of B cells and PDCs requires completely different delivery and presentation of CpG ODNs. Possible explanations for these differences might be:

- a) Polymorphic types of TLR9 do exist in PDCs and B cells, which require different structural prerequisites of their particular ligands.
- b) A non-identified CpG co-receptor exists in one of the two cell populations.
- c) TLR9 is located in different compartments of the endosome with different accessibility and/or activation requirements.

Summarizing, CpG-GNP formulations of CpG-B ODN 2006 and CpG-C ODN M362, represent a promising alternative tool to CpG-A ODN 2216 for the endogenous secretion of IFN- α . Even though the induced *in vitro* secretion of these new formulations is only slightly higher than that of CpG-A ODN 2216, CpG-GNPs comprise another aspect which makes this approach so auspicious. The highly defined and reproducible formulation procedure of CpG-GNPs offers exact formulation optimization and will consequently facilitate a future approval by the authorities.

CpG-A ODN 2216 represents an undefined mixture of various secondary and tertiary structures, that consist of different numbers of molecules (Kerkmann *et al.* 2005). Moreover, CpG ODN-A 2216 is also very unstable to external parameters such as freeze-thaw-cycles. These arguments make the development of a future formulation that will fulfil the requests for approval rather difficult.

4. CONCLUSION

We were able to demonstrate that gelatin nanoparticles are efficiently taken up into various APCs. Thus, they possess immense potential as carrier for immunogenic drugs that have their target receptors within these cells. CpG ODNs adsorbed onto the surface of cationized gelatin nanoparticles were a first drug delivery approach we extensively evaluated. Initial murine MDC data demonstrated in detail that this newly established way of CpG ODN delivery leads to strongly enhanced cytokine secretions. The cytokine pattern is still T_H1 and CTL specific such as the one of plain CpG ODNs. Moreover, it could be shown that maturation of the MDCs is intensively induced, thus supporting the overall immune response even more.

Since the recognition of CpG ODNs differs remarkably between humans and rodents, it was essential to proceed from the murine model to primary human cells. Experiments were performed with nanoparticles that were loaded with the three different classes of CpG ODNs that exist for humans. The applied cell-types were primary human B cells and PDCs, the only cells within humans that can recognize CpG ODNs. The data derived from these experiments provided additional precious information on the activation principles of CpG ODNs in humans.

It can be concluded that the respective ODN sequence is responsible for the intensity of B cell activation. Particulate delivery rather attenuates the strength of activation. Consequently, soluble CpG-B and CpG-C ODN are the most appropriate. PDCs, the other cell type being sensitive to CpG ODNs by inducing the production of IFN- α and indirectly T_H1 /CTL-supportive cytokine milieu, behaves completely converse to B cells. For this cell line particulate presentation of CpG ODN could be demonstrated to be favorable in congruency with previous murine MDC data. Thereby, the importance of a specific ODN sequence could be disproved. Solely the presence of CpG-motifs is essential. The sequence of CpG-A ODN, which was originally stated as optimum PDC activator is not essential for ideal receptor activation. Instead, this specific sequence facilitates only the formation of colloidal particles via self-assembly in physiological media. The key for efficient TLR9 stimulation in PDCs is the presentation of CpG motifs in particulate form. Presentation of the other two CpG ODN classes in particulate form by attaching them onto cationized gelatin nanoparticles, led to comparable or even better activation of IFN- α secretion. Present *in vitro* data suggest cationized gelatin nanoparticles with an averaging diameter of ~ 300 nm and a payload of 5-

10% (w/w) are most promising. Summarizing, CpG-B/CpG-C ODNs adsorbed onto cationized gelatin nanoparticles bear great potential as new immunogenic formulations. Consequently, the very positive and comprehensive *in vitro* results recommended the straight forward proceeding to investigate this new established approach *in vivo* (see Chapter IV).

5. REFERENCES

- Alexopoulou, L., Holt, A. C., Medzhitov, R., and Flavell, R. A.; (2001) Recognition of double-stranded RNA and activation of NF-kappaB by Toll-like receptor 3. *NATURE*, 413[6857], 732-738.
- Arrighi, J. F., Rebsamen, M., Rousset, F., Kindler, V., and Hauser, C.; (2001) A critical role for p38 mitogen-activated protein kinase in the maturation of human blood-derived dendritic cells induced by lipopolysaccharide, TNF- α , and contact sensitizers. *JOURNAL OF IMMUNOLOGY*, 166[6], 3837-3845.
- Ashkar, A. A., Bauer, S., Mitchell, W. J., Vieira, J., and Rosenthal, K. L.; (2003) Local delivery of CpG oligodeoxynucleotides induces rapid changes in the genital mucosa and inhibits replication, but not entry, of herpes simplex virus type 2. *JOURNAL OF VIROLOGY*, 77[16], 8948-8956.
- Ballas, Z. K., Krieg, A. M., Warren, T., Rasmussen, W., Davis, H. L., Waldschmidt, M., and Weiner, G. J.; (2001) Divergent therapeutic and immunologic effects of oligodeoxynucleotides with distinct CpG motifs. *JOURNAL OF IMMUNOLOGY*, 167[9], 4878-4886.
- Banchereau, J. and Steinman, R. M.; (1998) Dendritic cells and the control of immunity. *NATURE*, 392[6673], 245-252.
- Battiany, J.; (2006) Identifizierung einer neuen CpG-Oligonukleotidklasse und deren Wirkung auf B-Zellen und plasmazytoide dendritische Zellen. Dissertation, Munich.
- Bird, A. P., Taggart, M. H., Nicholls, R. D., and Higgs, D. R.; (1987) Non-methylated CpG-rich islands at the human alpha-globin locus: implications for evolution of the alpha-globin pseudogene. *EMBO JOURNAL*, 6, 999-1004.
- Bourquin, C., Schreiber, S., Beck, S., Hartmann, G., and Endres, S.; (2006) Immunotherapy with dendritic cells and CpG oligonucleotides can be combined with chemotherapy without loss of efficacy in a mouse model of colon cancer. *INTERNATIONAL JOURNAL OF CANCER*, 118[11], 2790-2795.
- Chu, R. S., Targoni, O. S., Krieg, A. M., Lehmann, P. V., and Harding, C. V.; (1997) CpG oligodeoxynucleotides act as adjuvants that switch on T helper 1 (Th1) immunity. *JOURNAL OF EXPERIMENTAL MEDICINE*, 186[10], 1623-1631.
- Coley, W. B.; (1893, republished 1991) The treatment of malignant tumors by repeated inoculations of erysipelas. With a report of ten original cases. *CLINICAL ORTHOPAEDICS AND RELATED RESEARCH*, 262, 3-11.
- Cooper, C. L., Davis, H. L., Morris, M. L., Efler, S. M., Al Adhami, M., Krieg, A. M., Cameron, D. W., and Heathcote, J.; (2004a) CPG 7909, an Immunostimulatory TLR9 Agonist Oligodeoxynucleotide, as Adjuvant to Engerix-B HBV Vaccine in Healthy Adults: A Double-Blind Phase I/II Study. *JOURNAL OF CLINICAL IMMUNOLOGY*, 24[6], 693-701.
- Cooper, C. L., Davis, H. L., Morris, M. L., Efler, S. M., Krieg, A. M., Li, Y., Laframboise, C., Al Adhami, M. J., Khaliq, Y., Seguin, I., and Cameron, D. W.; (2004b) Safety and immunogenicity of CPG 7909 injection as an adjuvant to Fluarix influenza vaccine. *VACCINE*, 22[23-24], 3136-3143.

Costa, L. T., Kerkmann, M., Hartmann, G., Endres, S., Bisch, P. M., Heckl, W. M., and Thalhammer, S.; (2004) Structural studies of oligonucleotides containing G-quadruplex motifs using AFM. *BIOCHEMICAL AND BIOPHYSICAL RESEARCH COMMUNICATIONS*, 313[4], 1065-1072.

Dalpke, A. H., Zimmermann, S., Albrecht, I., and Heeg, K.; (2002) Phosphodiester CpG oligonucleotides as adjuvants: polyguanosine runs enhance cellular uptake and improve immunostimulative activity of phosphodiester CpG oligonucleotides in vitro and in vivo. *IMMUNOLOGY*, 106[1], 102-112.

Davis, A. T., Estensen, R., and Quie, P. G.; (1971) Cytochalasin B. III. Inhibition of human polymorphonuclear leukocyte phagocytosis. *PROCEEDINGS OF THE SOCIETY FOR EXPERIMENTAL BIOLOGY AND MEDICINE*, 137[1], 161-164.

Diehl, S. and Rincon, M.; (2002) The two faces of IL-6 on Th1/Th2 differentiation. *MOLECULAR IMMUNOLOGY*, 39[9], 531-536.

Diwan, M., Elamanchili, P., Cao, M., and Samuel, J.; (2004) Dose sparing of CpG oligodeoxynucleotide vaccine adjuvants by nanoparticle delivery. *CURRENT DRUG DELIVERY*, 1[4], 405-412.

Diwan, M., Tafaghodi, M., and Samuel, J.; (2002) Enhancement of immune responses by co-delivery of a CpG oligodeoxynucleotide and tetanus toxoid in biodegradable nanospheres. *JOURNAL OF CONTROLLED RELEASE*, 85, 247-262.

Eastcott, J. W., Holmberg, C. J., Dewhirst, F. E., Esch, T. R., Smith, D. J., and Taubman, M. A.; (2001) Oligonucleotide containing CpG motifs enhances immune response to mucosally or systemically administered tetanus toxoid. *VACCINE*, 19[13-14], 1636-1642.

Elamanchili, P., Diwan, M., Cao, M., and Samuel, J.; (2004) Characterization of poly(D,L-lactic-co-glycolic acid) based nanoparticulate system for enhanced delivery of antigens to dendritic cells. *VACCINE*, 22[19], 2406-2412.

Elkins, K. L., Rhinehart-Jones, T. R., Stibitz, S., Conover, J. S., and Klinman, D. M.; (1999) Bacterial DNA containing CpG motifs stimulates lymphocyte-dependent protection of mice against lethal infection with intracellular bacteria. *JOURNAL OF IMMUNOLOGY*, 162[4], 2291-2298.

Fearon, K., Marshall, J. D., Abbate, C., Subramanian, S., Yee, P., Gregorio, J., Teshima, G., Ott, G., Tuck, S., Van Nest, G., and Coffman, R. L.; (2003) A minimal human immunostimulatory CpG motif that potently induces IFN- γ and IFN- α production. *EUROPEAN JOURNAL OF IMMUNOLOGY*, 33[8], 2114-2122.

Foged, C., Brodin, B., Frokjaer, S., and Sundblad, A.; (2005) Particle size and surface charge affect particle uptake by human dendritic cells in an in vitro model. *INTERNATIONAL JOURNAL OF PHARMACEUTICS*, 298[2], 315-322.

Gramzinski, R. A., Doolan, D. L., Sedegah, M., Davis, H. L., Krieg, A. M., and Hoffman, S. L.; (2001) Interleukin-12- and gamma interferon-dependent protection against malaria conferred by CpG oligodeoxynucleotide in mice. *INFECTION AND IMMUNITY*, 69[3], 1643-1649.

Gursel, I., Gursel, M., and Klinman, D. M.; (2001) In vivo immune responses induced by CpG oligonucleotides encapsulated in sterically stabilized cationic liposomes. 28th International

Symposium on Controlled Release of Bioactive Materials and 4th Consumer & Diversified Products Conference, San Diego, USA, Conference Proceeding, 1057-1058.

Gursel, M., Verthelyi, D., Gursel, I., Ishii, K. J., and Klinman, D. M.; (2002) Differential and competitive activation of human immune cells by distinct classes of CpG oligodeoxynucleotide. *JOURNAL OF LEUKOCYTE BIOLOGY*, 71[5], 813-820.

Halperin, S. A., Van Nest, G., Smith, B., Abtahi, S., Whiley, H., and Eiden, J. J.; (2003) A phase I study of the safety and immunogenicity of recombinant hepatitis B surface antigen co-administered with an immunostimulatory phosphorothioate oligonucleotide adjuvant. *VACCINE*, 21[19-20], 2461-2467.

Hartmann, G. and Krieg, A. M.; (2000) Mechanism and function of a newly identified CpG DNA motif in human primary B cells. *JOURNAL OF IMMUNOLOGY*, 164[2], 944-953.

Hartmann, G., Battiany, J., Poeck, H., Wagner, M., Kerkmann, M., Lubenow, N., Rothenfusser, S., and Endres, S.; (2003) Rational design of new CpG oligonucleotides that combine B cell activation with high IFN- α induction in plasmacytoid dendritic cells. *EUROPEAN JOURNAL OF IMMUNOLOGY*, 33[6], 1633-1641.

Hayashi, F., Smith, K. D., Ozinsky, A., Hawn, T. R., Yi, E. C., Goodlett, D. R., Eng, J. K., Akira, S., Underhill, D. M., and Aderem, A.; (2001) The innate immune response to bacterial flagellin is mediated by Toll-like receptor 5. *NATURE*, 410[6832], 1099-1103.

Heckelsmiller, K., Rall, K., Beck, S., Schlamp, A., Seiderer, J., Jahrsdorfer, B., Krug, A., Rothenfusser, S., Endres, S., and Hartmann, G.; (2002) Peritumoral CpG DNA elicits a coordinated response of CD8 T cells and innate effectors to cure established tumors in a murine colon carcinoma model. *JOURNAL OF IMMUNOLOGY*, 169[7], 3892-3899.

Heikenwalder, M., Polymenidou, M., Junt, T., Sigurdson, C., Wagner, H., Akira, S., Zinkernagel, R., and Aguzzi, A.; (2004) Lymphoid follicle destruction and immunosuppression after repeated CpG oligodeoxynucleotide administration. *NATURE MEDICINE*, 10[2], 187-192.

Hemmi, H., Takeuchi, O., Kawai, T., Kaisho, T., Sato, S., Sanjo, H., Matsumoto, M., Hoshino, K., Wagner, H., Takeda, K., and Akira, S.; (2000) A Toll-like receptor recognizes bacterial DNA. *NATURE*, 408[6813], 740-745.

Hornung, V., Rothenfusser, S., Britsch, S., Krug, A., Jahrsdorfer, B., Giese, T., Endres, S., and Hartmann, G.; (2002) Quantitative expression of Toll-like receptor 1-10 mRNA in cellular subsets of human peripheral blood mononuclear cells and sensitivity to CpG oligodeoxynucleotides. *JOURNAL OF IMMUNOLOGY*, 168[9], 4531-4537.

Hornung, V., Schlender, J., Guenther-Biller, M., Rothenfusser, S., Endres, S., Conzelmann, K., and Hartmann, G.; (2004) Replication-dependent potent IFN- α induction in human plasmacytoid dendritic cells by a single-stranded RNA virus. *JOURNAL OF IMMUNOLOGY*, 173[10], 5935-5943.

Hoshino, K., Takeuchi, O., Kawai, T., Sanjo, H., Ogawa, T., Takeda, Y., Takeda, K., and Akira, S.; (1999) Cutting edge: Toll-like receptor 4 (TLR4)-deficient mice are hyporesponsive to lipopolysaccharide: evidence for TLR4 as the LPS gene product. *JOURNAL OF IMMUNOLOGY*, 162[7], 3749-3752.

Iijima, N., Yanagawa, Y., and Onoe, K.; (2003) Role of early- or late-phase activation of p38 mitogen-activated protein kinase induced by tumour necrosis factor- α or 2,4-dinitrochlorobenzene during maturation of murine dendritic cells. *IMMUNOLOGY*, 110[3], 322-328.

Ilardia, D., Martinez, R., Gamazo, C., Irache, J. M., and Espuelas, S.; (2006) Encapsulation of CpG oligonucleotides in Gantrez AN nanoparticles: Study of integrity and in vitro activation of mice bone marrow derived dendritic cells. World Meeting on Pharmaceutics, Biopharmaceutics and Pharmaceutical Technology, Geneva, Switzerland, Conference Proceeding.

Jakob, T., Walker, P. S., Krieg, A. M., Von Stebut, E., Udey, M. C., and Vogel, J. C.; (1999) Bacterial DNA and CpG-containing oligodeoxynucleotides activate cutaneous dendritic cells and induce IL-12 production: implications for the augmentation of Th1 responses. *INTERNATIONAL ARCHIVES OF ALLERGY AND IMMUNOLOGY*, 118[2-4], 457-461.

Joseph, A., Louria-Hayon, I., Plis-Finarov, A., Zeira, E., Zakay-Rones, Z., Raz, E., Hayashi, T., Takabayashi, K., Barenholz, Y., and Kedar, E.; (2002) Liposomal immunostimulatory DNA sequence (ISS-ODN): an efficient parenteral and mucosal adjuvant for influenza and hepatitis B vaccines. *VACCINE*, 20[27-28], 3342-3354.

Jurk, M., Heil, F., Vollmer, J., Schetter, C., Krieg, A. M., Wagner, H., Lipford, G., and Bauer, S.; (2002) Human TLR7 or TLR8 independently confer responsiveness to the antiviral compound R-848. *NATURE IMMUNOLOGY*, 3[6], 499.

Kaisho, T. and Akira, S.; (2002) Toll-like receptors as adjuvant receptors. *BIOCHIMICA ET BIOPHYSICA ACTA*, 1589[1], 1-13.

Kerkmann, M., Costa, L. T., Richter, C., Rothenfusser, S., Battiany, J., Hornung, V., Johnson, J., Englert, S., Ketterer, T., Heckl, W., Thalhammer, S., Endres, S., and Hartmann, G.; (2005) Spontaneous Formation of Nucleic Acid-based Nanoparticles Is Responsible for High Interferon- α Induction by CpG-A in Plasmacytoid Dendritic Cells. *JOURNAL OF BIOLOGICAL CHEMISTRY*, 280[9], 8086-8093.

Kline, J. N., Waldschmidt, T. J., Businga, T. R., Lemish, J. E., Weinstock, J. V., Thorne, P. S., and Krieg, A. M.; (1998) Modulation of airway inflammation by CpG oligodeoxynucleotides in a murine model of asthma. *JOURNAL OF IMMUNOLOGY*, 160[6], 2555-2559.

Klinman, D. M., Yi, A. K., Beaucage, S. L., Conover, J., and Krieg, A. M., (1996) CpG motifs present in bacteria DNA rapidly induce lymphocytes to secrete interleukin 6, interleukin 12, and interferon gamma. *PROCEEDINGS OF THE NATIONAL ACADEMY OF SCIENCES OF THE UNITED STATES OF AMERICA*, 93[7], 2879-2883.

Klinman, D. M.; (2004) Immunotherapeutic uses of CpG oligodeoxynucleotides. *NATURE REVIEWS. IMMUNOLOGY*, 4[4], 249-258.

Klinman, D. M., Conover, J., and Coban, C.; (1999) Repeated administration of synthetic oligodeoxynucleotides expressing CpG motifs provides long-term protection against bacterial infection. *INFECTION AND IMMUNITY*, 67[11], 5658-5663.

Krieg, A. M., Hartmann, G., and Yi, A. K.; (2000) Mechanism of action of CpG DNA. *CURRENT TOPICS IN MICROBIOLOGY AND IMMUNOLOGY*, 247, 1-21.

- Krieg, A. M.; (2002) CpG motifs in bacterial DNA and their immune effects. *ANNUAL REVIEW OF IMMUNOLOGY*, 20, 709-760.
- Krieg, A. M., Love-Homan, L., Yi, A. K., and Harty, J. T.; (1998) CpG DNA induces sustained IL-12 expression in vivo and resistance to *Listeria monocytogenes* challenge. *JOURNAL OF IMMUNOLOGY*, 161[5], 2428-2434.
- Krieg, A. M., Yi, A. K., Matson, S., Waldschmidt, T. J., Bishop, G. A., Teasdale, R., Koretzky, G. A., and Klinman, D. M.; (1995) CpG motifs in bacterial DNA trigger direct B-cell activation. *NATURE*, 374, 546-549.
- Krug, A., Rothenfusser, S., Hornung, V., Jahrsdorter, B., Blackwell, S., Ballas, Z. K., Endres, S., Krieg, A. M., and Hartmann, G.; (2001) Identification of CpG oligonucleotide sequences with high induction of IFN- α/β in plasmacytoid dendritic cells. *EUROPEAN JOURNAL OF IMMUNOLOGY*, 31, 2154-2163.
- Kuramoto, E., Yano, O., Kimura, Y., Baba, M., Makino, T., Yamamoto, S., Yamamoto, T., Kataoka, T., and Tokunaga, T.; (1992) Oligonucleotide sequences required for natural killer cell activation. *JAPANESE JOURNAL OF CANCER RESEARCH*, 83[11], 1128-1131.
- Kurt-Jones, E. A., Popova, L., Kwinn, L., Haynes, L. M., Jones, L. P., Tripp, R. A., Walsh, E. E., Freeman, M. W., Golenbock, D. T., Anderson, L. J., and Finberg, R. W.; (2000) Pattern recognition receptors TLR4 and CD14 mediate response to respiratory syncytial virus. *NATURE IMMUNOLOGY*, 1[5], 398-401.
- Lee, S. W., Song, M. K., Baek, K. H., Park, Y., Kim, J. K., Lee, C. H., Cheong, H. K., Cheong, C., and Sung, Y. C.; (2000) Effects of a hexameric deoxyriboguanosine run conjugation into CpG oligodeoxynucleotides on their immunostimulatory potentials. *JOURNAL OF IMMUNOLOGY*, 165[7], 3631-3639.
- Lipford, G. B., Sparwasser, T., Zimmermann, S., Heeg, K., and Wagner, H.; (2000) CpG-DNA-mediated transient lymphadenopathy is associated with a state of Th1 predisposition to antigen-driven responses. *JOURNAL OF IMMUNOLOGY*, 165[3], 1228-1235.
- Lutz, M. B., Kukutsch, N., Ogilvie, A. L., Rossner, S., Koch, F., Romani, N., and Schuler, G.; (1999) An advanced culture method for generating large quantities of highly pure dendritic cells from mouse bone marrow. *JOURNAL OF IMMUNOLOGICAL METHODS*, 223[1], 77-92.
- Marshall, J. D., Fearon, K., Abbate, C., Subramanian, S., Yee, P., Gregorio, J., Coffman, R. L., and Van Nest, G.; (2003) Identification of a novel CpG DNA class and motif that optimally stimulate B cell and plasmacytoid dendritic cell functions. *JOURNAL OF LEUKOCYTE BIOLOGY*, 73[6], 781-792.
- Marshall, J. D., Higgins, D., Abbate, C., Yee, P., Teshima, G., Ott, G., dela Cruz, T., Passmore, D., Fearon, K. L., Tuck, S., and Van Nest, G. (2004) Polymyxin B enhances ISS-mediated immune responses across multiple species. *CELLULAR IMMUNOLOGY* 229[2], 93-105.
- Marty, J. J., Oppenheim, R. C., and Speiser, P.; (1978) Nanoparticles - a new colloidal drug delivery system. *PHARMACEUTICA ACTA HELVETIAE*, 53, 17-23.
- Matzinger, P.; (2002) An innate sense of danger. *ANNALS OF THE NEW YORK ACADEMY OF SCIENCES*, 961, 341-342.

- Means, T. K., Wang, S., Lien, E., Yoshimura, A., Golenbock, D. T., and Fenton, M. J.; (1999a) Human toll-like receptors mediate cellular activation by *Mycobacterium tuberculosis*. *JOURNAL OF IMMUNOLOGY*, 163[7], 3920-3927.
- Means, T. K., Lien, E., Yoshimura, A., Wang, S., Golenbock, D. T., and Fenton, M. J.; (1999b) The CD14 ligands lipoarabinomannan and lipopolysaccharide differ in their requirement for toll-like receptors. *JOURNAL OF IMMUNOLOGY*, 163[12], 6748-6755.
- Medzhitov, R. and Janeway, C. A.; (1997a) Innate immunity: impact on the adaptive immune response. *CURRENT OPINION IN IMMUNOLOGY*, 9[1], 4-9.
- Medzhitov, R. and Janeway, C. A.; (1997b) Innate immunity: the virtues of a nonclonal system of recognition. *CELL*, 91[3], 295-298.
- Meng, Y., Carpentier, A. F., Chen, L., Boisserie, G., Simon, J. M., Mazon, J. J., and Delattre, J. Y.; (2005) Successful combination of local CpG-ODN and radiotherapy in malignant glioma. *INTERNATIONAL JOURNAL OF CANCER*, 116[6], 992-997.
- Messina, J. P., Gilkeson, G. S., and Pisetsky, D. S.; (1991) Stimulation of in vitro murine lymphocyte proliferation by bacterial DNA. *JOURNAL OF IMMUNOLOGY*, 147[6], 1759-1764.
- Milas, L., Mason, K. A., Ariga, H., Hunter, N., Neal, R., Valdecanas, D., Krieg, A. M., and Whisnant, J. K.; (2004) CpG Oligodeoxynucleotide Enhances Tumor Response to Radiation. *CANCER RESEARCH*, 64[15], 5074-5077.
- Moldoveanu, Z., Love-Homan, L., Huang, W. Q., and Krieg, A. M.; (1998) CpG DNA, a novel immune enhancer for systemic and mucosal immunization with influenza virus. *VACCINE*, 16[11-12], 1216-1224.
- Monks, C. R. F., Freiberg, B. A., Kupfer, H., Sciaky, N., and Kupfer, A.; (1998) Three-dimensional segregation of supramolecular activation clusters in T cells. *NATURE*, 395[6697], 82-86.
- Morales, A.; (1978) Adjuvant immunotherapy in superficial bladder cancer. *NATIONAL CANCER INSTITUTE MONOGRAPH*, [49], 315-319.
- Müller, R. H.; (1996) Zetapotential und Partikelladung in der Laborpraxis. Wissenschaftliche Verlagsgesellschaft mbH, Stuttgart.
- Ohashi, K., Burkart, V., Flohe, S., and Kolb, H.; (2000) Cutting edge: heat shock protein 60 is a putative endogenous ligand of the toll-like receptor-4 complex. *JOURNAL OF IMMUNOLOGY*, 164[2], 558-561.
- Okamura, Y., Watari, M., Jerud, E. S., Young, D. W., Ishizaka, S. T., Rose, J., Chow, J. C., and Strauss, J. F., III.; (2001) The extra domain A of fibronectin activates Toll-like receptor 4. *THE JOURNAL OF BIOLOGICAL CHEMISTRY*, 276[13], 10229-10233.
- Peiser, Leanne, Mukhopadhyay, Subhankar, and Gordon, Siamon. Scavenger receptors in innate immunity. *CURRENT OPINION IN IMMUNOLOGY*, 14[1], 123-128. 2002.
- Pisetsky, D. S. and Reich, C. F., III.; (1998) The influence of base sequence on the immunological properties of defined oligonucleotides. *IMMUNOPHARMACOLOGY*, 40[3], 199-208.

Poock, H., Wagner, M., Battiany, J., Rothenfusser, S., Wellisch, D., Hornung, V., Jahrsdorfer, B., Giese, T., Endres, S., and Hartmann, G.; (2004) Plasmacytoid dendritic cells, antigen, and CpG-C license human B cells for plasma cell differentiation and immunoglobulin production in the absence of T-cell help. *BLOOD*, 103[8], 3058-3064.

Pralle, A., Keller, P., Florin, E. L., Simons, K., and Horber, J. K. H.; (2000) Sphingolipid-cholesterol rafts diffuse as small entities in the plasma membrane of mammalian cells. *JOURNAL OF CELL BIOLOGY*, 148[5], 997-1007.

Pyles, R. B., Higgins, D., Chalk, C., Zalar, A., Eiden, J., Brown, C., Van Nest, G., and Stanberry, L. R.; (2002) Use of immunostimulatory sequence-containing oligonucleotides as topical therapy for genital herpes simplex virus type 2 infection. *JOURNAL OF VIROLOGY*, 76[22], 11387-11396.

Qureshi, S. T., Lariviere, L., Leveque, G., Clermont, S., Moore, K. J., Gros, P., and Malo, D.; (1999) Endotoxin-tolerant mice have mutations in Toll-like receptor 4 (Tlr4). *THE JOURNAL OF EXPERIMENTAL MEDICINE*, 189[4], 615-625.

Rankin, R., Pontarollo, R., Ioannou, X., Krieg, A. M., Hecker, R., Babiuk, L. A., and van Drunen Littel-van den Hurk.; (2001) CpG motif identification for veterinary and laboratory species demonstrates that sequence recognition is highly conserved. *ANTISENSE & NUCLEIC ACID DRUG DEVELOPMENT*, 11[5], 333-340.

Raychaudhuri, S. and Rock, K. L.; (1998) Fully mobilizing host defense: building better vaccines. *NATURE BIOTECHNOLOGY*, 16[11], 1025-1031.

Robinson, D. S., Hamid, Q., Ying, S., Tsicopoulos, A., Barkans, J., Bentley, A. M., Corrigan, C., Durham, S. R., and Kay, A. B.; (1992) Predominant TH2-like bronchoalveolar T-lymphocyte population in atopic asthma. *THE NEW ENGLAND JOURNAL OF MEDICINE*, 326[5], 298-304.

Roser, M. and Kissel, T.; (1993) Surface-modified biodegradable albumin nano- and microspheres. Part 1. Preparation and characterization. *EUROPEAN JOURNAL OF PHARMACEUTICS AND BIOPHARMACEUTICS*, 39, 8-12.

Rothenfusser, S., Hornung, V., Krug, A., Towarowski, A., Krieg, A. M., Endres, S., and Hartmann, G.; (2001) Distinct CpG oligonucleotide sequences activate human gd T cells via interferon-a/-b. *EUROPEAN JOURNAL OF IMMUNOLOGY*, 31[12], 3525-3534.

Rothenfusser, S., Tuma, E., Endres, S., and Hartmann, G.; (2002) Plasmacytoid dendritic cells: the key to CpG. *HUMAN IMMUNOLOGY*, 63[12], 1111-1119.

Singh, M. and O'Hagan, D. T.; (2002) Recent Advances in Vaccine Adjuvants. *PHARMACEUTICAL RESEARCH* 19[6], 715-728.

Singh, M., Ott, G., Kazzaz, J., Ugozzoli, M., Briones, M., Donnelly, J., and O'Hagan, D. T.; (2001) Cationic microparticles are an effective delivery system for immune stimulatory CpG DNA. *PHARMACEUTICAL RESEARCH*, 18[10], 1476-1479.

Stahl, Philip D., Alan, R., and Ezekowitz, B.; (1998) The mannose receptor is a pattern recognition receptor involved in host defense. *CURRENT OPINION IN IMMUNOLOGY*, 10[1], 50-55.

Sur, S., Lam, J., Bouchard, P., Sigounas, A., Holbert, D., and Metzger, W. J.; (1996) Immunomodulatory effects of IL-12 on allergic lung inflammation depend on timing of doses. *JOURNAL OF IMMUNOLOGY*, 157[9], 4173-4180.

Sur, S., Wild, J. S., Choudhury, B. K., Sur, N., Alam, R., and Klinman, D. M.; (1999) Long term prevention of allergic lung inflammation in a mouse model of asthma by CpG oligodeoxynucleotides. *JOURNAL OF IMMUNOLOGY*, 162[10], 6284-6293.

Suzuki, Y., Wakita, D., Chamoto, K., Narita, Y., Tsuji, T., Takeshima, T., Gyobu, H., Kawarada, Y., Kondo, S., Akira, S., Katoh, H., Ikeda, H., and Nishimura, T.; (2004) Liposome-encapsulated CpG oligodeoxynucleotides as a potent adjuvant for inducing type 1 innate immunity. *CANCER RESEARCH*, 64[23], 8754-8760.

Takeuchi, O., Kaufmann, A., Grote, K., Kawai, T., Hoshino, K., Morr, M., Muhlradt, P. F., and Akira, S.; (2000) Cutting edge: preferentially the R-stereoisomer of the mycoplasmal lipopeptide macrophage-activating lipopeptide-2 activates immune cells through a toll-like receptor 2- and MyD88-dependent signaling pathway. *JOURNAL OF IMMUNOLOGY*, 164[2], 554-557.

Takeuchi, O., Kawai, T., Muhlradt, P. F., Morr, M., Radolf, J. D., Zychlinsky, A., Takeda, K., and Akira, S.; (2001) Discrimination of bacterial lipoproteins by Toll-like receptor 6. *INTERNATIONAL IMMUNOLOGY*, 13[7], 933-940.

Takeuchi, O., Kawai, T., Sanjo, H., Copeland, N. G., Gilbert, D. J., Jenkins, N. A., Takeda, K., and Akira, S.; (1999) TLR6: A novel member of an expanding toll-like receptor family. *GENE* 231[1-2], 59-65.

Thiele, L., Rothen-Rutishauser, B., Jilek, S., Wunderli-Allenspach, H., Merkle, H. P., and Walter, E.; (2001) Evaluation of particle uptake in human blood monocyte-derived cells in vitro. Does phagocytosis activity of dendritic cells measure up with macrophages? *JOURNAL OF CONTROLLED RELEASE*, 76[1-2], 59-71.

Tokunaga, T., Yamamoto, H., Shimada, S., Abe, H., Fukuda, T., Fujisawa, Y., Furutani, Y., Yano, O., and Kataoka, T.; (1984) Antitumor activity of deoxyribonucleic acid fraction from *Mycobacterium bovis* BCG. I. Isolation, physicochemical characterization, and antitumor activity. *JOURNAL OF THE NATIONAL CANCER INSTITUTE*, 72[4], 955-962.

Underhill, D. M., Ozinsky, A., Haijar, A. M., Stevens, A., Wilson, C. B., Bassetti, M., and Aderem, A.; (1999) The toll-like receptor 2 is recruited to macrophage phagosomes and discriminates between pathogens. *NATURE*, 401[6755], 811-815.

Vabulas, R. M., Ahmad-Nejad, P., da Costa, C., Miethke, T., Kirschning, C. J., Hacker, H., and Wagner, H.; (2001) Endocytosed HSP60s use toll-like receptor 2 (TLR2) and TLR4 to activate the toll/interleukin-1 receptor signaling pathway in innate immune cells. *THE JOURNAL OF BIOLOGICAL CHEMISTRY*, 276[33], 31332-31339.

Verthelyi, D., Gursel, M., Kenney, R. T., Lifson, J. D., Liu, S., Mican, J., and Klinman, D. M.; (2003) CpG Oligodeoxynucleotides Protect Normal and SIV-Infected Macaques from *Leishmania* Infection. *JOURNAL OF IMMUNOLOGY*, 170[9], 4717-4723.

Vollmer, J., Weeratna, R., Payette, P., Jurk, M., Schetter, C., Laucht, M., Wader, T., Tluk, S., Liu, M., Davis, H. L., and Krieg, A. M.; (2004) Characterization of three CpG oligodeoxynucleotide classes with distinct immunostimulatory activities. *EUROPEAN JOURNAL OF IMMUNOLOGY*, 34[1], 251-262.

Weber, C., Coester, C., Kreuter, J., and Langer, K.; (2000) Desolvation process and surface characterization of protein nanoparticles. *INTERNATIONAL JOURNAL OF PHARMACEUTICS*, 194, 91-102.

Weeratna, R. D., McCluskie, M. J., Xu, Y., and Davis, H. L.; (2000) CpG DNA induces stronger immune responses with less toxicity than other adjuvants. *VACCINE*, 18[17], 1755-1762.

Weigel, B. J., Rodeberg, D. A., Krieg, A. M., and Blazar, B. R.; (2003) CpG Oligodeoxynucleotides Potentiate the Antitumor Effects of Chemotherapy or Tumor Resection in an Orthotopic Murine Model of Rhabdomyosarcoma. *CLINICAL CANCER RESEARCH*, 9[8], 3105-3114.

Wiemann, B. and Starnes, C. O.; (1994) Coley's toxins, tumor necrosis factor and cancer research: a historical perspective. *PHARMACOLOGY AND THERAPEUTICS*, 64[3], 529-564.

Wu, C. C. N., Lee, J., Raz, E., Corr, M., and Carson, D. A.; Necessity of Oligonucleotide Aggregation for Toll-like Receptor 9 Activation. *JOURNAL OF BIOLOGICAL CHEMISTRY*, 279[32], 33071-33078.

Yamamoto, S., Yamamoto, T., Shimada, S., Kuramoto, E., Yano, O., Kataoka, T., and Tokunaga, T.; (1992) DNA from bacteria, but not from vertebrates, induces interferons, activates natural killer cells and inhibits tumor growth. *MICROBIOLOGY AND IMMUNOLOGY*, 36, 983-997.

Yoshimura, A., Lien, E., Ingalls, R. R., Tuomanen, E., Dziarski, R., and Golenbock, D.; (1999) Cutting edge: recognition of gram-positive bacterial cell wall components by the innate immune system occurs via toll-like receptor 2. *JOURNAL OF IMMUNOLOGY*, 163[1], 1-5.

Zillies, J. and Coester, C.; (2004) Evaluating gelatin based nanoparticles as a carrier system for double stranded oligonucleotides. *JOURNAL OF PHARMACY AND PHARMACEUTICAL SCIENCES*, 7[4], 17-21.

Zimmermann, S., Egeter, O., Hausmann, S., Lipford, G. B., Rocken, M., Wagner, H., and Heeg, K.; (1998) CpG oligodeoxynucleotides trigger protective and curative Th1 responses in lethal murine leishmaniasis. *JOURNAL OF IMMUNOLOGY*, 160[8], 3627-3630.

Chapter IV

In vivo characterization of CpG ODN-loaded gelatin nanoparticles – Application as efficient and safe vaccine adjuvant

1. INTRODUCTION

1.1 Novel vaccine adjuvants

In the early 20th century, the introduction of vaccines led to an enormous improvement of the average life expectancy by almost completely abolishing various deadly infectious diseases. Thus, currently available vaccines prevent up to 3 million deaths and >750,000 children are kept from serious disability (O'Hagan & Rappuoli 2004). Vaccination is typically performed with live attenuated pathogens, inactivated bacterial toxins, or inactivated organisms. Even though those traditional approaches have been highly successful for a number of diseases, a lot of unsolved and new challenges still exist. Of course, attenuated or related but less virulent live pathogens are mostly very efficient, but bear always the danger of reversion into the full virulent form. Whole-killed antigens however, lack often cell-mediated immunity and are sometimes difficult to be grown in cell culture.

Recent novel approaches that use recombinant protein subunit vaccines, synthetic peptides, protein-polysaccharide conjugates, and DNA plasmids are free of infectious hazards, but are very often poorly immunogenic and have high production costs (McCluskie & Weeratna 2001). Consequently, further efforts such as the co-administration of adjuvants are required.

Adjuvants are substances that are used in combination with a specific antigen and support the antigen to give a more robust immune response. This can be achieved by various modes of action that e.g. include:

- a) an increased antigen uptake and presentation,
- b) an enhancement of the biological or immunological half-life of the co-administered antigen,
- c) an induction of a specific immune response supporting cytokine milieu.

Already back in 1926, aluminum compounds were the first adjuvants to be reported in literature, since they were demonstrated to enhance the immunogenic effect of diphtheria toxoids (Glenny et al. 1926). Even 80 years later, aluminum-based compounds, which are also called alum, still represent the only adjuvants that are currently approved by the FDA. But even though alum possesses well documented safety properties, it features also various significant drawbacks. Thus, aluminum salts are only weak potentiators of recombinant vaccines, rather polarizing towards T_H2 instead of T_H1 or CTL-mediated immune responses (Gupta 1998). Moreover, the appearance of allergic reactions has been reported for some patients due to the induction of IgE antibodies. Finally, alum cannot be utilized as adjuvant for mucosal immunization, since it is unable to induce IgA antibody immune response (Relyveld *et al.* 1998; Gupta 1998). Actually, a lot of scientific work is currently concentrated on the development of promising new adjuvants.

In principle, the two major alternative strategies to alum are the use of antigen delivery systems, such as liposomal or particulate systems, virosomes, and virus-like particles, or the use of substances bearing an immunomodulatory influence on the *in vivo* cytokine milieu. The most relevant of the immunomodulatory adjuvants are:

- a) Synthetic ODNs containing CpG motifs
- b) Monophosphoryl lipid A (MPLA) and derivatives
- c) Saponin derivatives (Quil A)
- d) Muramyl dipeptide (MDP) and derivatives
- e) Double-stranded RNA (dsRNA)
- f) Small molecule immune potentiators
- g) Cytokines

Already in the previous chapter, co-administration as adjuvant in conjunction with an antigen has been described as a potential field of application for CpG ODNs (see Chapter III).

MPLA is derived from lipopolysaccharide (LPS), which is constituent of the cellular membrane in gram-negative bacteria. LPS itself is too toxic to be utilized in clinical trials, since it induces excessive amounts of inflammatory cytokines. However, MPLA is investigated in various clinical trials as it interacts with TLR4 on APCs and induces T_H1 /CTL immune response supporting cytokine milieu. Thus, MPLA was already proven as an effective adjuvant for vaccines against

infectious diseases, cancer, and allergies (Evans *et al.* 2003). Additionally, our cooperation partners at University of Alberta have demonstrated that the immunogenic efficiency of MPLA can be enhanced when incorporating it into PLGA nanoparticles (Diwan *et al.* 2003; Chong *et al.* 2005).

Immunostimulatory saponin derivatives, also known as Quil A, are typically obtained from the bark of the *Quillaja saponaria* tree and are already a common constituent of various veterinary vaccines (e.g. CattleMaster GOLD FP 5; Pfizer). The mechanism of action of Quil A is supposed as intercalation with the cholesterol in cell membranes, thereby forming holes or pores that may facilitate the antigen uptake into APCs (Singh & O'Hagan 2002). Especially QS21, a highly purified fraction of Quil A, has shown the highest potential in clinical trials (Kensil & Kammer 1998). But it was reported that QS21 induces only enhanced T cell proliferation but no CTL-mediated cytotoxic immune response (Evans *et al.* 2001).

N-acetylmuramyl-L-alanyl-D-isoglutamine, also called muramyl dipeptide (MDP), is the active component of Freund's complete adjuvant (FCA), a mycobacterial extract in oil emulsion. FCA is a commonly used adjuvant in laboratory settings, but its toxic properties prohibit clinical use (McCluskie & Weeratna 2001). MDP itself is pyrogenic, thus a number of synthetic derivatives have been synthesized and revealed immunostimulatory activity by inducing high amounts of proinflammatory and chemotactic cytokines. Consequently, those derivatives have shown great potential as adjuvants (Azuma 1992).

Double-stranded RNA (dsRNA) is recognized by TLR3 on APCs. Poly [I]:poly [C] is the prototype synthetic dsRNA and was shown to induce T_H1-biased cytokines. But, it has also been found to be clinically toxic, causing renal failure, coagulopathies and hypersensitivity reactions (Robinson *et al.* 1976). However, an analogue of poly [I]:poly [C], poly [I]:poly [C₁₂U] (Ampligen[®]), has been demonstrated to have minimal toxicity in clinical studies (Thompson *et al.* 1996). Our cooperation partners at LMU's Department of Pharmaceutical Biotechnology just recently utilized the high anti-tumoral potential of poly [I]:poly [C] dsRNA. They showed that specific delivery of poly [I]:poly [C] dsRNA, complexed with a non-viral vector targeting for the epidermal growth factor (EGF) receptor, could eliminate glioblastoma, breast cancer, and adenocarcinoma in mice (Shir *et al.* 2006). Thereby, a polyethelenimine, polyethyleneglycol, and EGF conjugate was complexed with poly [I]:poly [C] dsRNA.

Among small molecular immune potentiators, imidazoquinolines such as resiquimod have to be mentioned. This class of a small nucleoside-like molecules are promising substances that induce T_H1 immune responses (Wu *et al.* 2004).

Finally, also cytokines can be used directly to modify and/or redirect an immune response. IL-1, IL-2, IL-12, IFN- γ , and GM-CSF represent the most extensively investigated cytokines (Singh & O'Hagan 2002).

1.2 Aim of the study and potential safety hazards

In the previous chapter, cationized gelatin nanoparticles loaded with CpG ODN (CpG-GNPs) have been presented as highly effective immunogenic formulation *in vitro*. In the present chapter, the results of subsequent *in vivo* experiments are described. A first goal was to investigate the immunological effects of CpG-GNPs depending on the administration route. In addition to this, CpG-GNPs were tested as adjuvant in conjunction with the model protein antigen ovalbumin (OVA) in soluble or particulate bound form.

Basically it is also always mandatory to have an eye on possible safety issues when using immunomodulatory substances. This is especially the case when new delivery systems are evaluated that potentially increase the immunogenicity of the substance. Fig. 1 summarizes the various deleterious effects that might be caused by CpG ODNs (Klinman 2004).

One aspect is that enhanced immune response against pathogen antigens might also promote autoimmune diseases. A certain predisposal towards systemic autoimmune reactions might occur due to the conjunction of polyclonal B-cell activation, increased production of autoantibodies, and attenuated apoptosis of lymphocytes. A predisposing factor for organ-specific autoimmunity is the over-induction of T_H1 -biased cytokines in conjunction with the presence self-antigens. Finally, the production of TNF and IFN- γ might cause septic shocks in patients. These hypotheses were further substantiated by studies, where bacterial DNA was administered in high doses to healthy mice and caused the production of autoantibodies against double-stranded DNA (Gilkeson *et al.* 1995).

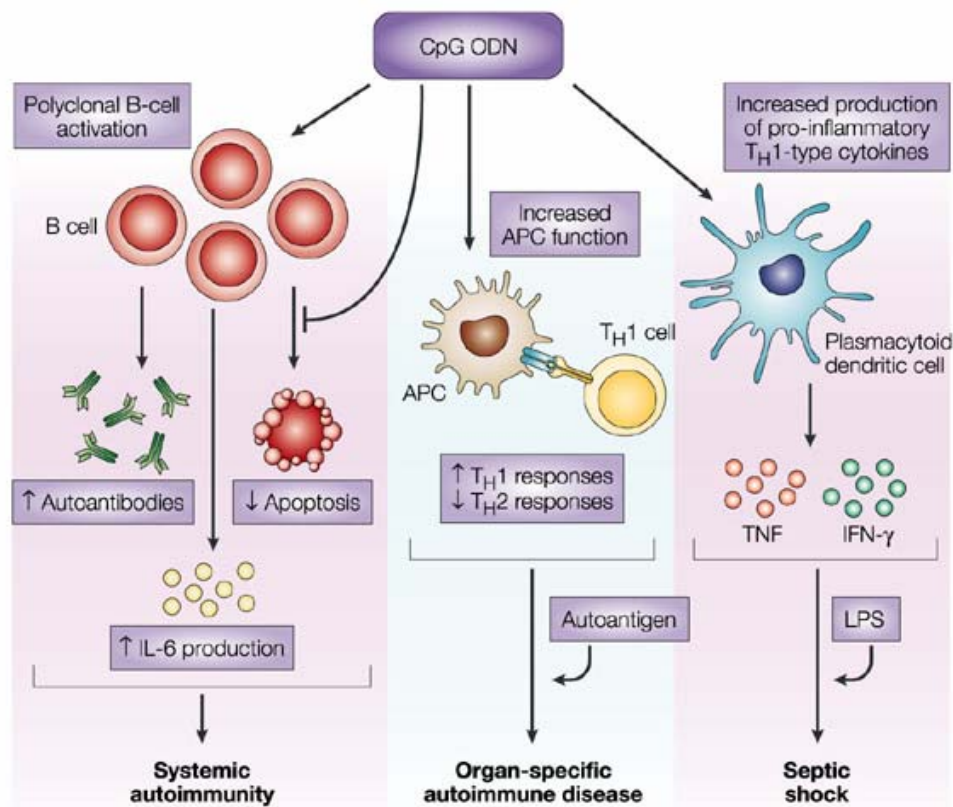


Fig. 1: Potential safety issues concerning the use of CpG ODNs (Klinman 2004)

To further investigate these issues, various experiments were performed in mice. Subsequent to continuous administration of CpG DNA, indeed DNA-specific IgGs were detectable in the blood serum of some mice, but the IgG amount was not sufficient to initiate an autoimmune response or pronounce an existing one (Katsumi *et al.* 1994). The potential hazards of septic shocks was investigated with BALB/c mice that were weekly treated with CpG ODN doses that were usually administered to patients in ongoing clinical vaccination trials (Elkins *et al.* 1999). All animals remained healthy and neither macro- nor microscopic indications for inflammations could be observed. Clinical studies as well did not show any evidence of toxicity so far.

Another theoretical source of safety hazards might also be the delivery system itself, gelatin nanoparticles. Even though, gelatin possesses a very well safety record, there were certain epidemiological observations made among the Japanese population, which indicated the rare presence of allergies against gelatin in some individuals (Kelso 1999; Saito *et al.* 2005). This local concentration of gelatin hypersensitivity reports is mainly attributed to historical evolutionary reasons.

Traditionally, the Japanese population derived in the past, in contrast to other populations, their nutrient protein predominantly from grain and soy beans. However, Japanese people shifted their dietary habits and started increased eating of animal protein such as beef and pork and gelatin containing food. Consequently, these dramatic nutrition changes within only a short period of time are discussed as cause of this local phenomenon. Nevertheless, this antigenicity issue has to be kept in mind when investigating gelatin nanoparticles *in vivo*. This is even more the case when gelatin nanoparticles are used as drug delivery system for an immunomodulatory adjuvant, e.g. CpG ODNs and/or vaccines. Consequently, this issue was another focus in the present study.

2. MATERIALS AND METHODS

2.1 Reagents

Reagent	Description	Supplier
BD Pharm Lyse TM Lysing Buffer	ammonium chloride buffer	BD Biosciences (Heidelberg, Germany)
BSA	Bovine serum albumin; fraction V; endotoxine-free	Carl Roth (Karlsruhe, Germany)
H ₂ SO ₄	Sulfuric acid; 1 M, p.a.	Sigma Aldrich (Taufkirchen, Germany)
OVA	Chicken egg ovalbumin; 99% endotoxine free	Sigma Aldrich (Taufkirchen, Germany)
o-phenylenediamine dihydrochloride	crystalline	Sigma Aldrich (Taufkirchen, Germany)
PBS	Phosphate buffered saline pH 7.4; endotoxine free	Sigma Aldrich (Taufkirchen, Germany)
Tween 20	Polysorbate 20	Carl Roth (Karlsruhe, Germany)

CpG ODN 1826 (5'-TCCATGACGTTTCCTGACGTT-3') was obtained from Coley Pharmaceutical Group (Langenfeld, Germany). For flow cytometry analysis, cells were stained with anti-mouse B220-PE, CD4-PE, CD8-PerCP, CD11c-APC, CD69-FITC, and isotype controls (BD Biosciences, Heidelberg, Germany).

2.2 Preparation of gelatin nanoparticles

2.2.1 Cationized gelatin nanoparticles

Cationized gelatin nanoparticles and Alexa-Fluor 488-labeled nanoparticles were prepared according to the procedures being described in Chapter II and III.

2.2.2 Gelatin nanoparticles with encapsulated OVA

OVA was added to the gelatin solution before the second desolvation step in a 1:10 ratio (m/m). The further particle preparation was performed according to the standard procedure for gelatin nanoparticles. The amount of incorporated OVA was semi-quantitatively determined via SDS-PAGE electrophoresis (NuPAGE

Novex, Invitrogen, Karlsruhe Germany). Therefore, staining was performed via Coomassie-Blue and quantitative analysis was done with ScanPack 3.0 Software (Biometra, Goettingen, Germany).

2.3 CpG ODN or OVA loading of cationized gelatin nanoparticles

Nanoparticle loading was performed according to the standard protocol that was described in the previous chapters for ODNs and pDNA.

2.4 Mice

Female Balb/c and C57BL/6 mice were purchased from Harlan-Winkelmann (Borchen, Germany). Mice were 5-12 weeks of age at the onset of experiments. Animal studies were approved by the local regulatory agency (Regierung von Oberbayern, Munich, Germany).

2.5 Immunostimulation *in vivo* and immunization

All immunological *in vivo* experiments were performed in cooperation with our partners at the Division of Clinical Pharmacology at LMU Munich's Department of Internal Medicine.

For *in vivo* immunostimulation, 500 µg cationized gelatin nanoparticles were incubated with 50 µg of oligonucleotides and 100 µL PBS for 20 min and injected i.v. into the retroorbital plexus or s.c.. Single cell suspensions were prepared from spleen and draining lymph nodes 18 h after injection and treated with ammonium chloride buffer to lyse erythrocytes. For analysis of activation markers, cells were stained with fluorochrome-coupled mAbs and analyzed by flow cytometry. Data were acquired on a FACSCalibur (BD Biosciences) and analyzed using CellQuest software (BD Biosciences). Blood was obtained by retroorbital puncture at the indicated time points. Serum was prepared by centrifugation and stored at -20°C.

For OVA immunization, formulations were injected s.c. on day 0 and day 14. Soluble OVA and both OVA formulations were administered in doses of 50 µg OVA each. Those groups that were additionally treated with CpG-GNPs or soluble CpG ODN became also doses containing 50 µg CpG ODN s.c. injected close to

the injection site of the OVA formulation. All formulations were administered in a volume of 100 μ L. Spleens and serum were collected on day 21.

2.6 Quantification of cytokines in serum

Cytokine concentrations were determined by ELISA for IL-6 (BioSource, Solingen, Germany) and IL-12p70 (BD Biosciences) according to the manufacturers' protocol. IFN- α was measured according to the following protocol: rat monoclonal antibody to mouse IFN- α (clone RMMA-1) was used as the capture antibody, rabbit polyclonal antibody to mouse IFN- α for detection (both from PBL Biomedical Laboratories, Piscataway, NJ, USA) together with HRP-conjugated donkey antibody to rabbit IgG as the secondary reagent (Jackson Immunolaboratories, West Grove, PA, USA). Recombinant mouse IFN- α (PBL Biomedical Laboratories) was used as standard (IFN- α concentration in IU/mL).

2.7 OVA-specific immune response

Serum antibodies to OVA were determined by ELISA: 96-well plates were coated overnight with 10 μ g/mL OVA in PBS and blocked 1 h with 1% BSA in PBS. After incubation of serum samples for 1 h at a dilution of 1/200, plates were washed with PBS/1% Tween 20 and goat anti-mouse IgG, IgG1 or IgG2a conjugated to horseradish peroxidase (Southern Biotech, Birmingham, AL, USA) was added at 1 μ g/mL for 1 h. Plates were again washed and ELISA was developed by o-phenylenediamine. Reaction was stopped by 1 M H₂SO₄ and optical density (OD) was read by photometer at 450 nm. For the detection of OVA-specific CD8⁺ T cells, freshly isolated splenocytes were lysed by ammonium chloride buffer and stained with H-2kb-OVA257-264-PE pentamers (Proimmune, Oxford, UK) and anti-CD8. Cells were stained with anti-CD8, then fixed with 2% paraformaldehyde and treated with permeabilizing solution (0.5% bovine serum albumin, 0.5% saponin, 0.02% sodium azide in PBS). The fixed cells were stained with FITC-conjugated anti-IFN- γ antibody (BD Biosciences) for 25 min. The percentage of CD8⁺ T cells expressing IFN- γ was determined by flow cytometry.

2.8 Biodistribution studies via CLSM

500 μg fluorescence-labeled GNPs loaded with 50 μg CpG ODN were injected i.v. into the retroorbital plexus or s.c. into the footpads of Balb/c mice. After 4h, the mice were sacrificed and liver, spleen, kidneys, and the draining lymph nodes were resected. The distribution into the different organs was determined by David Anz (Clinical Pharmacology, LMU Munich) via confocal laser scanning microscopy (CLSM).

2.9 FACS analysis of lymph node tissue

500 μg cationized gelatin nanoparticles were incubated with 50 μg of oligonucleotides and 100 μL PBS for 20 min and injected s.c.. Single cell suspensions were prepared from draining lymph nodes 18 h after injection. Cells were stained with fluorochrome-coupled mAbs and analyzed by flow cytometry. Data were acquired on a FACSCalibur (BD Biosciences) and analyzed using CellQuest software (BD Biosciences).

2.10 Gelatin-specific immune response

Serum antibodies to gelatin were determined by ELISA: 96-well plates were coated overnight with 10 $\mu\text{g}/\text{mL}$ gelatin in PBS and blocked 1 h with 1% BSA in PBS. After incubation of serum samples for 1 h at a dilution of 1/200, plates were washed with PBS/1% Tween 20 and goat anti-mouse IgG1 or IgG2a conjugated to horseradish peroxidase (Southern Biotech) was added at 1 $\mu\text{g}/\text{mL}$ for 1 h. Plates were again washed and ELISA was developed by o-phenylenediamine. Reaction was stopped by 1 M H_2SO_4 and optical density (OD) was read by photometer at 450 nm. Further details are given in the Results and Discussion part of this chapter (see 3.3).

3. RESULTS AND DISCUSSION

3.1 Systemic immunogenic activity of CpG-GNPs *in vivo*

The previously obtained *in vitro* results indicated that CpG-GNPs stimulate an enhanced T_{H1} /CTL-type immune response. Due to this it was the first focus to analyze if these well-plate-derived data correlate with *in vivo* activation patterns in mice. In these first *in vivo* experiments, we wanted to characterize the systemic immunogenic activity of CpG-GNPs. The two investigated routes of administration were intravenous and subcutaneous injection. Aside from the immunogenic activity, the biodistribution of CpG-GNPs following both injection pathways was the second factor to be studied.

3.1.1 Intravenous injection

Intravenous injection into the retroorbital plexus of the mice was the first route of administration to be examined. In analogy to *in vitro* experiments, again two differently sized nanoparticle batches were utilized: ZW IV1 (average size: 289.4 nm; PI: 0.047) & ZW IV2 (average size: 150.7 nm; PI: 0.068). Fig. 2 displays the induced IL-12p70 (Fig. 2A) and IL-6 (Fig. 2B) levels that were detected 6 h past injection.

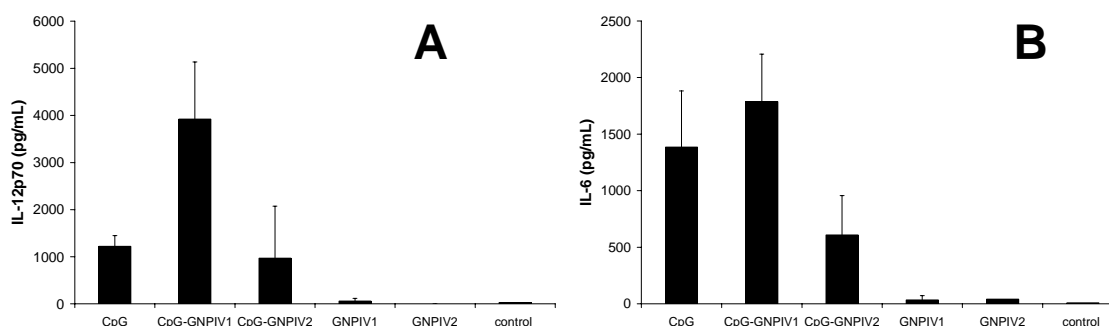


Fig. 2: IL-12p70 (A) & IL-6 (B) levels per mL blood serum at 6 hours past injection ($n=3$). CpG: 50 μ g soluble CpG ODN; CpG-GNPIV1: 500 μ g GNPs (batch ZW IV1: 289 nm) loaded with 50 μ g CpG ODN; CpG-GNPIV2: 500 μ g GNPs (batch ZW IV2: 150 nm) loaded with 50 μ g CpG ODN; GNPIV1/GNPIV2: 500 μ g unloaded GNPs controls; control: untreated control mice.

Both CpG ODN formulations being tested in this setup resulted in successful cytokine secretion, whereas the controls did not show any activity. Moreover, *in*

in vitro results indicating that larger sized nanoparticles are more efficient than smaller ones were confirmed. However, the respective differences between ~150 nm and ~300 nm sized particles concerning the amount of induction were bigger than in *in vitro* experiments (see Chapter III). 300 nm sized nanoparticles ZW IV1, led to more than threefold higher IL-12p70 concentrations than soluble CpG ODN and slightly enhanced IL-6 values. The 150.7 nm large nanoparticle batch reached comparable IL-12p70 levels to soluble CpG ODN, but only reduced secretion of IL-6.

As already discussed in Chapter III, the lack of strong enhancement of IL-6 levels in comparison to soluble CpG ODN is not necessarily unfavorable, since only IL-12p70 is the key cytokine to trigger T_H1 immune responses and IL-6 is discussed to show even adverse effects on a T_H1 differentiation (Diehl & Rincon 2002).

While observing the treated animals during the experiments, none of them showed signs of toxicity. However as we applied a third nanoparticle batch with even larger nanoparticles (500.8 nm) to determine if these particles are even more efficient, some of the animals died. As a consequence, maximum particle size of intravenously administered CpG-GNPs should not exceed 300 nm.

Another method to monitor the activity of immunogenic CpG-GNPs is to detect the percentage of activated immune cells. Therefore, activation markers on various previously purified cell types were analyzed by FACS. Thus, both types of DCs showed enhanced maturation as detected via CD86, in comparison to control mice and mice treated with gelatin nanoparticles alone. However, the percentage of matured cells of both DC types was slightly below soluble CpG ODN (Fig. 3). CpG-GNP's activation enhancement of B cells and CD8⁺ cells that was detected via the early activation marker CD69, was comparable or even slightly higher than soluble CpG ODN. Hence, CpG-GNPs are also *in vivo* able to activate the cells that are important for a successful immune response.

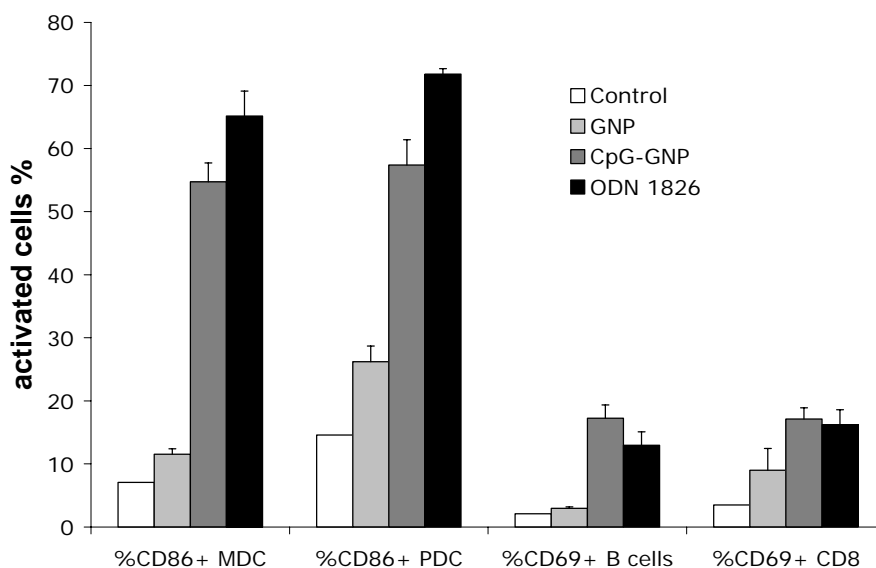


Fig. 3: Percentage of immunologically activated MDCs, PDCs, B cells, and CD8⁺ cells 2 h after intravenous administration; white columns: untreated control mice; light grey columns: mice treated with cationized gelatin nanoparticles alone; dark grey columns: mice treated with CpG-GNPs; black columns: mice treated with soluble CpG ODN.

3.1.2 Subcutaneous injection

Aside from intravenous injection, the subcutaneous route was the second examined type of administration. Again, systemic IL-12p70 and IL-6 levels were quantified to measure the systemic stimulation of the immune system. As depicted in Fig. 4, 50 µg soluble CpG ODN was able to induce systemic activation of the immune system also after s.c. administration.

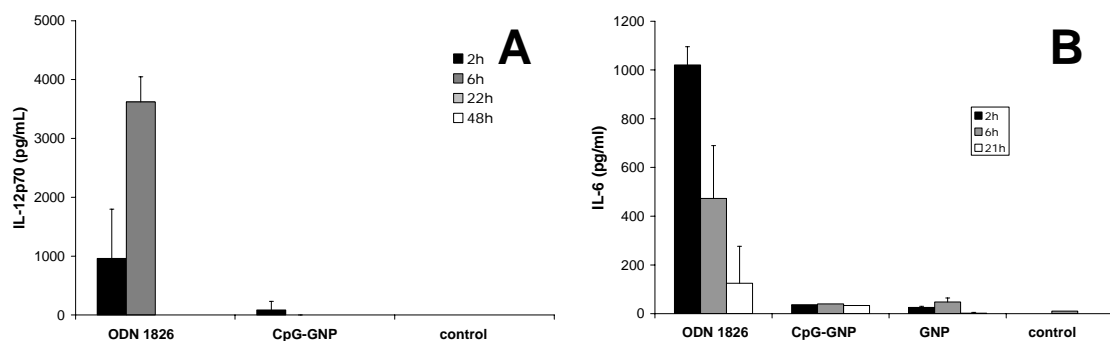


Fig. 4: Serum cytokine levels induced by s.c. administered soluble CpG ODNs and CpG-GNPs. A: IL-12p70 in blood serum after 2, 6, 22 & 48 h; B: IL-6 in blood serum after 2, 6, & 21h

IL-12p70 reached its highest level after 6 hours whereas IL-6 achieved its peak concentration already at the first detection point after 2 h. In contrast to i.v. results,

none of the CpG-GNP batches was able to increase cytokine levels. In fact, all tested CpG-GNP batches were unable to induce any significant cytokine amounts, as exemplarily displayed by the results of 289.4 nm sized CpG-GNP IV1. Even though it was already known from *in vitro* kinetic studies that particulate delivery of CpG ODNs does not induce any sustained or delayed activation of the immune system in comparison to soluble CpG ODNs, this possible aspect was surveyed once more. But even after very late detection points (IL-12p70: 21 h; IL-6: 22 & 48 h), no cytokine secretions could be observed. Summarizing, subcutaneous administration does not induce systemic activation of the immune system.

Nevertheless, this absence of systemic activity was not automatically judged negatively. For feasible applications of CpG ODNs, such as e.g. the co-administration as vaccine adjuvant, an unspecific systemic cytokine secretion is rather a undesirable side effect bearing the potential risk of immunological over-reactions (Klinman 2004). To give a final statement on this issue, further investigations of e.g. the biodistribution properties of s.c. administered formulations had to be performed.

3.1.3 *In vivo* localization of fluorescence-labeled CpG-GNPs

To track the *in vivo* fate of CpG-GNPs, mice were injected with fluorescence-labeled CpG-GNPs. After 4 hours, the mice were sacrificed and their major organs were resected. Surveying selected tissue samples that were obtained from animals receiving intravenously administered CpG-GNPs under a confocal laser scanning microscope, it was possible to localize fluorescence-labeled CpG-GNPs in addition to blood cells also in liver, spleen and kidney (Fig. 5A). These data correlated nicely with other biodistribution data that were obtained with gelatin nanoparticles (Kaul & Amiji 2004; Zillies et al. 2005). Subcutaneously administered CpG-GNPs could not be detected in those tissues (Fig. 5B), thus the particles were obviously not further processed by the systemic bloodstream, at least not above the visually detectable limits.

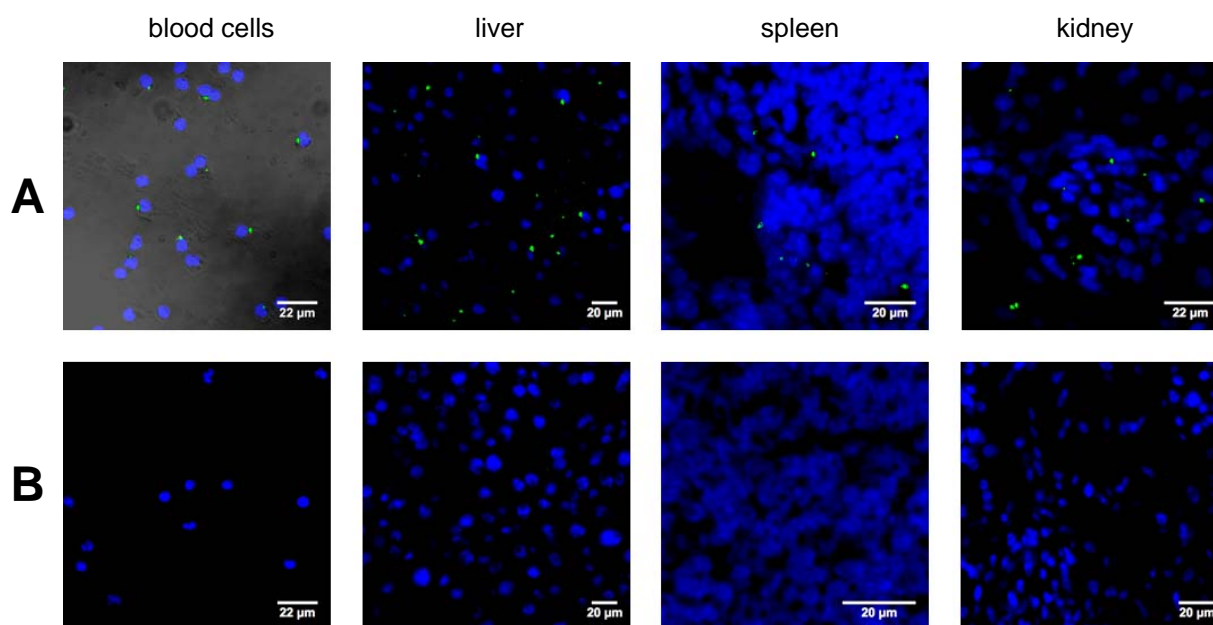


Fig. 5: CLSM images of various tissues. Blue: cell nuclei; Green: fluorescence-labeled CpG-GNPs. A: intravenous injection; B: subcutaneous injection

Consequently, CpG-GNPs were only systemically distributed via the blood stream following intravenous injection instead of subcutaneous. These findings agree with those previously described for other colloidal drug delivery systems, such as solid lipid nanoparticles (Reddy *et al.* 2005) and liposomes (Oussoren *et al.* 1997). Those references describe that s.c. administered colloidal carriers frequently remain at the injection site and are partially transferred via the lymphatic system to the draining lymph nodes. In detail, the carriers are taken up at the site of injection by local phagocytotic cells such as immature DCs. Following this uptake the cells transform into their mature state and are transferred to the lymph nodes where they start to induce a local immune response, such as e.g. the T_{H1} /CTL-type response that is activated by CpG ODNs.

Due to this theoretical background, it was decided to further investigate tissue samples of the site of injection and the draining lymph nodes. Since the subcutaneous injections were conducted into the footpads, the next draining lymph nodes were located in the popliteal fossa and the inguinal region. However, confocal laser scanning microscopic analysis 4 h past injection revealed only a massive amount of nanoparticles at the site of injection. No nanoparticles could be identified in the draining lymph nodes (Fig. 6).

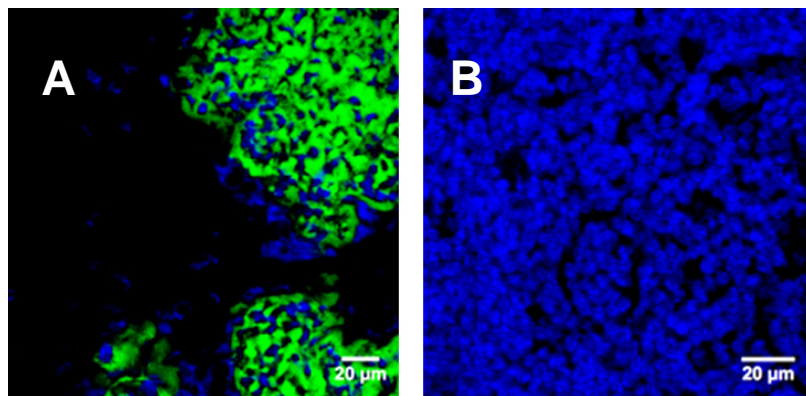


Fig. 6: CLSM images of tissue samples at 4 h past subcutaneous injection; A: tissue at the site of injection; B: tissue of the popliteal lymph node

Even though the nanoparticles could not be visually detected under the microscope after 4 h, it was decided to analyze the tissue of the popliteal and inguinal lymph nodes by more sensitive FACS analysis at various time points. In Fig. 7, a typical quadrant analysis of the cells derived from popliteal (Fig. 7A) and inguinal (Fig. 7B) lymph nodes is shown.

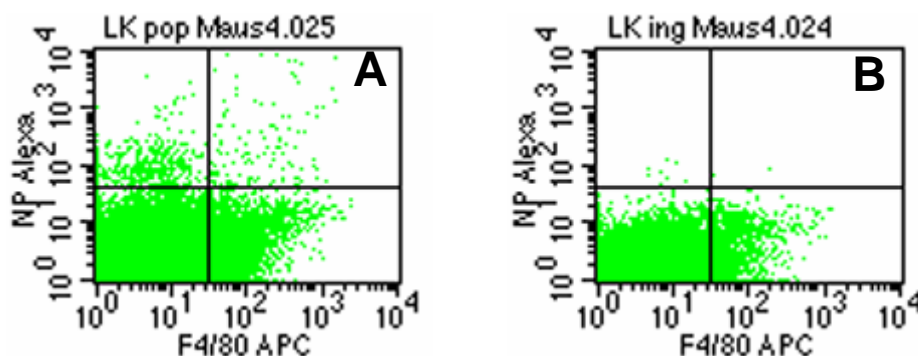


Fig. 7: 2-color FACS analysis of cells that were derived from the draining lymph nodes being closest to the site of CpG-GNP injection. Sacrificed: 18 h post injection; y-axis: FL-1 fluorescence (Alexa Fluor™ 488 labeled CpG-GNPs); x-axis: FL-2 fluorescence: Allophycocyanin (APC) anti-mouse F4/80 antigen; A: popliteal lymph node; B: inguinal lymph node

In the displayed two-color analysis macrophages have been additionally stained with F4/80 APC. They can be identified in the upper and lower right quadrants. Cells that have taken up nanoparticles are located in the upper quadrants. The results show that nanoparticles could be located within the cells of lymph nodes. In total, more nanoparticles could be located after 18 h in the popliteal lymph nodes that are located closest to the site of administration (Fig. 7A), whereas only a few cells indicated the presence of nanoparticles in the inguinal lymph nodes (Fig. 7B). Moreover, since cells can be found in both upper quadrants, the particles are

apparently taken up by various distinct cell-types, such as macrophages and other phagocytotic cells (DCs, etc.).

Based on these histological results, the conclusion can be drawn that s.c. administered CpG-GNPs do not cause a systemic immune activation since they are, in contrast to soluble CpG ODN, not removed via the blood stream from the site of injection. But, as a certain movement towards the draining lymph nodes could be observed, it was potentially possible that an activation of the immune system by CpG-GNPs occurs. However this would only happen within a regionally restricted area encompassing the injection site.

3.1.4 Summary

The results of these first experiments to characterize the systemic immunogenic activity of CpG-GNPs revealed significant differences to soluble CpG ODN. Whereas soluble CpG ODN induces a systemic secretion of T_H1 /CTL-polarizing cytokines subsequent to both types of administration, CpG-GNPs did only cause a systemic immune response after intravenous injection.

Analyzing the systemic cytokine levels that were induced with i.v. administered CpG-GNPs, *in vitro* results indicating the size of the applied gelatin nanoparticles as significant factor on the immunogenic activity of CpG-GNPs were confirmed. The ideal nanoparticle size to excite the secretion of enhanced levels of IL-12p70, the key cytokine to promote T_H1 differentiation, is apparently ~ 300 nm. Observing the maturation or activation levels of myeloid DCs (MDCs), plasmacytoid DCs (PDCs), B cells, and $CD8^+$ cells as second important benchmark aside from cytokine secretion revealed that CpG-GNPs led to comparable enhanced numbers of activated cells as soluble CpG ODN.

Searching for possible explanations, why subcutaneous administration did not result in any detectable systemic cytokine levels, CLSM analysis gave valuable insights. S.c. administered CpG-GNPs are in contrast to i.v. injected CpG-GNPs not biodistributed via the bloodstream, thus remaining basically at the site of injection. Nevertheless, FACS analysis revealed that some nanoparticles are also transported to the closest draining lymph nodes.

Consequently, it might be possible that CpG-GNPs are still able to induce an immune response. But due to the lack of systemic distribution, no systemic cytokine secretion occurs. If this potential local immune reaction would be

sufficient to e.g. boost the immune response against a co-administered antigen in comparable manner to soluble CpG ODNs, but without systemic side-effects, this would be a highly auspicious application.

3.2 CpG-GNPs as immunization adjuvant for chicken egg ovalbumin (OVA) as model protein vaccine

Summarizing the first results of s.c. administered CpG-GNPs it was hypothesized that they might possibly cause a locally restricted immune reaction in the area comprising the site of injection. As a consequence, the potential local immunological activity of s.c. injected CpG-GNPs should now be evaluated as adjuvant for a co-administered antigen protein. The chosen antigen was chicken egg ovalbumin (OVA), a commonly used model protein antigen. Other groups had recently demonstrated with different types of nanoparticulate delivery systems for CpG ODNs in combination with OVA, that strong immune induction can be observed *in vitro*, which might indicate also enhanced OVA specific immunization efficiency *in vivo* (Kwon *et al.* 2005; Jain *et al.* 2005).

3.2.1 Orientation study to evaluate the applicability of CpG-GNPs as adjuvant for OVA

In this orientation study with 3 mice per group, 2 groups were immunized with 25 µg OVA by s.c. injection, whereas one group received additionally 100 µL of a CpG-GNP dispersion (containing 500 µg nanoparticles loaded with 50µg CpG ODN) s.c. injected (Fig. 8). Analyzing the blood sera that were collected on day 21 past the initial injection, it could be revealed that CpG-GNPs led to increased anti-OVA IgG titers in serum. Thus, the previously claimed hypothesis that CpG-GNPs are able to induce immune responses when subcutaneously injected, but only in regionally limited manner and without unwanted systemic secretion of unspecific cytokines was confirmed.

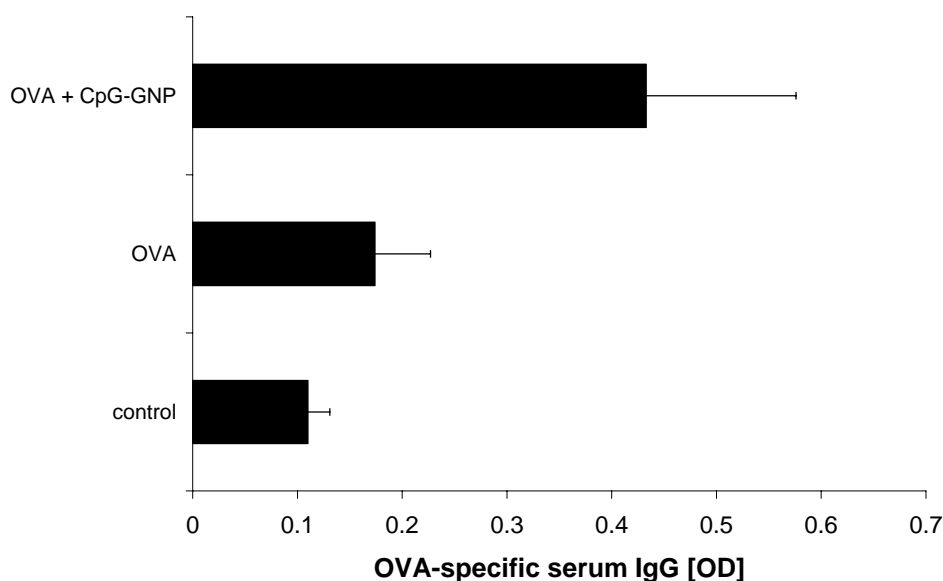


Fig. 8: OVA-specific IgG titers in serum after s.c. immunization (n=3). OVA+CpG-GNP: 25 μ g soluble OVA + 500 μ g gelatin nanoparticles loaded with 50 μ g CpG ODN; OVA: 25 μ g soluble OVA; control: untreated control mice.

3.2.2 Rational design of an applicable OVA delivery by gelatin nanoparticles

A second project of this study was to evaluate if OVA can either be encapsulated into the matrix of gelatin nanoparticles or be adsorbed onto the surface of cationized gelatin nanoparticles, since OVA has a ζ potential of -7.3 mV in physiological PBS pH 7.4. To analyze the amount of OVA that was loaded onto the nanoparticles, UV-metrical detection of OVA in the particle supernatant, in analogy to the quantification method for free unbound nucleotides (see Chapter II), failed since the signal was too low for exact detection. So it was decided to use SDS-Page electrophoresis to quantify the OVA loading. Staining was performed via Coomassie-Blue to enable the semi-quantitative analysis.

The cationized gelatin nanoparticles that were used in these experiments belonged to the same batch (ZW IV1; average size: 289.4 nm; PI: 0.047) that was previously evaluated as optimum carrier for intravenously injected CpG ODNs. When trying to attach various amounts of OVA onto the surface of the cationized gelatin nanoparticles, 1.5 μ g OVA were completely loaded onto 30 μ g nanoparticles (~5% [w/w]), as it can be visually derived from Fig. 9A. Furthermore, the reduction of the band intensities of the other, higher OVA amounts could be quantified as averaging 1.47 ± 0.17 μ g OVA and were in good agreement with the maximum

amount of completely loaded OVA. Repetitive experiments with the same and different nanoparticle batches, led to the comparable results (data not shown).

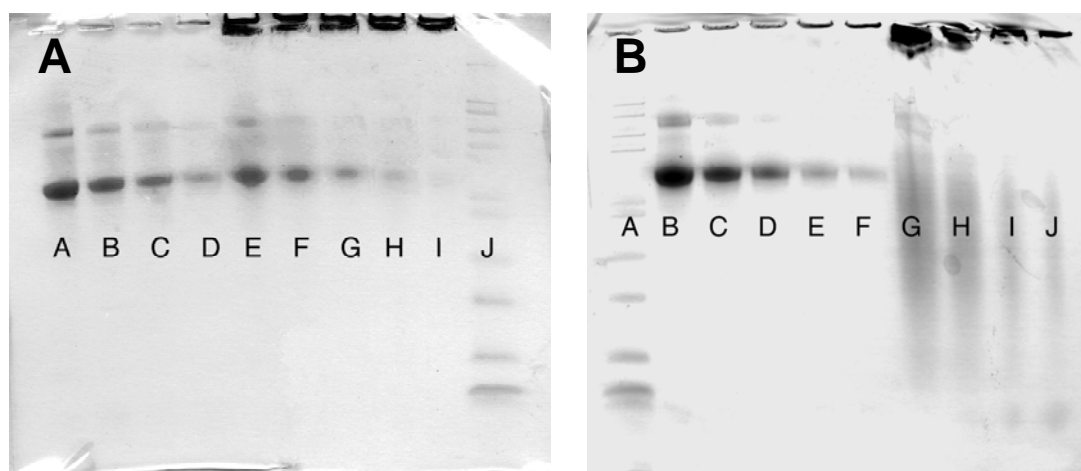


Fig. 9: A: semi-quantitative analysis of OVA loading properties onto the surface of cationized gelatin nanoparticles; OVA standards (A-D): A=12µg B=6µg; C=3µg; D=1.5µg OVA; Nanoparticle samples (E-I) incubated with 30 µg nanoparticles each: E=12 µg; F=6 µg; G=3 µg; H=2 µg; I= 1.5 µg OVA administered; J= control markers **B:** semi-quantitative analysis of OVA encapsulation properties of gelatin nanoparticles; OVA Standards (B-F): B=18µg, C=9µg, D=4.5µg, E=2.25, F=1.125 µg OVA; Nanoparticle dispersion aliquots (G-J) containing nanoparticles prepared in 1:10 (OVA:gelatin) ratio: G =76.4 µg, H =38.2 µg, I= 19.1 µg J=9.6 µg OVA administered; A= control markers

In the other formulation approach, the efficiency of the OVA incorporation into the nanoparticle matrix was also analyzed via gel electrophoresis (Fig. 9B). This analysis was performed with freshly prepared nanoparticles. All samples resulted with a rather broad and smearing background signal. The reason was remaining soluble non-desolvated gelatin that was still present in these samples, since no purification could be performed before the gel electrophoresis, because the unbound OVA, the factor that should be determined, would thereby get discarded as well. Assuming that the signal in the typical region of OVA is only an OVA signal, then our yield of incorporated OVA would be ~97%, regarding to ScanPack calculation. Interestingly, the addition of OVA in 1:10 ratio to the gelatin solution before the second desolvation step had also significant impact on the size of the later nanoparticles. All three batches that were produced using standard conditions to achieve an averaging mean size of 250 nm resulted between 113 and 139 nm. The obtained PIs (0.09 – 0.13) were slightly worse than those typically known for pure gelatin nanoparticles, but still acceptable concerning their homogeneity.

Readily prepared nanoparticles were purified from non-desolvated gelatin and non-incubated OVA by three-fold centrifugation and redispersion.

Finally, both novel OVA formulations were applied for immunization in comparison to soluble OVA (Fig. 10). In these experiments, the previous results of the orientation study were substantiated, which indicated that additional administration of CpG-GNPs leads to a strong immunization boost.

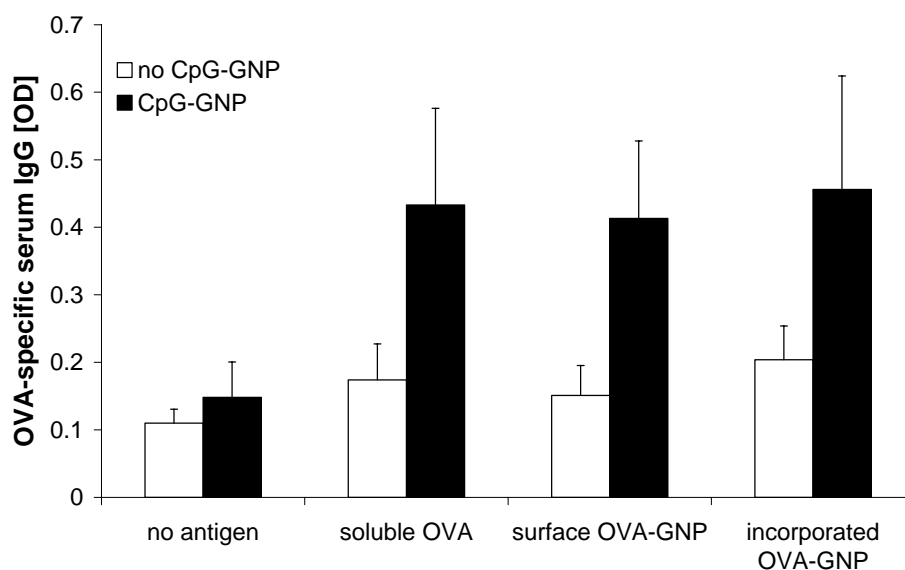


Fig. 10: OVA-specific IgG titers in serum after s.c. immunization ($n=3$). Additionally administered CpG-GNPs: white columns \rightarrow no; black columns \rightarrow yes; no antigen: no OVA administered to mice; soluble OVA: soluble OVA administered to mice; surface OVA-GNP: OVA adsorbed onto cationized GNPs administered to mice; incorporated OVA-GNP: OVA entrapped into the gelatin nanoparticle matrix administered to mice

Both of the new OVA formulations were able to induce comparable OVA-specific IgG titers to soluble OVA. Thus, it was demonstrated that no inactivation of the antigen's immunogenicity occurred. Otherwise, also no additional increase of the immunization via particulate antigen delivery could be observed, although nano- or microparticulate delivery are referred as further adjuvant approach in literature (Singh *et al.* 2001; McCluskie & Weeratna 2001).

Nevertheless, the performed new approaches are giving an outlook for potential future antigen formulations, where particulate delivery might be advisable.

3.2.3 Comparison of the adjuvant potential of CpG-GNPs vs. soluble CpG ODN

In this study we wanted to determine the actual adjuvantive strength of s.c. administered CpG-GNPs in comparison to soluble CpG ODN. To keep the number of necessary groups of mice limited it was decided to perform the experiments with OVA being adsorbed onto the surface of cationized gelatin nanoparticles as only antigen formulation. Due to the results of the previous experiment soluble OVA or OVA incorporated into the particle matrix should expectedly result similar.

As shown in Fig. 11, previous experiments indicating that additional administration of CpG-GNPs led to strongly enhanced production of OVA-specific IgG, were again substantiated. Thus, the IgG titer of mice that were immunized with OVA-loaded nanoparticles and CpG-GNPs being co-administered was more than 3-fold higher than the one of OVA-loaded gelatin nanoparticles alone. But, comparing the induced IgG titers, CpG-GNPs resulted also slightly better as co-administered adjuvant than soluble CpG ODN (Fig. 11A).

Aside from the actual IgG titer, an important benchmark of successful T_H1 /CTL-biased immunization is the percentage of antigen specific $CD8^+$ cells. While co-administered soluble CpG ODN led only to a slight increase of OVA-specific $CD8^+$ cells in blood serum in comparison to OVA-loaded gelatin nanoparticles alone, a 4-fold amount of specific $CD8^+$ cells was obtained with CpG-GNPs that were co-administered with OVA-loaded nanoparticles (Fig. 11B). Hence, CpG-GNPs are an ideal new adjuvant to selectively promote the immunization via a T_H1 /CTL-mediated pathway.

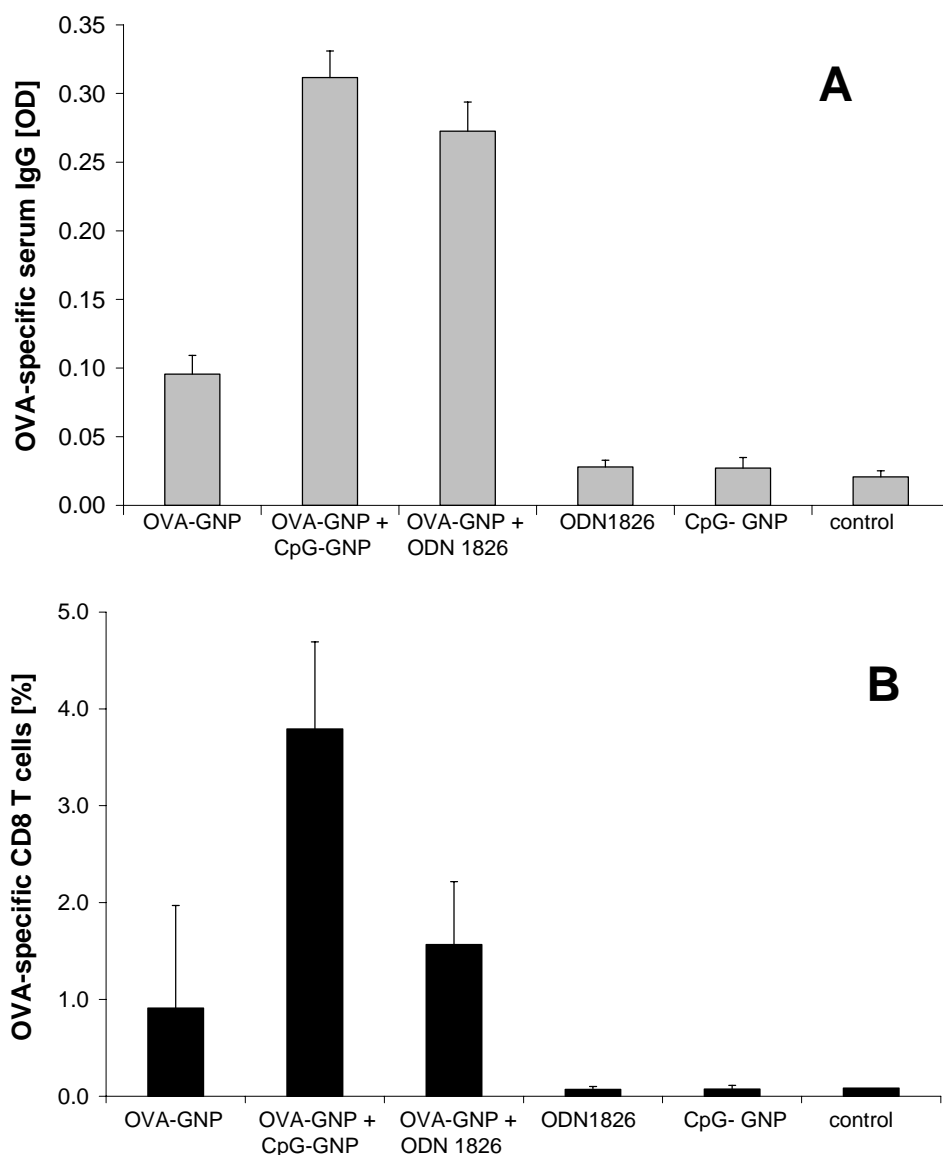


Fig. 11: OVA-specific IgG titer (A) and amount of OVA-specific CD8⁺ cells (B) in serum after s.c. immunization (n=5). OVA-GNP: Mice treated with OVA adsorbed onto gelatin nanoparticles; OVA-GNP + CpG-GNP; Mice treated with OVA adsorbed onto gelatin nanoparticles and co-administered CpG-GNPs; OVA-GNP + ODN 1826: Mice treated with OVA adsorbed onto gelatin nanoparticles and co-administered soluble CpG ODN 1826; ODN 1826: Mice treated with soluble CpG ODN 1826; CpG-GNP: Mice treated with CpG-GNPs; control: untreated control mice.

3.2.4 Summary

Present data revealed that CpG-GNPs are a highly potent vaccine adjuvant. Whereas previous findings raised the question, if s.c. administered CpG-GNPs possess immunological activity at all, since no enhanced blood-levels of immunogenic and inflammatory cytokines could be detected (see 3.1), it was now demonstrated that this immune activation occurs in a local manner.

Nevertheless, this local restriction encompassing the area around the injection site and the closest draining lymph nodes turned out to be sufficient to induce strongly enhanced specific immune against the co-administered antigen OVA. Moreover, the immunization efficiency with co-administered CpG-GNPs concerning the obtained percentage of specific CD8⁺ cells was significantly better than with soluble CpG ODN.

In addition to these findings, it was demonstrated that the protein antigen remains comparably active as the soluble antigen, when it is adsorbed onto the surface of gelatin nanoparticles or incorporated in the particles matrix.

3.3 Do gelatin nanoparticles induce anti-gelatin IgGs in mice?

In all *in vitro* experiments that have been described in this Ph.D. thesis, gelatin nanoparticles behaved biologically neutral. However, since gelatin nanoparticles were used as carrier for an immunomodulatory adjuvant here, certain antigenicity concerns have been raised. To investigate these issues, we established a specific ELISA. Therefore, we injected dissolved gelatin in combination with FCA (Freund's Complete Adjuvant) to a group of mice. Immunization with gelatin and FCA as adjuvant induces the production of specific anti-gelatin IgG1 and IgG2a antibodies. Thus, we generated mice bearing these gelatin-specific serum antibodies as a positive control. To detect the antibodies via ELISA, we coated well-plates with gelatin and incubated them with serum samples of CpG-GNP-immunized mice.

After the CpG/OVA-immunization experiments, serum samples of all mice were taken and analyzed for anti-gelatin IgG1 and IgG2a in comparison to PBS as negative control and serum of gelatin/FCA-immunized mice as positive control. As depicted in Fig. 12, all serum samples of CpG/OVA-immunized mice did not contain significant anti-gelatin IgG. So, no undesired immunogenicity against gelatin was induced. Nevertheless, certain focus has to be put on this issue also in future.

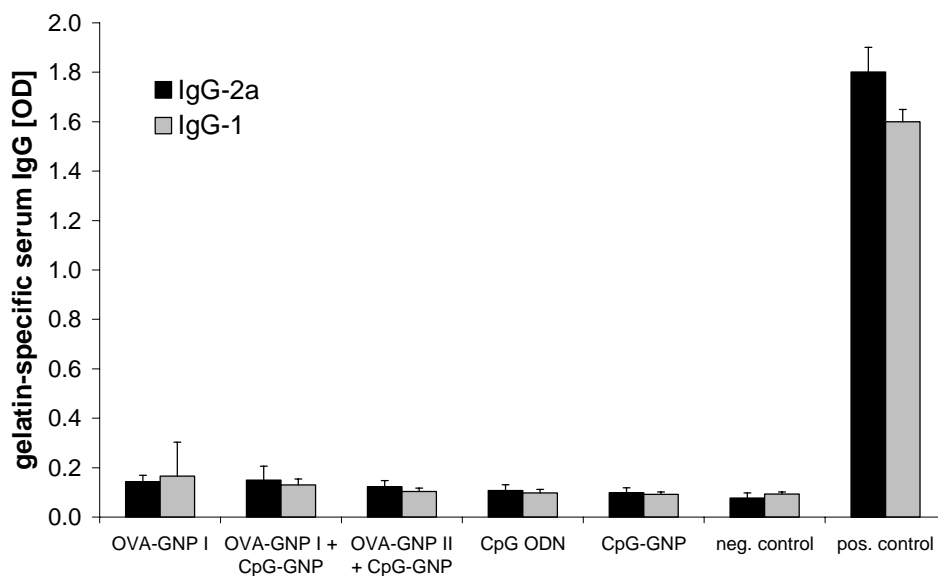


Fig. 12: Serum titers of anti-gelatin IgG of all gelatin nanoparticle samples administered in vivo; OVA-GNP I: gelatin nanoparticles with incorporated OVA; OVA-GNP I + CpG-GNP: gelatin nanoparticles with incorporated OVA and additional CpG-GNP; OVA-GNP II + CpG-GNP: gelatin nanoparticles with adsorbed OVA and additional CpG GNP; CpG ODN: soluble CpG ODN; CpG-GNP; neg. control: PBS; pos. control: mice treated with gelatin and additional FCA.

4. CONCLUSION

When performing first characterization experiments to investigate the *in vivo* immunological activity of CpG-GNPs, it was noteworthy that the route of administration was decisive for systemic secretion of immunogenic and inflammatory cytokines. While intravenous injection of CpG-GNPs induces high amounts of those cytokines in the blood stream, subcutaneously applied CpG-GNPs do not cause this systemic kind of immune response. On the other hand, soluble CpG ODN induces systemic secretion of non-specific, immunogenic cytokines in both ways of application. Searching for explanations for this phenomenon, it was found that s. c. administered CpG-GNPs in contrast to soluble CpG ODN are not systemically distributed via the blood stream, but remain at the site of injection from where they are partially taken up by antigen presenting cells (APCs). After this cellular uptake they are transported to the closest draining lymph nodes, where finally T_H1 /CTL-mediated immune reactions against co-administered are initialized.

Due to the locally restricted distribution of CpG-GNPs, the potential appearance of unwanted systemic immunological side effects, such as septic shocks, can be almost excluded for this new adjuvant formulation. This circumstance alone represents already an enormous improvement against soluble CpG ODN. But even more, CpG-GNPs seem to be slightly more effective than soluble CpG ODN, when applied as vaccine adjuvant. Otherwise, it was also demonstrated that CpG-GNPs amplify only the immune reaction against the real antigen protein and did not cause immune responses against gelatin, the proteinaceous matrix material of the nanoparticles.

Due to its T_H1 /CTL specificity this new adjuvant might perfectly fit the needs of anti-viral or anti-tumoral antigens to enable successful and efficient vaccinations, a field where state-of-the-art adjuvant alum has its disadvantages.

Finally, it was successfully demonstrated that gelatin nanoparticles can also be used as carrier for antigens, by either entrapping them into the particle matrix or conjugating them onto the particle surface. This further expands the potential application repertoire also towards smaller antigenic substances, such as peptides, where particulate delivery might be advantageous.

5. REFERENCES

- Azuma, I.; (1992) Inducer of cytokines in vivo: overview of field and romurtide experience. *INTERNATIONAL JOURNAL OF IMMUNOPHARMACOLOGY*, 14[3], 487-496.
- Chong, C. S. W., Cao, M., Wong, W. W., Fischer, K. P., Addison, W. R., Kwon, G. S., Tyrrell, D. L., and Samuel, J.; (2005) Enhancement of T helper type 1 immune responses against hepatitis B virus core antigen by PLGA nanoparticle vaccine delivery. *JOURNAL OF CONTROLLED RELEASE*, 102[1], 85-99.
- Diehl, S. and Rincon, M.; (2002) The two faces of IL-6 on Th1/Th2 differentiation. *MOLECULAR IMMUNOLOGY*, 39[9], 531-536.
- Diwan, M., Elamanchili, P., Lane, H., Gainer, A., and Samuel, J.; (2003) Biodegradable Nanoparticle Mediated Antigen Delivery to Human Cord Blood Derived Dendritic Cells for Induction of Primary T Cell Responses. *JOURNAL OF DRUG TARGETING*, 11[8-10], 495-507.
- Elkins, K. L., Rhinehart-Jones, T. R., Stibitz, S., Conover, J. S., and Klinman, D. M.; (1999) Bacterial DNA containing CpG motifs stimulates lymphocyte-dependent protection of mice against lethal infection with intracellular bacteria. *JOURNAL OF IMMUNOLOGY*, 162[4], 2291-2298.
- Evans, J. T., Cluff, C. W., Johnson, D. A., Lacy, M. J., Persing, D. H., and Baldrige, J. R.; (2003) Enhancement of antigen-specific immunity via the TLR4 ligands MPL adjuvant and Ribi.529. *EXPERT REVIEW OF VACCINES*, 2[2], 219-229.
- Evans, T. G., McElrath, M. J., Matthews, T., Montefiori, D., Weinhold, K., Wolff, M., Keefer, M. C., Kallas, E. G., Corey, L., Gorse, G. J., Belshe, R., Graham, B. S., Spearman, P. W., Schwartz, D., Mulligan, M. J., Goepfert, P., Fast, P., Berman, P., Powell, M., and Francis, D.; (2001) QS-21 promotes an adjuvant effect allowing for reduced antigen dose during HIV-1 envelope subunit immunization in humans. *VACCINE*, 19[15-16], 2080-2091.
- Gilkeson, G. S., Phippen, A. M. M., and Pisetsky, D. S.; (1995) Induction of cross-reactive anti-dsDNA antibodies in preautoimmune NZB/NZW mice by immunization with bacterial DNA. *JOURNAL OF CLINICAL INVESTIGATION*, 95[3], 1398-1402.
- Gupta, R. K.; (1998) Aluminum compounds as vaccine adjuvants. *ADVANCED DRUG DELIVERY REVIEWS*, 32[3], 155-172.
- Jain, S., Yap, W. T., and Irvine, D. J.; (2005) Synthesis of Protein-Loaded Hydrogel Particles in an Aqueous Two-Phase System for Coincident Antigen and CpG Oligonucleotide Delivery to Antigen-Presenting Cells, *BIOMACROMOLECULES*, 6[5], 2590-2600.
- Katsumi, A., Emi, N., Abe, A., Hasegawa, Y., Ito, M., and Saito, H.; (1994) Humoral and cellular immunity to an encoded protein induced by direct DNA injection. *HUMAN GENE THERAPY*, 5[11], 1335-1339.
- Kaul, G. and Amiji, M.; (2004) Biodistribution and targeting potential of poly(ethylene glycol)-modified gelatin nanoparticles in subcutaneous murine tumor model. *JOURNAL OF DRUG TARGETING*, 12[9-10], 585-591.

- Kelso, J. M.; (1999) The gelatin story. *THE JOURNAL OF ALLERGY AND CLINICAL IMMUNOLOGY*, 103[2 Pt 1], 200-202.
- Kensil, C. R. and Kammer, R.; (1998) QS-21: a water-soluble triterpene glycoside adjuvant. *EXPERT OPINION ON INVESTIGATIONAL DRUGS*, 7[9], 1475-1482.
- Klinman, D. M.; (2004) Immunotherapeutic uses of CpG oligodeoxynucleotides. *NATURE REVIEWS IMMUNOLOGY*, 4[4], 249-258.
- Kwon, Y. J., Standley, S. M., Goh, S. L., and Frechet, J. M. J.; (2005) Enhanced antigen presentation and immunostimulation of dendritic cells using acid-degradable cationic nanoparticles. *JOURNAL OF CONTROLLED RELEASE*, 105[3], 199-212.
- McCluskie, M. J. and Weeratna, R. D.; (2001) Novel adjuvant systems. *CURRENT DRUG TARGETS: INFECTIOUS DISORDERS*, 1[3], 263-271.
- O'Hagan, D. T. and Rappuoli, R.; (2004) Novel Approaches to Vaccine Delivery. *PHARMACEUTICAL RESEARCH*, 21[9], 1519-1530.
- Oussoren, C., Zuidema, J., Crommelin, D. J. A., and Storm, G.; (1997) Lymphatic uptake and biodistribution of liposomes after subcutaneous injection. II. Influence of liposomal size, lipid composition and lipid dose. *BIOCHIMICA ET BIOPHYSICA ACTA, BIOMEMBRANES*, 1328[2], 261-272.
- Reddy, L. H., Sharma, R. K., Chuttani, K., Mishra, A. K., and Murthy, R. S. R.; (2005) Influence of administration route on tumor uptake and biodistribution of etoposide loaded solid lipid nanoparticles in Dalton's lymphoma tumor bearing mice. *JOURNAL OF CONTROLLED RELEASE*, 105[3], 185-198.
- Relyveld, E. H., Bizzini, B., and Gupta, R. K.; (1998) Rational approaches to reduce adverse reactions in man to vaccines containing tetanus and diphtheria toxoids. *VACCINE*, 16[9-10], 1016-1023.
- Robinson, R. A., DeVita, V. T., Levy, H. B., Baron, S., Hubbard, S. P., and Levine, A. S.; (1976) A phase I-II trial of multiple-dose polyriboinosic-polyribocytidylic acid in patients with leukemia or solid tumors. *JOURNAL OF THE NATIONAL CANCER INSTITUTE*, 57[3], 599-602.
- Saito, A., Kumagai, T., Kojima, H., Terai, I., Yamanaka, T., Wataya, Y., Umetsu, M., Umetsu, A., and Yano, S.; (2006) A sero-epidemiological survey of gelatin sensitization in young Japanese children during the 1979-1996 period. *SCANDINAVIAN JOURNAL OF IMMUNOLOGY*, 61[4], 376-379.
- Shir, A., Ogris, M., Wagner, E., and Levitzki, A.; (2006) EGF receptor-targeted synthetic double-stranded RNA eliminates glioblastoma, breast cancer, and adenocarcinoma tumors in mice. *PLOS MEDICINE*, 3[1], 125-135.
- Singh, M. and O'Hagan, D. T.; (2002) Recent Advances in Vaccine Adjuvants. *PHARMACEUTICAL RESEARCH*, 19[6], 715-728.
- Thompson, K. A., Strayer, D. R., Salvato, P. D., Thompson, C. E., Klimas, N., Molavi, A., Hamill, A. K., Zheng, Z., Ventura, D., and Carter, W. A.; (1996) Results of a double-blind placebo-controlled study of the double-stranded RNA drug polyI:polyC12U in the treatment of HIV infection. *EUROPEAN JOURNAL OF CLINICAL MICROBIOLOGY AND INFECTIOUS DISEASES*, 15[7], 580-587.

Wu, J. J., Huang, D. B., and Tyring, S. K.; (2004) Resiquimod: a new immune response modifier with potential as a vaccine adjuvant for Th1 immune responses. *ANTIVIRAL RESEARCH*, 64[2], 79-83.

Zillies, J., Goeppert, T. M., Hoffmann, F., Zahler, S., Vollmar, A., Müller, R. H., Winter, G., and Coester, C.; (2005) Correlation of Plasma Protein Adsorption Patterns and Biodistribution Data of Different Gelatin and Solid Lipid Nanoparticle Formulations. Annual Meeting of the AAPS, Nashville, USA, Conference Proceeding.

Chapter V

PEGylation and biodistribution of gelatin nanoparticles – Initial experiments

1. INTRODUCTION

1.1 Biodistribution of nanoparticles

When developing a new drug delivery system, exact knowledge of its fate *in vivo* is essential. This is even more the case, if the drug release and effect is only desired at a specific target tissue or organ within the body. Nanoparticles are a promising colloidal carrier system and due to their small size they can be applied for specific cell targeting purposes. Potential targets are the brain (across the blood brain barrier), tumors, or sites of inflammation. Thereby, intravenous administration represents still the main route for these colloidal applications. Unfortunately, nanoparticles are, similar to other colloidal carrier systems, in general quickly removed from the blood stream by the mononuclear phagocytotic system (MPS), formerly also known as reticuloendothelial system (RES). Consequently, this circumstance represents the major obstacle for the realization of most targeting goals (Gref *et al.* 1994; Owens & Peppas 2006). The cells of the MPS that are responsible for this rapid clearance are mainly Kupffer cells in the liver and macrophages in spleen and lung (Kreuter 1983). But MPS cells do not recognize nanoparticles by themselves. They are dependent on the adsorption of opsonin proteins (Gref *et al.* 1995). The function of these blood serum components is to make foreign particles recognizable for phagocytotic cells. Typical opsonins that are adsorbed onto the surface of nanoparticles are lectins, immunoglobulins, and complement proteins such as C1-C5. Nevertheless, the respective opsonization pattern and thus the clearance of the nanoparticles from the blood circulation depends very strongly on the particular surface of the nanoparticles. The knowledge of the specific adsorption pattern appears to be very helpful when estimating a biodistribution profile of a new intravenously injectable colloidal carrier system. While searching for appropriate analytical tools, methods like two-dimensional polyacrylamide gel electrophoresis have proven to be valuable for the

characterization of plasma protein absorption patterns (Blunk *et al.* 1993; Goepfert & Mueller 2005).

In our research group, we have just recently used this method to investigate the adsorption profile of solid lipid nanoparticles (SLNs) that were stabilized with poloxamer 188 (Pluronic™ F 68) versus plain gelatin nanoparticles (Zillies *et al.* 2005). Thereby, SLNs mainly adsorbed apolipoproteins on their surface, thus indicating a comparable adsorption pattern as polysorbate 80 or poloxamer coated poly (butyl 2-cyanoacrylate) nanoparticles (Douglas *et al.* 1986; Kreuter *et al.* 1995). Because of this opsonization profile, these nanoparticles are long circulating and are discussed to pass the blood brain barrier since apolipoprotein adsorption is postulated to induce active transfer via the LDL (low density lipoprotein) receptor (Kreuter *et al.* 2003). In contrast to that, gelatin nanoparticles adsorb mainly immunoglobulins, lectin, and components of the complement system. Thus, they are expected to be very quickly sequestered by the cells of the MPS.

Even though it is difficult to set up rules for the biodistribution of nanoparticles, it can be stated that adsorption of hydrophilic shells is beneficial for prolonged blood circulation. These hydrophilic chains are typically introduced by attaching poly(ethylene oxide) (PEO) onto the nanoparticle surface. One strategy is the adsorption of amphiphilic agents that contain PEO such as poloxamers and poloxamins (block copolymers of PEO and poly (propylene oxide)) or polysorbate (poly (ethylene oxide) sorbitanester). The second way is to covalently attach or entangle poly (ethylene glycol) (PEG) and PEG containing polymer layers. So far numerous approaches based on one of these concepts have been described for polymeric nanoparticles (for detailed information see review Owens & Peppas 2006). Most of them prolonged the bloodstream half-lives of the nanoparticles up to some hours. A second beneficial feature of the hydrophilic shell is that it prevents cationic nanoparticles or polyplexes, which are often used in non-viral gene therapy (see Chapter II.), from inducing erythrocyte aggregation by sterically neutralizing the formulation's zeta potential (Ogris *et al.* 1999).

However, when planning to develop specific cell targeting of e.g. tumor cells, it would be highly desirable to achieve separation of the colloidal carrier from its attached PEG chains during entrance into the target cell. Nanoparticles are typically internalized via phagocytosis. So, acidic pH sensitive separation within the endosome appears as promising potential mechanism. This concept led already to

highly increased gene transfections in gene therapeutic experiments with pH-sensitive PEGylated PEI/DNA polyplexes (Walker *et al.* 2005).

Performing the attachment of PEG onto the surface of colloidal carriers, it is essential to have detailed information on the total amount of PEG that has been successfully grafted (Veronese 2001; Moghimi & Szebeni 2003). Moreover, this information is also mandatory to prove the reproducible quality of commercial PEGylated products. Unfortunately, accurate analytical quantification of PEG is a quite crucial issue, since direct spectrophotometrical detection fails due to the molecular structure of PEG. Some quantification methods being described in literature that are based on colorimetric reactions with PEG (Childs 1975; Cole *et al.* 1983; Nag *et al.* 1996) are quite old, but due to the lack of alternatives still commonly used. Although, these methods feature only low accuracy and sensitivity and are quite susceptible to outside influences. A more recent detection method is direct refractive index detection of PEG in connection with previous separation (Philipsen *et al.* 1985) via e.g. HPLC or asymmetrical flow field-flow fractionation (AF4).

1.2 Real-time biodistribution analysis of gelatin nanoparticles via positron emission tomography (PET)

While investigating the fate of i.v. injected nanoparticles for their respective biodistribution profile, radiolabeling of the nanoparticle matrix with appropriate radioisotopes is still most favorable for a subsequent facile and reliable *in vivo/ex vivo* quantitative analysis.

In order to derive non-invasive real-time analytical data of radiolabeled colloidal carriers, positron emission tomography (PET) currently represents the method of choice (Oku 1999). Other common imaging techniques are the use of γ -camera or single photon emission computed tomography (SPECT). These techniques detect γ -rays that are emitted by radionuclides. However, the resolution of PET is superior since it detects two 511 keV γ -rays in coincidence that are produced by annihilation after positron emission a respective radionuclide. Thus, PET has become a routine tool in modern nuclear medicine diagnostics. Radioisotopes that are typically utilized in PET diagnostics are those with short half-lives such as fluorine-18 (^{18}F ; $T_{1/2}=109.7$ min), carbon-11 (^{11}C ; $T_{1/2}=20.4$ min), nitrogen-13 (^{13}N , $T_{1/2}=10$ min), oxygen-15 (^{15}O ; $T_{1/2}=2$ min), iodine-124 (^{124}I ; $T_{1/2}=100.8\text{h}$) and

copper-64 (^{64}Cu ; $T_{1/2}=12.7\text{h}$). The most relevant isotope at present is ^{18}F . Similar to the others, it can be produced using small cyclotrons, so called ‘baby cyclotrons’. Compared to other positron emitting radioisotopes ^{18}F shows almost ideal decay characteristics: 96% positron branching and with 0.63 MeV a low maximum positron energy allowing detection in high resolution.

The ^{18}F -labeled glucose analogue 2-deoxy-2- ^{18}F -fluoro-D-glucose (^{18}F FDG) is currently one of the most often used radiopharmaceuticals being applied for tumor diagnosis worldwide (Fukuda *et al.* 1982; Brix *et al.* 2002). Due to the development of more and more tumor-specific peptides and antibodies, ^{18}F -labeling of these amino-acid-based compounds for highly specific diagnostic applications is rising more and more interest (for overview see Varagnolo *et al.* 2000; Okarvi 2001).

However, direct nucleophilic incorporation of ^{18}F fails due to the presence of acidic functionalities in those biomolecules and the necessity of harsh reaction conditions that occur during ^{18}F -labeling experiments. Electrophilic radiofluorination is theoretically possible when residual tyrosine groups are available in the protein, but bad regioselectivity, the low specific activity (only available in carrier added (^{19}F -added) form) and the low finally obtained radioactive yields (<50%, ^{18}F - ^{19}F) rather question the applicability of this approach. Consequently, the use of prosthetic groups is necessary. Preferred conjugation reactions being described are labeling reactions via amino-reactive conjugates, sulfhydryl-reactive conjugates, carboxyl-reactive couplings or photochemical conjugation.

When targeting sulfhydryl groups, common strategies are selective alkylation reactions with activated halides and maleimides. Well established examples of activated halides as prosthetic groups for ^{18}F -labeling are α -halo ketones such as ^{18}F fluorophenacyl bromide and N-(4- ^{18}F fluorobenzyl)-2-bromoacetamide (Kilbourn *et al.* 1987; Kuhnast *et al.* 2002). They react with soft nucleophiles like sulfhydryl groups to corresponding α -keto thioethers. Maleimide-containing compounds such as N-(4- ^{18}F fluorophenyl)maleimide (Wuest 2005) react with sulfhydryl groups according to a Michael-reaction to give thioethers.

N-terminal amines and ϵ -amino groups of lysine residues represent the most commonly targeted functional group for conjugation of ^{18}F -containing groups to peptides and proteins. Photochemical conjugation reactions are performed with azides such as 4-Azidophenacyl- ^{18}F fluoride (Wester *et al.* 1996), which react via

highly reactive nitrene intermediates with the amino groups. However, these reactions are very unspecific.

More often used conjugation reactions via prosthetic groups and residual amino groups are acylations, amidations, imidations, and oxim-forming reactions (for overview see Okarvi 2001; Wuest 2005). The most prominent reaction being applied is the formation of amide linkages. These fluoroacylation reactions can either be introduced via previously in-situ activated carboxylic groups that have been activated with carbodiimide agents such as the DCC (Wuest 2005). Other more prominent approaches induce direct aminolysis via ^{18}F -labeled active esters.

Table 1: Frequently used ^{18}F -labeled active esters for peptide and protein labeling via acylation

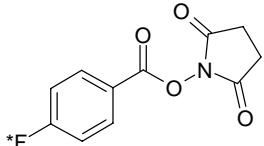
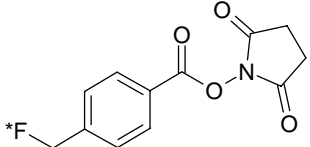
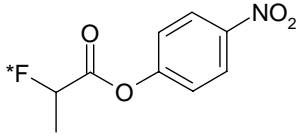
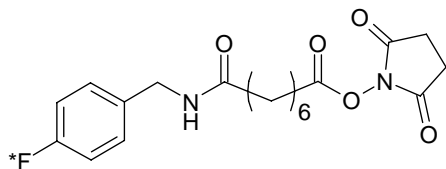
Prosthetic group	References
 <p>N-Succinimidyl 4-^{18}Ffluorobenzoate (^{18}FSFB)</p>	(Vaidyanathan & Zalutsky 1992; Vaidyanathan & Zalutsky 1994; Wester <i>et al.</i> 1996; Wuest <i>et al.</i> 2003)
 <p>N-Succinimidyl 4-^{18}F (fluoromethyl)benzoate</p>	(Lang & Eckelman 1994)
 <p>4-Nitrophenyl 2-^{18}Ffluoropropionate (^{18}FNPFP)</p>	(Guhlke <i>et al.</i> 1994)
 <p>N-Succinimidyl-8-[4'-^{18}Ffluorobenzyl]-amino] suberate</p>	(Garg <i>et al.</i> 1991)

Table 1 gives an overview of the most relevant acylation agents (Okarvi 2001; Wester 2003; Wuest 2005). Each of these approaches comprises advantages and limitations. But summarizing all relevant aspects such as low number of synthesis steps, short preparation time, high radiochemical yield, and good *in vivo* stability, N-Succinimidyl 4-[¹⁸F]fluorobenzoate (ISTU-mediated) ([¹⁸F]SFB) and 4-Nitrophenyl 2-[¹⁸F]fluoropropionate appear to be suitable acylation agents for ¹⁸F protein and peptide labeling.

The most attractive conjugation approach, chemoselective labeling via oxime ligation, comprises the use of ¹⁸F-benzaldehydes, since the achievable radioactive yield is high and the syntheses are very quick and simple (Poethko *et al.* 2004). The principle of this approach is that aldehydes react with high efficiency and chemoselectivity with previously aminoxy functionalized proteins, by forming stable oximes. A similar approach has been developed for using radiolabeled aldehydes and hydrazides to form hydrazones (Bruus-Jensen *et al.* 2006).

1.3 Aim of the study

In the present study initial experiments were performed to build a fundament for a potential future application of gelatin nanoparticles as highly specific and multi-functional carrier system for intravenous injection. A first focus was to establish PEGylation on the surface of the nanoparticles to shield them from the phagocytotic clearance via the MPS. Special care was taken on the development of new analytical tools for the monitoring of the PEGylation process. The second aim of the study was to develop a strategy for radiolabeling of plain and PEGylated gelatin nanoparticles to track their respective biodistribution *in vivo*. Thereby, a first goal was to investigate the biodistribution profile of standard 150-200 nm sized plain gelatin nanoparticles and subsequently to compare the biodistribution profiles of plain and PEGylated particles.

2. MATERIALS AND METHODS

2.1 Reagents

Reagent	Description	Supplier
Acetone	p.a.	VWR International GmbH (Ismaning, Germany)
Cholaminechloride hydrochloride	(2-aminoethyl)-trimethyl-ammoniumchloride hydrochloride	Sigma-Aldrich GmbH (Taufkirchen, Germany)
EDC	1-ethyl-3-(3-dimethyl-aminopropyl) carbodiimide hydrochloride	Sigma-Aldrich GmbH (Taufkirchen, Germany)
Gelatin type A	175 Bloom	Sigma-Aldrich GmbH (Taufkirchen, Germany)
Glutaraldehyde	25%	Sigma-Aldrich GmbH (Taufkirchen, Germany)
HCl	1 N	VWR International GmbH (Ismaning, Germany)
MPEG-NH ₂	Methoxy-poly (ethylene glycol)amine (Mw 5 kDa)	Nektar (Huntsville, AL, USA)
NaOH	1 N	VWR International GmbH (Ismaning, Germany)

2.2 Preparation of plain and PEGylated gelatin nanoparticles

Plain gelatin nanoparticles were produced in reference to previously established optimized conditions (see Chapter I). For PEGylation, 50 μ L of an aqueous nanoparticle dispersion (20 mg/mL) were incubated for 2 h under constant shaking (800 rpm; 25°C; Thermomixer comfort, Eppendorf AG, Hamburg, Germany) with various amounts of an MPEG-NH₂ solution in 0.5 M borate buffer pH 8.4 (20 mg/mL). Thereby, MPEG-NH₂ reacts with residual aldehyde groups on the surface of the gelatin nanoparticles. After incubation the total volume was filled up to 1 mL with highly purified water to get a nanoparticle concentration of 1 mg/mL. Aliquots of this non-purified dispersion were now taken to assess the quantity of conjugated MPEG-NH₂ by AF4. The remaining particles were purified by 3-fold centrifugation and redispersion.

Nanoparticles being used in the AFM experiments furthermore demanded a cationic surface charge to enable fixation on the anionic sample grid. The

cationization was performed according to the previously described method with the cationization agent cholamine (see Chapter II- 2.2).

2.3 Quantitative monitoring of nanoparticle PEGylation by AF4

AF4 measurements were performed in cooperation with my colleague Jan Zillies on an Eclipse2 AF4 system (Wyatt Technology, Santa Barbara, CA, USA). Autosampler, isocratic HPLC pump, degasser, UV-, and RI-detector were parts of the Agilent 1100 series (Agilent Technologies, Palo Alto, CA, USA). A fractionation-channel height of 350 μm and a regenerated cellulose ultrafiltration membrane (5 kDa cut-off; Nadir Filtration, Wiesbaden, Germany) were chosen as experimental settings as well as a phosphate buffer pH 7.0 (50 mM Phosphate 150 mM NaCl) as mobile phase. The flow-rate at the channel-outlet was 1 mL/min. PEG was quantified via the AUC of the RI signal according to a PEG-standard calibration curve. The amount of covalently bound PEG was assessed via the detected amount of unbound PEG.

2.4 Atomic force microscopy analysis of plain and PEGylated cationized gelatin nanoparticles

Size and surface morphology of cationized plain and PEGylated gelatin nanoparticles were analyzed by atomic force microscopy (AFM) in cooperation with Christian Lobbe (JPK Instruments, Berlin, Germany). Therefore, we used a JPK NanoWizard™ Life science version (JPK Instruments) in intermittent contact (ic) mode with a so called super sharp silicon (SSS) cantilever (NanoWorld, Schaffhausen, Switzerland). These special cantilevers were chemically etched and end with a slim 200 nm long and 2 nm-radius tip. Used cantilevers had a spring constant of about 42 N/m measured. Measurements in water were utilized with softer cantilevers having spring constants of about 0.2 N/m (10-15 nm-radius tip). In both cases the cantilever was excited close to its resonance frequency (air: ~ 300 kHz; water: ~ 12 kHz).

2.5 Synthesis of 4-Nitrophenyl 2-[¹⁸F]fluoropropionate ([¹⁸F]NPPF)

The synthesis of [¹⁸F] NPPF according to a previously described protocol (Wester et al. 1996) is well established as it is a routine labeling agent in our cooperation partner's facility. Consequently, the respective agent was obtained as aliquots from large scale batches.

2.6 Adopted synthesis of N-succinimidyl-[¹⁸F]fluorobenzoate ([¹⁸F]SFB)

The synthesis of [¹⁸F]SFB was performed according to the previously described protocol (Wester *et al.* 1996) of the improved synthesis using O-(N-succinimidyl)-N,N,N',N'-tetramethyluronium tetrafluoroborate (TSTU) as activating reagent. In cooperation with Dr. Norman Koglin (Nuclear medicine, TU Munich), the original protocol was further optimized resulting in the following procedure:

[¹⁸F]Fluoride was produced via the ¹⁸O-(p,n)¹⁸F nuclear reaction by bombardment of isotopically enriched [¹⁸O] water target with a 11-MeV proton beam at the RDS-112 cyclotron (Siemens/CTI, Munich, Germany).

The resulting aqueous [¹⁸F]fluoride solution was separated from [¹⁸O]H₂O using an anion exchange cartridge. After elution with ~200 µL 1 M potassium carbonate solution, the aqueous [¹⁸F]fluoride solution was transferred to a 2.5 mL conical vial containing 500 µL of anhydrous acetonitril and 10 mg Kryptofix 2.2.2 (Merck, Darmstadt, Germany). The solution was azeotropically dried with 3 x 300 µL acetonitrile portions in a stream of argon.

11 mg of the triflate salt of ethyl p-trimethylammonium benzoate were dissolved in 250 µL anhydrous dimethylsulfoxide. This solution was added to the dry cryptate (K⁺[2.2.2]/¹⁸F⁻). Subsequently, the reaction vessel was heated at 90°C for 5 min. Afterwards 0.5 mL of 0.3 M sodium hydroxide were added and stirred at 90°C for 10 min hydrolyzing the ester. This reaction was stopped by acidification with 1 mL of 0.3 M HCl. The reaction vessel was rinsed twice with 0.03 M HCl. The obtained 4-[¹⁸F]fluorobenzoic acid was fixed by passing the reaction mixture through a Sep-Pak C18 cartridge. The product was eluted from the cartridge with 2 x 2 mL ether and collected in a new reaction vessel. The aqueous phase was discarded. The

remaining organic solution was treated with 50 μL 20% tetramethylammonium hydroxide. Afterwards, the solvent was evaporated under a stream of argon. Drying was repeated three times by addition and evaporation of acetonitrile. For activation a solution of 10 mg TSTU, dissolved in 400 μL acetonitrile was added and heated for 2 min at 90°C. Instant acidification was performed by addition of 2 mL 0.1% TFA/ H_2O . Subsequently, the solution was passed through a Sep-Pak C-18 cartridge and the column was washed with 2 mL 20% acetonitrile/0.1% TFA/ H_2O and the activated ester eluted with 50% acetonitrile/0.1% TFA/ H_2O . The acetonitrile was evaporated by rotary evaporation.

Preparative chromatography was performed using a LiChrosorb RP-18 select B column (7 μm , 250 x 4 mm) at a flow rate of 5 mL/min and a gradient 20 \rightarrow 50% acetonitrile/ H_2O over 20 min. The product peak was fractionated, diluted with 10 mL H_2O and fixed on a HR-P cartridge (Macherey-Nagel, Dueren, Germany). The cartridge was dried under a stream of argon and [^{18}F]SFB was eluted with ether.

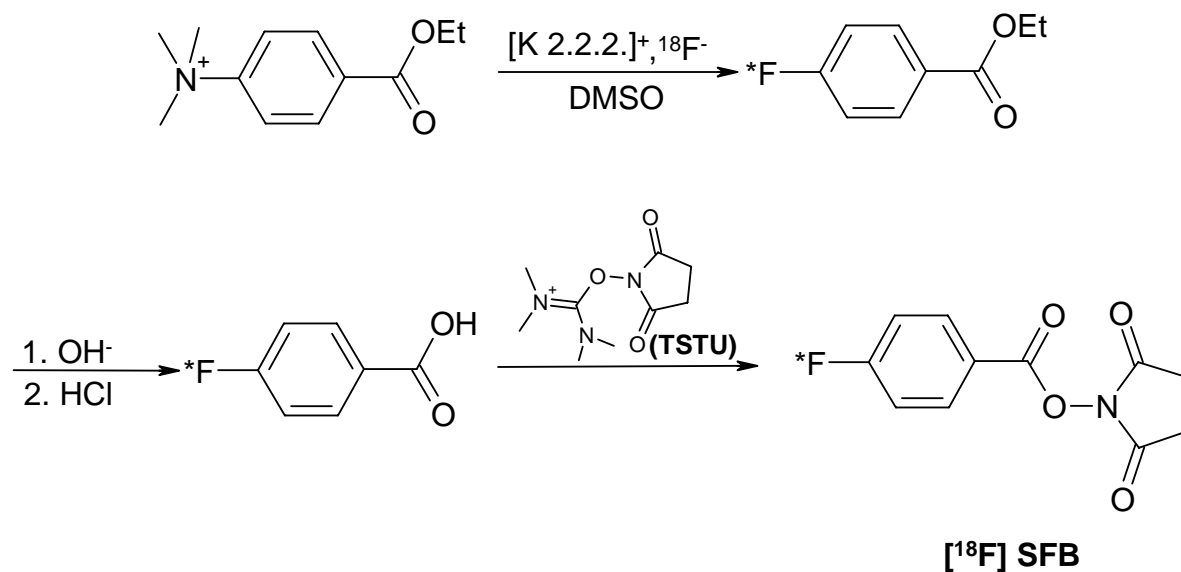


Fig. 1: Scheme of the preparation of [^{18}F] SFB.

2.7 ^{18}F -Radiolabeling of gelatin nanoparticles with [^{18}F]SFB/ [^{18}F]NPFP

[^{18}F]SFB dissolved in ether was transferred to a reaction cap and the ether was removed in a stream of argon. 100 μL of a gelatin nanoparticles dispersion in 0.5 M borate buffer (pH 8.0, if not differently stated) were added to the residue. Furthermore, 20 μL of acetone were added. The mixture was incubated for 30 min at 37°C under constant shaking (800 rpm). Purification was performed by 3 times centrifugation and redispersion of the gelatin nanoparticles. After every centrifugation step, the supernatant was collected and measured in a Capintec CRC Dose Calibrator (Capintec Inc., Ramsey, NJ, USA) to determine unbound [^{18}F] fluorobenzoic acid/SFB. Finally, the particles were dispersed in physiological PBS (pH 7.4).

[^{18}F]NPFP labeling was performed according to the same protocol.

2.8 $^{125}\text{I}/^{123}\text{I}$ labeling of gelatin nanoparticles

Radioiodination was performed according to the standard protocol being described by Pierce Biotechnology Inc. (Rockford, IL, USA; www.piercenet.com) with slight modifications. Thereby, Iodogen (1,3,4,6-tetrachloro-3a,6a-diphenylglycouril) was dissolved in chloroform in a concentration of 1.5 mg/mL. 100 μL of this solution (corresponding to 150 μg Iodogen) were added to a 2 mL Eppendorf reaction cap (Eppendorf AG, Hamburg, Germany) Chloroform was evaporated under gentle heating in a water bath and constant rotation. Thus, water-insoluble Iodogen was plated onto the inner surface of the cap. The Iodogen coated caps were stored at -20°C until usage. Gelatin nanoparticles dispersed in PBS pH 7.4 were added to the Iodogen coated reaction vessel. Subsequently, 10-20 μL radioiodide solution in 0.05 N NaOH (^{125}I : Hartmann Analytic, Braunschweig, Germany; ^{123}I : GE/Amersham Health, Eindhoven, The Netherlands) were added. This mixture was incubated at ambient temperature under slight shaking. After 30 min, an aliquot sample was taken to quantify the percentage of successful ^{125}I or ^{123}I conjugation via thin layer chromatography (TLC). TLC was performed using silica gel 60 F254 TLC plates from Merck (Darmstadt, Germany). To separate free iodine from that being linked onto the nanoparticle a mixture of acetone, butanol, ammonia, and water (65:20:10:5) was chosen as mobile phase. The resulting radioactive spots on the TLC plate were

quantified by an automatic TLC analyzer, Tracemaster 20 (Berthold, Wildbad, Germany).

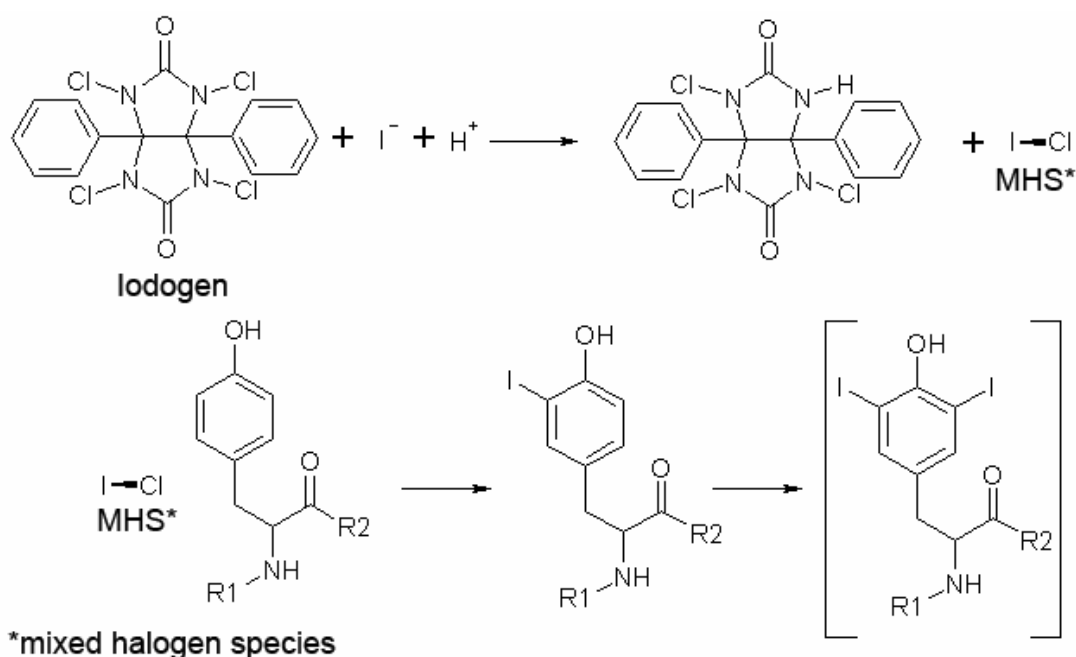


Fig. 2: Mechanism of radioiodide incorporation into proteins; a) formation of the reactive mixed halogen species by Iodogen; b) Iodination of tyrosine (to a lower extent also histidine and tryptophan) resulting in a mixture of monoiodinated and rare diiodinated tyrosyl moieties.

2.9 Biodistribution experiments

For biodistribution studies the radiolabeled gelatin nanoparticles dispersed in PBS 7.4 were injected into the tail vein of Balb/c mice. Concentrations were adjusted to injection doses of 100 μ L containing nanoparticles labeled with 50 μ Ci radioactivity. During injection, the mice were slightly anesthetized via inhalation of ether. At selected time points after injection, organs of interest were dissected. The radioactivity was measured in weighted tissue samples using a γ -counter (1480 Wizard3 gamma counter from Wallac, Turku, Finland). Results are expressed as the percentage injected dose per gram (%ID/g) (mean \pm s.d., 3–5 animals per group) if not stated otherwise.

2.10 PET imaging

For PET imaging, respective amounts of 18 F-labeled gelatin nanoparticles were dispersed in PBS 7.4. Similar to the biodistribution studies, the dispersions were

adjusted to injection doses of 100 μ L containing 50 μ Ci radioactivity. These doses were injected intravenously into the tail vein of white Balb/c mice that were anesthetized using a combination of xylazine and ketamine. Dynamic PET images (10-60 min after injection) of the anesthetized mice were acquired using a Philips MOSAIC small animal PET scanner (Philips, Hamburg, Germany).

2.11 γ -camera imaging

¹²³I-labeled nanoparticles were dispersed in PBS 7.4 and adjusted to injection doses of 100 μ L containing 80-140 μ Ci. During injection, mice were slightly anesthetized with inhalation of ether. Mice were sacrificed 15 min p.i.. For acquisition of γ -camera images mice were directly positioned on one medium energy general purpose collimator of a dual-headed γ -camera (Skylight, ADAC/Philips, Hamburg, Germany). Data acquisition was performed for 20 min.

3. RESULTS AND DISCUSSION

3.1 PEGylation of gelatin nanoparticles

3.1.1 Quantitative analysis of the PEGylation properties of gelatin nanoparticles via AF4

As mentioned, PEGylation is currently a very popular method to prolong the blood circulation time of biomolecules or colloidal carrier systems by shielding them from detection by the MPS. In order to achieve pH-sensitive linkage of PEG, we chose MPEG-NH₂ as PEGylation agent to give imines with available aldehyde groups on the nanoparticle surface that could be attributed to only monofunctionally bound glutaraldehyde. Resulting imine bonds are pH-sensitive and hydrolyze under acidic pH conditions. To quantify the amount of MPEG-NH₂ that was finally grafted onto the nanoparticles, our idea was to detect the amount of free, unbound PEG directly with the present AF4 setup.

The complete development and validation of the analytical method was performed by Jan Zillies. Data concerning these issues will be published in his thesis (Zillies 2007).

According to its molecular properties, the PEG signal is only detected as peak in the RI detector, whereas the gelatin nanoparticles appear as stronger signal within the UV-detector. However, gelatin nanoparticles induce also a certain RI signal. Consequently, particle separation from PEG as realized with the AF4 system was mandatory to avoid any disturbance of the PEG signal.

Aside from the PEG quantification, it was a further goal of our analytical approach to determine a certain saturation-threshold dose of PEG when the nanoparticles are completely loaded with MPEG-NH₂. Therefore, 1 mg of gelatin nanoparticles were incubated with increasing amounts of MPEG-NH₂, ranging from 31.25 µg up to 1 mg MPEG-NH₂.

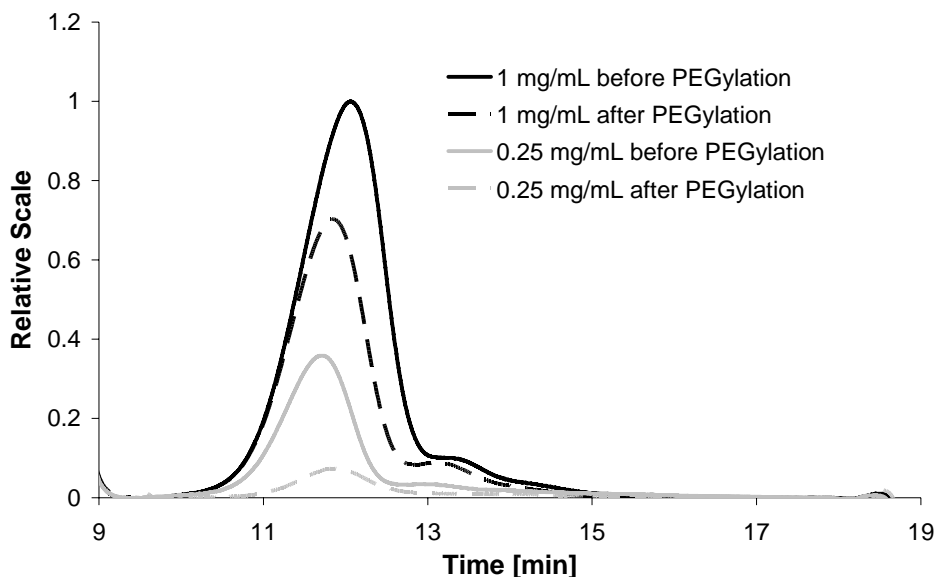


Fig. 3: Exemplary fractograms of two different MPEG-NH₂ concentrations (1 mg/mL: black; 0.25 mg/mL: grey) before and after the incubation with gelatin nanoparticles. Solid lines represent the fractograms before and dotted lines those after incubation.

Analyzing the AUCs of MPEG-NH₂ before and after incubation with 1 mg nanoparticles (Fig. 3), a certain dose dependent saturation became visible. A significant peak of unbound PEG could be detected when administering 1mg PEG per mg nanoparticles, whereas only a low signal could be detected when 0.25 mg PEG was administered. The amount of bound PEG was calculated by the following equation:

$$m_x = (AUC_0 - AUC_x) \times m_0$$

m_x = mass of MPEG-NH₂ being loaded onto the nanoparticles

m_0 = initially administered mass of MPEG-NH₂

AUC_x = AUC of the RI signal being detected for the amount of residual free of MPEG-NH₂ after incubation

AUC_0 = AUC of the RI signal being detected for the amount m_0 of MPEG-NH₂ before incubation

The so calculated values of the various amounts of PEG bound per mg nanoparticles are plotted versus their pertaining originally administered amounts per mg nanoparticles in Fig. 4. Analyzing this diagram, ~350 µg MPEG-NH₂ could be identified as the maximum dose that could be covalently linked onto the surface of 1 mg gelatin nanoparticles. This complete loading can be achieved with the

utilized incubation settings of 1 mg gelatin nanoparticles in 50 μL highly purified water being incubated over 2 h with ~ 0.8 mg MPEG-NH₂ in 50 μL 0.5 M borate buffer pH 8.4.

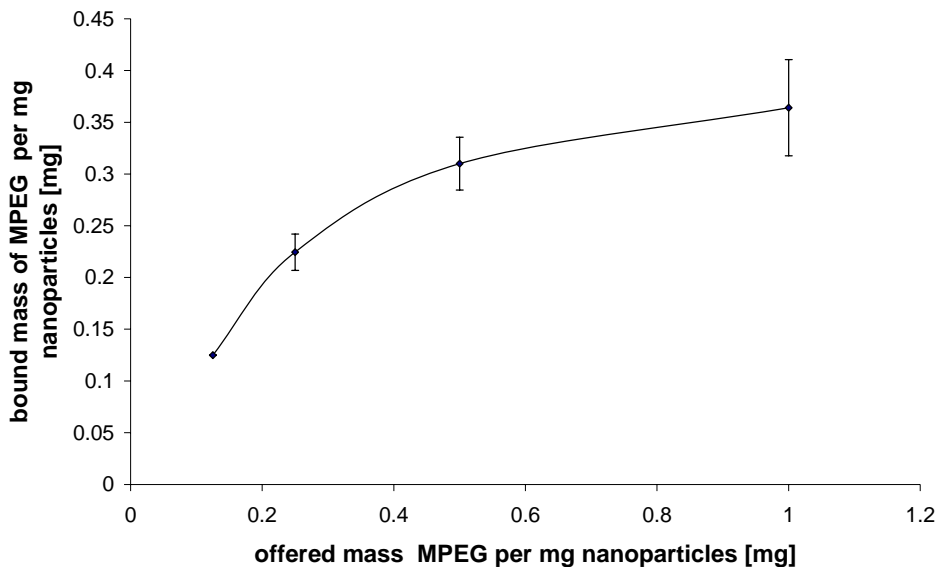


Fig. 4: Amount of MPEG-NH₂ being loaded onto 1 mg nanoparticles in dependency of the originally offered amount of MPEG-NH₂.

In a final experiment we wanted to scrutinize the impact of the applied pH conditions during the incubation process. Successful linking was performed in 0.5 M borate buffer pH 8.4, since alkaline conditions are beneficial for the reaction of aldehyde groups with primary amino groups. Hence, changing the pH towards acidic conditions should have negative impact on the reaction yield. Comparing the chromatograms of 1 mg PEG that has been incubated with 1mg nanoparticles in an acidic aqueous solution (pH 3.0) versus 1 mg PEG standard, both peaks were almost identical (data not shown). Thus, we could demonstrate that no conjugation occurs under these unfavorable acidic reaction conditions. Moreover, this experiment represents a successfully coped negative control, to prove the accuracy of the new established analytical method.

For further detailed information on the performed experiments, see Jan Zillies' dissertation (Zillies 2007).

3.1.2 Visual comparison of the surface morphology of plain and PEGylated gelatin nanoparticles by AFM

Searching for other modes to characterize the nanoparticles we investigated AFM as an interesting method, since it is obviously dedicated for the analysis of various surfaces due to its measurement principle. Summarizing the microscopic visualization techniques it is the method of choice for the analysis of surface morphologies, since it allows the highest resolution. Other groups have already demonstrated this as they were even able to visualize the helical structure of DNA (Ravi Kumar, V *et al.* 2004; Bakowsky 2005) via AFM. Prior measurement, the nanoparticles were fixed on the sample grid by electrostatic interactions. Since the sample grid had a negatively charged coating, the nanoparticles had to be cationized to ensure sufficient fixation. Certainly, it has to be mentioned that the measured nanoparticles were not identical to those that were analyzed via AF4 and applied in later *in vivo* biodistribution experiments. But it was supposed that this modification with cholamine, a low molecular weight substance (Mw 175.10 Da) should not have crucial impact on the particle's morphology. Otherwise, this is a good example that both modifications can be performed on one nanoparticle batch. Dynamic light scattering (DLS) revealed that neither cationization *or* PEGylation nor cationization *and* PEGylation led to changes in particle homogeneity. All batches still had polydispersity indices below 0.1 (Table 2).

Table 2: DLS size determination data of the applied nanoparticle batches; ZWAFM: plain nanoparticles; ZWAFM-PEG: PEGylated batch ZWAFM

	plain nanoparticles		cationized nanoparticles	
	size (nm)	PI	size (nm)	PI
ZWAFM	179.7	0.041	180.4	0.064
ZWAFM-PEG	185.2	0.072	184.5	0.097

The images derived from AFM analysis of the cationized versions of ZWAFM and ZWAFM-PEG are depicted below (Fig. 5):

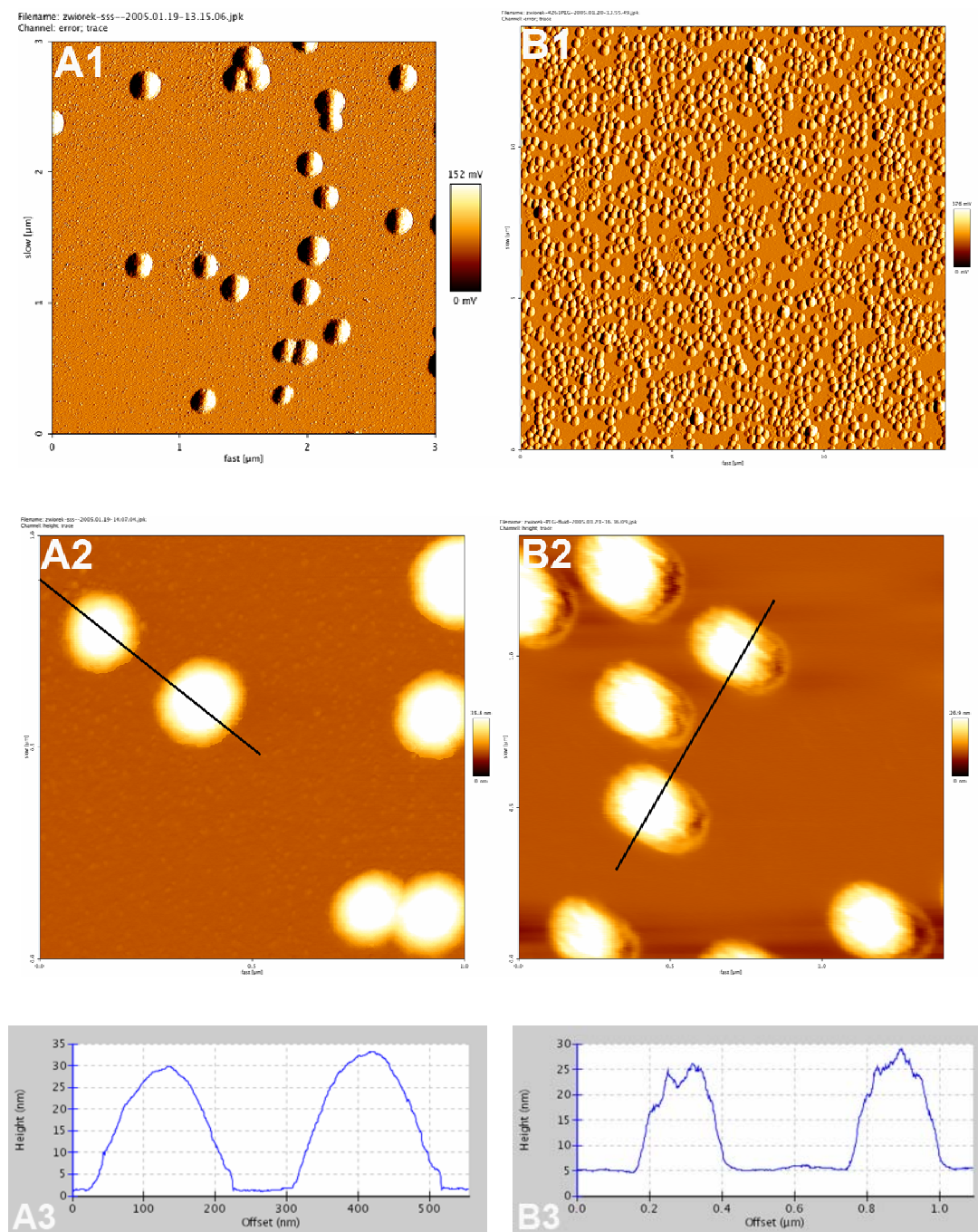


Fig. 5: AFM analysis of plain (A1-A3) and PEGylated (B1-B3) gelatin nanoparticles; A/B 1: error channel image; A/B 2: height channel image; A/B 3: cross section of the height image (see black lines)

Overview images being employed in the amplitude mode demonstrated the good homogeneity of the applied samples (Fig. 5-A/B1). No significant differences between both batches could be noticed. So, previous SEM data, where those

gelatin nanoparticles were assessed as homogeneous smooth spheres were substantiated (see Chapter I – 3.1). But analyzing height images, PEGylated nanoparticles seemed to possess a more indifferent surface (Fig. 5-A/B2). Observing the respective cross sections of these height images finally revealed more detailed information (Fig. 5-A/B3). Contrary to the smooth surface of plain gelatin nanoparticles, PEGylated nanoparticles featured a cragged surface when analyzing their height profile in highly purified water, which obviously indicates the presence of PEG-chains on the nanoparticles' surface.

3.1.3 Summary

Present data indicate that PEGylation of gelatin nanoparticles with MPEG-NH₂ is possible. Thus, the residual amino group of MPEG reacts with free aldehyde groups on the nanoparticle surface by forming an imine. Quantitative analysis via AF4 demonstrated that up to ~0.35 mg PEG can be attached onto the surface of 1 mg nanoparticles in dependency of the amount of MPEG-NH₂ being offered. The absence of successful conjugation while performing the incubation of gelatin nanoparticles and MPEG-NH₂ under acidic aqueous conditions leads to the conclusion that the conjugation is mainly based on the covalent linkage as imine, since this reaction is suppressed under acidic conditions.

AFM as second analytical tool finally completed the set of data and demonstrated its strength by visualizing the presence of PEG chains on the nanoparticles' surface. Especially the combination of both techniques appears to be ideal to track the PEGylation of colloidal carrier systems, even more due to the certain lack of other appropriate techniques.

3.2 Biodistribution experiments with radiolabeled gelatin nanoparticles

3.2.1 Evaluation of the applicability of prosthetic groups for radioactive ^{18}F labeling of gelatin nanoparticles

The necessity of prosthetic groups for ^{18}F labeling of proteinaceous material has already been discussed. Searching for the ideal radiofluorination agent, the use of ^{18}F -benzaldehydes appeared very attractive, because of their fast synthesis and high radioactive yield. However, this process could not be applied for gelatin nanoparticles due to the necessary conjugation conditions, since gelatin nanoparticles contain free aldehyde groups according to only monofunctionally bound crosslinking-agent glutaraldehyde. Thus, additional aminoxy functionalization of the nanoparticles would induce immediate aggregation.

Moreover, it was refrained from labeling sulfhydryl groups on the nanoparticle surface since none are present in the primary sequence of gelatin. Thus, previous introduction would have been necessary. Considering these facts and summarizing the pros and cons of the remaining amino-reactive prosthetic groups, it was decided that [^{18}F]SFB (TSTU-mediated) and [^{18}F]NPFP seem to be the most promising radiolabeling agents worth to be further investigated. To find the most efficient agent for gelatin nanoparticle radiolabeling, we tested the potential of both in parallel. Therefore, 100 μL of gelatin nanoparticle dispersion were applied (conc. 29 mg/mL). Dynamic light scattering analysis resulted with an averaging mean size of 180.4 nm and 0.053 as corresponding polydispersity index for the chosen plain nanoparticle batch ZW1F18. Aliquots of this batch were incubated with low dose amounts of the respective ^{18}F prosthetic groups ($\sim 100 \mu\text{Ci}$: [^{18}F]SFB; $\sim 180 \mu\text{Ci}$: [^{18}F]NPFP). Fig. 6 shows the radiochemical yields (RCYs) that were achieved when labeling the described gelatin nanoparticles with both radioactive acylation agents at various pH conditions.

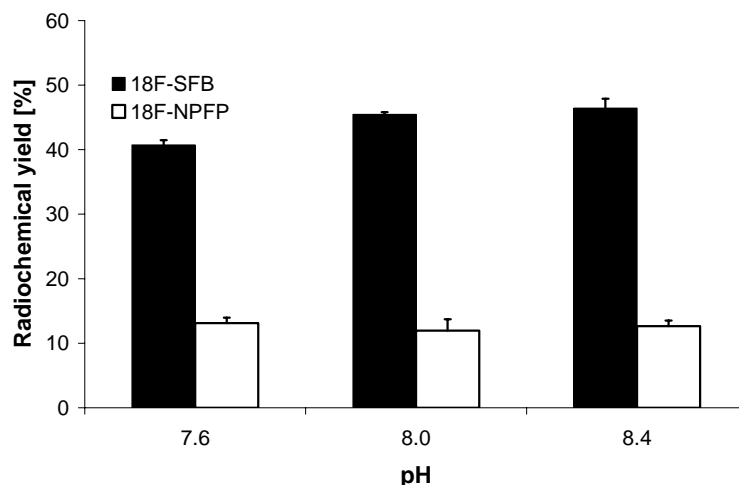


Fig. 6: Comparative study of radiolabeling efficiency of [^{18}F]NPFP and [^{18}F]SFB to evaluate their potential as ^{18}F -labeling agents for gelatin nanoparticles at various pH conditions.

The resulting RCYs of successfully labeled gelatin nanoparticles differed remarkably between both radioacylation agents. Whereas only 12-13% RCY could be achieved for labeling with [^{18}F]NPFP, [^{18}F]SFB was more efficiently linked onto the nanoparticles (40.7-46.5% RCY) and able to exceed [^{18}F]NPFP by far. Moreover, the RCY was improved when using 0.5 M borate buffer at pH 8.0 and 8.4 (45.5-46.5% RCY) instead of pH 7.6 (40.7% RCY) as conjugation medium. Performing size determination of the respective [^{18}F]SFB-labeled nanoparticle samples (batch ZW1F18), no significant changes could be detected (Fig. 7).

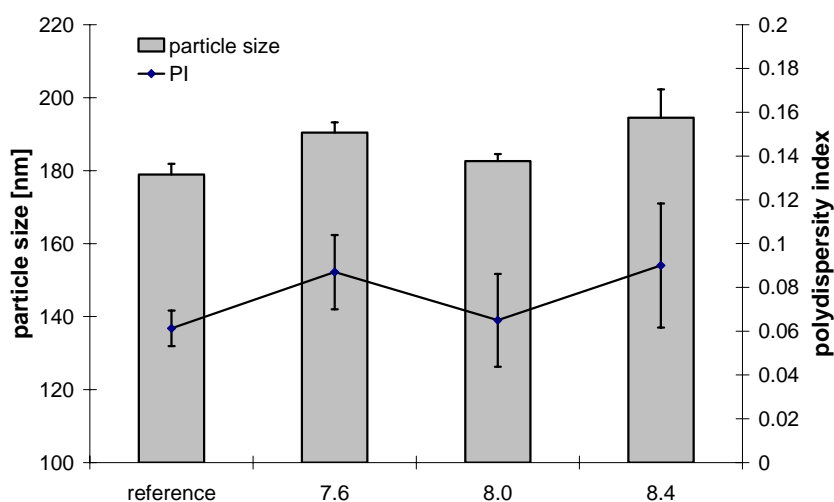


Fig. 7: Dynamic light scattering control experiments of [^{18}F]SFB-labeled gelatin nanoparticles being conjugated at various pH conditions.

According to these results, it was decided that [^{18}F]SFB was the prosthetic group of choice for ^{18}F -labeling of gelatin nanoparticles in high radiochemical yields. The second parameter we examined was the influence of the offered amount of gelatin nanoparticles on the achievable RCYs. Fig. 8 indicates that ^{18}F conjugation yields of up to 50% can be achieved with increasing amounts of gelatin nanoparticles. Thereby, the underlying correlation of both parameters can be very well described with a logarithmical fit. Changes of the initially utilized ^{18}F - respectively [^{18}F]SFB-dose did not influence this phenomenon. Thus, optimum yield was achieved above a concentration of 3 mg nanoparticles in 100 μL 0.5 M borate buffer (\rightarrow conc.=30 mg/mL).

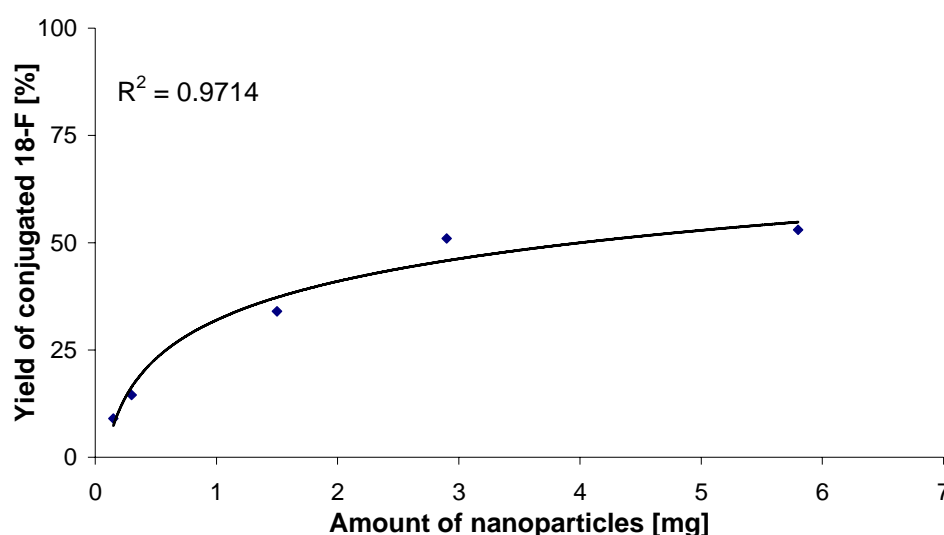


Fig. 8: RCY in dependence of the offered amount of gelatin nanoparticles; conjugation buffer: (0.5 M borate buffer pH 8.0)

3.2.2 Biodistribution experiments with ^{18}F -labeled gelatin nanoparticles

Since it was demonstrated that gelatin nanoparticles can successfully be labeled with [^{18}F]SFB produced in the established small scale setup, first *in vivo* biodistribution experiments could be initiated. In this study, 2 mg ^{18}F -labeled gelatin nanoparticles being dispersed in 100 μL PBS 7.4 were injected to 2 groups of mice containing 4 individuals each. The injected radioactive dose was ~ 50 μCi per animal. The first group was sacrificed after 30 min and the other after 60 min. Subsequently the biodistribution of the nanoparticles was assessed by detection of the accumulated radioactivity in various organs. Additionally, the biodistribution

was tracked online via a dynamic PET scan of one mouse (Fig. 9). Early PET images after 10 min revealed that the nanoparticles accumulated very quickly in lung and liver. This distribution pattern remained constant over 60 min. Solely certain radioactivity became visible in the bladder with increasing time, which might indicate cleavage of the radioactive agent and/or initial degradation of the nanoparticles. The signal in the tail region of the mouse referred to particles that remained at the site of injection.

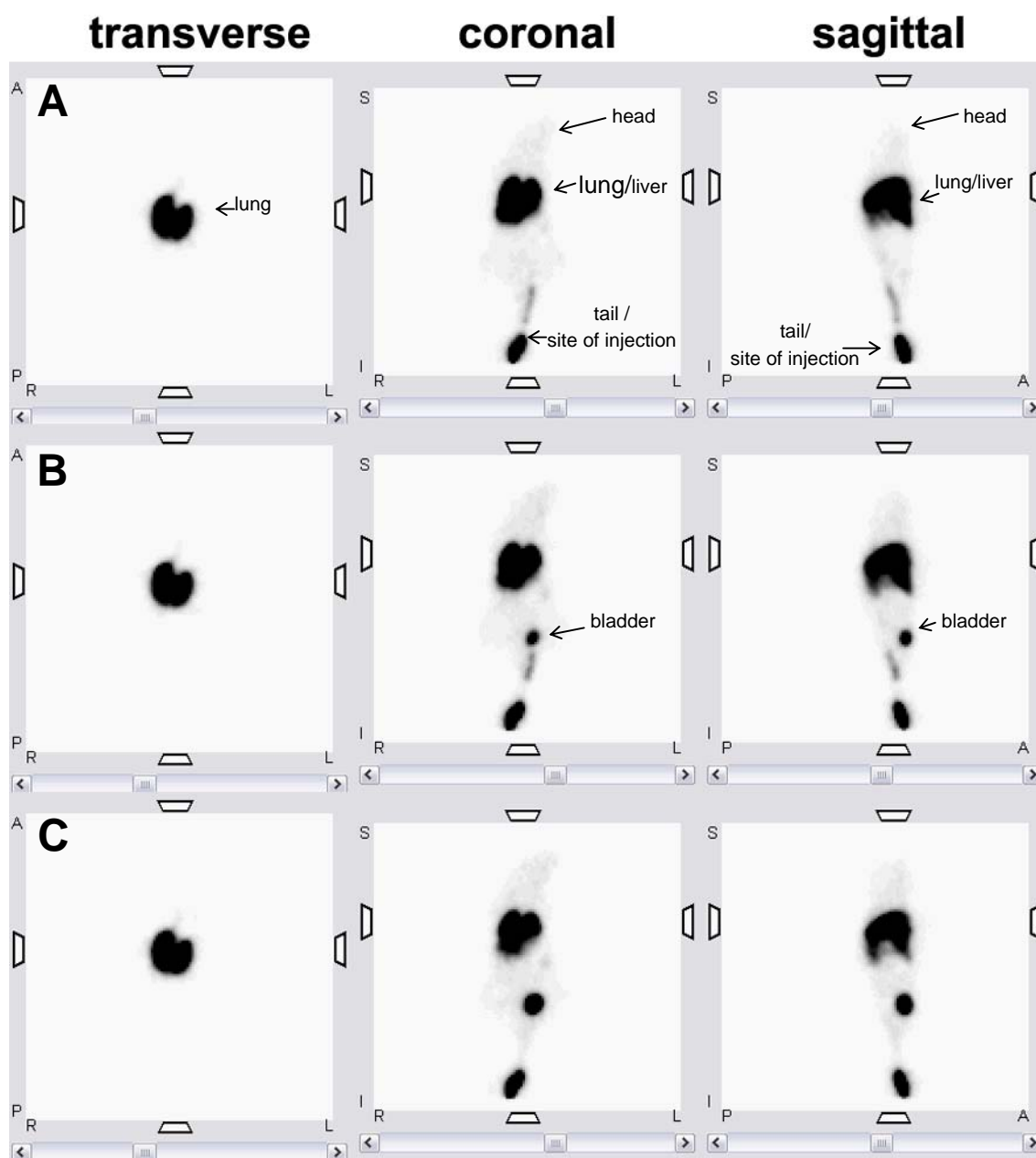


Fig. 9: PET images after 1-10 min (A), 21-30 min (B), and 51-60 min (C) after injection of 2 mg nanoparticles.

The quantification of the biodistribution substantiated these observations very well (Fig. 10). The highest concentration of radioactivity (depicted as %ID/g) was determined in the lungs. In addition, edema could be observed in the lung tissue of some mice when dissecting their organs after sacrificing. Consequently, this strong lung accumulation had to be attributed to the occurrence of thromboses in the lung capillaries which are caused by the high amount (2 mg) and concentration (20 mg/mL) of nanoparticles that was injected.

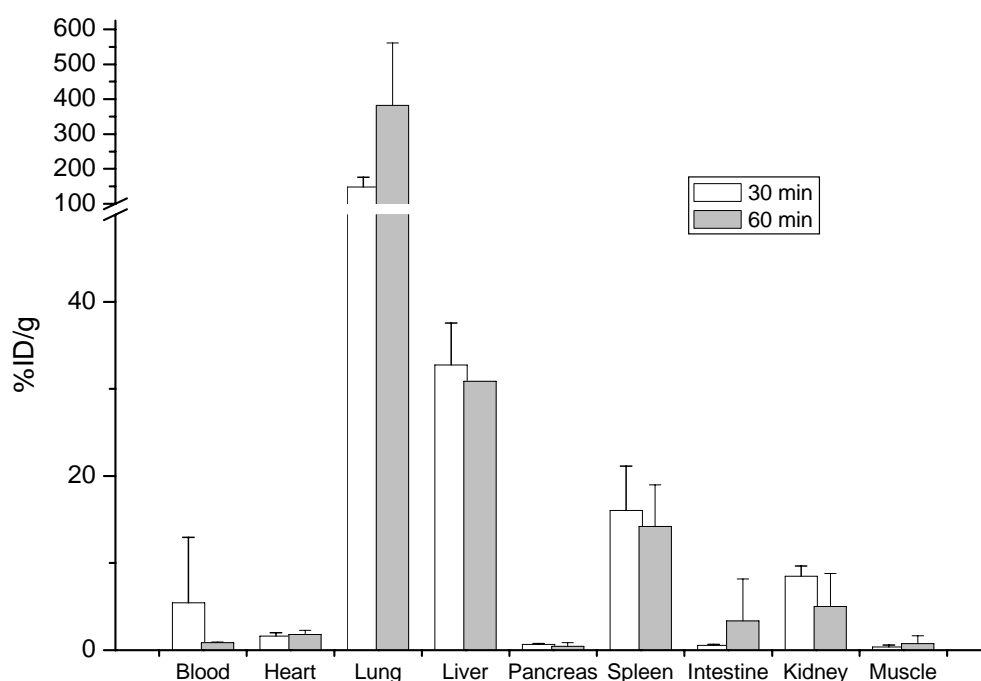


Fig. 10: Biodistribution of gelatin nanoparticles in mice after injection into the tail vein ($n=4$); radioactivity concentrations are given as percent of the injected radioactive dose per gram tissue (%ID/g).

However, in the small ‘lab-scale’ [^{18}F]SFB, the radioactivity that could be linked onto the nanoparticles was too low for the administration of less concentrated nanoparticle dispersions. Therefore, upscaling from the present setup was necessary to obtain [^{18}F]SFB with higher radioactivity. Simultaneously, this required also a higher initial radioactivity of ^{18}F at the start of the synthesis (~ 100 mCi). Due to safety reasons these syntheses could no longer be manually prepared in the lab. Thus, the [^{18}F]SFB synthesis had to be transferred for a large-scale setup into a radiation shielded hot-cell. Although scale up was carried out successfully

concerning the obtained [^{18}F]SFB yield and subsequent conjugation, the resulting ^{18}F -labeled nanoparticles tended towards strong aggregation, thus could not be applied for animal experiments. Searching for reasons, the used nanoparticle batch (ZW1F18) could be excluded as originating factor, since no aggregation occurred when performing control experiments with Texas Red-XTM succinimidylester instead of [^{18}F]SFB. These control-experiments were performed following the identical procedure as that for [^{18}F]SFB labeling. But also the [^{18}F]SFB could be almost excluded, since the molar amount administered was not significantly increased in comparison to the previous low scale experiments. Finally, we discovered the presence of an impurity peak with variable intensity in the UV-signal which is co-eluted at similar retention time as [^{18}F]SFB in the preparative HPLC purification step. Unfortunately, the origin of this impurity could not be located so far and is still under investigation.

3.2.3 Biodistribution experiments with $^{123}\text{I}/^{125}\text{I}$ -labeled gelatin nanoparticles

While we were searching for reasons that caused the nanoparticle aggregation during labeling with [^{18}F]SFB derived from large scale production, we considered radioiodination of the gelatin nanoparticles as an alternative strategy, since it is a well established method for proteins and peptides. Furthermore, ^{125}I had been used in recently published biodistribution experiments with nanoparticles based on a gelatin-PEG co-polymer (Kaul & Amiji 2004). In order to evaluate the applicability of this approach, we performed initial experiments with iodine isotope ^{123}I due to its shorter radioactive half-life (13h) in comparison to commonly used ^{125}I ($T_{1/2} = 60$ d) and the possibility to image the *in vivo* distribution via planar γ - or SPECT-Imaging. Furthermore, after a 6d decay period of the ^{123}I -iodine label, the nanoparticles could be analyzed without considerations by DLS for changes concerning their average mean sizes. Moreover, we now compared for the first time plain with PEGylated gelatin nanoparticles. The PEGylated nanoparticles that were used in this experiment were prepared according to the previously described method, incubating 1 mg MPEG-NH₂ with 1 mg plain gelatin nanoparticles in 0.5 M borate buffer pH 8.4 to achieve a complete saturation of the free aldehyde groups on the nanoparticle surface.

With respect to labeling efficiency, TLC analysis demonstrated that ^{123}I was almost completely introduced into the accessible tyrosyl groups of plain and PEGylated

gelatin nanoparticles within 30 min (Fig. 11). No relevant amounts of free ^{123}I could be measured for both, plain and PEGylated gelatin nanoparticles.

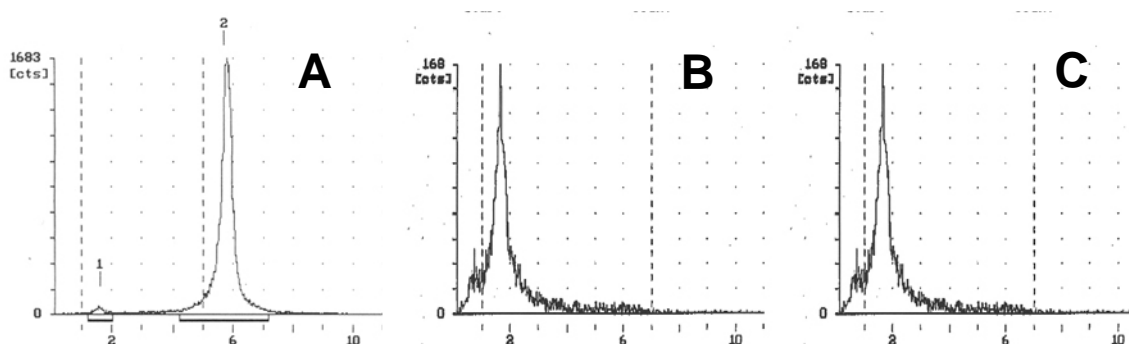
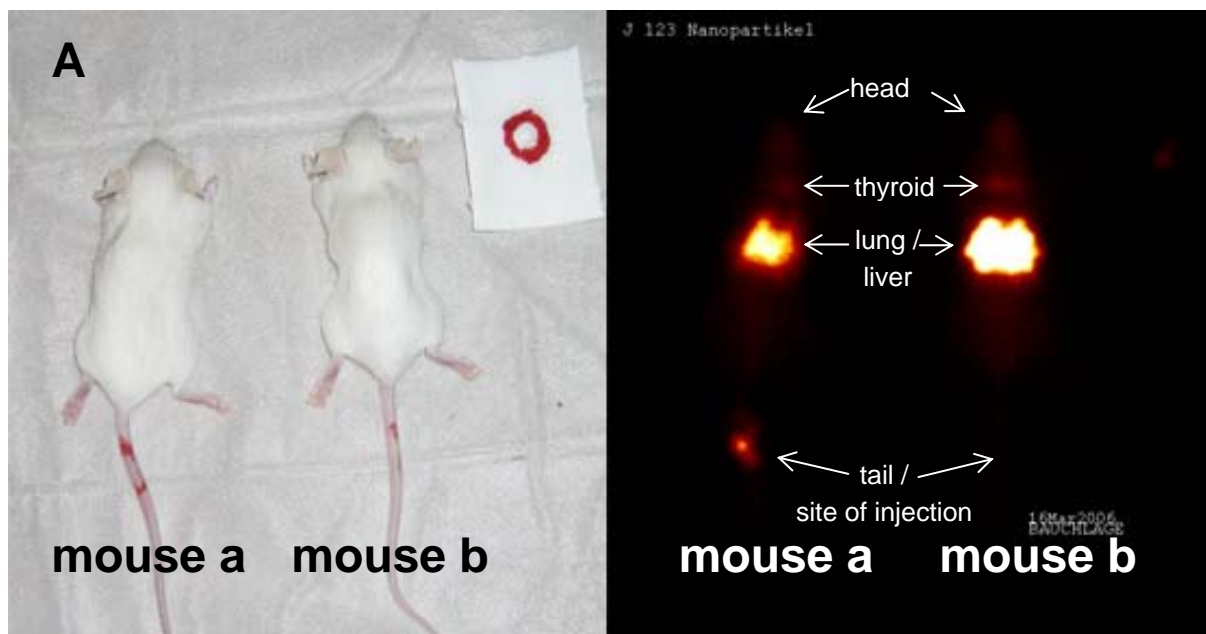


Fig. 11: Quality control of ^{123}I -labeled nanoparticles via TLC after 30 min of incubation; A: [^{123}I]iodide control without nanoparticles; B: [^{123}I]iodide reacted with plain nanoparticles; C: [^{123}I]iodide reacted with PEGylated nanoparticles

Consequently, it could be refrained from further nanoparticle purification and nanoparticles were only diluted with PBS 7.4, to a concentration of 1 mg/mL. Finally, formulations of 100 ng (corresponding to 100 μL of 1 mg/mL nanoparticles) were injected into the tail vein of one mouse each.



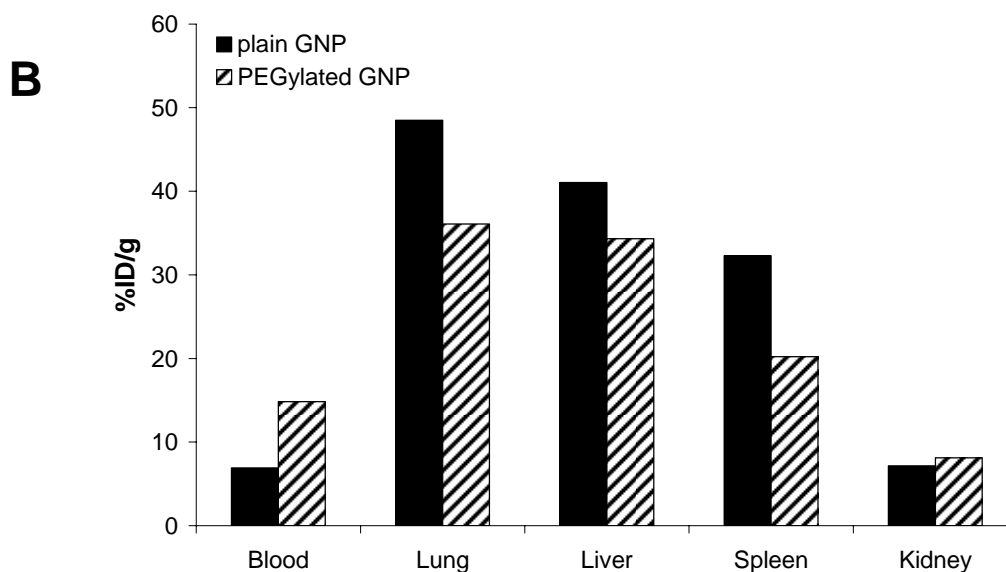
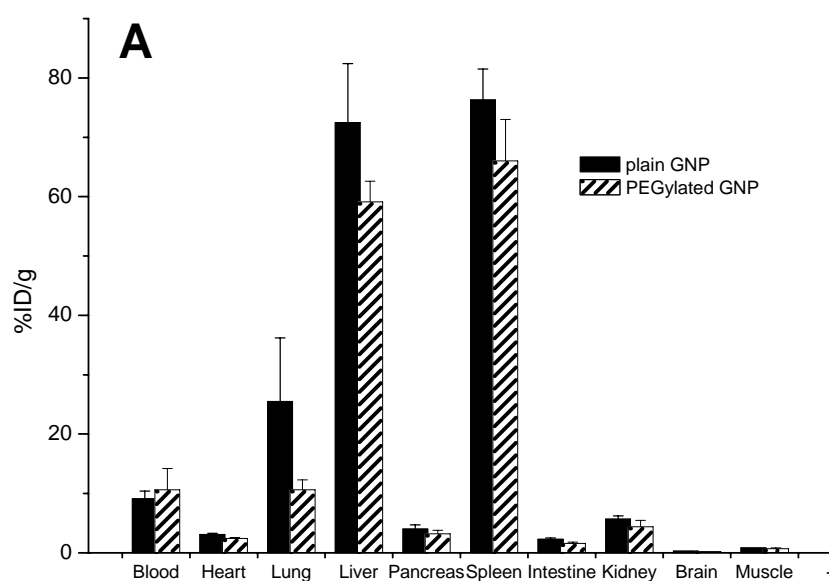


Fig. 12: Rough estimation of biodistribution pattern of plain and PEGylated ^{123}I -labeled nanoparticles; injected dose of nanoparticles: 100 ng in 100 μL PBS 7.4; time point of sacrifice: 30 min. A: γ -camera scan; mouse a: PEGylated nanoparticles; mouse b: plain nanoparticles. B: Semi-quantitative analysis of the accumulated radioactive dose (%ID/g) in the major organs of these two mice as measured by a γ -counter.

The obtained data are only based on single shots and consequently without any statistical significance. Even though, the strong accumulation within the lung tissue did not occur in both mice. In addition, no edemas caused by thromboses were observed with this 20-fold reduced dose when dissecting the lung tissue of both mice. Concurrently, it could be seen that γ -camera imaging enables only visual distribution data of limited precision and accuracy in comparison to PET (Fig. 12A). Again, the signal in the tail region of the mouse being treated with PEGylated nanoparticles referred to particles that remained at the site of injection. Slight radioactivity within the thyroid gland region occurs due to free ^{123}I formed by *in vivo*-deiodination. Measuring size and homogeneity of particles in previously taken aliquots of the ^{123}I -labeled nanoparticles after their radioactive decay demonstrate no significant changes when compared to the original nanoparticles (data not shown).

In the final experiment of the present study, we investigated the biodistribution of ^{125}I -labeled nanoparticles over 15 and 60 min after injection. Again, both types of nanoparticles, plain and PEGylated were administered to two groups of mice (6 mice each). In analogy to the previous ^{123}I experiment, also ^{125}I was completely incorporated into the nanoparticles as monitored with TLC (data not shown), so

that no further purification of the nanoparticles was necessary to separate them from free iodide. This time we conjugated higher amounts of radioactive iodide with the nanoparticles than in the first experiment. Consequently we were able to administer again a lowered nanoparticle concentration of only 20 ng nanoparticles per mouse which was only 1% of the originally administered dose in the [^{18}F]SFB-study that had caused the thromboses. Screening the biodistribution of both batches, the accumulation within the lung was now even more reduced, thus no obstruction of the lung capillaries was detected. Liver and spleen, two characteristic tissues of the MPS were the organs containing the highest concentrations of radioactively labeled nanoparticles (Fig. 13). Calculating the absolute amount of recovered radioactivity of the originally injected dose, the liver was identified as the predominant site that contains nanoparticles with ~50% of the originally injected radioactive nanoparticles. This observation was made for both, PEGylated and plain gelatin nanoparticles.



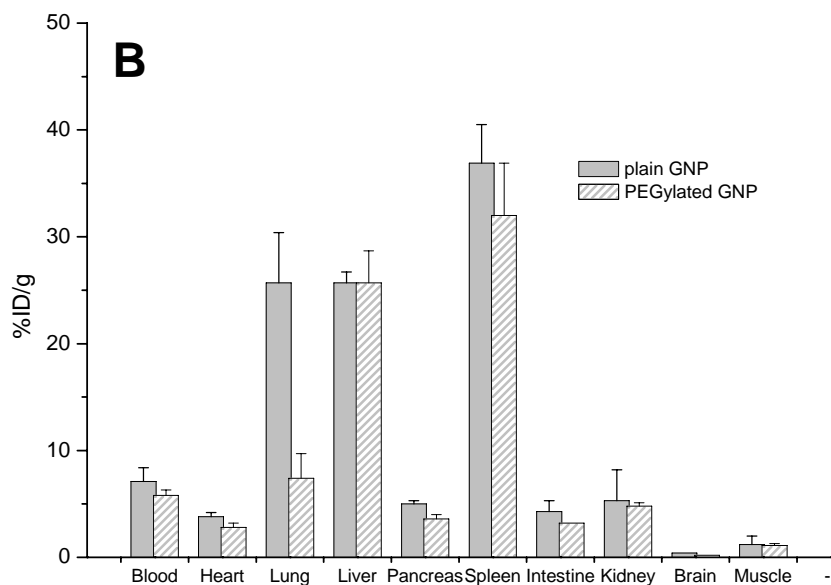


Fig. 13: Biodistribution of plain and PEGylated gelatin nanoparticles in mice after injection into the tail vein; radioactivity concentrations are given as percent of the injected radioactive dose per g (%ID/g). A: Biodistribution after 15 min; B: Biodistribution after 60 min.

A first observation made was that the radioactive dose within liver and spleen was significantly reduced after 60 min (Fig. 13B) in comparison to 15 min (Fig. 13A). Furthermore, significant radioactivity could be detected within samples of the urine after 60 min. Obviously, the MPS already begins to degrade the nanoparticles at this time point. Similar findings were made when analyzing the data that were obtained with 100-fold more concentrated [^{18}F]SFB-labeled nanoparticles, but less pronounced (see 3.3.2). One reason for the distinct appearance of this phenomenon is the lower administered dose of nanoparticles, since it is most likely that degradation activity underlies zero-order-kinetics due to saturation of the respective degradation enzymes.

The second conclusion that can be drawn from these data is that the goal of prolonged blood circulation of PEGylated gelatin nanoparticles was not achieved with the present setup. Possible reasons might be that the length of the grafted PEG-chains (Mw. 5 kDa) was not appropriate, since literature suggests using PEG chains of higher molecular weights to achieve prolonged blood circulation. However, prolonged circulation effect was observed by other researcher's when

preparing nanoparticles based on gelatin-PEG co-polymer containing a 5 kDa PEG (Kaul & Amiji 2004).

Another aspect might be that the linkage of MPEG-NH₂ with free aldehyde groups represents only a reversible balance reaction, since the imine function is easily hydrolyzed under acidic conditions. If this is the case, PEG needs to be linked onto the nanoparticles in a more stable way. One possible approach would be to add cyanoborohydride (NaCNBH₃) during the condensation reaction. NaCNBH₃ induces the reduction of the imine giving a stable amine bond. But the use of this approach is due to the high toxicity of NaCNBH₃ questionable. Other approaches of MPEG-NH₂ linkage would be direct conjugation with previously activated carboxyl groups, or the utilization of different functional groups. However, both approaches do not allow quick cleavage of the nanoparticles when entering the cell, which was the original idea behind the present approach. The applicability of the highly promising technique to introduce pH-triggered linkage via acylhydrazides or pyridylhydrazines (Walker *et al.* 2005) appears also questionable for gelatin nanoparticles due to the complex synthesis that might facilitate particle-aggregation. Another interesting approach might be the linkage via reducible disulfide bonds that would be cleaved within the reductive intracellular milieu of the target cell. Therefore, introduction of sulfhydryl groups onto the gelatin nanoparticles is necessary. Respective methods using cysteine or cystaminiumdichloride have been described in literature (Coester 2000; Weber *et al.* 2000).

3.2.4 Summary

It has been demonstrated in the present study that gelatin nanoparticles can be linked with ¹⁸F prosthetic groups or radioactive iodide to enable the study of their *in vivo* biodistribution noninvasively by PET or SPECT. Moreover, [¹⁸F]SFB could be characterized as a promising prosthetic group for this purpose. Small-scale synthesis and labeling reaction for gelatin nanoparticles were established. However, the initial radioactivity at the start of the synthesis that can be utilized in the small-scale setup was too low to allow the application of appropriate nanoparticle concentrations that do not cause thromboses in the lung capillaries. Preparation of 'large-scale' [¹⁸F]SFB-conjugated nanoparticles failed so far due to nanoparticle aggregation. Although the exact reason could not be identified yet, the effect is most likely induced by the introduction of impurities during [¹⁸F]SFB synthesis.

Thus, radioactive iodine isotopes which are well established for radioactive protein and peptide labeling were chosen as alternative radiolabeling agent for gelatin nanoparticles. Both, plain and PEGylated gelatin nanoparticles could be almost quantitatively labeled with $^{123}\text{I}/^{125}\text{I}$, so high amounts of radioactivity could be introduced to the gelatin nanoparticles. This higher radioactivity introduced allowed to lower the concentration that was injected to the tail vein of mice by two orders of magnitude. Consequently, quick accumulation of the nanoparticles in the main organs of the MPS could be already observed after 15 min. PEGylated nanoparticles were unable to improve the blood circulation time. Reasons might be *in vivo* instability of the PEG-linkage via an imine bond, or too low molecular weight of the applied PEG chains. Consequently, different approaches such as reducible disulfide linkage and different sized PEG chains should be evaluated in future. Furthermore, the impact of the applied particle size should be studied. Finally, surfactant coating with e.g. polysorbate, in analogy to the findings with solid lipid nanoparticles (Zillies *et al.* 2005) and poly (butyl 2-cyanoacrylate) nanoparticles (Douglas *et al.* 1986; Kreuter *et al.* 1995) should be evaluated as alternative strategy to change the opsonization profile of gelatin nanoparticles.

4. CONCLUSION

This chapter gives another outlook on possible future projects with gelatin nanoparticles.

Aside from successful PEGylation experiments, special attention was paid to the development of innovative and precise analytical tools for the assessment of the quality and quantity of PEG chains grafted onto the nanoparticles. Thereby, AF4 and AFM were demonstrated as complementing instruments for the quantification and visualization of successful linkage. The obtained results are of high quality and suggest transferring both methods as state-of-the-art for various other colloidal systems as the number of existing techniques is rather limited.

As second focus, radioactive labeling of gelatin nanoparticles was performed to enable the analysis of their biodistribution. Moreover, ^{18}F labeling was established, which allows real-time tracking of the nanoparticles' biodistribution by PET. Thereby, [^{18}F]SFB could be identified as a prosthetic group for ^{18}F labeling. Initial biodistribution revealed that plain gelatin nanoparticles behave like most other non-modified nanoparticles and are quickly cleared from the blood stream by the MPS. The first PEGylation approach grafting a 5 kDa PEG-chains via a pH-sensitive and reversible imine bonds onto the surface of gelatin nanoparticles did not succeed in prolonged blood circulation in comparison to plain gelatin nanoparticles.

Nevertheless, the analytical setup is prepared for further investigations. The next steps should include the evaluation of various nanoparticle batches with various surface modifications concerning their circulation in the blood stream. In addition to this, targeting ligands for e.g. cancer cells should be attached onto the particle surface, thus resulting in a new application of gelatin nanoparticles as highly specific colloidal delivery system or diagnostic tracer.

5. REFERENCES

- Bakowsky, U.; (2005) Novel nanoscale drug delivery systems: Physicochemical properties and visualisation. Annual Meeting of the Controlled Release Society, Miami, USA, Conference Proceeding.
- Blunk, T., Hochstrasser, D. F., Sanchez, J. C., Muller, B. W., and Muller, R. H.; (1993) Colloidal carriers for intravenous drug targeting: plasma protein adsorption patterns on surface-modified latex particles evaluated by two-dimensional polyacrylamide gel electrophoresis. *ELECTROPHORESIS*, 14[12], 1382-1387.
- Brix, G., Nosske, D., Glatting, G., Minkov, V., and Reske, S. N.; (2002) A survey of PET activity in Germany during 1999. *EUROPEAN JOURNAL OF NUCLEAR MEDICINE AND MOLECULAR IMAGING*, 29[8], 1091-1097.
- Bruus-Jensen, K., Poethko, T., Schottelius, M., Hauser, A., Schwaiger, M., and Wester, H. J.; (2006) Chemoselective hydrazone formation between HYNIC-functionalized peptides and 18F-fluorinated aldehydes. *NUCLEAR MEDICINE AND BIOLOGY*, 33[2], 173-183.
- Childs, C. E.; (1975) Determination of polyethylene glycol in gamma globulin solutions. *MICROCHEMICAL JOURNAL*, 20[2], 190-192.
- Coester, C.; (2000) Entwicklung peptidischer oberflächenmodifizierter nanopartikulärer Trägersysteme für Antisense-Wirkstoffe und präklinische Testung gegen HIV. Dissertation, Frankfurt.
- Cole, S. C., Christensen, G. A., and Olson, W. P.; (1983) Poly(ethylene glycol) quantitation by laser nephelometry. *ANALYTICAL BIOCHEMISTRY*, 134[2], 368-373.
- Douglas, S. J., Davis, S. S., and Illum, L.; (1986) Biodistribution of poly(butyl 2-cyanoacrylate) nanoparticles in rabbits. *INTERNATIONAL JOURNAL OF PHARMACEUTICS*, 34[1-2], 145-152.
- Fukuda, H., Matsuzawa, T., Abe, Y., Endo, S., Yamada, K., Kubota, K., Hatazawa, J., Sato, T., and Ito, M.; (1982) Experimental study for cancer diagnosis with positron-labeled fluorinated glucose analogs: [18F]-2-deoxy-D-mannose: a new tracer for cancer detection. *EUROPEAN JOURNAL OF NUCLEAR MEDICINE*, 7[7], 294-297.
- Garg, P. K., Garg, S., and Zalutsky, M. R.; (1991) Fluorine-18 labeling of monoclonal antibodies and fragments with preservation of immunoreactivity. *BIOCONJUGATE CHEMISTRY*, 2[1], 44-49.
- Goepfert, T. M. and Mueller, R. H.; (2005) Protein adsorption patterns on poloxamer- and poloxamine-stabilized solid lipid nanoparticles (SLN). *EUROPEAN JOURNAL OF PHARMACEUTICS AND BIOPHARMACEUTICS*, 60[3], 361-372.
- Gref, R., Domb, A., Quellec, P., Blunk, T., Mueller, R. H., Verbavatz, J. M., and Langer, R.; (1995) The controlled intravenous delivery of drugs using PEG-coated sterically stabilized nanospheres. *ADVANCED DRUG DELIVERY REVIEWS*, 16, 215-233.
- Gref, R., Minamitake, Y., Peracchia, M. T., Trubetskoy, V., Torchilin, V., and Langer, R.; (1994) Biodegradable long-circulating polymeric nanospheres. *SCIENCE*, 263[5153], 1600-1603.

- Guhlke, S., Coenen, H. H., and Stoecklin, G.; (1994) Fluoroacylation agents based on small n.c.a. [18F]fluorocarboxylic acids. *APPLIED RADIATION AND ISOTOPES*, 45[6], 715-727.
- Kaul, G. and Amiji, M.; (2004) Biodistribution and targeting potential of poly(ethylene glycol)-modified gelatin nanoparticles in subcutaneous murine tumor model. *JOURNAL OF DRUG TARGETING*, 12[9-10], 585-591.
- Kilbourn, M. R., Dence, C. S., Welch, M. J., and Mathias, C. J.; (1987) Fluorine-18 labeling of proteins. *JOURNAL OF NUCLEAR MEDICINE*, 28[4], 462-470.
- Kreuter, J.; (1983) Evaluation of nanoparticles as drug-delivery systems. II: Comparison of the body distribution of nanoparticles with the body distribution of microspheres (diameter greater than 1 micron), liposomes, and emulsions. *PHARMACEUTICA ACTA HELVETIAE*, 58, 217-226.
- Kreuter, J., Alyautdin, R. N., Kharkevich, D. A., and Ivanov, A. A.; (1995) Passage of peptides through the blood-brain barrier with colloidal polymer particles (nanoparticles). *BRAIN RESEARCH*, 674, 171-174.
- Kreuter, J., Ränge, P., Petrov, V., Hamm, S., Gelperina, S. E., Engelhardt, B., Alyautdin, R., von Briesen, H., and Begley, D. J.; (2003) Direct Evidence that Polysorbate-80-Coated Poly(Butylcyanoacrylate) Nanoparticles Deliver Drugs to the CNS via Specific Mechanisms Requiring Prior Binding of Drug to the Nanoparticles. *PHARMACEUTICAL RESEARCH*, 20, 409-416.
- Kuhnast, B., Dolle, F., and Tavitian, B.; (2002) Fluorine-18 labeling of peptide nucleic acids. *JOURNAL OF LABELLED COMPOUNDS & RADIOPHARMACEUTICALS*, 45[1], 1-11.
- Lang, L. and Eckelman, W. C.; (1994) One-step synthesis of 18F labeled [18F]-N-succinimidyl 4-(fluoromethyl)benzoate for protein labeling. *APPLIED RADIATION AND ISOTOPES*; 45[12], 1155-1163.
- Moghimi, S. M. and Szebeni, J.; (2003) Stealth liposomes and long circulating nanoparticles: critical issues in pharmacokinetics, opsonization and protein-binding properties. *PROGRESS IN LIPID RESEARCH*, 42[6], 463-478.
- Nag, A., Mitra, G., and Ghosh, P. C.; (1996) A colorimetric assay for estimation of polyethylene glycol and polyethylene glycolated protein using ammonium ferrothiocyanate. *ANALYTICAL BIOCHEMISTRY*, 237[2], 224-231.
- Ogris, M., Brunner, S., Schuller, S., Kircheis, R., and Wagner, E.; (1999) PEGylated DNA/transferrin-PEI complexes: reduced interaction with blood components, extended circulation in blood and potential for systemic gene delivery. *GENE THERAPY*, 6[4], 595-605.
- Okarvi, S. M.; (2001) Recent progress in fluorine-18 labelled peptide radiopharmaceuticals. *EUROPEAN JOURNAL OF NUCLEAR MEDICINE*, 28[7], 929-938.
- Oku, N.; (1999) Delivery of contrast agents for positron emission tomography imaging by liposomes. *ADVANCED DRUG DELIVERY REVIEWS*, 37[1-3], 53-61.
- Owens, D. E. and Peppas, N. A.; (2006) Opsonization, biodistribution, and pharmacokinetics of polymeric nanoparticles. *INTERNATIONAL JOURNAL OF PHARMACEUTICS*, 307[1], 93-102.

Philipsen, E., Batsberg, W., and Larsen, E.; (1985) The determination of polyethylene glycol in untreated urine samples by high performance liquid chromatography for intestinal permeability studies. *JOURNAL OF TRACE AND MICROPROBE TECHNIQUES*, 3[3], 255-271.

Poethko, T., Schottelius, M., Thumshirn, G., Hersel, U., Herz, M., Henriksen, G., Kessler, H., Schwaiger, M., and Wester, H. J.; (2004) Two-step methodology for high-yield routine radiohalogenation of peptides: (18)F-labeled RGD and octreotide analogs. *JOURNAL OF NUCLEAR MEDICINE*, 45[5], 892-902.

Ravi Kumar, M. N. V., Bakowsky, U., and Lehr, C. M.; (2004) Preparation and characterization of cationic PLGA nanospheres as DNA carriers. *BIOMATERIALS*, 25[10], 1771-1777.

Vaidyanathan, G. and Zalutsky, M. R.; (1992) Labeling proteins with fluorine-18 using N-succinimidyl 4-[18F]fluorobenzoate. *INTERNATIONAL JOURNAL OF RADIATION APPLICATIONS AND INSTRUMENTATION*, 19[3], 275-281.

Vaidyanathan, G. and Zalutsky, M. R.; (1994) Improved synthesis of N-succinimidyl 4-[18F]fluorobenzoate and its application to the labeling of a monoclonal antibody fragment. *BIOCONJUGATE CHEMISTRY*, 5[4], 352-356.

Varagnolo, L., Stokkel, M. P. M., Mazzi, U., and Pauwels, E. K. J.; (2000) 18F-labeled radiopharmaceuticals for PET in oncology, excluding FDG. *NUCLEAR MEDICINE AND BIOLOGY*, 27, 103-112.

Veronese, F. M.; (2001) Peptide and protein PEGylation: a review of problems and solutions. *BIOMATERIALS*, 22[5], 405-417.

Walker, G. F., Fella, C., Pelisek, J., Fahrmeir, J., Boeckle, S., Ogris, M., and Wagner, E.; (2005) Toward synthetic viruses: Endosomal pH-triggered deshielding of targeted polyplexes greatly enhances gene transfer in vitro and in vivo. *MOLECULAR THERAPY*, 11[3], 418-425.

Weber, C., Reiss, S., and Langer, K.; (2000) Preparation of surface modified protein nanoparticles by introduction of sulfhydryl groups. *INTERNATIONAL JOURNAL OF PHARMACEUTICS*, 211[1-2], 67-78.

Wester, H. J.; (2003) 18F: labeling chemistry and labeled compounds. *HANDBOOK OF NUCLEAR CHEMISTRY*, 4, 167-209.

Wester, H. J., Hamacher, K., and Stocklin, G.; (1996) A comparative study of N.C.A. fluorine-18 labeling of proteins via acylation and photochemical conjugation. *NUCLEAR MEDICINE AND BIOLOGY*, 23[3], 365-372.

Wuest, F.; (2005) Aspects of positron emission tomography radiochemistry as relevant for food chemistry. *AMINO ACIDS* 29[4], 323-339.

Wuest, F., Hultsch, C., Bergmann, R., Johannsen, B., and Henle, T.; (2003) Radiolabelling of isopeptide N epsilon-(gamma-glutamyl)-L-lysine by conjugation with N-succinimidyl-4-[18F]fluorobenzoate. *APPLIED RADIATION AND ISOTOPE*, 59[1], 43-48.

Zillies, J.; Dissertation, to be published 2007.

Zillies, J., Goepfert, T. M., Hoffmann, F., Zahler, S., Vollmar, A., Müller, R. H., Winter, G., and Coester, C.; (2005) Correlation of Plasma Protein Adsorption Patterns and Biodistribution Data

of Different Gelatin and Solid Lipid Nanoparticle Formulations. Annual Meeting of the AAPS, Nashville, USA, Conference Proceeding.

Final summary and conclusions of this thesis

The present work highlights the potential of gelatin nanoparticles as delivery system for nucleotide-based drugs.

Detailed analysis of the original manufacturing process and exact characterization of the effect of process parameters on the later nanoparticle quality, as described in **Chapter I**, allowed significant improvement of the two-step desolvation technique. Now it is possible to prepare standardized homogeneous colloidal spheres in a range between 100 and 300 nm with excellent reproducibility. Another essential result was the analytical determination of the optimum molecular weight constitution of the gelatin raw material to prepare homogeneous and stable nanoparticles. Our partners at Gelita AG prepared specific gelatin batches that allow to refrain from the first fractionating desolvation step in the preparation procedure. Now, stable gelatin nanoparticles can be directly generated by a simple single desolvation process.

In **Chapter II**, surface modification strategies were investigated to enable the electrostatic loading of nucleotide-based drugs onto the nanoparticle surface. Among the various tested modification agents, cholamine, containing a terminal quaternary amino group that induces a pH independent cationic charge on the nanoparticle surface, was selected as the most promising one for further investigations. The first application examined *in vitro*, was the use as gene delivery system. In this study it could be demonstrated that cationized gelatin nanoparticles are able to successfully transfect murine melanoma cells. However, transfection occurred with a little delay and achieved results were unable to top the efficiency of the current ‘gold standard’ PEI-polyplexes. But, gelatin nanoparticles were also shown to be a biocompatible carrier, as they did not induce significant cytotoxicity in contrast to other non-viral delivery systems. Consequently, this simple approach promises high potential.

The most auspicious and advanced results were obtained with immunogenic CpG ODNs (**Chapter III** and **Chapter IV**). In these studies, short single-stranded ODNs were attached onto the surface of cholamine-modified gelatin nanoparticles. During first *in vitro* experiments with murine myeloid dendritic cells (MDCs), phagocytotic uptake and enhanced induction of T_H1/CTL-polarizing cytokines in comparison to soluble CpG ODNs could be observed. Comparing the activation

kinetics of particulate bound CpG ODN with soluble CpG ODN, no delay could be observed. Hence, CpG interacts most likely with the receptor when still being attached onto the nanoparticle surface. Admittedly, those experiments with murine MDCs can only be seen as model setup because TLR9, the specific receptor for CpG motifs is not present in this cell-type in humans. Thus, the setup was successfully transferred to primary human B cells and plasmacytoid dendritic cells (PDCs), the two cell-types that have exclusively expressed TLR9 in humans and non-human primates.

For humans three different classes of CpG ODNs (CpG-A – CpG-C) exist. *In vitro* experiments on PDCs and B cells with all three ODN types being loaded onto gelatin nanoparticles led to novel insights on the different activation prerequisites of both CpG-ODN-sensitive cell-types. Particulate presentation of CpG motifs is rather counterproductive for the activation of B cells. In PDCs, activation conditions were found to be completely contrary to B cells. They are stimulated best by particulate CpG ODN presentation. Hence, optimized nanoparticulate presentation led to strongly enhanced induction of CpG-C. Even CpG-B, which does not activate PDCs in soluble form, was now able to induce slightly more IFN- α than the original ‘gold standard’, soluble CpG-A. Furthermore, it was proven that the high efficiency of CpG-A has to be attributed to the fact that the sequence of CpG-A facilitates the formation of colloidal particulate aggregates in physiological media.

Due to the success *in vitro*, CpG formulations were then transferred to *in vivo* trials in mice (**Chapter IV**). In first characterization studies, comparing the subcutaneous and intravenous administration route, it could be observed that only i.v. administration of CpG-GNPs induces systemic immune activation, whereas soluble CpG ODN is active after both types of injection. The explanation is that particulate bound CpG ODN basically remained at the site of administration after s.c. injection. Solely a few nanoparticles could be detected in the draining lymph nodes that were closest to the site of injection.

However, for an application as adjuvant for vaccines, the absence of unspecific systemic immunoactivation is highly advantageous, because the systemic effect of soluble CpG ODNs potentially is a source of immunological side effects.

While performing immunization experiments with the model antigen ovalbumin (OVA) and CpG ODN-loaded gelatin nanoparticles as additional adjuvant, this

local restriction of the immunological effect turned out to be sufficient to achieve enhanced immunization. The obtained specific IgG titers were comparable and the activation of specific CD8⁺ cells was significantly better than that achieved with soluble CpG ODN as adjuvant, which is currently investigated in various clinical trials. Thus, these preclinical data suggest the development of CpG ODN-loaded gelatin nanoparticles towards clinical trials as new adjuvant for vaccine formulations. Due to its T_H1/CTL specificity, this new formulation might be ideal for anti-viral and anti-tumoral antigens, a field where standard adjuvant alum has its weaknesses.

Finally, it was demonstrated that the immunological activity of OVA remains identical with soluble OVA, when adsorbed onto the surface of cationized gelatin nanoparticles or incorporated into the matrix of plain nanoparticles. These might be potential options when particulate delivery and presentation of an antigen peptide is advantageous.

Summarizing the applications presented in this work, gelatin nanoparticles are a versatile carrier that can be used for both, transfection with large double-stranded pDNAs as well as for short single-stranded ODNs. However, the optimum payloads of both applications differ remarkably. Whereas best gene transfections were obtained with 0.5% (w/w) payload, best activation of the immune system were achieved with 5-10% (w/w) CpG ODN loaded onto nanoparticles, a payload where pDNA loaded nanoparticles were unstable and aggregated.

Additionally, it was interesting to see that the optimum nanoparticle size depends also on the respective target. Best gene transfections on murine melanoma cells were obtained with small gelatin nanoparticles (~150 nm). In contrast to that, best dendritic cell activation occurred with ~300 nm large CpG ODN loaded nanoparticles. This fits perfectly with the preferably phagocytosed size of antigen presenting cells.

Comparing the results of gene transfection with the ones of CpG delivery it is noticeable that the same carrier platform showed different success. Whereas the gene transfection efficiency of cationized gelatin nanoparticles was lower than that of PEI-polyplexes, it is known that PEI rather reduces the immunological effect of CpG ODNs when delivered as polyplexes. An explanation for this phenomenon is that TLR9, the receptor of CpG ODNs, is located within the endosomal

compartment. Consequently good transfection reagents, such as PEI, that are known to promote a quick endosomal escape, are inappropriate for this purpose. On the other hand cholamine-modified nanoparticles apparently comprise a rather delayed escape from the endosome.

Special attention was paid in this work to safety and biocompatibility of gelatin nanoparticles. During gene delivery studies, cationized gelatin nanoparticles were demonstrated as highly biocompatible, low cytotoxic transfection system in contrast to other very efficient non-viral carriers such as cationic liposomes and PEI-polyplexes. CpG delivery experiments proved that gelatin nanoparticles themselves are an immunologically inert delivery system. The immunogenic effect of CpG ODNs led only to efficient immunization against the co-administered protein antigen but did not induce the production of anti-gelatin IgGs.

In the final **Chapter V**, first PEGylations of the nanoparticle surface were performed to achieve prolonged circulation within the blood-stream. The major focus here was to establish new analytical tools for quantitative and qualitative monitoring of the coupling reaction. AF4 and AFM demonstrated to be highly valuable to characterize the successful PEGylation of nanoparticles, since existing alternatives are limited.

In the second part of this chapter, radiolabeling was applied to track the biodistribution of gelatin nanoparticles. Aside from radioiodination, ^{18}F -coupling via prosthetic groups was evaluated for real-time monitoring of the biodistribution with positron emission tomography (PET). N-Succinimidyl 4- ^{18}F fluorobenzoate (^{18}F SFB) was identified as ideal prosthetic group for gelatin nanoparticle labeling. Initial biodistribution experiments showed typical quick elimination via the mononuclear phagocytotic system (MPS).

However, no significantly prolonged blood circulation could be achieved using PEGylated nanoparticles in a first approach. Nevertheless, various other potential PEGylation strategies exist and should be evaluated. If one of these PEGylation approaches succeeds, a future application as parenteral carrier system for tumor targeting seems possible. The target specificity would occur, since long-circulating gelatin nanoparticles are expected to accumulate at the target site due to the enhanced permeability and retention (EPR) effect, a phenomenon which allows colloidal carriers to penetrate deep into the leaky vasculature surrounding solid tumor cells. Aside from this passive targeting approach, covalent coupling of a

tumor-specific ligand onto the nanoparticle surface would allow additional active targeting. In combination with the established radiolabeling, diagnostic as well as therapeutic applications seem feasible.

List of abbreviations

AF 4	Asymmetrical flow field-flow fractionation
AFM	Atomic force microscopy
APC	Antigen presenting cell
AUC	Area under the curve
BSA	Bovine serum albumin
CD	Cluster of differentiation
CLSM	Confocal laser scanning microscopy
CMV	Cytomegalovirus
CpG	Cytosine-phosphate-guanosine
CpG motif	Cytosine-phosphate-guanosine dinucleotide in a particular sequence context
CpG ODN	Synthetic ODN containing CpG motifs
CpG-A	CpG ODN 2216
CpG-B	CpG ODN 2006
CpG-C	CpG ODN M362
CpG-GNP	CpG ODN loaded cationized gelatin nanoparticle
CTL	Cytotoxic T lymphocytes
DC	Dendritic cell
DLS	Dynamic light scattering
DMEM	Dulbeco's modified eagles medium
DMSO	Dimethyl sulfoxide
DNA	Deoxyribonucleic acid
DOPC	1,2-Dioleoyl-sn-glycero-3-phosphocholine
DOTAP	1,2-Dioleoyl-3-trimethylammonium-propane chloride
dsRNA	Double-stranded RNA
EDC	1-Ethyl-3-(3-dimethyl-aminopropyl) carbodiimide hydrochloride
EGF	Epidermal growth factor

List of abbreviations

ELISA	Enzyme-linked immunosorbent assay
FACS	Fluorescence-activated cell sorting
FCA	Freund's complete adjuvant
FCS	Fetal calf serum
FDA	US Food and Drug Administration
FITC	Fluoresceine-isothiocyanate
GM-CSF	Granulocyte-macrophage colony stimulating factor
GNP	Gelatin nanoparticle
GRAS	Generally recognized as safe
GTA	Glutaraldehyde
HBG	HEPES-buffered glucose
HBS	HEPES-buffered saline
hmw	High molecular weight
HPLC	High pressure liquid chromatography
ID	Injected dose
IEP	Isoelectric point
IFN	Interferon
Ig	Immunoglobulin
IL	Interleukin
lmw	Low molecular weight
LPS	Lipopolysaccharide
MACS	Magnetic-activated cell sorting
MALS	Multi-angle light scattering
MDC	Myeloid dendritic cell
MHC	Major histocompatibility complex
MPS	Mononuclear phagocytotic system
mRNA	Messenger ribonucleic acid
Mw	Molecular weight

N/P-ratio	Molar ratio of PEI nitrogen to DNA phosphate
NF- κ B	Nuclear factor kappa B
NK cells	Natural killer cells
NPEP	4-Nitrophenyl 2-fluoropropionate
OD	Optical density
ODN	Oligodesoxynucleotide
OVA	Ovalbumin
PACA	Poly(alkylcyanoacrylate)
PAMP	Pathogen-associated molecular pattern
PBMC	Peripheral blood mononuclear cell
PBS	Phosphate-buffered saline
PCA	Poly(cyanoacrylate)
PCL	Poly(ϵ -caprolactone)
pCMVLuc	Plasmid encoding for luciferase under control of the CMV promoter/enhancer
PCS	Photon correlation spectroscopy
PDC	Plasmacyoid dendritic cell
pDNA	plasmid DNA
PE	Phycoerythrin
PEA	Poly(ester-anhydride)
PEG	Polyethyleneglycol
PEI	Polyethylenimine
PEO	Polyethyleneoxide
PET	Positron emission tomography
PI	Polydispersity index
PLA	Poly lactide
PLG	Polyglycolide
PLGA	Poly(D,L-lactide-co-glycolide)

PRR	Pattern recognition receptor
QELS	Quasi-elastic light scattering
RCY	Radiochemical yield
RES	Reticuloendothelial system
RGD	Rayleigh-Gans-Debye
RLU	Relative light units
RNA	Ribonucleic acid
SE-HPLC	Size exclusion HPLC
SEM	Scanning electron microscopy
SFB	N-Succinimidyl 4-fluorobenzoate
SLN	Solid lipid nanoparticle
SLS	static light scattering
SPECT	Single photon emission computed tomography
TEPA	Tetraethylenpentamine
TETA	Triethylenetetramine
T _H cells	T helper cells
TLC	Thin-layer chromatography
TLR	Toll-like receptor
TNF	Tumor necrosis factor
TSTU	O-(N-succinimidyl)-N-N,N',N'-tetramethyluronium tetrafluoroborate
W/O	Water in oil
ζ potential	Zeta potential

Publications and presentations associated with this work

ORIGINAL PAPERS

Zwiorek, K., Klöckner, J., Wagner, E., Coester, C., Gelatin nanoparticles as a new and simple gene delivery system. *J. Pharm. Pharm. Sci.*, 7(4), 22-28, 2004.

In preparation:

Zwiorek, K., Bourquin, C., Battiany, J., Anz, D., Endres, S., Winter, G., Hartmann, G., Coester, C., Cationized gelatin nanoparticles as novel biodegradable carrier system for immunogenic CpG oligonucleotides.

Bourquin, C., Zwiorek, K., Anz, D., Sandholzer, N., von der Borch, P., Winter, G., Coester, C., Endres, S., CpG ODN bound gelatin nanoparticles induce antigen-specific immune responses without systemic immune stimulation.

Zillies, J., Zwiorek, K., Loebbe, C., Winter, G., Coester, C., Quantifying the PEGylation of gelatin nanoparticle drug carrier systems via asymmetrical flow field-flow fractionation (AF4) and refractive index (RI) detection.

PATENTS

DE 102004041340/WO 2006021367

Nanopartikel und Verfahren zu deren Herstellung

POSTER PRESENTATIONS

Zwiorek, K. , Bourquin, C., Endres, S., Coester, C., CpG oligonucleotide-loaded gelatin nanoparticles as an effective biodegradable vaccine adjuvant. 5th World Meeting on Pharmaceutics, Biopharmaceutics and Pharmaceutical Technology, March 27-30, 2006, Geneva , Switzerland.

Zwiorek, K., Elamanchili, P., Samuel, J., Coester, C., In vitro evaluation of various biodegradable colloidal carrier systems for dendritic cell targeting. 32nd Annual Meeting of the Controlled Release Society, June 18-22, 2005, Miami, USA.

Zwiorek, K., Coester, C., Evaluation of surface-modified gelatin nanoparticles as delivery system for oligonucleotides and plasmids. 2003 AAPS Annual Meeting and Exposition, October 26-30, 2003, Salt Lake City, USA.

ORAL PRESENTATIONS

Zwiorek, K., Klöckner, J., Wagner, E., Coester, C., In vitro transfection with surface-modified gelatin nanoparticles. 2004 Canada-Japan Nanopharmaceutical Symposium, August 23-26, 2004, Banff, Canada.

Zwiorek, K., Stock, N., Coester, C., A new method for characterization and analysis of nanocolloidal drug delivery systems based on biological polymers. 2003 Annual Meeting of the Controlled Release Society (German Chapter), April 4, 2003, Munich, Germany.

Acknowledgments

Foremost, I wish to express my deepest gratitude to my supervisor, Prof. Dr. Gerhard Winter for his highly professional guidance and numerous inspiring discussions. In addition to his scientific brilliance, I especially appreciated his dedication to create an excellent working atmosphere.

Moreover I would like to thank my direct tutor Dr. Conrad Coester for his support during my work, especially the great efforts he made to facilitate my research stay at University of Alberta.

Consequently, I am also exceptionally grateful to Prof. Dr. John Samuel for giving me the great opportunity to work for three months in his labs at University of Alberta and to learn a lot about immunological issues and cell culture.

My very special appreciation goes out to my cooperation partners, who were essential for the success of this work:

- Prof Dr. Ernst Wagner and his awesome research team at the Department of Pharmaceutical Biotechnology (LMU Munich) for our successful gene delivery cooperation. Very special thanks to Dr. Julia Klöckner; aside from her brilliant scientific expertise, I will also miss the fun we had outside of the lab, e.g. on the tennis court.
- Prof. Dr. Stefan Endres and his research team at the Division of Clinical Pharmacology (LMU Munich) for our successful cooperation on CpG oligonucleotide delivery. Concerning the studies with primary human blood cells, I would like to thank Prof. Dr. Gunther Hartmann and his research group, especially Dr. Julia Battiany who was also a very pleasant scientific partner. For the perfect processing of the following *in vivo* applications, I want to thank Dr. Dr. Carole Bourquin and her nice team, Nadja Sandholzer, Philip von der Borch, and David Anz.
- Prof. Dr. Hans-Jürgen Wester and his research team at the Department of Nuclear Medicine (TU Munich) for their support and assistance during my biodistribution experiments. In this cooperation especially Dr. Norman Koglin has to be mentioned as highly pleasant scientific partner who put immense personal effort into our projects.

Thanks are extended to Dr. Michael Ahlers from our partner Gelita AG, who generously provided all kinds of specific gelatin batches.

Dr. Wolfgang Fraunhofer and Jan Zillies are acknowledged for their scientific support and great entertainment during AF4 experiments.

Due to their outstanding assistance during the optimization of the nanoparticle preparation, I am very grateful to Alice Hirschmann and Arianna Albertella.

Many thanks to Christian Löbbe (JPK Instruments, Berlin) and Dr. Norbert Stock (Department of Physical Chemistry, LMU) who were responsible for the high quality of AFM and SEM images.

Furthermore, I want to thank Ingo, Andi, Jan, Johannes, Richard, and Martin for joining me in the computer-administration team during the last years.

I am very thankful to Dr. Friedrich Gruber, Jan Zillies, and Lars Schiefelbein for their quick and accurate revision of this thesis and encouraging words during the final time.

Overall, I extremely enjoyed working in our department. Thus, I want to thank all present and former members of our research groups for the brilliant atmosphere and the good time we had. Here, especially Jan has to be mentioned for being the perfect lab buddy through all the years.

Finally, I want to thank my parents and Melanie for their love and support.

Curriculum Vitae

KLAUS ZWIOREK

Date of birth: September 01, 1975

Place of birth: Munich, Germany

Marital status: unmarried

EDUCATION

10/2002 to present: PhD studies at the Department of Pharmaceutical Technology and Biopharmaceutics at LMU Munich

Supervisor: Prof. Dr. Gerhard Winter

07/2004 - 09/2004: Research stay at the Faculty of Pharmacy at University of Alberta, Edmonton, Canada

Supervisor: Prof. Dr. John Samuel

08/2002: Licensure as pharmacist

11/2001 – 05/2002: 2nd part of practical education (retail): Weissenburger Pharmacy in Munich

05/2001 – 10/2001: 1st part of practical education (industry): Klinge Pharma GmbH in Munich

11/1996 – 04/2001: Study of pharmacy at LMU Munich

10/1995 – 10/1996: Civilian service: Supervision of mentally disabled persons at the sheltered workshop of Care Centre Munich West

07/1995: General qualification for university entrance

09/1982 – 07/1995: School education (Grundschule Esting & Gymnasium Olching)